SC

Photochemical Applications of the Intercalation of Organic Cations in Clay Minerals.

by

Gilles Villemure

A thesis
presented to the University of Ottawa
in fulfillment of the
thesis requirement for the degree of
Ph.D.
in
Chemistry

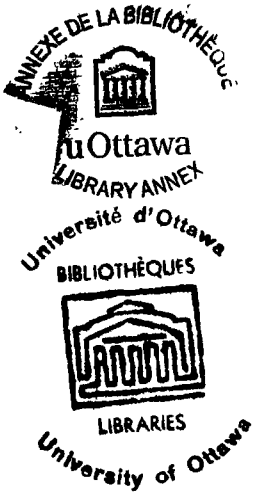

ACKNOWLEDGMENTS

I would very much like to thank my research director, Dr. C. Detellier for his support, enthusiasm and encouragement throughout my studies.

Many thanks also to Dr. H. Kodama for introducing me to the wonderful world of clay minerals, to Dr. A. Szabo for his help and patience in the deciphering and the interpretation of the fluorescence results and to Dr. T. Wrzesniewska for her assistance with the SEM measurements.

I would further like to thank my colleagues Harold Stover, Claude Dupressoir, Helen Graves, Kathy Brière and Mahmoud Tajik for creating an enjoyable working atmosphere.

Thank you to the professors, students and staff members of the department of chemistry and to all those who contributed to this work.

Finally I wish to thank my family for their patience and support throughout my studies in Ottawa. It is to them that I dedicate this thesis

ABSTRACT

We have observed hydrogen formation when a buffered system (pH 7), containing methylviologen (MV^{2+}), ruthenium tris bipyridyl ($Ru(bpy)_3^{2+}$), triethanolamine and the smectite clay minerals montmorillonite, hectorite or nontronite was irradiated with visible light. The effect of varying either the clay or the electron relay (methylviologen) concentrations on the hydrogen evolution efficiency is discussed. From the results of the competitive adsorption of MV^{2+} and $Ru(bpy)_3^{2+}$ by montmorillonite a proposal is put forward to interpret the function of the clay minerals in the hydrogen photoproduction process.

The fluorescence of the methylviologen cation could be observed when it was incorporated into the lamellae of colloidal montmorillonite or hectorite suspensions. The intensity, the anisotropy and the lifetime of the fluorescence of methylviologen intercalated in these two clays were studied as a function of the cation to clay ratio.

The segregation of $Ru(bpy)_3^{2+}$ and MV^{2+} in the interlayer spaces of hectorite and montmorillonite was studied by X-ray diffraction by oriented films of the clays.

The configuration of isolated montmorillonite particles exchanged with various amounts of either $Ru(bpy)_3^{2+}$ or MV^{2+} was examined by scanning electron microscopy.

TABLE OF CONTENTS

LIST OF FIGURES

LIST OF TABLES

Part 1

CLAY-ASSISTED HYDROGEN PHOTOPRODUCTION.

CHAPTER I

STORAGE OF SOLAR ENERGY.

1.1 Introduction.

In the past decade, water photoreduction has attracted considerable interest because of its potential use for the storage of solar energy.[1] [2]

One of the chief obstacles in the use of the sun as an energy source in today's industrial society is the intermittent nature of this form of energy. Unless sunlight is collected in space[3] one must deal with the night and day cycle and with variable weather conditions. A lot of progress has been made recently in the conversion of sunlight into electrical energy, in particular the development of the amorphous silicon solar cell,[4] but electricity is difficult to store or to transport over large distances. It is the ease of storage and transportation that makes attractive the conversion of solar energy to chemical energy, via a light driven fuel producing reaction.[5] This fuel can be stored and used when and where it is needed.

In order for a chemical reaction to be a good candidate for storage of solar energy, it must meet certain requirements.[6] First it must be a reaction driven by visible light, producing a stable fuel. The photochemical reaction must operate over a large portion of the solar spectrum so as to store a significant fraction of the light energy. To have a good yield of fuel, the quantum yield of the reaction must be high. For large scale applications the system must be cyclic, with no important side reactions leading to consumption of the reaction reagents or catalysts. And finally, those reagents and the other components of the system should be readily available, inexpensive, nontoxic and easy to handle.

Not many reactions can meet all of these requirements. Among them, one of the most interesting is the photosplitting of water.[7]

$$H_2O \longrightarrow H_2 + 1/2\ O_2 \qquad (E^o = 1.229\ V) \qquad [1]$$

Water is the cheapest and most abundant starting material there is. Its reduction yields hydrogen. Hydrogen is an ideal non-polluting fuel since it is a stable compound whose combustion produces only water.

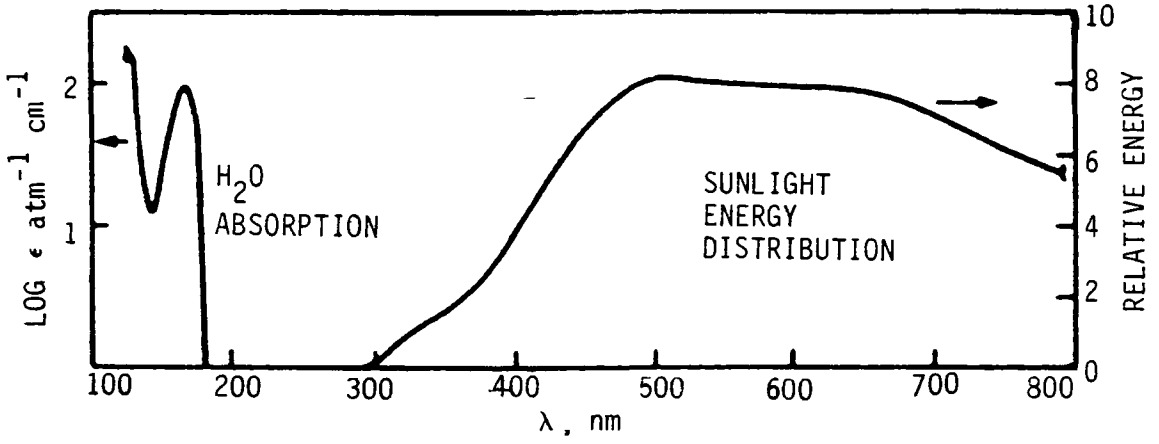

Figure 1: Absorption spectrum of water and sea level solar spectrum. (reproduced with permission from reference 8)

In figure 1, the absorption spectrum of water is compared to the distribution of sunlight at sea level. Pure water is colorless. Thus its sea level photochemistry is quickly described: there is none.[8] To make water splitting useful for solar energy storage, one must somehow succeed in driving the reaction with visible light.

Visible light contains enough energy to induce water photosplitting. The heat of dissociation of water into molecular hydrogen and molecular oxygen is only 58 kcal/mole. This means that about 16% of the sunlight contains enough energy to split water via a one photon process and as much as 40% via a two photons process.[9]

Direct photodissociation of water requires ultraviolet light because it proceeds via the formation of radicals. This is a waste of energy since radicals cannot be stored. One must look therefore for cycles in which water is split without the need of the formation of intermediate radicals. In the past decade there has been a lot of work done, on a wide variety of photoelectrochemical,[10] photobiological[11] and photochemical[12 13] systems, aimed at the development of such cycles.

1.2 Limits on the conversion efficiency.

The storage of solar energy via an endergonic photochemical reaction is shown in figure 2. Some of the energy is lost at several points in the conversion scheme. First, because of the quantum nature of light, only photons having a certain minimum energy, E^*, will be absorbed. The system will therefore have a threshold wavelength λ_{E^*}. If the photons have more energy than E^*, the excited state produced, R^*, will have large amounts of vibrational energy. In condensed media internal relaxation is rapid, the system will return to its lowest vibrational level in less than 10 picoseconds[7] and any energy in excess of E^* will be lost to the surroundings as heat.

A further fraction of the energy is lost in going from the excited state R^*, to the product P. In order to form a stable product, there must be an energy barrier between P and the starting material R. These limiting factors on the conversion efficiency of sunlight to chemical energy, have been treated by Ross et al.[14] The Ross treatment allows optimization of the various loss terms to give the maximum conversion efficiency of an ideal system, as a function of the threshold wavelength λ_{E^*}, of the light driven reaction.

This model predicts that the maximum conversion efficiency attainable in water photosplitting via a two photon process, is approximately 31%, if the system threshold wavelength is 775 nm.[7] The maximum conversion efficiency can be increased by using a

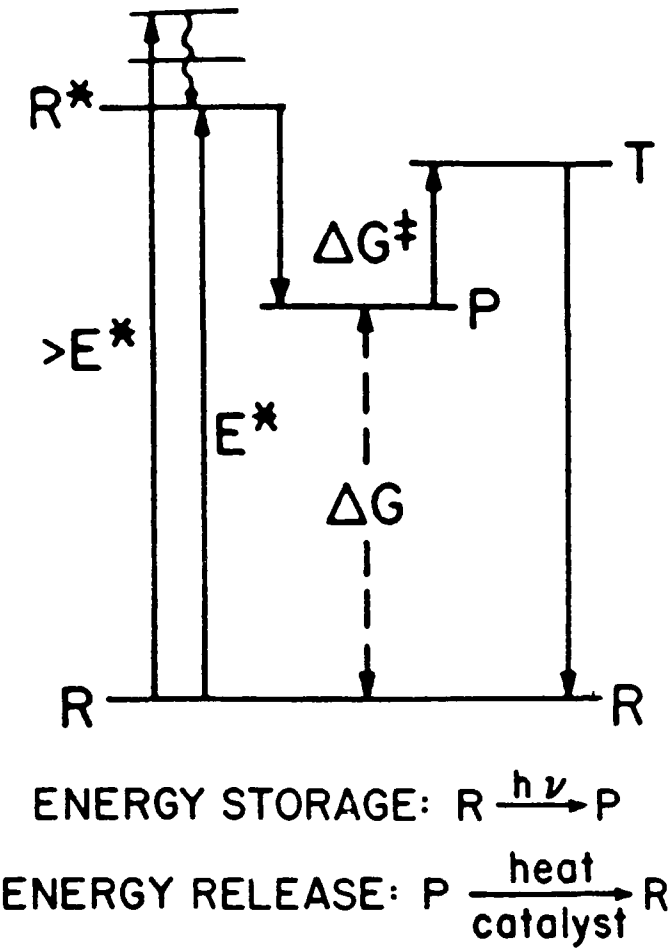

Figure 2: Photochemical energy-storage cycle. in which a fuel P is produced by a photochemical reaction of R.

dual system which contains two light driven processes. In such a system the conversion efficiency reaches 42% when the threshold wavelengths are 655 and 930 nm respectively.

These values are for ideal systems, where all photons having energy larger than the threshold energy, E^*, are absorbed and in which the formation of the product P, occurs with a quantum yield of one. In practice this will not be the case. Furthermore there will be additional losses that cannot be avoided. For example, some energy may be lost due to the reflection of some of the light or during the collection of the products, compression of the gases etc.

Being optimistic, one hope that a single two photons process could give 10% conversion, while a dual two photons process could give 16% conversion. These results may appear to be low, but when this treatment is applied to photosynthesis, considered as a dual system with both threshold wavelengths equal to 690 nm, the ideal conversion efficiency is only 12.4%.[7] Under controlled laboratory conditions conversion efficiencies of 5-6% have been obtained.[6] The yields in field conditions are lower.[15]

1.3 Photoreduction of Water : Microheterogeneous Systems.

One way to overcome the great disparity in wavelength which exists between the upper limit of absorption of water and the lower limit of the sea level solar spectrum, is to use a photosensitizer. A photosensitizer is a compound that absorbs visible light and can transfer the energy thus absorbed, via a series of relays, to a water molecule, where it can then be used to split the molecule into hydrogen and oxygen. This is essentially the function fulfilled by chlorophyll in photosynthesis.

One example of a photosensitizer used for water splitting is the dye acridine yellow (AY). As shown in figure 3, when AY is irradiated in the presence of an electron donor D, such as cysteine or ethylenediamine tetraacetic acid (EDTA) the dye is reduced. In 1977, Shilov et al[16] have shown that this reduced dye could reduce methylviologen (1,1'-dimethyl-4,4'-dipyridinium, MV^{2+}) to give the radical $MV^{+\cdot}$ and that the radical produced could reduce water in the presence of a dispersion of small particles of PtO_2 catalyst. This is the first report of a completely artificial water photoreduction scheme, involving such a microheterogeneous dispersion of a catalyst.

Since then, the efficiency of this scheme has been improved by replacing PtO_2 by a colloidal suspension of metallic platinum.[2] This system is sacrificial. The hydrogen evo-

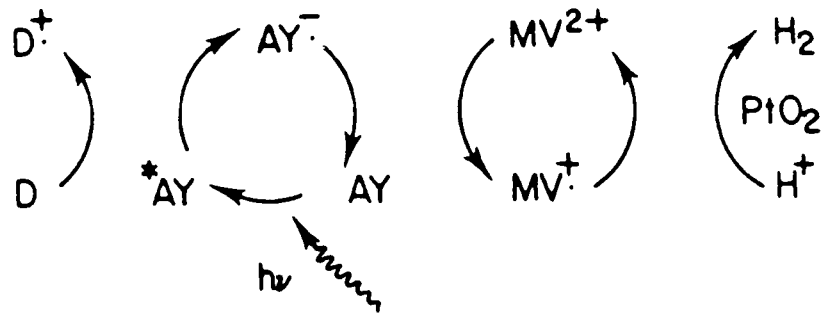

Figure 3: Sacrificial water photoreduction scheme, using acridine yellow (AY) as photosensitizer.

lution relies on the irreversible decomposition of an electron donor, thus blocking the thermodynamically favored back reactions between $AY^{-\cdot}$ and $D^{+\cdot}$, or between $MV^{+\cdot}$ and $D^{+\cdot}$. Of course, in a practical system, oxygen would be produced in another subcycle, supplying the electrons for water reduction and making the decomposition truly cyclic.

What are the requirements of a good photosensitizer for water splitting? First it must absorb visible light. Figure 1 shows that very little light with a wavelength of less than 400 nm reaches earth's surface. On the other hand, it is unlikely that light with a wavelength longer than 850 nm will have enough energy to split water. Therefore the ideal chromophore should absorb all the light having wavelengths between 400 and 850 nm.[2] Secondly, the excited state, formed by light absorption, must be produced with a high quantum yield, and have a long enough lifetime to allow time for useful chemical reactions to take place. It will almost certainly be a triplet state since, not only do triplet states generally have longer lifetimes, they also usually allow more efficient product separation. In a triplet state, spin rephasing must occur within the solvent cage before the thermodynamically favorable reverse electron transfer can take place. As a result, ions can escape from the solvent cage in better yields.[2] (see figure 7)

In addition to the photophysical requirements just described, a photosensitizer must also meet some thermodynamic requirements to be capable of mediating the splitting of water. The reduction potential of water is pH dependent. At pH 7 it is -0.41 V. To reduce water, a redox couple with a potential more negative than -0.41 V at pH 7 is required.

The excited state of the photosensitizer can be quenched by either oxidative or reductive electron transfer. If the photosensitizer is oxidized, then water reduction proceeds via equations 2 and 3.

$$S^{*} + A \longrightarrow S^{\cdot +} + A^{-\cdot} \qquad [2]$$

$$A^{-\cdot} + H^{+} \longrightarrow 1/2\ H_2 + A \qquad [3]$$

Where S stands for the photosensitizer and A is the electron acceptor which acts as a relay between S and water. To be capable of reducing water at pH 7

$$E_0(S^{+\cdot}/S^{*}) < E_0(A/A^{-}) < E_0 H^{+}/H_2 = -0.41\ V \qquad [4]$$

On the other hand, if the photosensitizer's excited state is reduced, then water reduction proceeds via equations 5 and 6

$$S^{*} + D \longrightarrow S^{-\cdot} + D^{+\cdot} \qquad [5]$$

$$S^{-\cdot} + H^{+} \longrightarrow 1/2\ H_2 + S \qquad [6]$$

And to reduce water at pH 7

$$E_0(S/S^{-\cdot}) < E_0(H^{+}/H_2) = -0.41\ V \qquad [7]$$

Finally, even if a chromophore meets all the photophysical and thermodynamic requirements, it still may not be a suitable photosensitizer for water reduction for a num-

ber of reasons. S, $S^{-\cdot}$ and $S^{+\cdot}$ must not be hydrolyzed by water or undergo other decomposition reactions; nor must they be involved in any side reactions which lead to unwanted products. Finally, S^* must be efficiently quenched by electron transfer with good cage escape yields (i.e. good charge separation) and quenching rates. These criteria do not guarantee that a chromophore will be a good photosensitizer, but only that it may be one. If it does not meet the requirements of equation 4 or 7 it is certain that it could never be useful for hydrogen photoproduction.

1.4 Tris(bipyridyl)ruthenium(II) as a Photosensitizer.

The sensitizer which has received the most attention, in connection with its potential use in water photosplitting, is tris(bipyridyl)ruthenium(II) dichloride ($Ru(bpy)_3^{2+}Cl_2$). This water soluble complex has an absorption band in the visible (λ_{max} = 452 nm; ε = 14,400 $M^{-1}cm^{-1}$), attributed to a "metal to ligand" charge transfer process, (MLCT) in which an electron is promoted from the metal t_2 orbital to a t_1 orbital associated with the ligand.[17] Irradiation at 452 nm produces an excited state with a quantum yield of one.[18] This excited state has a lifetime of 0.62 μs, and is luminescent at room temperature in water, emitting light at 607 nm with a quantum yield of 0.042.[17]

The nature of the luminescent state of $Ru(bpy)_3^{2+}$ has been the object of some controversy. At 77 K the emitted light could be resolved into three peaks at 584, 630 and 690 nm respectively. It has been established, that at 77 K the luminescence of RuL_3^{2+} type complexes was essentially of the charge transfer type and was spin-forbidden.

If one compares the photophysical properties of $Ru(bpy)_3^{2+}$ with those of the ideal photosensitizer for water splitting described in the previous section, one sees that $Ru(bpy)_3^{2+}$ is far from an ideal chromophore. It absorbs light only between 400 and 500 nm (see figure 4) and the lifetime of its excited state is relatively short. When the Ross

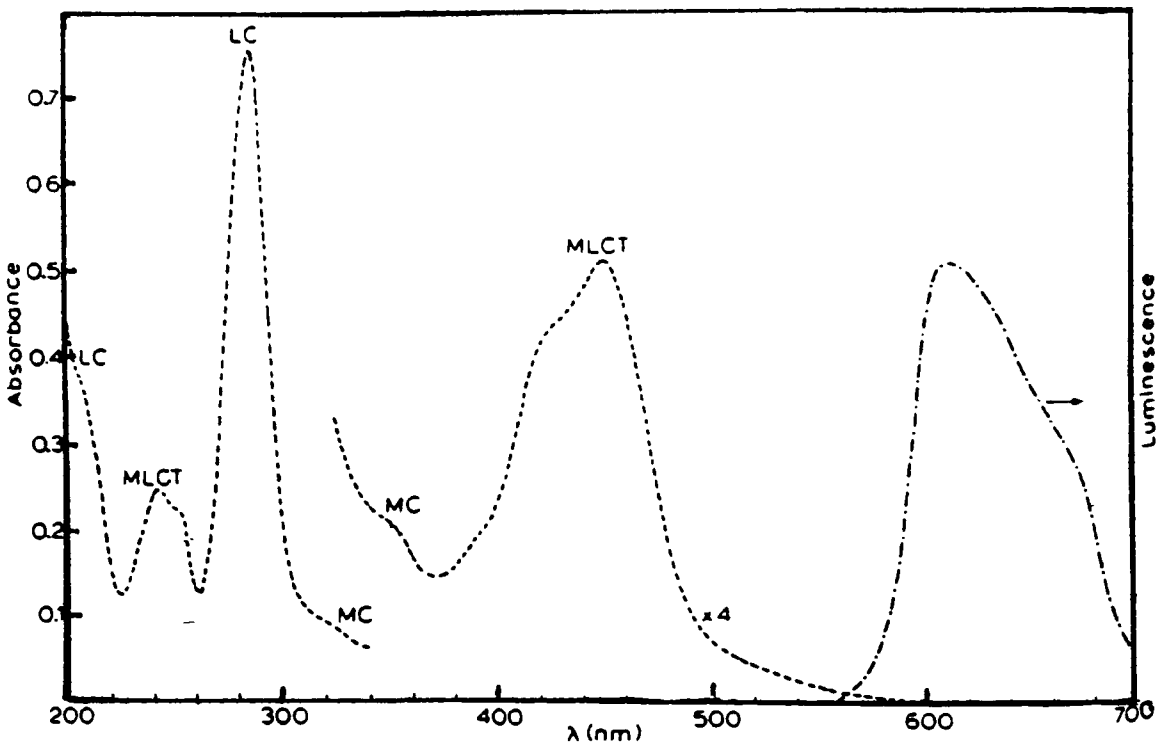

Figure 4: Absorption and emission spectrum of $Ru(bpy)_3^{2+}$ in water. (reproduced with permission form reference 17)

treatment, for the maximum efficiency of solar energy conversion attainable, (see section 1.2) was applied to $Ru(bpy)_3^{2+}$ the result was only approximately 8%.[7] $Ru(bpy)_3^{2+}$ does fulfill the thermodynamic requirements discussed in section 1.3. The potential involving the ruthenium excited state can be evaluated from the redox potentials of the ground state ions and the energy of the luminescent excited state, 2.12 V, obtained by spectroscopy, by assuming that all this energy is available as free energy for the excited state redox processes.

$$E_o(Ru^{3+}/_{2+}^*) = E_o(Ru^{3+}/_{2+}) \quad E_o(Ru^{2+}/_{2+}^*) \qquad [8]$$

$$= 1.26 - 2.12 = -0.86 \text{ V}$$

$$E_o(Ru^{2+*/+}) = E_o(Ru^{2+/+}) + E_o(Ru^{2+}/_{2+}^*) \qquad [9]$$

$$= -1.28 + 2.12 = +0.84 \text{ V}$$

Experimental support for the potential estimated via equations 8 and 9 is given by studies of the quenching of $Ru(bpy)_3^{2+}$ luminescence by series of quenchers covering a range of redox potentials.[17]

The results of equations 8 and 9 imply that the excited state of $Ru(bpy)_3^{2+}$ is at the same time a better reductant and a better oxidant than the ground state. This is accounted for by a model in which the excited state has complete charge transfer character, with an electron deficient $d_5(Ru^{3+})$ center and excess electron localized on one of the complex bipyridyl ligand. (i.e. $Ru^{3+}(bpy)_{2+}(bpy)^-$)

$Ru(bpy)_3^{2+}$ fulfills the thermodynamic requirements set forth in equation 4 and 7. The potentials for the couples $Ru(bpy)_3^{+3/2+*}$ and $Ru(bpy)_3^{2+/+}$ are both below -0.41 V, the reduction potential of water at pH 7. Therefore this photosensitizer can be used to reduce water via both reductive and oxidative quenching of its excited state.

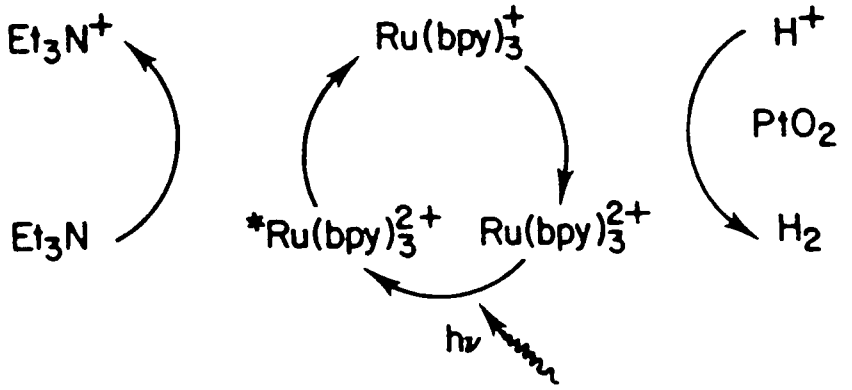

Figure 5: Water reduction via reductive electron transfer quenching of $*Ru(bpy)_3^{2+}$.

In figure 5, an example of the use of $Ru(bpy)_3^{2+}$ to reduce water in a reductive cycle is shown. Excited $Ru(bpy)_3^{2+}$ can be reduced by triethylamine (Et_3N) in acetoni-

trile to give $Ru(bpy)_3^{+}$.[19] If PtO_2 is also present, hydrogen is produced with a quantum yield of about 0.44 mol/ein.

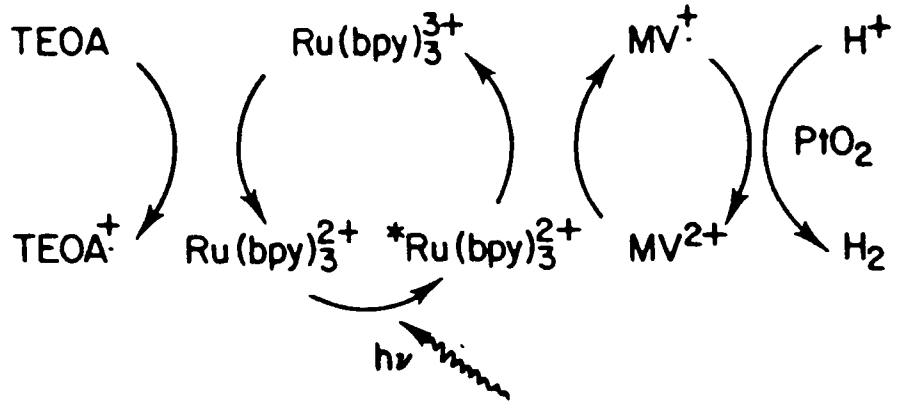

Figure 6: Water reduction via oxidation electron transfer quenching of $*Ru(bpy)_3^{2+}$.

As shown in figure 6, $Ru(bpy)_3^{2+}$ can also mediate the evolution of hydrogen via an oxidative cycle. This is one the most extensively studied and best characterized scheme for visible light photoreduction of water. Despite the efficient quenching of excited $Ru(bpy)_3^{2+}$ by MV^{2+}, relatively large concentrations of the quencher are needed because of the relatively short lifetime of the $Ru(bpy)_3^{2+}$ excited state. With high MV^{2+} concentrations, the quantum yield of hydrogen in this system is 0.13 mol/ein.[20]

The main limitation of this system is the relatively low cage escape yield. In no cases was the quantum yield of reduced methylviologen, produced by irradiation of $Ru(bpy)_3^{2+}$ in the presence of a sacrificial donor, larger than 0.25.[21] This low quantum yield is attributed to poor charge separation.[2] The back electron transfer within the solvent cage, reaction k_2 in figure 7 is thermodynamically favored (see equation 10).

$$k_1/(k_1 + k_2) < 0.3^{22} \qquad [10]$$

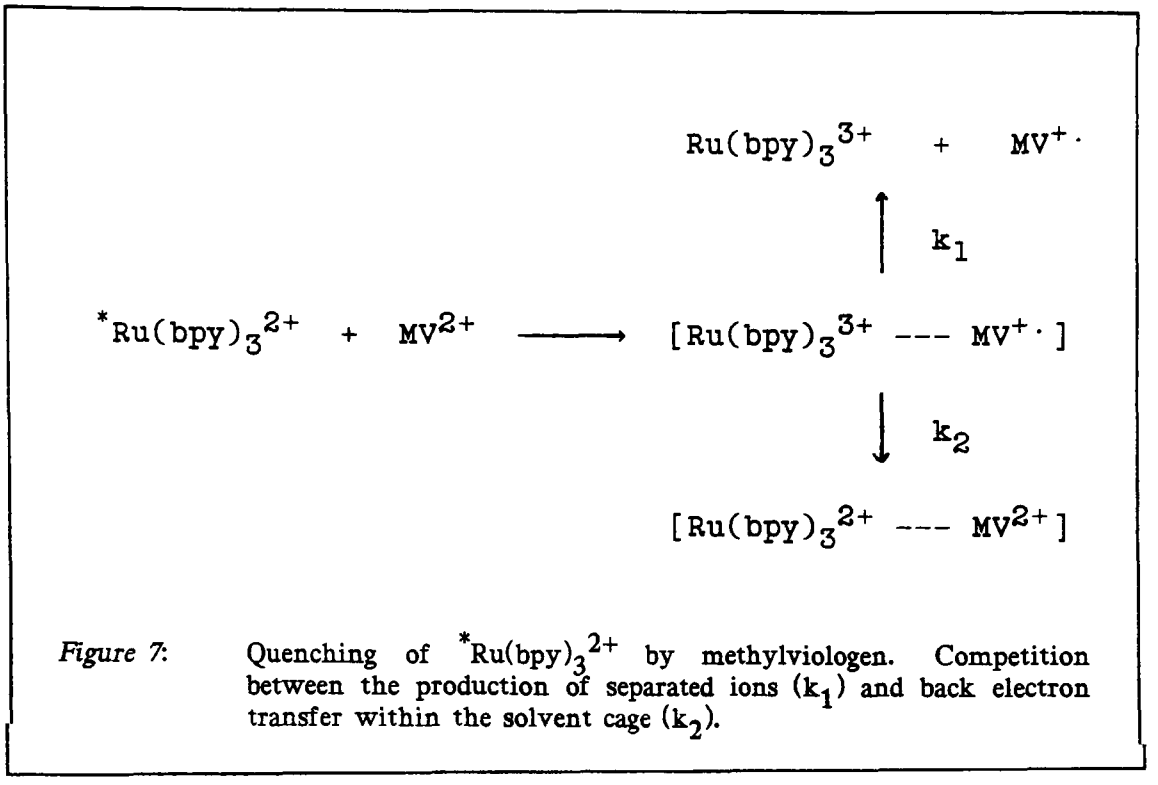

Figure 7: Quenching of $^{*}Ru(bpy)_3^{2+}$ by methylviologen. Competition between the production of separated ions (k_1) and back electron transfer within the solvent cage (k_2).

Therefore the quantum yield of hydrogen, which is half the quantum yield of $MV^{+\cdot}$, is limited to about 0.15 mol/ein.

A wide range of sacrificial donors has been tested in this system. The most efficient ones are ethylenediamine tetraacetic acid (EDTA) or triethanolamine (TEOA), depending on the pH. Many different catalysts have also been studied. The most widely used are colloidal suspensions of platinum[23] or platinum deposited on inorganic supports.[24] Other metal suspensions, like iridium[25] or preparations of the enzyme hydrogenase[26] have also been used.

One mechanism proposed for the action of the metal catalysts involves the transfer of an electron from the relay, $MV^{+\cdot}$ in this case, to the metal particle, followed by protonation leading to formation of an H atom on the metal surface, and finally evolution of H_2.[25] Hydrogenase is an enzyme involved in hydrogen evolution in nature. It has been known for a long time that it catalyzes the reduction of water by reduced methylviologen. This reaction is in fact used to assay hydrogenase.[2]

$$MV^{+\cdot} + H^{+} \xrightarrow{\text{hydrogenase}} 1/2\ H_2 + MV^{2+} \qquad [11]$$

The action of the catalysts will be discussed in more detail in a subsequent section of this thesis.

1.5 Porphyrin Photosensitizer.

Aside from $Ru(bpy)_3^{2+}$, the most investigated class of chromophores as possible photosensitizers for water splitting are the metalloporphyrins. This is due, in part, to the similarity of their structures to chlorophyll, which is a magnesium porphyrin. Chlorophyll itself is too fragile and expensive to be used for large scale solar energy conversion.

The work done on these chromophores has been concentrated on the preparation of stable water soluble metalloporphyrins. The most success has been obtained with zinc porphyrins. Two of them, zinc tetra(N-methylpyridyl)porphyrin ($ZnTMPyP^{4+}$) and zinc tetrasulphonated phenylporphyrin ($ZnTSPP^{4-}$), will be briefly discussed here.

Metalloporphyrins have better photophysical properties than $Ru(bpy)_3^{2+}$ for water reduction. They absorb more visible light. In some cases they can collect up to 45% of the energy available in sunlight.[27] Visible light irradiation of these porphyrin produces a triplet state with a long lifetime in high quantum yield, but there is a large energy gap between the initially produced singlet state and the lowest triplet state. More than 20% of the energy available in the excited singlet state is lost during intersystem crossing to the triplet manifold.

The photophysical properties of these two porphyrins, along with those of $Ru(bpy)_3^{2+}$ and chlorophyll-a, are given in table 1, and their thermodynamic properties are given in table 2.

As is the case for $Ru(bpy)_3^{2+}$, the potentials for the redox couples of both porphyrins meet the requirements of equations 4 and 7. Therefore, they can be used to mediate water reduction via both oxidative and reductive cycles.

Table 1: Photophysical properties of some typical photosensitizers.

Sensitizer	λ max(nm)	$\tau_t(\mu s)$	Φ_t	E_t (eV)
$Ru(bpy)_3^{2+}$	452	0.65	1.0	2.12
$ZnTSPP^{4-}$	555	---	---	1.61
$ZnTMPyP^{4+}$	560	655	0.9	1.57
Chlorophyll-a	661	1000	0.6	1.33

λ_{max} of the lowest spin allowed absorption band, τ_t, Φ_t and E_t are to the lifetime, quantum yield and energy of the triplet photoactive state.

Table 2: Redox Potentials of some typical photosensitizers.

	$E_o(V)$			
Sensitizer	(S^+/S)	(S/S^-)	(S^+/S^*)	(S^*/S^-)
$Ru(bpy)_3^{2+}$	1.3	-1.3	-0.86	0.84
$ZnTSPP^{4-}$	0.9	-1.2	-0.75	0.45
$ZnTMPyP^{4+}$	1.2	-0.9	-0.4	0.7
Chlorophyll-a	0.8	-0.9	-0.5	0.4

Redox potentials are referred to the NHE. They were calculated using equations 8 and 9 together with the excited state energies shown in table 1.

Figure 8 shows an example of an oxidative cycle involving $ZnTMPyP^{4+}$ as photosensitizer and MV^{2+}as electron relay. Quantum yields of 0.75 for $MV^{+.}$[27] and of 0.3 mol/ein for hydrogen[28] have been reported for this system. Because of the instability of the reduced porphyrin, which leads to the lost of the chromophore, the reductive cycle is much less efficient.

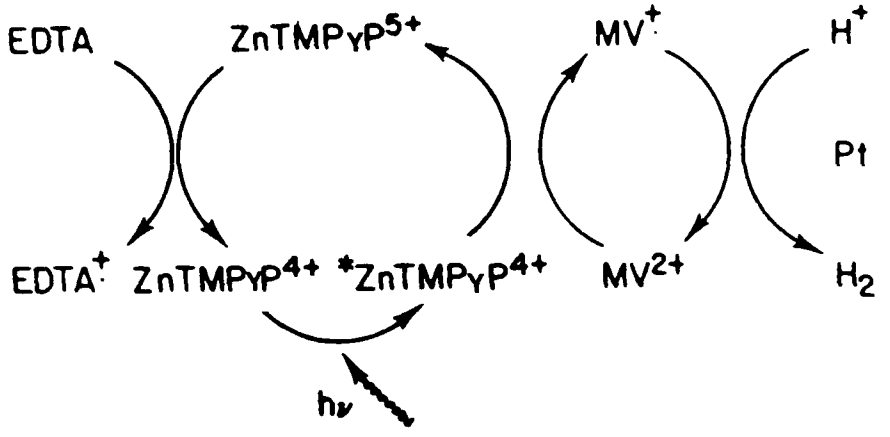

Figure 8: Water reduction via an oxidative quenching of $ZnTMPyP^{4+}$.

The yield of $MV^{+\cdot}$ obtained from an analogous system, using $ZnTSPP^{4-}$ instead of $ZnTMPyP^{4+}$ was less than 0.01. This difference was attributed to a very low charge separation quantum yield, Φ_s. The overall yield of $MV^{+\cdot}$, Φ_{ion}, by such a system can be separated into three parts according to equation 12.

$$\Phi_{ion} = \Phi_t \Phi_q \Phi_s \qquad [12]$$

Where Φ_t is the quantum yield of the excited triplet state and Φ_q is the quantum yield of quenching of this triplet state MV^{2+}. In the case of $ZnTMPyP^{4+}$ Φ_t = 0.9, and if we assume Φ_q to be approximately 1.0 then to get the observed Φ_{ion} of 0.75, Φ_s must be about 0.8. For $ZnTSPP^{4-}$, the strong attraction between the two oppositely charged ions MV^{2+} and $ZnTSPP^{4-}$ leads to a very small Φ_s, explaining the low Φ_{ion} found. Further, $ZnTSPP^{4-}$ is known to form ground state complexes with MV^{2+}, complexes which do not yield photoproducts.[29]

1.6 Simultaneous Photoproduction of Hydrogen and Oxygen.

All the systems discussed so far have been sacrificial systems. The hydrogen evolution observed depended on the irreversible decomposition of an electron donor. In a practical solar energy storage scheme, the photoreduction of water, will have to be coupled with water oxidation to provide a truly cyclic splitting of water.

A few complete systems, in which both oxygen and hydrogen are produced simultaneously, have been reported. One example is shown in figure 9. If a dispersion of RuO_2 was added to the system shown in figure 6, illumination produced hydrogen without the need for a sacrificial donor. $Ru(bpy)_3^{2+}$ was regenerated by RuO_2 catalyzed oxidation of water by $Ru(bpy)_3^{3+}$, with concomitant evolution of oxygen.[30 31]

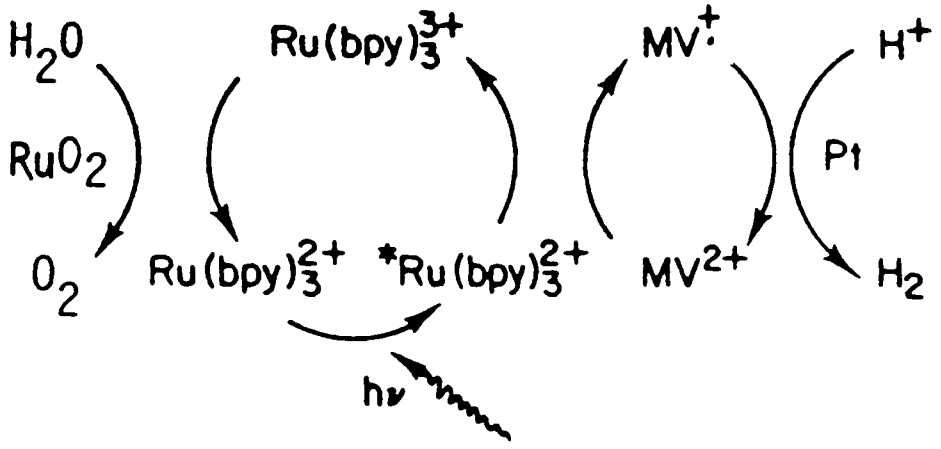

Figure 9. Simultaneous photoproduction of oxygen and hydrogen.

The oxidation catalyst, RuO_2, and the reduction catalyst, Pt, could be deposited on a dispersion of TiO_2 semiconductor particles, producing what is called a bifunctional catalyst. In this case the mechanism of water splitting was described as follows. The excited

state of $Ru(bpy)_3^{2+}$, produced by illumination, transfers one of its electrons to the conduction band of a TiO_2 semiconductor particle. From there, it is channelled to a Pt site where hydrogen evolution occurs. The reconversion of the oxidized sensitizer into its original form is coupled to oxygen formation at a RuO_2 site.

Aside from a few reports in which PtO_2 or IrO_2 were used, RuO_2 is practically the only oxidation catalyst ever used for water photooxidation with visible light. It was chosen on the basis of its very low overvoltage for O_2 evolution.[32] The mechanism of oxygen evolution has been less studied than that for hydrogen evolution. It is known that only hydrated RuO_2 is effective. This is explained by the intervention in the water oxidation process of Ru-OH species.[33]

The action of the colloidal platinum catalyst was described by the model of colloidal microelectrodes.[31] To be effective in realizing hydrogen generation, the metal catalyst has to intercept diffusion controlled processes in the microsecond range. Moreover it has to be selective and stable. Platinum is very efficient because of its low overvoltage for H_2 evolution. The most efficient catalyst preparation involved Pt particles of 1.5 nm radius prepared in aqueous solution by citrate reduction of H_2PtCl_6. The 1.5 nm Pt-cluster size was favorable since it ensured large dispersion of the platinum, while maintaining a minimum size necessary for the Pt to have metallic character.[32]

Several attempts have been made to improve the catalyst efficiency, such as the deposition of the platinum on TiO_2. There has also been some work on the coating of the Pt particles with Carbowax 20M[34] or cationic polysoap like polyvinylpyridine-C_{16} to prevent aggregation of the particles. More will be said on this topic in a subsequent section of this thesis. A measure of the success of the platinum catalyst is given by noting, for example, that the quantum yield of $MV^{+\cdot}$ given by illumination of $ZnTMPyP^{4+}$ was 0.75, while H_2 was obtained with a yield 0.3 mol/ein in this system. Since two $MV^{+\cdot}$ ions were needed for each H_2 molecule produced, the catalytic reduction of water by $MV^{+\cdot}$ was

very efficient, at least for short irradiation times. The problem lies more in insuring the long term stability of the systems.[35]

1.7 Hydrogen Evolution over Suspensions of Semi-conductor Particles.

An alternative to dye sensitized systems, involving microheterogeneous dispersions of solid catalyst particles, is the use of an heterogeneous dispersion of semiconductor particles. In these systems the energy of the photon is used to promote an electron from the valence band to the conduction band of a semiconductor, instead of being used to excite a photo-sensitizer. The aim is to use the electron-hole pair formed, for the splitting of water.

To do so, the problem of the rapid electron-hole recombination reaction must be solved. The use of semiconductors is exemplified by TiO_2 dispersions, upon which Pt and RuO_2 are codeposited. Figure 10 shows what happens when such a semiconductor suspension is subjected to ultraviolet light.

The light causes the formation of an electron-hole pair according to equation 13.

$$TiO_2 + h\nu \longrightarrow h^+ + e^- \qquad [13]$$

The electron is channelled to a Pt site where an ohmic contact develops and hydrogen is evolved. The promotion of an electron also causes an increase in the Fermi level of TiO_2, as Pt seeks to equalize its own Fermi level with TiO_2 and the electrolyte through the formation of an ohmic contact. A potential A-B is produced. Band bending takes place, originating a Schottky barrier, to equalize the Fermi level of RuO_2 and TiO_2. Because of the low overvoltage of RuO_2 for oxygen evolution, hole capture is very efficient, thus limiting the importance of the electron hole recombination reaction.

TiO_2 has a band gap of 3.0 eV,[32] so only light with a wavelength less than 400 nm can be used to promote an electron to its conduction band. Visible light does not have

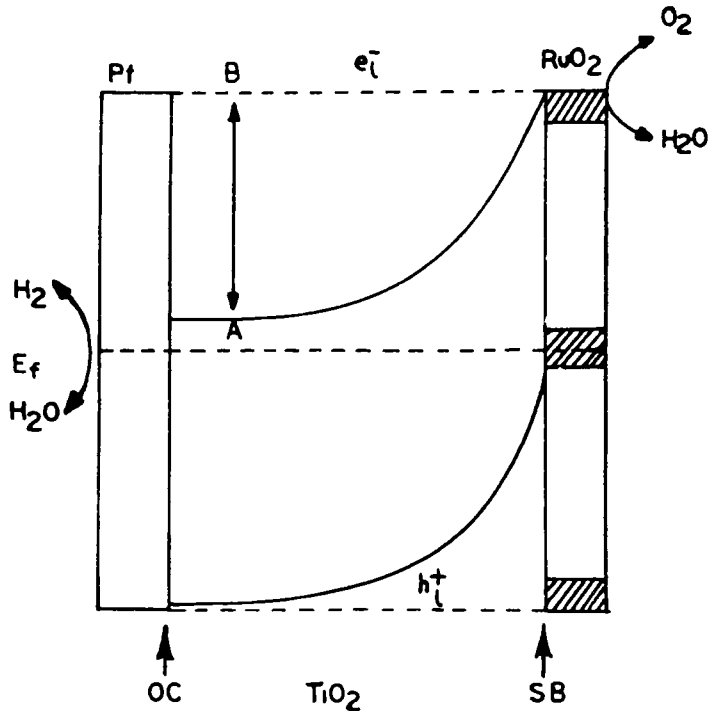

Figure 10: Water splitting with semiconductor particles. Ohmic contact (OC) and Schottky barrier (SB) developed when band bending occurs (A-B) on TiO_2. Semiconductor loaded with islands of Pt and RuO_2 and in contact with electrolyte solution. E_f = Fermi level, e_l^- = electron level and h_l^+ = hole level. (reproduced with permission from reference 32)

enough energy. The problem with using semiconductors is finding a species that is capable of forming a suspension in water, is stable in sunlight, and has a band gap larger than the 1.23 volts needed to split water at pH 7, but small enough to absorb visible light. This has proven to be a difficult problem.

One semiconductor that has been studied is CdS. It has a suitable band gap, 2.4 eV, but it is not stable, being sensitive to photocorrosion.[35] Fe_2O_3 has also been studied. Its band gap is 2.2 eV. Photocatalytic production of hydrogen from water has been observed in a system containing a p-type semiconductor, made by doping Fe_2O_3 with magnesium, and an n-type semiconductor of silicon doped Fe_2O_3.[36]

CHAPTER II

THE CHEMISTRY OF CLAY MINERALS.

2.1 Introduction.

We have observed the evolution of hydrogen when a system containing $Ru(bpy)_3^{2+}$, MV^{2+} and the sacrificial donor, triethanolamine, was illuminated with visible light in the presence of the clay mineral montmorillonite,[37 38] without the need for a platinum catalyst.

The idea of using clay minerals in a photocatalytic water splitting system is attractive for many reasons. Aside from the fact that they are cheap and widely available, clay minerals have a number of properties that can make them potentially very useful for water photoreduction. In recent years, their chemistry and the chemistry of reactions taking place on their surfaces has been receiving increased attention.[39-42]

There are many advantages of performing reactions on solid supports such as clays. Adsorption of the reagents can result in a faster reaction because of the increase in local concentration of reagents,[43] or the support can induce shape selectivity,[44] changing the distribution of products. Also, in many cases, solid supports lead to a simplification of the experimental procedure by, for example, facilitating product isolation.[45] Clays can also activate the adsorbed reagents, either via their acid sites, (clays are known to have both Lewis and Bronsted acidity) or via their electron acceptor or donor sites.[46] Furthermore, clays have interesting adsorption capabilities, being capable of intercalating molecules[47] or of adsorbing them on their external surfaces, by either cation exchange or simple replacement of adsorbed water molecules.[48 49] Finally, clay minerals may have

played a key role in the origin of life.[50-52] In this respect, the role of photochemistry on clay surface in prebiotic evolution is of particular interest.

In the following sections, a brief description of the structure of clay minerals will be given, followed by a discussion of the properties of clay suspensions and of the reactions of clay adsorbed reagents. Then a few words will be said on the reactions of clay adsorbed reagents. Finally we will look at the uses of clay minerals in assisting water photoreduction.

2.2 Structure of Clay Minerals.

Clays are naturally occurring minerals,[53] characterized by a layered structure. The main building elements of clay minerals are two-dimensional arrays of silicon-oxygen tetrahedra and two-dimensional arrays of aluminum or magnesium oxygen-hydroxyl octahedra. These tetrahedral and octahedral sheets are superimposed in different fashions to form the clay layers.

The arrangement of the clay sheets forming the clay layers is the first characteristic used in classifying a clay mineral. There are essentially two groups. The 1:1 minerals, in which the layers are made up of one tetrahedral sheet and one octahedral sheet and the 2:1 minerals, in which the layers are made up of two tetrahedral sheets, one on either side of a central octahedral sheet. Montmorillonite, hectorite and nontronite, the three minerals which will be used in this work, are 2:1 clays. A schematic representation of unit cell of the these 2:1 minerals is given in figure 11.

The tetrahedral sheets are formed by linked silicon oxygen tetrahedra. They are linked by the sharing of three of their four oxygens by neighboring silicons. The fourth oxygen of each tetrahedron points down. It is the sharing of these apical oxygens between the silicon of the tetrahedral sheet and the aluminum or magnesium of the octahedral

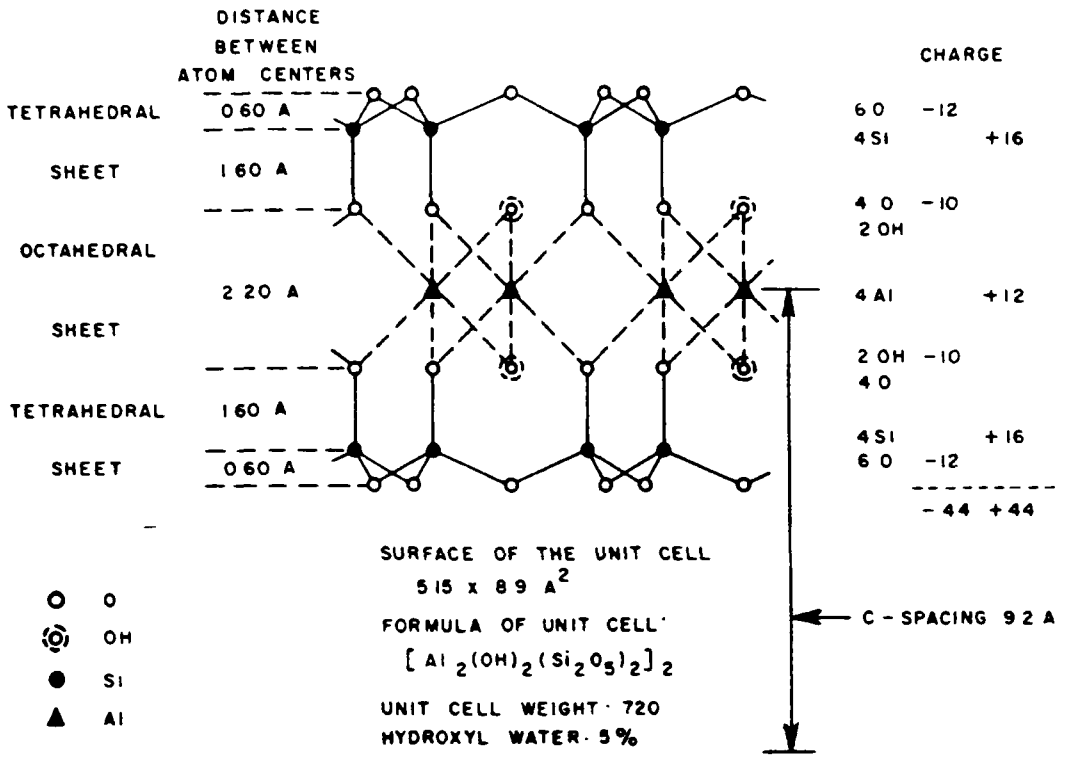

Figure 11: Schematic representation of the arrangement of the atoms in the unit cell of 2:1 layer minerals. (reproduced with permission from reference 54)

sheet that holds the clay layer together. This linking is only possible because of the almost identical dimensions of the two types of sheets and their analogous symmetry.[54]

The second important characteristic of a clay is the degree of occupancy of its octahedral sheet. Looking at the unit cell of the 2:1 mineral shown in figure 11, one sees an empty octahedral site. When the octahedral sheets are made up of Al(III), only 2/3 of the available octahedral positions need to be fill to maintain the electrical neutrality of the layers. Therefore, minerals such as montmorillonite that contain mainly Al(III) in their octahedral sheets are called dioctahedral clays. Hectorite, on the other hand contains mostly Mg(II) in its octahedral positions. In this case one must fill all available octahedral

positions to achieve the electrical neutrality of the layers. This clay belongs to the trioctahedral group.

The most important property of clay minerals is the existence of a net negative charge on their layers. The unit cell shown in figure 11, is the cell of the mineral pyrophillite. If the octahedral sheet contained Mg(II) atoms, and all the octahedral positions were filled, it would be the unit cell of the mineral talc. The layers of these minerals are not charged so they are not clays, but pyrophillite and talc are the parent minerals of the clays montmorillonite and hectorite respectively. The two clays are derived from these minerals by substitution of some of the tetrahedral Si(IV) atoms by Al(III) or of some of the octahedral Al(III) or Mg(II) by Mg(II) or Li(I). This substitution by a lower valency atom causes a deficiency of positive charge, resulting in the observed negative layer charge. Since these atoms are of similar sizes, this substitution does not cause much distortion of the layer structure. It is therefore called an isomorphous substitution. The clay can also undergo substitution of some of its aluminum, magnesium or silicon by other atoms like Fe, Cr, Zn etc. In fact, a particular clay can have a wide range of compositions,[55] depending on its origin in nature.

The negative charge of the clay layer is counter balanced by adsorbed or intercalated exchangeable cations, usually a mixture of alkali and alkaline earths metal cations. These are called exchangeable cations since they can be replaced by other cations from solution. The extent of isomorphous substitution, and therefore the magnitude of the layer charge, is measured by the clay cation exchange capacity (CEC), the amount of adsorbed cations needed to neutralized it.

Clay minerals are also characterized by the nature of their interlayer spacings. A clay particle is made up of a stack of clay layers, themselves composed of clay sheets. The distance between two clay layers in a stack is called the interlayer spacing. In some clays this distance is not fixed, but variable. When dispersed in water these clays can swell,

intercalating up to four water layers. They are called expandable clays. Montmorillonite, hectorite and nontronite are all expandable clays. This expandability allows them to intercalate large cations, such as $Ru(bpy)_3^{2+}$ and MV^{2+}.

Figure 12 shows a classification of clay minerals. A particular clay mineral can be classified according to three characteristics, layer structure, (1:1 and 2:1 minerals) occupancy of octahedral sheet, (dioctahedral and trioctahedral) and nature of interlayer spacings, (stable and expandable clays). The individual clays are then obtained by a combination of their chemical composition, extent and location of isomorphous substitution and type of layer stacking.

For example, the 1:1 minerals kaolinite and dickite both belong to the kaolinites group. They are very similar in composition, containing an octahedral Al(III) sheet and a tetrahedral Si(IV) sheet with very little isomorphous substitution, but the order of stacking of their layers is different.[55] The kaolinite layers are stacked in such a way that the empty octahedral sites of the Al(III) sheets are line up, while in dickite they are not. In other words, if A, B and C represent the three possible octahedral sites, the stacking of the empty sites in dickite is BCBCBC, while in kaolinite it is AAAAAA.

The location of isomorphous substitution is also used to differentiate between some clays. For example, it has been suggested that the division between beidellite and montmorillonite should be made at the composition at which the lattice charges due to octahedral and tetrahedral substitution equal each other.[55] Both these clays are 2:1 dioctahedral expandable minerals with similar chemical composition and surface charge, but the charge of montmorillonite comes mainly from substitution for Al(III) in the octahedral sheets, while in beidellite it comes mainly from substitution for Si(IV) in the tetrahedral sheets.

Aside from the 1:1 and 2:1 clays shown in figure 12, there are other types of clay minerals. The mixed layer clays are clays whose stacks are composed of the interstratification of the layer of different minerals, in either a regular or a random order. For exam-

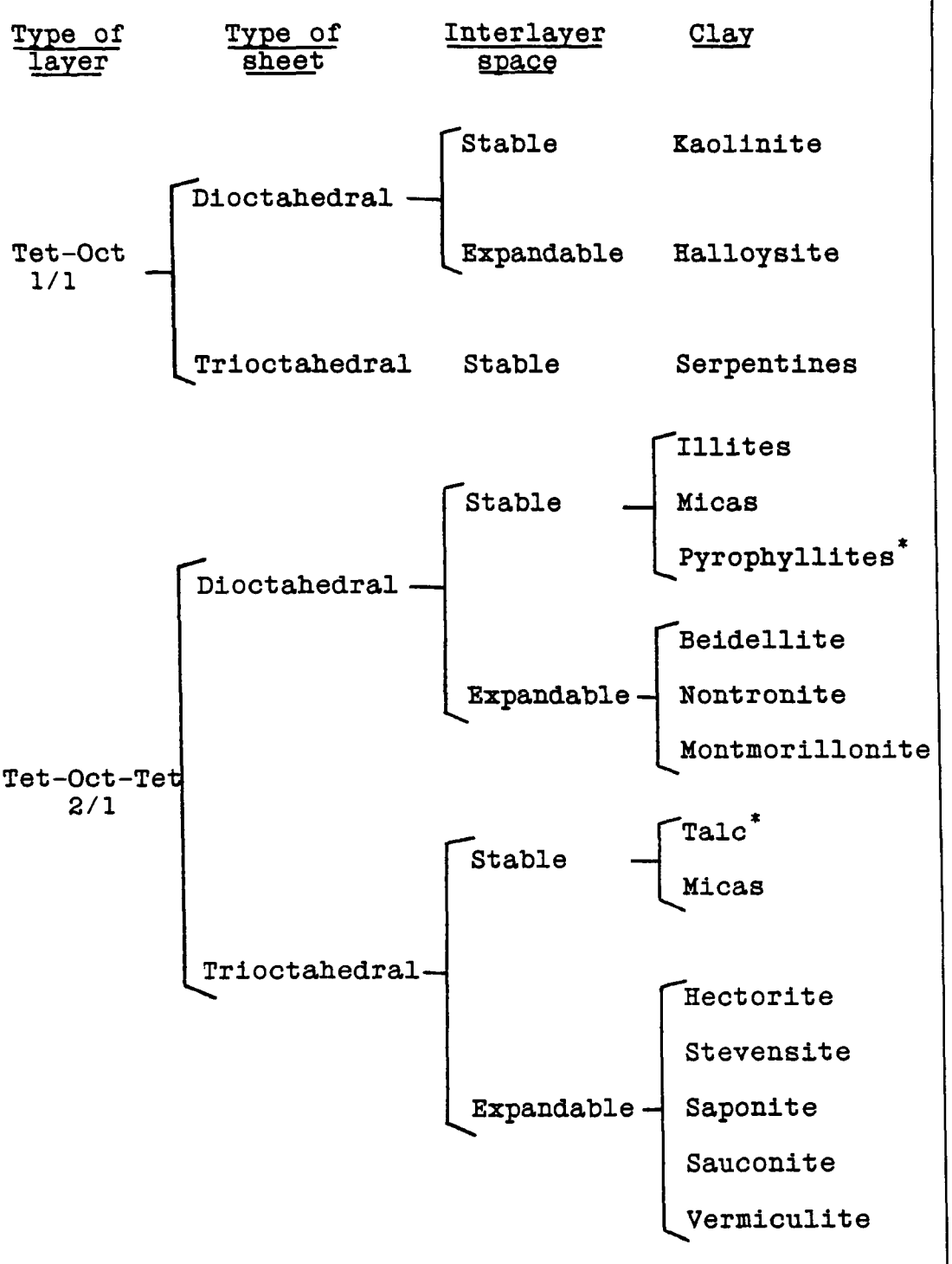

Figure 12: Classification of clay minerals. (* parent minerals of the clays montmorillonite and hectorite respectively, see text)

ple, the montmorillonite-illite mixed clay contains layers having the chemical composition of the layers of montmorillonite stacked with layers having the chemical composition of illite. There is also the chlorite group in which the negative surface charge is counter balanced, not by intercalated cations, but by intercalation of an octahedral magnesium hydroxide sheet, in which substitution of some Mg(II) by Al(III) causes a positive charge. They can be considered to be 2:2 minerals. Finally, some clays do not have a layer structure at all: attapulgite, for example, has a chain structure.[55]

In conclusion the "impure" nature of clay minerals should be stressed. In doing chemistry with them, one must always keep in mind that the composition of a particular mineral may vary depending on its source. To get a "pure" clay, one must use synthetic clays prepared in laboratory.[56]

2.3 Properties of Clay Suspensions.[54]

Depending on the size of the particles, the dispersion of a clay in water is called a clay suspension or a clay sol. A suspension contains particles of more than 1 μm, while a sol contains particles smaller than 1 μm. This is an arbitrary division. Both terms are applied to clays, especially since most dispersions contain a range of particle sizes. The term suspension is most used. Clays are classified as hydrophobic colloids, despite their high affinity for water. This unfortunate nomenclature comes form the historical developments of colloid chemistry, before the nature of suspension was well understood. Today, it is applied to all colloids formed by the dispersion of small solid particles in a liquid. The term hydrophilic is reserved for true solutions of macromolecules, where the colloidal properties come from the large size of the dissolved molecules.[54]

A clay particle is a stack of clay layers. In a suspension the number of layers in a stack depends on many factors. In a colloidal suspension of sodium montmorillonite for

example, the stacks contain only 2 or 3 layers, while in the same suspension of calcium montmorillonite, there are approximately 8 layers per stack.[54] This property is called the degree of aggregation of the clay. Na^{+}-montmorillonite forms dispersed suspensions, while Ca^{2+}-montmorillonite forms more aggregated suspensions. (see figure 14)

The stability of a colloidal clay suspension depends on a delicate equilibrium of forces. The particles repel each other because of their negative surface charges. On the other hand there are van der Waals attractions between the atoms of the particles. Stability is attained because of the different ranges of action for the two types of forces. In pure water, the electrostatic repulsion acts over long distances, not allowing the particles to approach each other close enough for the van der Waals attraction to be felt.

This simple view of suspensions accounts for the flocculation effect of electrolytes. The negative charge of the particles leads to the formation of an electric double layer at the particle surfaces. The negative charge attracts cations from the solution, increasing their concentrations close to the surfaces. In the same way anion concentrations near the surface are decreased. Entropy on the other hand seeks to equalize the ion concentrations over the entire bulk of the suspension. This is analogous to the competition between gravity and diffusion in earth's atmosphere. This competition of forces leads to an "atmospheric" distribution of ion concentrations near the surfaces of the particles, called the electric double layer.

The thickness of this layer is the key to the stability of a clay suspension. By neutralizing the surface charge, the excess cation concentration near the surfaces curtails the range of the electrostatic repulsion forces. The effect of increasing the bulk electrolyte concentration is to compress this double layer. Since the clay surface charge is constant, with a larger bulk concentration of cations the neutralization of that charge is achieved closer to the particle surface. Thus, the range of the electrostatic repulsion force is shortened. If the electrolyte concentration is large enough the clay particles can get close

enough for the van der Waals force to act. There is an aggregation of the clay particles; the suspension flocculates. Figure 13 shows the balance of forces at low and high electrolyte concentrations as a function of the distance between particles. In the first case an energy maximum exists between the most stable state, the flocculated state in which interparticle distances are small, and the colloidal state at larger interparticle distances. At high electrolyte concentration no such maximum exists. The clay cannot form a stable colloidal suspension. Note that even a so called stable colloidal suspension is only meta-stable. All clay suspensions will eventually flocculate.

The model presented here is a simplified representation of clay suspensions. It ignores such factors as the existence of regions of positive charge at the edges of the clay particles, the size of particles, the aggregation of small particles is faster, or refinements of the double layer model such as the Stern layer and the Gouy layer.[54] Nonetheless it is adequate for our purpose. In figure 14 the various types of particles aggregation are summarized.

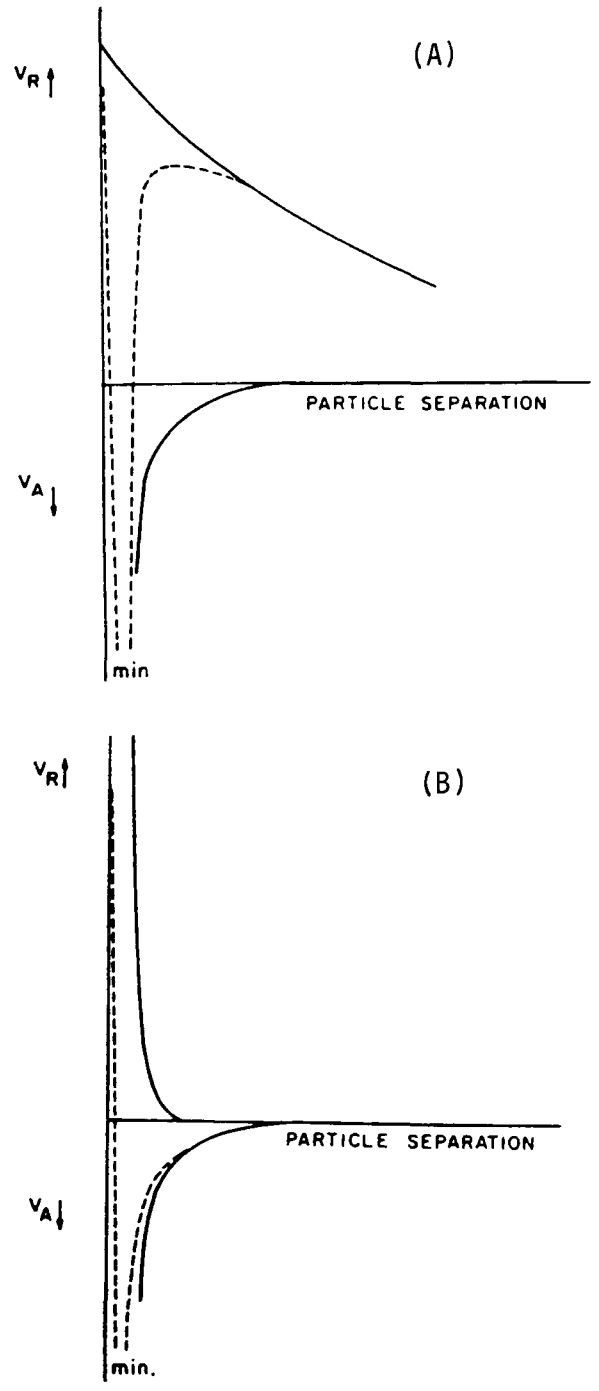

Figure 13: Net interaction energy as a function of particle separation. A) Low electrolyte concentration, B) High electrolyte concentration. (reproduced with permission from reference 54)

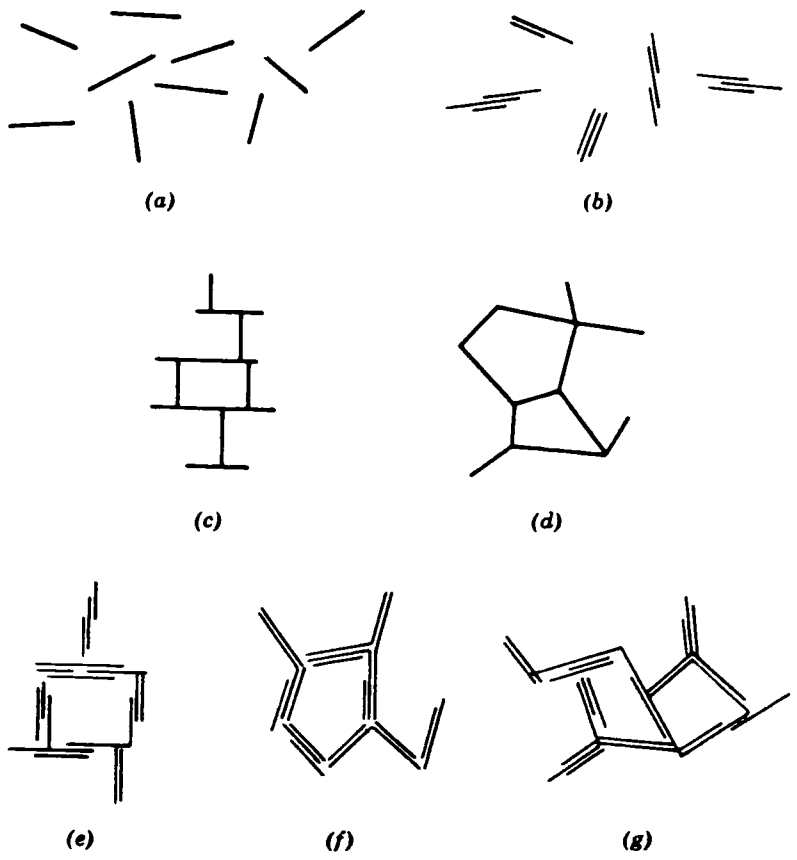

Figure 14: Model of the various types of particle association that can be found in clay suspensions. a) dispersed, b) aggregated, c) and d) dispersed and flocculated, e), f) and g) aggregated and flocculated. (reproduced with permission from reference 54)

2.4 The Chemistry of Supported Reagents.

There is growing interest in the use of insoluble inorganic supports in organic synthesis.[43] [57] Many factors make them potentially useful. The adsorption of the reagents on a solid support can have two types of effects on a chemical reaction. First there are physical effects such as a decrease in the entropy of the reaction, which is due to

the increase in the local concentrations of the reagents caused by their adsorption on a solid surface, or shape selectivity , a variation in the product distribution imposed by the geometry of the support. Secondly there are chemical effects, such as the activation of one of the reagents by its interaction with the support surface.

The increased reactivity resulting from an increase in the local concentration of an adsorbed reagent has been observed, for example, in the reaction of ozone with an hydrocarbon to give an alcohol by direct oxygen insertion.[58] Although this reaction provides a one step hydroxylation, it has been rarely used because ozone is only slightly soluble in organic solvents. O_3 is very efficiently adsorbed by silica gel at low temperatures. (4.5% by weight at -78^0C). Therefore, by adsorbing ozone on SiO_2, the reagent could be brought into contact with an hydrocarbon, in a high enough concentration for the reaction to proceed at a good rate.

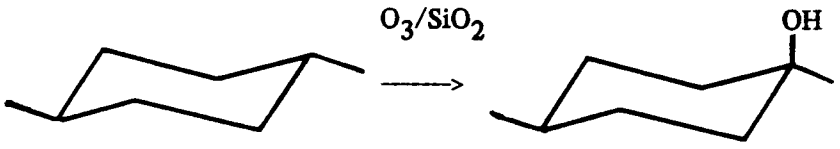

[14]

In reaction 14, the alcohol was produced with a yield of 79% in 30 minutes with retention of configuration.[58] Further, the addition of silica supported ozone to the hydrocarbon eliminated the problem of the reaction of O_3 with the solvent and greatly simplified the experimental procedure,[59] especially the isolation of the product.

The production of olefins from methanol in the zeolite H-ZSM-5,[60 61] is an example of support induced shape selectivity. Zeolites contain channels, whose size and geometries can control the product distribution.[61] Support induced shape selectivity in zeolites can be divided into three classes: 1) reactant selectivity, in which only reactants of a given geometry can enter into the channels and reach the reaction sites, 2) product selectivity, in

which only products of a given geometry can leave the reaction sites and 3) restricted transition state selectivity, in which the geometry of the reaction sites allows only certain types of products to be formed, those which are formed by reaction whose transition states geometries corresponds with that of the reaction sites.

The other types of effects of the support, the chemical effects, are those in which the support is an active participant in the chemical reaction. When methanol was heated in the presence of silica-alumina gel,[62] dimethyl ether was produced.

$$2CH_3OH \xrightarrow{SiO_2\text{-}Al_2O_3} CH_3OCH_3 + H_2O \qquad [15]$$

In this example the support catalyzed the reaction by generating a key intermediate. It could act by either protonation of the methanol by one of its Bronsted acid sites, as in equation 16,

$$CH_3OH + H^+ \longrightarrow CH_3OH_2^+ + CH_3OH \longrightarrow CH_3OCH_3 + H_2O + H^+ \qquad [16]$$

or by adsorbing the methanol in one of its Lewis acid sites, as in equation 17.

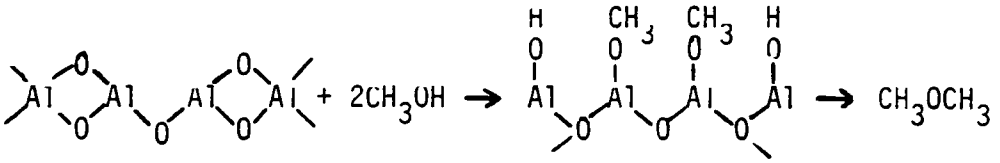

[17]

So far a few examples showing the advantages of using inorganic insoluble supports, like zeolite, silica or alumina have been presented. In the next section, examples of the uses of clay minerals as supports will be discussed.

2.5 Reactions on Clay Surfaces.

Clays can be used as supports for reagents. They have some of the advantages of the supports described in the previous section.

Before the description of some of the unusual chemical conversions that can take place on clay surfaces, the adsorption of chemical compounds by clay minerals will be shortly reviewed. The smectites used in this work can intercalate various species between their layers. In a water suspension, besides the exchangeable cations such as calcium and sodium, the interlayer spaces of these clays can contain up to four layers of intercalated water molecules. This water can be displaced by other neutral molecules. For example, pyridine has been shown to form four different intercalates with montmorillonite. Their basal spacings (i.e. the sum of the thickness of the clay layers, 9.6 Å and of the clay interlayer spacings defined in section 2.2) were 29.3, 23.3, 19.4 and 14.8 Å, depending on the water to pyridine ratio.[48] The intercalation of the organic base, p-phenylenediamine, in montmorillonite[49] was another example. (see figure 15) In this case, the clay protonated the base and more than one layer could be intercalated.

The clay's exchangeable cations can also be replaced by large organic cationic species.[63] In fact large organic ions are more strongly held by the clay than are the inorganic cations, including hydrogen ions. Their presence markedly alters the dispersibility of the clay and practically destroys their ability to swell in water.[49]

Aside from the clay adsorption properties, other factors will have an influence on chemical reactions taking place on their surfaces. The most important ones are the presence of Bronsted[42] and Lewis acid sites[39] in clays and the clays' ability to act as both electron donors or electron acceptors.[46] Further the water molecules present in the interlayer spaces are highly activated. They are polarized by interaction with the negative surface charges of the clays and with the exchangeable cations located at the mineral surface.[64]

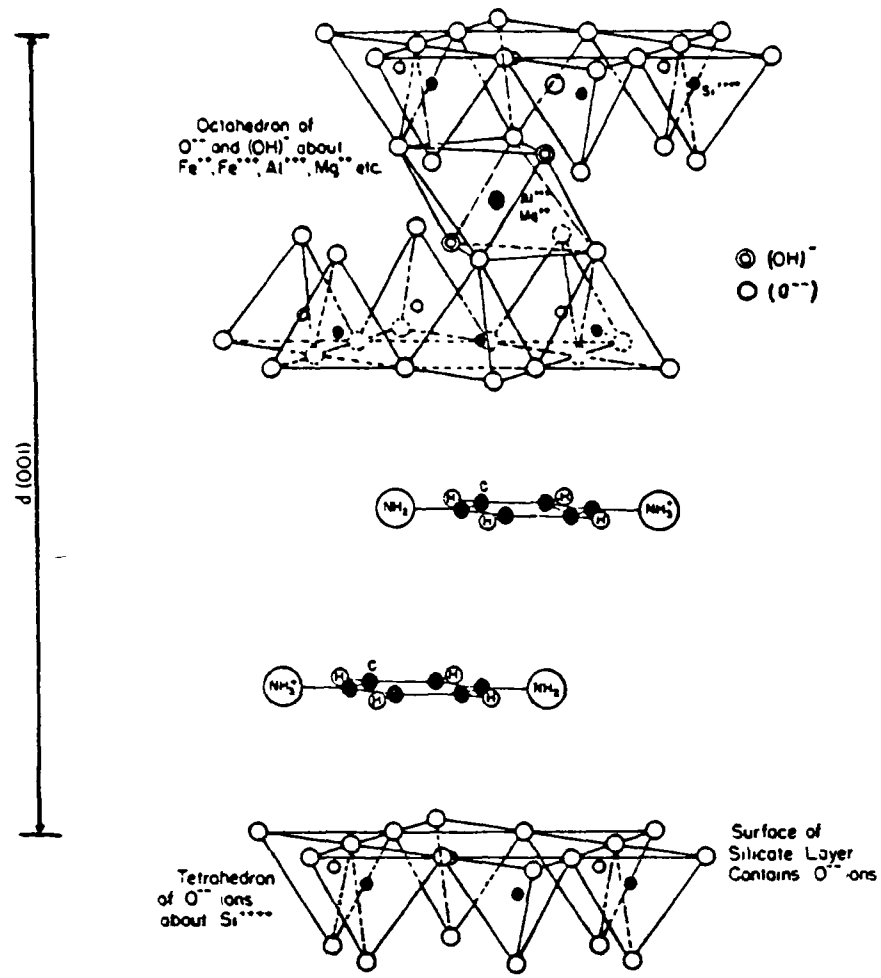

Figure 15: Intercalation of p-phenylenediamine in sodium-montmorillonite. (reproduced with permission from reference 49)

The identification of the various donor and acceptor sites in montmorillonite can be credited, in a large part, to D. H. Solomon and his group.[41 46] The existence of these sites is perhaps best exemplified by the results shown in figure 16.

If tetracyanoethylene is brought in contact with reduced montmorillonite, a clay treated in such a way as to reduce all its structural iron to the Fe(II) state, the clay is oxidized and the tetracyanoethylene radical anion can be detected by esr spectroscopy.[46] If one uses the oxidized clay, no reaction takes place. In this case, the clay is an electron

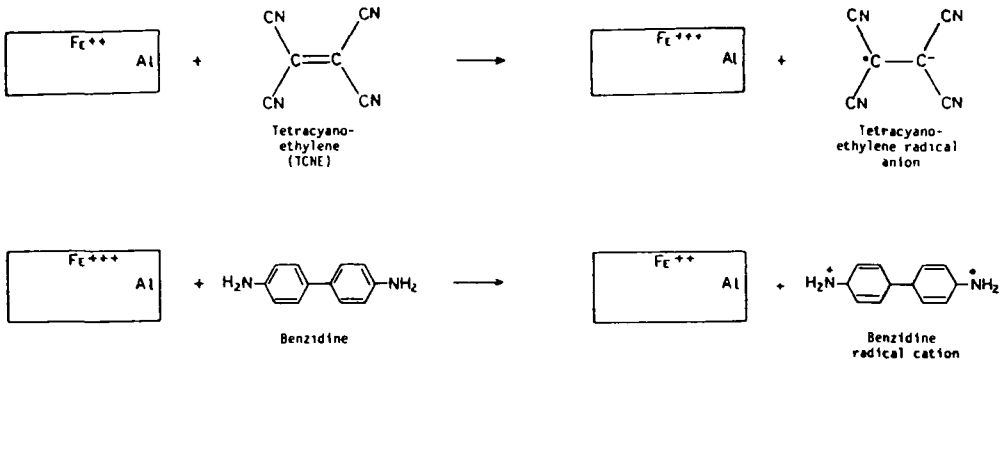

Figure 16: Montmorillonite as an electron donor and an electron acceptor.

donor, the donor sites being Fe(II). On the other hand, oxidized montmorillonite in contact with benzidine leads to the formation of the blue benzidine monocation radical, while the clay is reduced.[65-67] In this case the clay is an electron acceptor, the acceptor sites being structural Fe(III).

In addition to the acceptor and donor sites involving atoms that can exist in more than one oxidation states, clays like kaolinite and montmorillonite have another type of electron accepting site, namely aluminum at the edges of the clay layers that have an incomplete coordination shell.

This is shown by the conversion of triphenylmethyl radicals to triphenylmethyl carbonium ions in the presence of these clays.

$$Ph_3C^{\cdot} + \boxed{Al} \longrightarrow Ph_3C^{+} + \boxed{{}^{\cdot}Al} \longrightarrow Ph_3COH \qquad [18]$$

This reaction does not take place in the presence of talc, since talc contains Mg(II) instead of Al(III) in its octahedral sheets.

The model of clays having two types of electron acceptor sites and one type of electron donor site is very successful in accounting for the effect of the presence of clays in many chemical processes.[41] For example, it accounts for the catalysis or the inhibition by clays of some polymerization reactions. The polymerization of styrene is catalyzed, since the donation of an electron to the clay by the styrene monomer produces a radical cation which is an initiator for the polymerization. The inactivity of talc in this reaction shows that this radical is produced by donation of an electron to an Al(III) site at the edge of the clay layers. On the other hand the inhibition of the polymerization of methyl metacrylate by montmorillonite is attributed to the destruction of the propagating free radicals by the clay.[46]

Table 3: Some of the types of organic reactions that have been shown to take place on the surface of clays.

Rx types	Example
Thermal decomposition	Esters --› acids and hydrocarbons
Dimerization	trans-stilbene
Reduction - Oxidation	1,1'-diphenylethylene to 1,1 diphenylethane and benzophenone
Hydrogen transfer	9,10 dihydroanthracene and 1,1 diphenylethylene
Lactonization	Cyclooctene carboxylic acid --› 1,4 and 1,3 lactanes
Ether formation	$(CH_3)_2CH_2 + CH_3OH$ --› $(CH_3)_3OCH_3$
Ester formation	$CH_2CH_2 + CH_3COOH$ --› $C_2H_5COOC_2H_5$
Eliminations	$2RCH_2NH_2$ ---› $(RCH_2)_2NH + NH_3$

Many of the unusual organic reactions taking place in the smectite interlayers involve the activation of the reagents by the clay acid sites. Some of the types of organic reactions that have been found to proceed in the presence of clay minerals are summarized in table 3.[39] The first step in many of these reactions is the protonation of one of the reagents by the Bronsted acid sites of the clay. The thermal break down of cyclohexyl ethanoate in the presence of montmorillonite, proceeds according to equation 19.[42]

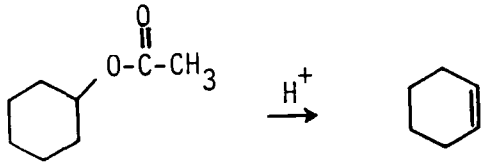

[19]

In the dimerization of trans-stilbene, shown in equation 20, the reaction is initiated by the protonation of the reagent, [39]

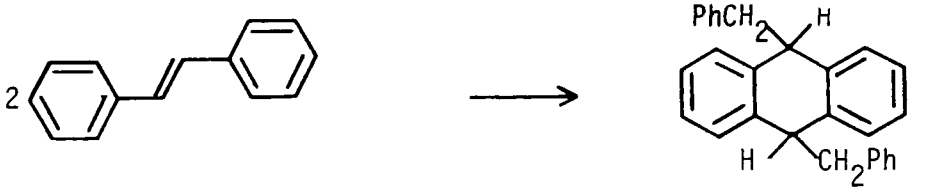

[20]

as is the lactonization of cyclooctene carboxylic acid,

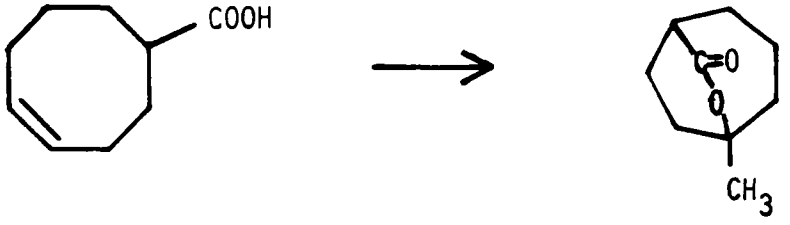

[21]

the formation of methyl t-butyl ether in the presence of Cu^{2+}-montmorillonite,[67]

$$CH_3OH + CH_2{=}C(CH_3)_2 \xrightarrow{Cu^{2+}\ Mont.} (CH_3)_3COCH_3 \qquad [22]$$

and the addition of acids to alkenes[68] to give esters in the presence of Al^{3+}-montmorillonite.

$$CH_2{=}CH_2 + CH_3COOH \xrightarrow{Al^{3+}\ Mont.} CH_3COOCH_2CH_3 \qquad [23]$$

The conversion of primary amines to secondary amines in the presence of montmorillonite is also initiated by protonation of the amine group,[39]

$$2RCH_2NH_2 \xrightarrow{Mont.} (RCH_2)_2NH + NH_3 \qquad [24]$$

and so is the similar elimination of H_2S and H_2O, from thiol[69] and alcohol[70] respectively.

Other types of acid catalyzed reactions found to occur in clays were oxidation reduction processes such as the conversion of 1,1-diphenylethylene to benzophenone and 1,1-diphenylethane,[71] and hydrogen transfer reactions between 9,10-dihydroanthracene and 1,1-diphenylethylene which took place on synthetic hectorite.[72]

In all the examples discussed so far, the clay was used as a support for the reagents. When catalysis was found it was by the mineral itself via its acid sites. There are also cases in which the clay was used to adsorb a catalyst in addition to the reagents. The advantages of adsorbing catalysts are the same as those described previously for the adsorption of reagents. An increased reactivity and a variation in the catalyst selectivity, imposed by the support geometry, could result from the immobilization of a reagent and of

a catalyst in close proximity on the surface. Also, in some cases, it was found that the clay induced the catalytic activity. That is, the catalyst was not the adsorbed species, but the clay adsorbate complex.

An example of a catalyst whose selectivity was changed by intercalation into clays is the rhodium hydrogenation catalyst RhL_n^+ (L = triphenyl phosphine n = 2 or 3) adsorbed in hectorite.[63] In homogenous solution, this complex catalyzed the hydrogenation of both terminal and nonterminal olefins, while in the clay interlayer space terminal olefins were selectively hydrogenated. The same preference for the hydrogenation of terminal alkyne was found. The adsorbed catalyst was also more specific, almost no isomerization took place in the presence of the clay. This was an example of shape selectivity. Figure 17 shows the proposed arrangement of the catalyst in the hectorite interlayer space. One can see how an interlayer spacing of 7.7 Å favors the reaction of terminal alkynes.

Uranyl ions (UO_2^{2+}) incorporated in different clays have been tested as catalysts for the photooxidation of isopropyl alcohol.[73] In general they were more active than UO_2^{2+} incorporated into zeolites. The UO_2^{2+} hectorite intercalate was the most active. Their stability was less than that of the zeolite supported ones and they were not as selective for the production of acetone.

A pillared clay, prepared by adding a montmorillonite suspension to a solution containing cationic polychromium oligomers was tested as a catalyst for the conversion of cyclohexane to benzene at 550°C. Its activity was found to be substantially higher than that of a commercial chromia catalyst supported on alumina.[74] Similar pillared clays, intercalated with alumina and zirconia were found to be petroleum cracking catalysts having shape selectivity comparable to that of commercial zeolite catalysts.

The greater catalytic activity of chromia pillared montmorillonite was attributed in part to the greater degree of dispersion of the chromia. A possible use of clays was to help in the preparation of such highly dispersed catalysts. Pinnavaia et al[75] found that

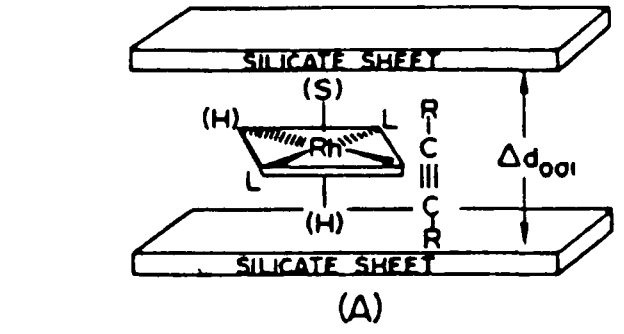

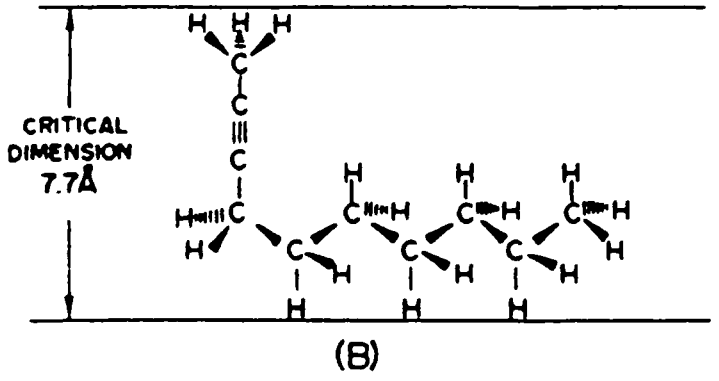

Figure 17: Shape selectivity in the interlayer spaces of a clay. A) Proposed orientation of the alkyne-rhodium triphenyl phosphine complex between the silicate sheets of hectorite B) The critical dimension of 2 decyne. (reproduced with permission from reference 63)

they could prepare highly dispersed $Os_3(CO)_{12}$ by reacting $HOs(CO)_{12}^+$ with hectorite. The cation reacted at the edges of the clay layers, producing $Os_3(CO)_{12}$ more highly dispersed than what could be achieved by impregnation of the neutral clusters from solution. Although the catalytic activity of this preparation was not tested, the ability to make highly dispersed metal carbonyl clusters may prove to be useful in enhancing their catalytic activity.

CHAPTER III

USES OF SUPRAMOLECULAR ORGANIZATIONS IN WATER REDUCTION.

3.1 Introduction.

One of the main obstacles that must be overcome to achieve efficient water photosplitting is charge separation. This problem can be divided into two parts, achieving charge separation in the first place, and then maintaining it a time long enough for the production of useful chemicals. For example, the photoreduction scheme depicted in figure 6, involves quenching of excited $Ru(bpy)_3^{2+}$ by MV^{2+}. The key reaction in this system is electron transfer between $^*Ru(bpy)_3^{2+}$ and MV^{2+}.

$$^*Ru(bpy)_3^{2+} + MV^{2+} \longrightarrow Ru(bpy)_3^{3+} + MV^{+\cdot} \qquad [25]$$

The quantum yield of separated ions in equation 25 is limited by the cage escape yield of the reaction to less than 0.3.[22] The cage escape yield is defined as the ratio of ions $Ru(bpy)_3^{3+}$ and $MV^{+\cdot}$ produced per encounter of $^*Ru(bpy)_3^{2+}$ with MV^{2+}

Once charge separation is achieved, the challenge is to maintain it. The back electron transfer reaction between $MV^{+\cdot}$ and $Ru(bpy)_3^{3+}$ is thermodynamically favored. It is one of the major energy wasting processes found in this system.

$$Ru(bpy)_3^{3+} + MV^{+\cdot} \longrightarrow Ru(bpy)_3^{2+} + MV^{2+} \qquad [26]$$

Some success can be achieved in limiting the importance of this back reaction by varying the experimental conditions. One can increase the concentration of the sacrificial donor to consume $Ru(bpy)_3^{3+}$ more efficiently or one can look for a more efficient catalyst to make the reaction of $MV^{+\cdot}$ with water faster. However, such changes have very little effect on the cage escape yield which is an inherent limitation of electron transfer between these two cations.

The third problem encountered in water photoreduction is that two electrons are needed for the production of one hydrogen molecule, while $MV^{+\cdot}$ is a one electron carrier.[12] Somehow, the electrons from two $MV^{+\cdot}$ must be combined. Two approaches have been used to attempt to solve this problem. One solution is to use a catalyst that can act as an electron accumulator, such as a metallic platinum particle. The other is to use a surface on which adsorbed hydrogen atoms can be produced. The production of a hydrogen radical is not a solution because it requires too much energy.

A possible solution to these three problems is once again found in nature. Compartmentalization is an essential feature of natural photosynthesis. The components of the photosynthetic apparatus are bound to the thylacoid membrane. Their arrangement makes light harvesting, charge separation, electron transfer, water oxidation and carbon fixation possible.[12] The solution thus suggested is the engineering of the water splitting system on the supramolecular level, by using molecular assemblies like micelles, vesicles and membranes, polyelectrolytes or inorganic colloids such as silica, alumina, zeolites and clays.[11 76]

The following section will cover a few examples of how using compartmentalization can help to solve the problems outlined above: charge separation, back electron transfer and performing a two electron reduction with a one electron carrier. In particular, the last section of this chapter will deal with the use of clay minerals in water photosplitting.

3.2 Organized Molecular Assemblies in Water Reduction.

The first problem that compartmentalization can help to solve is achieving charge separation. Since direct electron transfer between $^*Ru(bpy)_3^{2+}$ and MV^{2+} is so inefficient, and since Φs, the cage escape yield is not markedly altered by changes in experimental conditions, one can try to use an intermediate which will help to transfer the energy between those two ions more efficiently. Increasing the concentration of MV^{2+} or $Ru(bpy)_3^{2+}$ will increase the number of encounters between the ions, but will not increase Φs, the number of $MV^{+\cdot}$ ions produced per encounter. The yield of $MV^{+\cdot}$ can be increased by adding an intermediate to the system such as 9-anthracenecarboxylic acid (AA^-).[77] Electron transfer between the excited triplet state of this soluble anion and MV^{2+} proceeds with a cage escape yield close to unity, as opposed to only 0.25 between MV^{2+} and $^*Ru(bpy)_3^{2+}$. Unfortunately the production of the AA^- triplet state proceeds by excitation of the anion into its singlet state, at a much higher energy, requiring light of less than 392 nm. However the triplet state of AA^- can be made indirectly, in high yield, by the very efficient quenching of $^*Ru(bpy)_3^{2+}$ by AA^- via energy transfer. Electron transfer can then take place between this triplet AA^- state and MV^{2+}. In this enlarged system, (see figure 18) the yield of $MV^{+\cdot}$ approaches 100% and the yield of H_2 is close to 90%. Unfortunately the system is not stable. AA^- tends to dimerize or to decarboxylate when it is irradiated.

Instead of adding a soluble intermediate, another approach to improve charge separation is to physically separate the two ions, $Ru(bpy)_3^{2+}$ and MV^{2+}, for example, by placing one inside and the other outside of a vesicle. Of course there must be a mechanism for the transport of the electrons from one ion to the other through the barrier. For example, Fendler et al[78] prepared a system in which MV^{2+} and Pt catalyst were placed inside a vesicle of dihexadecylphosphate, while $Ru(bpy)_3^{2+}$ and EDTA were outside. They

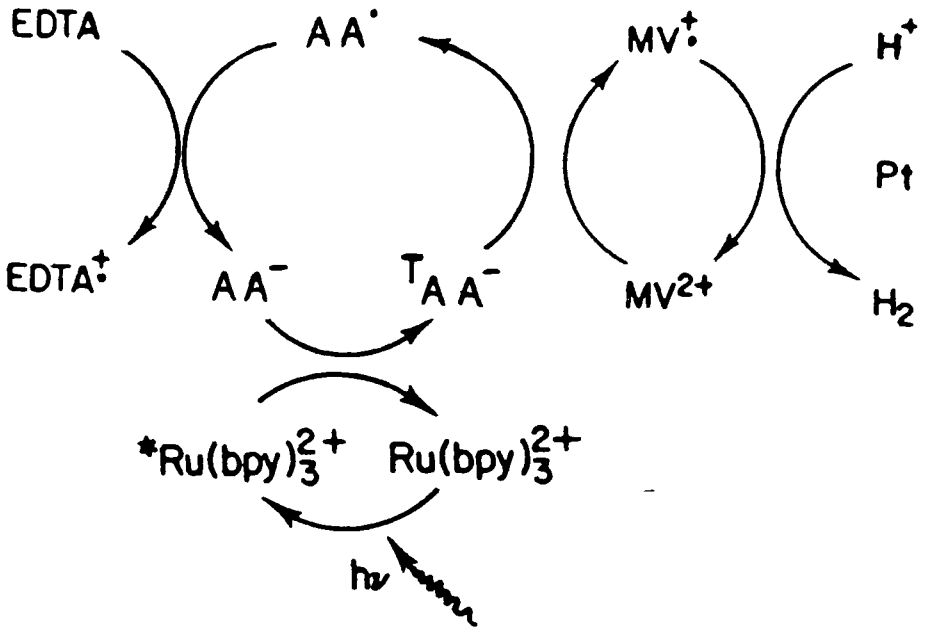

Figure 18: Water reduction with a system containing 9-anthracenecarboxylic acid (AA^-), MV^{2+} and $Ru(bpy)_3^{2+}$.

found that the electrons were free to move through the bilayer, and since MV^{2+} and $Ru(bpy)_3^{2+}$ were not in direct contact no problem with the cage escape yield was encountered.

Alternatively the ions could be immobilized on a solid support like cellulose.[79 80] The results indicated that the electron transfer between adsorbed excited $Ru(bpy)_3^{2+}$ and MV^{2+} tooks place in an active sphere of up to 20 Å, a distance which is larger than the sum of the van der Waals radii of the reacting molecules (about 10 Å). The quenching of excited $Ru(bpy)_3^{2+}$ by MV^{2+} in a cellulose matrix was therefore assumed to proceed by an electron tunneling mechanism,[79] rather than by a collision mechanism, eliminating the problem of cage escape yield.

The investigation of the uses of compartmentalization in water photoreduction has been mostly applied to the problem of maintaining charge separation once it has been achieved. After all, the cage escape problem can be solved by simply using a different photosensitizer. The quenching of $^{*}ZnTMPyP^{4+}$ by MV^{2+} for example, proceeds with a cage escape yield of about 0.8,[27] (see equation 12) but the problem of the thermodynamically favored back electron transfer reaction remains.

The use of micelles or vesicles can help in preventing the recombination of the two ions, by physically separating them. An example was provided by the use of $C_{14}MV^{2+}$ (figure 19) as electron relay to quench $^{*}ZnTMPyP^{4+}$ in the presence of the micelle cetyltrimethylammonium chloride.[81] The radical cation $C_{14}MV^{+\cdot}$ produced was stable for several milliseconds in the presence of the micelle, while the back electron transfer was very fast in its absence. The system worked because both $C_{14}MV^{2+}$ and $ZnTMPyP^{4+}$ were hydrophilic, while $C_{14}MV^{+\cdot}$ was hydrophobic. As soon as $C_{14}MV^{+\cdot}$ was formed it entered into the hydrophobic center of the micelles, while $ZnTMPyP^{5+}$ remained in the bulk water phase. The micelle physically separated the two ions after their formation, preventing them from reacting with each other.

The donor and the acceptor can also be physically separated prior to electron transfer. This was the case in the photoproduction of reduced heptylviologen ($HV^{+\cdot}$) (see figure 19) in the presence of a microemulsion of cetyltrimethylammonium bromine in dodecane containing small amounts of water.[82] In such a system the surfactant molecules formed inverted micelles, in which small water droplets were isolated from the hydrophobic bulk phase by being surrounded by the surfactant. In this system, $Ru(bpy)_3^{2+}$ was located in the water pool inside the micelles, while amphiphilic HV^{2+} was embedded in the interface boundary. In the same system no $MV^{+\cdot}$ was produced, since both $Ru(bpy)_3^{2+}$ and MV^{2+} were located exclusively in the water pools, making the back electron transfer very efficient.

An alternative to the physical separation of the ions by a membrane or is the induction of a favorable spacial distribution of the cations in solution by the electric field of a polyelectrolyte.[83-86] For example, the addition of polyvinylsulphate to the system retarded back electron transfer between $Ru(bpy)_3^{3+}$ and the electron relay, $BSV^{-\cdot}$. p-disulphonated benzylviologen (BSV), (see figure 19) a neutral zwitterionic viologen, was not affected by the negatively charged polyelectrolyte,[83] while $Ru(bpy)_3^{2+}$ was concentrated near it by electrostatic attraction. After electron transfer, the negatively charged $BSV^{-\cdot}$ was repelled away from the polyelectrolyte, and therefore away from $Ru(bpy)_3^{3+}$, insuring the persistence of the charge separation. In a related system, the anionic field of the inorganic colloid SiO_2, has been used to suppress the reverse electron transfer in a $Ru(bpy)_3^{2+}$ zwitterionic viologen system.[87]

Back electron transfer can also be hindered by the immobilization of the cations on a solid support. Cellulose retarded back electron transfer between $MV^{+\cdot}$ and $Ru(bpy)_3^{3+}$ by some three orders of magnitude. This was attributed in part to Franck-Condon factors, but also to the reduction of $Ru(bpy)_3^{3+}$ by the cellulose.[79] This reduction was assumed to be more efficient than reduction by the usual sacrificial electron donors, and it resulted in the accumulation of $MV^{+\cdot}$.

Finally, with regards to the problem of doing a two electrons reduction with a one electron carrier, the use of supramolecular organizations, such as inorganic colloids, can be very useful. They can provide sites where electrons can be accumulated. This was proposed as one of the functions of the colloidal platinum catalysts.[2] They can also provide a surface for the production of adsorbed H atoms. Further, many surfaces have acid sites that can be used to activate adsorbed water molecules. One proposed mechanism for the evolution of hydrogen on metal colloids involved protonation of the particle surfaces.[25] The inorganic colloids could be the source of these protons.

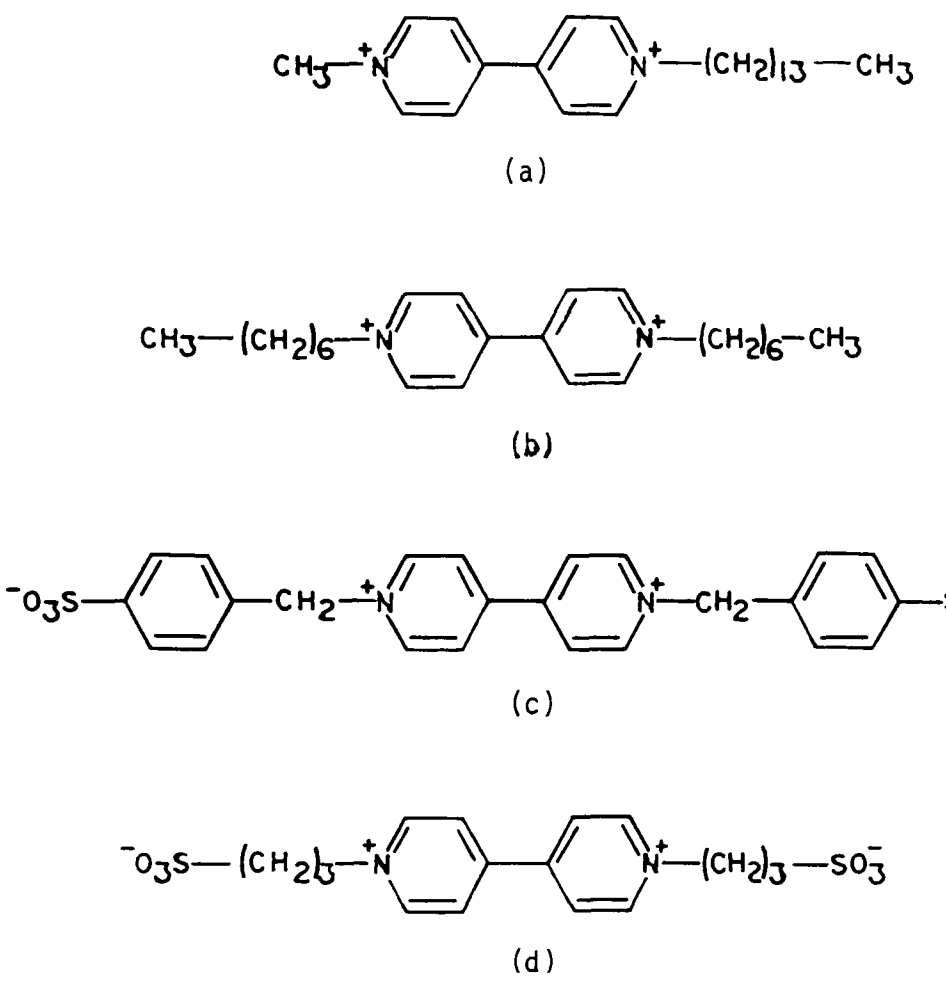

Figure 19: Structures of a) $C_{14}MV^{2+}$, b) heptylviologen (HV^{2+}), c) p-disulphonated benzylviologen (BSV), d) propylviologen sulphonate (PVS).

3.3 Water Photosplitting on Clay Surfaces.

Clay mineral suspensions have been used to promote hydrogen evolution in synthetic water photosplitting systems.

The negative charges of the clay particles were used by van Damme and his group to maintain charge separation in water photooxidation.[88-90] They observed the simultaneous evolution of hydrogen and oxygen in a system containing the photosensitizer $Ru(bpy)_3^{2+}$, a catalyst for water oxidation, RuO_2 (coadsorbed on the fibrous clay sepiolite), an electron acceptor Eu^{3+}, and a water reduction catalyst, colloidal Pt, coadsorbed on a positively charged $Al(OH)_x$ gel.[90] The use of two solid surfaces of opposite charges made possible the physical separation of the redox intermediates and their coupling with the corresponding catalysts.

The first system was made up of a negatively charged clay, sepiolite. This clay could only adsorb cations by exchange on its external surfaces. By coadsorbing $Ru(bpy)_3^{2+}$, the electron donor, and the water oxidation catalyst RuO_2 on those surfaces, the reaction of $Ru(bpy)_3^{3+}$ with water to give oxygen was very efficient. The other colloid was an ill-organized aluminum hydroxide gel, having a net positive charge. An electron acceptor, Eu^{3+} was embedded in the gel close to Pt particles making water reduction efficient. The rapid consumption of $Ru(bpy)_3^{3+}$ and Eu^{2+} thus diminished the importance of back electron transfer. The two systems were coupled through interparticle association in the reaction medium.

Interestingly, the gas evolution in the system displayed an oscillatory behavior. This was attributed to some type of cross catalytic effect arising from the presence of H_2 and O_2 on the one hand and from the presence of the oxidized and reduced catalysts on the other. Each of these catalysts was able to catalyze the oxidation or the reduction of the other by oxygen or hydrogen, consuming some of the gas produced in regenerating the catalysts. An oscillatory gas evolution could be an advantage in a practical water photosplitting system, provided its periodicity could be well controlled, since it could provide a means for the separation of hydrogen and oxygen via the time dependence of their evolution.

This system could be divided into two sacrificial subsystems, that were studied individually, by the addition of a sacrificial donor, EDTA, or a sacrificial acceptor, $Co(NH_3)_5Cl^{2+}$. When water photooxidation was tried in a system in which sepiolite was replaced by hectorite, no oxygen was found.[89] This was attributed to the location of the adsorbed photosensitizer, $Ru(bpy)_3^{2+}$, and of the oxidation catalyst RuO_2. $Ru(bpy)_3^{2+}$ was intercalated in hectorite, while the larger RuO_2 particles were restricted to the outside surfaces of the clay. This physical separation of the photosensitizer and the catalyst prevented the oxidation of water. If the hectorite layers were collapsed by heating them to 600°C, so that $Ru(bpy)_3^{2+}$ could no longer be intercalated, then the catalyst and the donor were in contact on the outside surface of the clay and oxygen evolution occurred. This confirmed the importance of the spacial arrangements of the catalysts and redox intermediates in building an efficient water photosplitting system.

The incorporation of semiconductor particles in clay films was studied by Bard and his coworkers.[91 92] The irradiation of an hectorite film in which TiO_2 and MV^{2+} were intercalated resulted in the photoproduction of $MV^{+\cdot}$. The immobilization of the semiconductor in close proximity to an electron acceptor resulted in the efficient capture of the electron of the photogenerated electron-hole pair. The hole had then time to react with the sacrificial donor TEOA. The persistence of charge separation was thus ensured.

Catalytic hydrogen evolution was found upon illumination of a montmorillonite film containing $Ru(bpy)_3^{2+}$, Pt and polyvinyl alcohol along with propylviologen sulphonate (PVS).[92] (see figure 19) In this system the clay was a direct chemical participant in maintaining charge separation. It was found by cyclic voltammetric measurements, that the ratio of the number of coulombs passed during the reduction of electrochemically generated $Ru(bpy)_3^{3+}$ to the number of coulombs passed during the oxidation of $Ru(bpy)_3^{2+}$ was 0.2. Further, when $Ru(bpy)_3^{3+}$, produced by the chemical oxidation of $Ru(bpy)_3^{2+}$ with PbO_2 in acidic solution, was mixed with colloidal montmorillonite, an immediate

reduction of $Ru(bpy)_3^{3+}$ to $Ru(bpy)_3^{2+}$ took place. These results were interpreted by postulating a reduction of $Ru(bpy)_3^{3+}$ by an unknown electron donating site in the clay. By removing $Ru(bpy)_3^{3+}$ from the system and thus allowing the accumulation of $PVS^{-\cdot}$, the persistence of charge separation was ensured. This is analogous to the previously discussed reduction of $Ru(bpy)_3^{3+}$ by cellulose.[89]

Finally, there was a recent report of hydrogen evolution upon irradiation of a mixture of the semiconductors ZnS and CdS in colloidal suspensions of montmorillonite,[93] without a noble metal catalyst. The efficiency was comparable to that previously found for a ZnS, CdS mixture on SiO_2 and on Nafion film[94] and to that of a Pt catalyzed CdS system. The behavior of the system was consistent with the following interpretation. The H_2 evolution was catalyzed by Zn metal formed by irradiation of ZnS in the system. It was proposed that an reactive layer of Zn metal was formed, coating the colloidal CdS particles.

In all of the systems discussed above, the clay acted as a support for both the reagents and the catalysts of the photoreduction cycles. Besides our own work,[37 38] we are not aware of any other reports of water photoreduction involving clay minerals as supports for reagents without the presence of an added external catalyst.

CHAPTER IV

IRON-SULFUR CLUSTERS IN WATER PHOTOREDUCTION.

4.1 Introduction.

The original objective of this work was to look at the potential use of iron-sulfur clusters in artificial water photosplitting. These iron-sulfur clusters are analogues of the active sites of iron-sulfur proteins such as hydrogenase, which catalyzes hydrogen evolution in natural systems.[95] Several intermediates in plant photosynthesis have also been shown to contain iron-sulfur sites.

The first section of this chapter will deal with the structures of the active sites in iron-sulfur proteins,[95] along with their roles in natural processes, in particular plant photosynthesis.[97] Then the synthesis and the activity of low molecular weight analogues of these proteins will be described.[98] The last section of this chapter will deal with the use of iron-sulfur proteins and their analogues in the photoreduction of water by visible light.[95 99]

4.2 Structures and Biological functions of Iron-Sulfur Proteins.

Iron-sulfur proteins have been found to contain three types of active sites. Their structures are illustrated in figure 20.

The 1-Fe site found in the protein rubedoxin is composed of a distorted tetrahedral arrangement of four sulfur ligands around a central iron atom.[96] The 2-Fe site is found in plant ferredoxin, where it plays a role in the electron transport chain. This site has a

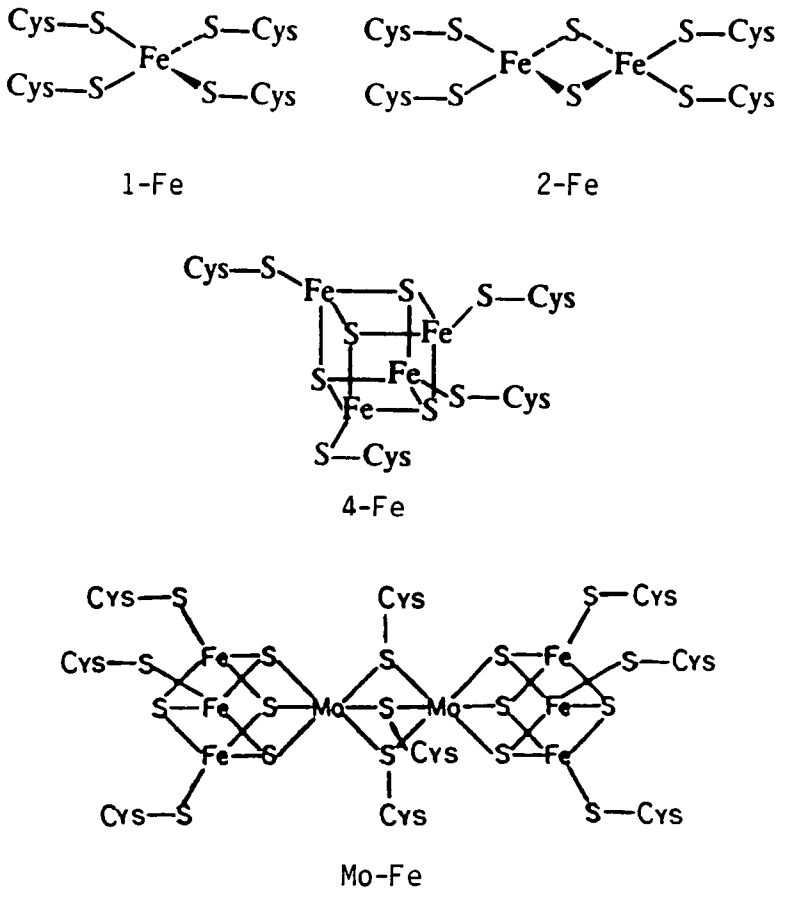

Figure 20: Structure of the active sites of the iron-sulfur proteins. (see text)

core formed by two irons bridged by two sulfur atoms. Each iron atom is further linked to the protein amino acid chain, via two other sulfurs, so that once again the iron atoms are at the center of distorted tetrahedra of four sulfurs. The third type of site, the 4-Fe site is formed by a cluster of four irons and 4 sulfurs linked to form a distorted cubane structure. A sulfur atom from the protein chain is linked to each of the four irons completing the iron-sulfur tetrahedra. This 4-Fe site is the structure of the active site of the protein hydrogenase.[95] Figure 20 also shows the structure of the active site of the protein nitrogenase,[104] which catalyzes nitrogen fixation. This site is made up of two 4-Fe

sites linked by the replacement of two irons by two molybdenum atoms and bridged by three sulfur atoms.

The biological function of the iron-sulfur proteins is redox coupling to enzymatic systems which catalyze a myriad of reactions.[96] They are electron relays. Because of their high reducing power they can function as electron carriers on the hydrogen side of $NADP^{+\cdot}$.[102] Plant ferredoxin, for example, has a redox potential of -420 mV, which is comparable to molecular hydrogen. (i.e. -413 mV at pH 7) By contrast, cytochromes, the better known group of protein electron carriers that contain heme iron, function on the oxygen side of $NADP.^{+\cdot}$

Five iron-sulfur sites have been identified in the electron transport chain in plant photosynthesis.[97] (see figure 21) The Rieske center, which is also a component part of mitochondria, is thought to be a 2-Fe center. It has a redox potential of +290 mV and functions as a link between the two photochemical systems. The other four are low potential centers. Three of them are membrane bound 4-Fe sites, call X, A and B, having redox potentials of -700 mV, -550 mV and -594 mV respectively. Their function is to transport the electron from Ch1, the primary electron acceptor of PS1, to the soluble protein ferredoxin. This protein (redox potential -420 mV) then reduces $NADP^{+\cdot}$ (-320 mV) to NADPH via an intermediate, the enzyme ferredoxin-NADP-reductase. (FNR) The multiple oxidation states of the flavin moiety of FNR allow this enzyme to couple the overall two electron reduction of $NADP^{+\cdot}$ by a one electron carrier in two one electron step reactions.[103]

Hydrogenase contains 4-Fe centers.[104] To explain its ability to mediate the reduction of water to hydrogen, by a one electron relay like $MV^{+\cdot}$ without the presence of a solid surface, it is assumed that the cluster can have several oxidation states. The cluster contains four iron atoms in which electrons can be placed. When three electrons are put into the iron-sulfur cluster, the result is molecular hydrogen with concomitant reoxidation of two Fe atoms.[11]

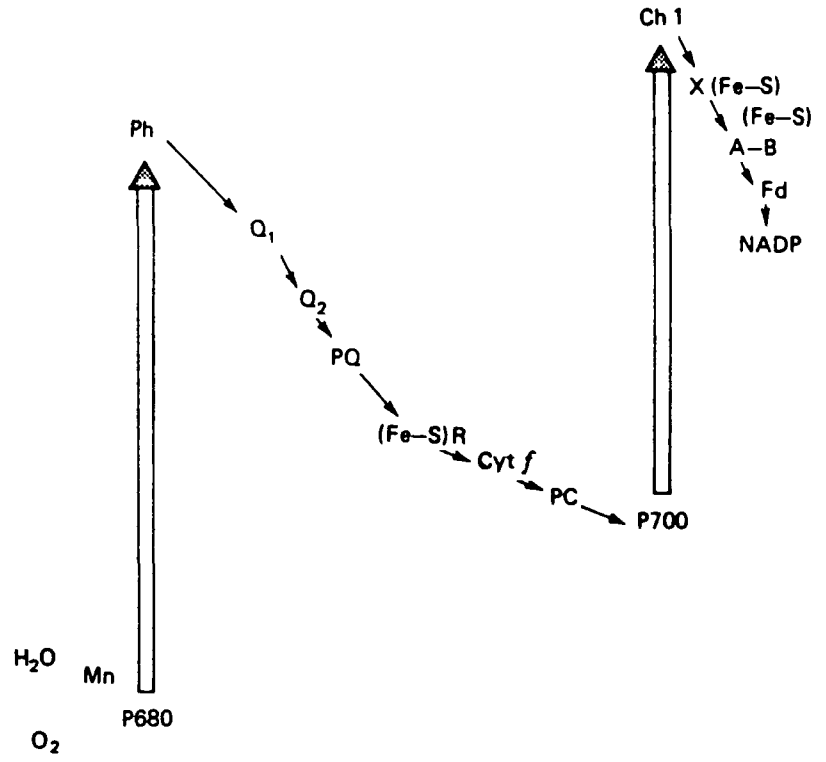

Figure 21: Electron transport chain in plant photosynthesis. (reproduced with permission from reference 97)

4.3 Synthesis of Analogues of Iron-Sulfur Proteins.

There has been a lot of work, in particular by Holm[98] and his group, on the preparation of low molecular weight iron-sulfur clusters analogues of the active sites of the iron-sulfur proteins. By an analogue one means that those clusters would mimic both the structures of the protein sites along with the proteins redox potentials. As a result of this work, analogues for all three types of active sites have now been successfully synthesized.[105 106 107] It turns out that in methanol, in the absence of air and moisture, the 4-Fe type clusters are the thermodynamically most stable soluble products of Fe(II) or Fe(III) salts and elemental sulfur in the presence of sufficient thiolate reductand.[98]

The structural and redox properties of a wide variety of these clusters have been measured.[96 108-110] They are found to be very similar to those of the proteins, making them true analogues of the proteins active sites.

The iron-sulfur clusters have been tested as catalysts in several reactions. For example the 4-Fe clusters were found to catalyze the oxidation of thiols to disulfides by oxygen.[111]

$$4PhSH + O_2 \xrightarrow{[Fe_4S_4(SPh)_4]^{2-}} 2RSSR + 2H_2O \qquad [27]$$

They also catalyzed some reduction reaction, such as the production of cis-stilbene from diphenylacetylene.[112]

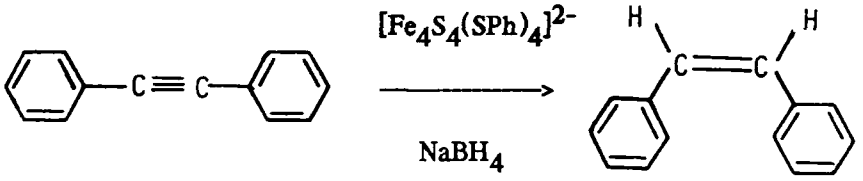

[28]

Further, the cluster $[Fe_4S_4(SPh)_4]^{2-}$ has been shown to have catalytic activity in two very important, and potentially very useful, reactions: the reduction of carbon dioxide and the fixation of nitrogen. In nonaqueous DMF solutions, addition of this cluster shifted the potential needed for the electroreduction of CO_2 to a more positive value by approximately 0.7 V.[113] The electrochemical reduction of $[Fe_4S_4(SPh)_4]^{2-}$ to $[Fe_4S_4(SPh)_4]^{3-}$ or $[Fe_4S_4(SPh)_4]^{4-}$, or of $[Mo_2Fe_6S_8(SPh)_9]^{3-}$ to $[Mo_2Fe_6S_8(SPh)_9]^{5-}$ in a protic solvent led to the production of NH_3 when nitrogen was bubbled through the solution.[144]

These two clusters have also been shown to be active in hydrogen evolution reactions. The electrogenerated reduced clusters were capable of reducing acetylene to ethylene with concomitant evolution of hydrogen.[115] Hydrogen was also produced in the reaction of the reduced clusters with PhSH.[104]

$$2[Fe_4S_4(SPh)_4]^{3-} + 2PhSH \longrightarrow [Fe_4S_4(SPh)_4]^{2-} + 2PhS^- + H_2 \qquad [29]$$

However the hydrogen evolution in these reactions depended on the irreversible consumption of the reduced clusters. What we are looking for is a light driven system in which the cluster catalyzes the evolution of hydrogen. The protein hydrogenase itself has been used as a catalyst in several such systems.[26] It was shown to catalyze water photoreduction in systems, such as the one of figure 6, where $Ru(bpy)_3^{2+}$ was the photosensitizer,[116] or of figure 8, where $ZnTSPP_3$[117 118] or $CdTSPP_3$[119] were the photosensitizers, or even in systems where triphenylamine[128] was the photosensitizer with near ultraviolet illumination. In all these examples MV^{2+} or a related viologen derivative[99] was used as the electron relay. The function of hydrogenase was the catalysis of the reduction of water by $MV^{+\cdot}$. However, in a practical water splitting system one cannot use hydrogenase as a catalyst, for the same reason that one cannot use chlorophyll as photosensitizer: it is too expensive and too fragile.

This is what makes the use of iron-sulfur clusters analogues so interesting. In one system the evolution of hydrogen was reported when $Ru(bpy)_3^{2+}$ was illuminated in the presence of the cluster $Fe_4S_4(SCH_2Ph)_4^{2-}$.[121] The excited ruthenium complex was assumed to reduce the cluster. The reduced cluster was then able to reduce $Ru(bpy)_3^{2+}$ to $Ru(bpy)_3^{+}$ giving hydrogen via a reductive cycle like the one of figure 5. The yield of hydrogen was very low and the system very unstable.

In general, the isolated clusters do not have the catalytic ability of hydrogenase. The ability of the protein must therefore be due in part to the structure of its amino acid

chain (tertiary structure). Attempts have been made to mimic the environment of the active site of iron-sulfur proteins, by placing the clusters in a matrix. For example, it was found that the cluster $[Fe_4S_4(SPh)_4]^{2-}$ incorporated into the protein Bovin Serum Albumin catalyzed the photoreduction of water by $MV^{+\cdot}$.[95] The yield of hydrogen was much lower than with hydrogenase, but this result showed the importance of the environment of the iron-sulfur cluster on its catalytic properties. There was a report on the adsorption of a 4-Fe cluster on silica gel.[122] In that case, the cluster was linked to the surface by a chemical bond. The surface was first modified by the attachment of thiol chains and the cluster was then linked to those surface thiol groups. This surface attached cluster did not display any catalytic activity.

We were therefore led to wonder what effect incorporating the clusters into other types of solid matrix, such as clays, would have on their ability to catalyze the reduction of water by $MV^{+\cdot}$.

CHAPTER V

EXPERIMENTAL.

5.1 Synthesis.

5.1.1 Iron-sulfur Cluster $[(n\text{-}Bu)_4N]_2[Fe_4S_4(SPh)_4]$

The iron-sulfur cluster $[Fe_4S_4(SPh)_4]^{2-}$ (see figure 22) was prepared according to the procedure reported by Christou et al.[105] The reagents, sulfur precipitated purified powder, tetra-n-butylammonium iodide 98% from Alfa Products, anhydrous ferric chloride, lithium metal from Aldrich and anhydrous thiophenol from Sigma were used without further purification. The solvents, acetonitrile and methanol were Fisher certified reagents. Prior to their use they were dried by distillation over calcium hydride and magnesium respectively.

All the manipulations were carried out under nitrogen. Care was taken to keep the reaction mixture free of moisture. The solvents were made free of dissolved oxygen by bubbling with N_2 for 15 minutes prior to their use.

Lithium (0.56 g, 80 mmol) was dissolved in 80 ml of methanol; 8.2 ml (80 mmol) benzenethiol was added followed by 3.24 g (20 mmol) anhydrous ferric chloride in 50 ml methanol. The black solution was added to 0.64 g (20 mmol) sulfur giving a brown reaction mixture. This mixture was stirred overnight at room temperature, filtered and added to a solution of 5.54 g (15 mmol) tetra-n-butylammonium iodide in 40 ml methanol. The mixture was left overnight in the cold (-5^{o}C) to allow time for crystallization of the product to take place. Filtration gave a black crystalline solid, (needles) which was vacuum dried.

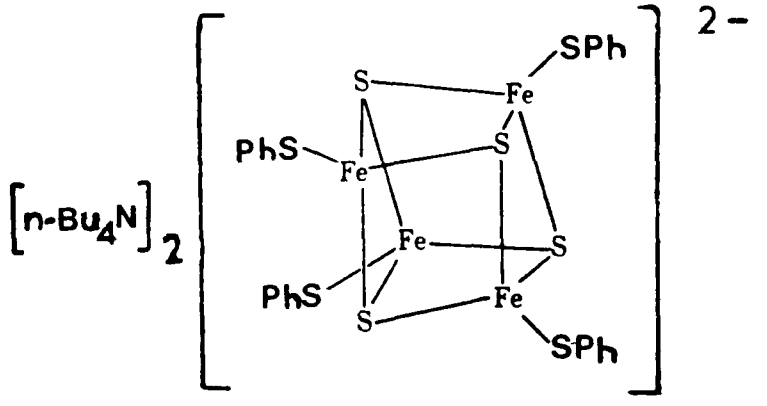

Figure 22: Structure of the iron-sulfur cluster $[n\text{-}Bu_4N]_2[Fe_4S_4(SPh)_4]$

The product was purified by recrystallization. The solid was dissolved in hot acetonitrile. After addition of methanol, cooling to -5°C gave 3.2 g of black needles, m.p. 187-192°C, for an experimental yield of 60%. (lit. m.p. 190-191°C, yield 76%[105]) The product was characterized by its UV-Visible spectrum and its ^1H NMR spectrum. Both were identical to those reported for the cluster $[n\text{-}Bu_4N]_2[Fe_4S_4(SPh)_4]$ in the literature.[123 124]

5.1.2 Adsorption of the Cluster on Montmorillonite.

The cluster prepared in section 5.1.1 was adsorbed on clay mineral in the following way. A suspension of the clay montmorillonite (a bentonite from Clay Spur Wyoming, see section 5.1.4) was made by dispersing 0.3 g of the clay in 15 ml of acetonitrile. A solution of 0.2 g $[n\text{-}Bu_4N]_2[Fe_4S_4(SPh)_4]$ in 20 ml acetonitrile was added. After 30 minutes of stirring under nitrogen, the solid was isolated by filtration, giving, after drying, 0.45 g of a black powder. This solid was not further characterized, but the cluster was shown to be intact after this treatment since this solid was active in catalyzing the oxida-

tion of benzenethiol to diphenyl disulfide by oxygen, according to the procedure described by Hirobe et al.[111] (see equation 27) A second clay incorporated material was prepared having a different ratio of cluster to montmorillonite (ie 0.1 g of cluster in 0.3 g of clay). The activity of these two preparations as water photoreduction catalysts was tested.

5.1.3 Zinc Tetramethylpyridine porphyrin. ($ZnTMPyP^{4+}$)

The photosensitizer $[ZnTMPyP^{4+}]I_4$ (see figure 23) was synthesized according to the procedure described by Harriman et al.[28] The reagents, methyl iodide and sodium iodide from Fisher, meso-tetrapyridylporphyrin 90% pure from Sigma and anhydrous zinc chloride from Alfa product were used without further purification. The solvents DMF and CH_2Cl_2 were Fisher certified reagents.

1.0 g meso-tetrapyridylporphyrin (TPyP) was stirred at room temperature under argon for 3 days in 100 ml methyl iodide. The product, tetra(N-methylpyridyl)porphyrin iodide ($[TMPyP^{4+}]I_4$) was isolated by filtration and purified by recrystallization. The solid was dissolved in hot water. A saturated solution of sodium iodide in water was added and the solution cooled in an ice bath. After filtration the solid was dried under vacuum over P_2O_5 giving 1.7 g of a purple red powder. The product yield was 88% and its purity was estimated at more than 95% from its UV-visible spectrum.[125] (See figure 23)

1.0 g of this product was dissolved in 75 ml of boiling DMF; 150 mg of anhydrous $ZnCl_2$ in 25 ml of DMF was added and the mixture was reflux for 2 hours under N_2. After cooling, 100 ml of $CHCl_3$ were added and the solution was left overnight in the cold (-5°C) to allow time for crystallization. The solid was separated by filtration, washed with cold $CHCl_3$ and purified by recrystallization from water with NaI as before, giving, after drying in vacuum over P_2O_5, 0.6 g of a purple powder, for a yield of 57%. From the UV-Visible spectrum (see figure 23 and table 4) the purity of the product was estimated at more than 90%. This product was used without further purification.

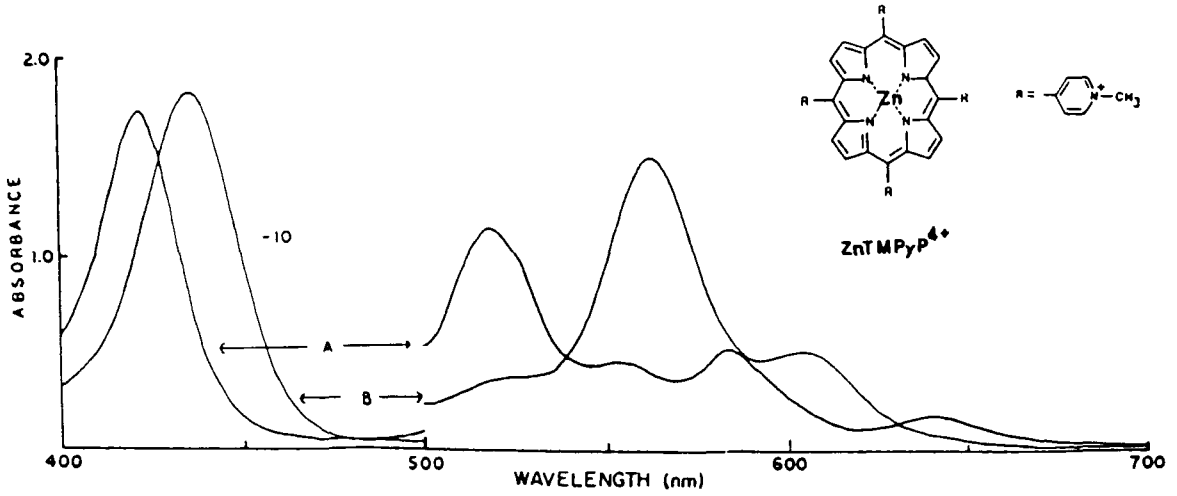

Figure 23: Characterization of the porphyrins. UV-Visible spectra of A) $TMPyP^{4+}$ (1.0×10^{-4}M) and B) $ZnTMPyP^{4+}$ (1.0×10^{-4}M) in H_2O.

Table 4: Characterization of the porphyrin $[ZnTMPyP^{4+}]I_4$

λ_{max} nm		ϵ $M^{-1}cm^{-1}$	
Observed	Literature	Observed	Literature
435	436	177,000	181,000
562	560	15,000	16,000
604	602	5,000	5,300

Position of the porphyrin absorption bands in water and their molar extinction coefficients. (Literature values taken from reference 125)

5.1.4 Purification and Characterization of the Clays.

1. *Hectorite*

Samples of this clay and of the two others that have been used in this work, montmorillonite and nontronite, were provided by Dr. H. Kodama from the Land Resource Research Center, Research Branch, Agriculture Canada, Ottawa. The sample was from San Bernardino county California U.S.A. Its elemental composition is given in table 5. It contained large amounts of calcium carbonate impurities.

Table 5: Elemental analysis of the clay minerals used in this work.

Oxide	Ca-Saturated Montmorillonite (Clay Spur Wyoming)	Ca-Saturated Hectorite (San Bernardino California)	Ca-Saturated Nontronite (Garfield Washington)
SiO_2	61.95 %	52.8	45.23 %
Al_2O_3	21.82	0.8	7.11
TiO_2	0.14	---	---
[a] Fe_2O_3	4.17	0.34	32.28
MnO	---	---	0.02
MgO	2.06	24.0	0.31
CaO	2.29	8.6	2.61
K_2O	0.07	---	---
Na_2O	---	0.3	0.13
Li_2O	---	0.13	---
[b] Ig Loss	7.60	12.8	10.56
total	100.1	99.8	98.25

a) All the iron present is assumed to be in the Fe(III) oxidation state, b) Ignition loss

Prior to use, these carbonate impurities were removed and the < 2.0 μm fraction separated by the procedure described by J. E. Brydon,[126] which was derived from the procedures reported by Jackson et al[127] and by Mackenzie[128] for the purification of clay minerals. A suspension of 15 g of the crude hectorite in 200 ml of water was prepared. To destroy the carbonates, 1 N HCl was added until the pH was reduced to 3.5 and remained

at or near that value for 10 minutes. The mixture was then centrifuged, the clear supernatant discarded and the sediment washed with HCl (pH 3.5) to remove soluble salts and exchangeable basic cations. After a second centrifugation, the sediment was redispersed in water, the suspension pH was adjusted to 8.0 with 0.1 N NaOH and the suspension was covered and allowed to stand overnight. It was then transferred to a 600 ml beaker marked 10 cm from the inside bottom, water was added to the mark and the suspension was stirred overnight.

The < 2.0 μm fraction of the clay was then separated by gravitation. After standing undisturbed and free from vibrations and drafts overnight, the suspension above the sediment was siphoned off and poured into a large vessel. Water was added to the sediment up to the mark and the sediment was redispersed. The suspension temperature was taken and it was allowed to stand for the length of time needed for all particles larger than 2.0 μm to deposit themselves at the bottom of the beaker, as specified in figure 1 of reference 129. (6 hours in our case) The suspension above the sediment was then siphoned off and combined with the one siphoned off previously. This was repeated until the supernatant liquid became clear after the 6 hours waiting period.

The siphoned suspension that contained all the < 2.0 μm clay was then acidified to pH 3.5 with 1 N HCl and 75 ml of a saturated $CaCl_2$ solution was added to prepare the homoionic < 2.0 μm Ca^{2+}-hectorite. This also caused the flocculation of the suspension. Most of the clear supernatant could then be siphoned off and discarded. The remaining clay water mixture (about 400 ml) was centrifuged at 4000 rpm on a Fisher Centrific centrifuge for 15 minutes. The sediment was washed, first with a saturated $CaCl_2$ solution, then water and water-acetone mixtures, increasing the acetone content each time until a negative chloride test was obtained. The sediment was transferred to a 250 ml beaker with acetone, the acetone was evaporated over a water bath and the sediment was dried in vacuum at 80°C. 6.3 g a of beige powder was obtained. This material was used for all experiments involving hectorite.

2. *Montmorillonite*

The montmorillonite used was a Bentonite from Clay Spur Wyoming U.S.A. The crude sample was used in some experiments, but purified montmorillonite was used in most of them. Dr. Kodama provided us with samples of < 2.0 μm Ca^{2+}, Ni^{2+}, Cu^{2+}, Zn^{2+}, Co^{2+}, Mg^{2+}, Sr^{2+}, Li^{2+} and NH_4^+ and a sample of < 0.2 μm Na^+ homoionic montmorillonite. They were prepared by conventional techniques, using gravitation and saturated chloride solutions of the cations. (see part 1 of this section) The elemental composition of this montmorillonite is given in table 5.

3. *Nontronite*

The nontronite was the < 2.0 μm fraction of a Ca^{2+} saturated nontronite from Garfield, Washington. Its elemental composition is also given in table 5.

4. *Calculation of the Clay Formulas*

A formula for each of the three clays was calculated by the procedure described by Van Olpen[54] using the general formula of smectite clays, (see equation 30) and the elemental composition of the three clays. (see table 5)

$$[(Si_{4-y}Al_y)^{IV}(Al_{a-y}Fe_b{}^3Fe_c{}^2Mg_dCr_e{}^3Mn_f{}^3Mn_g{}^2Li_h)^{VI}O_{10}(OH)_2]_2X_x \qquad [30]$$

TiO_2 and P_2O_5 were assumed to be mineral impurities and all the iron was assumed to be in the Fe(III) oxidation state. The following usual arbitrary assumptions were made: 1) all the Si present is in the tetrahedral sheet, 2) the remainder of the tetrahedral positions are filled by Al 3) the additional Al and all the other metals, except K, Na and Ca are assigned to the octahedral sheets and 4) Potassium, sodium and calcium are assumed to be intercalated exchangeable cations.

The analytical values for the percentage of the oxides of the crystal elements and exchangeable ions were reduced to atomic proportions by using the oxide formula and molecular weights. Equation 31 was then applied.

$$K(4Z + 3A + 3B + 2C + 2D + 3E + 3F + 2G + H + X) = 22 \qquad [31]$$

where Z, A, B, C, D, E, F, G, H and X are the atomic proportion of Si, Al, Fe(III), Fe(II), Mg, Cr(III), Mn(III), Mn(II), Li and the sum of the atomic proportion of the exchangeable cations. K is the factor by which the atomic proportion must be multiplied to obtain the actual amounts of a species in the formula. (see equation 30) Evaluation of K by equation 31 allows the formula of the clay to be computed. Y, the atomic proportion of Al in tetrahedral positions can be evaluated since $K(Z + Y) = 4$. Note that the value of X can be replaced by the cation exchanged capacity of the clay expressed in equivalent of exchangeable ions per 100 g of clay. This value will be called calculated cation exchange capacity, in table 15. Also, since hectorite contains carbonate impurities its formula cannot be evaluated in this way. The amount of $CaCO_3$ impurity has to be estimated in order to obtain the value of % CaO and the corrected elemental composition of the clay.

5.2 Hydrogen Evolution Experiments.

5.2.1 Illumination.

In the early hydrogen evolution experiments, visible light illumination was provided by a 300 W tungsten halogen lamp placed 25 cm from the center of the solution. Ultraviolet light was removed by < 395 nm filter. (Ealing GG-395)

For the majority of the experiments, illumination was provided by a Kratos Solar Simulator equipped with an ozone free XBO 450 W xenon arc lamp, an air mass 1 filter and a sun lens diffuser providing a 14^{o} uniform diverging beam. The same 395 nm filter was used to eliminate ultraviolet light. The temperature of the reaction mixture was approximately $30^{o}C$. The spectral distribution of the light given by this system is compared with that of the noon sun at sea level in figure 24.

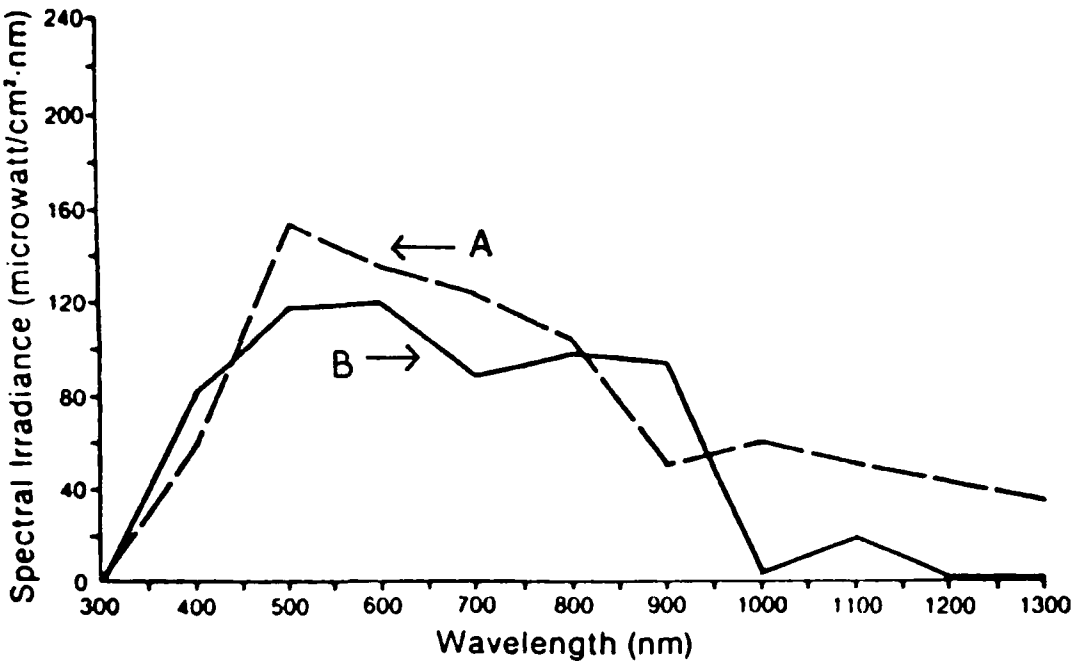

Figure 24: Spectrum of the Kratos Solar Simulator. A) Sea level noon solar spectrum and B) spectrum of the kratos solar simulator with air mass 1 filter.

The reaction mixture was contained in a 100 ml round bottom flask equipped with a valve and a septum. Its illuminated cross-sectional area was 25 $cm.^2$ The flask was placed 15 cm from the lens of the lamp. The diameter of the illuminated target at that point was 10 cm and the light intensity equivalent to 2.7 times that of the noon sun or about 270 $mW/cm.^2$

5.2.2 Preparation of the Mixture for Photolysis Experiments.

The reagents used in the water photolysis experiments, tris (2,2'bipyridyl)ruthenium(II) chloride ($Ru(bpy)_3Cl_2$) from Alfa products, methylviologen monohydrate dichloride (MV), triethanolamine (TEOA) and ethylenediamine tetraacetic

acid (EDTA) from Aldrich were used without further purification. The buffers were Fisher solutions, monobasic potassium phosphate and sodium hydroxide for pH 7.0 and potassium biphthalate for pH 4.0. A typical reaction mixture was prepared, keeping the same order of addition of the various reagents, in the following way: under an argon atmosphere 10 ml of the pH 7.0 buffer solution was added to 0.8 ml of TEOA followed by 0.20 g of one of the clay minerals, 0.0771 g of MV^{2+} and 0.0192 g of $Ru(bpy)_3^{2+}$ followed by deoxygenated deionized water so that the volume was constant at 60 ml. Argon was bubbled through the mixture for 20 minutes to remove all traces of air. The reaction flask was a 100 ml round bottom flask equipped with a valve and a septum. The flocculated clay mixture was stirred with a Teflon coated magnetic bar during illumination. After illumination the gas phase over the mixture was analyzed by gas chromatography (see section 5.2.3) by taking a gas sample through the septum with a syringe equipped with a valve.

In the experiments where the activity of the iron-sulfur cluster, $[n\text{-}Bu_4N][Fe_4S_4(SPh)_4]$ as water photoreduction catalyst was tested the mixtures were prepared in the same way, except that 0.150 g of clay incorporated cluster, prepared according to the procedure of section 5.1.2, was used instead of the clay.

The mixtures for the photolysis experiments performed at pH 5.3 were prepared in the same way, replacing the pH 7.0 buffer solution and the TEOA by 10 ml of the pH 4.0 buffer solution and 2.2 g of EDTA. In some experiments the photosensitizer $Ru(bpy)_3^{2+}$ was replaced by 0.030 g of the porphyrin photosensitizer $ZnTMPyP^{4+}$. In one case 0.335 g of EDTA, 0.123 g of MV^{2+} and 12 ml of a solution 1.0×10^{-4}M in $ZnTMPyP^{4+}$ were used giving a mixture having concentrations of the reagents of 1.5×10^{-2}M, 8.0×10^{-3}M and 2.0×10^{-5}M respectively. These are the optimum concentrations for the photoproduction of $MV^{+\cdot}$ with $ZnTMPyP^{4+}$.[28] The various blank experiments were performed by simply omitting one of the reagents in the mixture preparation.

The effect of using a nonflocculated clay mixture was also tested. A typical mixture in this series was prepared by mixing, under argon, 0.060 g of a clay with 10 ml of deoxygenated deionized water, followed by the addition of 0.1 ml of TEOA, 20 ml of a solution of MV 5.0×10^{-4}M and 30 ml of a solution of $Ru(bpy)_3^{2+}$ 1.0×10^{-4}M and bubbling argon through the mixture for 20 minutes. Some of those mixtures were placed in an ultrasound bath prior to illumination, to study the effect of ultrasound on hydrogen evolution.

5.2.3 Analysis of the Evolved Hydrogen.

Samples of the gas phase, taken over the reaction mixtures, were injected into a GOW-MAC 550P gas chromatograph equipped with a thermal conductivity detector and a 6' x 1/8" molecular sieve 5 Å column using argon as gas carrier. The output was recorded by a Spectra Physics SP4270 chromatography integrator. The conditions used for the analysis were: detector temperature 40°C, injection port temperature 45°C, oven temperature 40°C, detector bridge current 110 mV and flow rate of the argon carrier gas 30 ml/min. The attenuator was set at 2.

The amount of hydrogen in the injected samples was determined by comparison with a calibration curve. A mixture of hydrogen and argon containing a precisely known amount of hydrogen was prepared. Various volumes of this mixture were then injected into the gas chromatograph and the peak area were recorded. A calibration curve of amount of hydrogen versus peak area was then computed. A typical chromatograph obtained with this analysis system is given in figure 25. The hydrogen peak appears at a retention time of 0.34 min. The two peaks at retention times of 0.68 and 1.36 minutes are due to the oxygen and the nitrogen respectively, from residual traces of air in the system. It was estimated that the system detection limits was about 0.3 to 0.4 μmol per litre. (i.e. in such a case, a 1.0 ml sample of the gas phase contains about 0.01 μL of hydrogen)

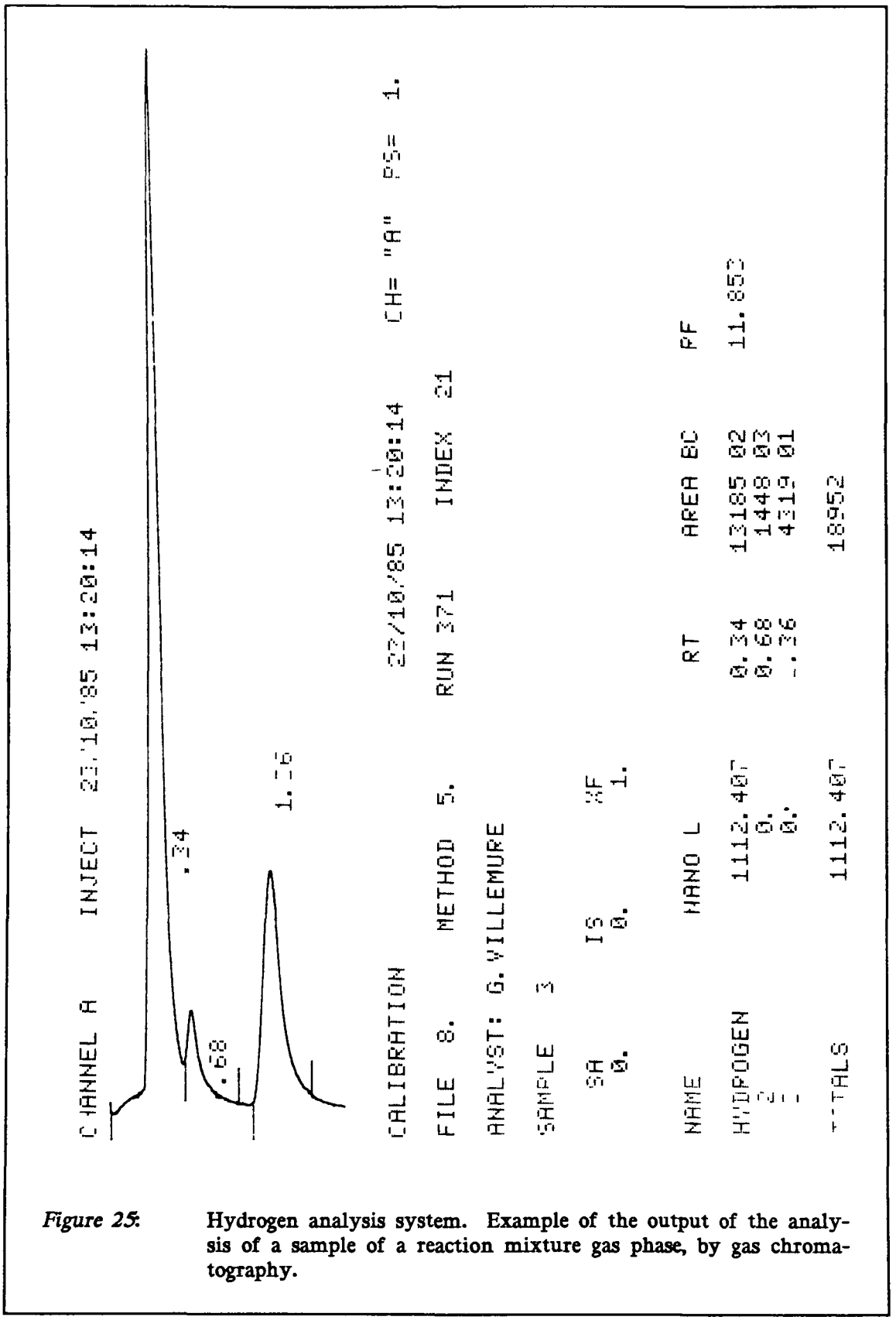

Figure 25: **Hydrogen analysis system. Example of the output of the analysis of a sample of a reaction mixture gas phase, by gas chromatography.**

5.3 Adsorption of MV^{2+}, $Ru(bpy)_3^{2+}$ and $ZnTMPyP^{4+}$ on Clays.

5.3.1 Amounts of the Cations Adsorbed by the Clays.

In order to determine the amount of MV^{2+} adsorbed by < 2.0 μm Ca^{2+}-montmorillonite, 0.150 g of this clay was dispersed in 25 ml of distilled water and 75 ml of a solution of MV^{2+} 2.00 x 10^{-3}M was added. The mixture was stirred overnight and then centrifuged for one hour. The solid was kept for further use described in section 5.3.2 c). The concentration of MV^{2+} remaining in the supernatant was determined by measuring its absorbance at 257.5 nm (lit. ϵ = 20,100 $M^{-1}cm^{-1}$ [130]). The amount of cation adsorbed by the clay was determined by difference

The same procedure was used to determine the amounts of $Ru(bpy)_3^{2+}$ and of $ZnTMPyP^{4+}$ that were adsorbed by montmorillonite, using their absorbances at 452 nm (lit. ϵ = 14,600$M^{-1}cm^{-1}$ [17] and 562 nm (lit. ϵ = 16,000 $M^{-1}cm^{-1}$ [125]) respectively. This procedure was repeated several times for all three cations. It gave always the same results within experimental error. The amounts of MV^{2+} and $Ru(bpy)_3^{2+}$ adsorbed by < 2.0 μm Ca^{2+} hectorite were also measured using this procedure.

5.3.2 Competitive Adsorption of two Cations.

a) *Simultaneous Addition of the two Cations*

The competitive adsorption of $Ru(bpy)_3^{2+}$ and MV^{2+} and of $ZnTMPyP^{4+}$ and MV^{2+} by montmorillonite was studied when both cations were added simultaneously. In each case a series of reaction mixtures was prepared in the following way: 0.025 g of montmorillonite was dispersed in 25 ml of distilled water and 25 ml of a solution containing various concentrations of MV^{2+} and $Ru(bpy)_3^{2+}$ or of MV^{2+} and $ZnTMPyP^{4+}$

was added, such that the total concentration of cations added was about twice the amount that the clay could adsorb, as measured in section 5.3.1. The mixtures were stirred overnight and the supernatants were isolated by centrifugation. The concentrations of MV^{2+} and $Ru(bpy)_3^{2+}$ or of MV^{2+} and $ZnTMPyP^{4+}$ left in solution were determined by UV-Visible spectroscopy, allowing the determination of the amounts of the various cations adsorbed as in the previous section. The composition of the solution phase versus the composition of the absorbed phase was then plotted to see if the clay adsorbed one of the cations preferentially.[131]

b) *Delayed Addition of one of the Cations*

The same procedure was repeated except that instead of adding mixed solutions of MV^{2+} and $Ru(bpy)_3^{2+}$ or of MV^{2+} and $ZnTMPyP^{4+}$ to the clay suspensions, a solution of one of the cations was added first, followed, 30 minutes later, by a solution of the other. Again, the total amount of both cations added was about twice the amount that the clay could adsorb, as determined in section 5.3.1. Four series of these mixtures were prepared in which $Ru(bpy)_3^{2+}$ was added first followed by MV^{2+}, MV^{2+} was added first followed by $Ru(bpy)_3^{2+}$, $ZnTMPyP^{4+}$ was added first followed by MV^{2+} and MV^{2+} was added first followed by $ZnTMPyP^{4+}$. After overnight stirring the compositions of the solutions phases and of the adsorbed phases were determined and plotted.

c) *The Displacement of a Pre-adsorbed Cation*

The ability of MV^{2+} to displace $Ru(bpy)_3^{2+}$ or $ZnTMPyP^{4+}$ from montmorillonite and the ability of $Ru(bpy)_3^{2+}$ or $ZnTMPyP^{4+}$ to displace preadsorbed MV^{2+} from montmorillonite were studied. The solids isolated by centrifugation in section 5.3.1 were washed several times with water and dried under vacuum over P_2O_5.

Suspensions of the MV^{2+} intercalated montmorillonite were prepared by dispersing 0.025 g of this solid in 25 ml of distilled water. A series of reaction mixtures were prepared by adding various volumes of a solution of $Ru(bpy)_3^{2+}$ such that the total amounts of $Ru(bpy)_3^{2+}$ added covered a range from about 0.1 to about 10 times the amounts of MV^{2+} present on the clay. After stirring overnight, the compositions of the solution and adsorbed phases were determined as before (see part a of this section) and plotted. The same procedure was repeated adding a solution of $ZnTMPyP^{4+}$ to the MV^{2+} intercalated montmorillonite. Then the reverse was done, solutions of MV^{2+} were added to suspensions of $Ru(bpy)_3^{2+}$ and $ZnTMPyP^{4+}$ exchanged clays. For each series the compositions of the solution and adsorbed phases were then plotted.

CHAPTER VI

RESULTS.

6.1 Production of hydrogen.

6.1.1 Hydrogen Evolution at pH 7.0.

Table 6: Production of hydrogen in the presence of the clay adsorbed cluster.

$Ru(bpy)_3^{2+}$ (M)	MV^{2+} (M)	Cluster (M)	H_2 (μmol/L) in 15 hours
5.0×10^{-4}	5.0×10^{-3}	--------	4.2
5.0×10^{-4}	5.0×10^{-3}	6.5×10^{-4}	2.0
5.0×10^{-4}	5.0×10^{-3}	1.3×10^{-3}	1.0
--------	5.0×10^{-3}	1.3×10^{-3}	---
5.0×10^{-4}	--------	1.3×10^{-3}	---

Cluster = $[n\text{-}Bu_4N]_2[Fe_4S_4(SPh)_4]$, in each case the montmorillonite concentration was 3.0 g/L.

Table 6 shows the amount of hydrogen produced after 15 hours of illumination, with a 300 W tungsten halogen lamp through a 395 nm filter, as a function of the concentration of the cluster $[n\text{-}Bu_4N]_2[Fe_4S_4(SPh)_4]$ adsorbed on montmorillonite. (see section 5.1.2) In each case, the concentration of the sacrificial donor TEOA was 5.0×10^{-2} M and the pH was adjusted to 7.0 with a buffer solution.

No hydrogen was produced if either $Ru(bpy)_3^{2+}$ or MV^{2+} were omitted from the reaction mixture. The cluster could not act as photosensitizer or electron relay. During the illumination the color of the reaction mixture turned from orange to deep purple, showing that reduced methylviologen, ($MV^{+\cdot}$) was produced. The evolution of hydrogen follows very likely the mechanism shown in figure 6 of chapter 1. The cluster adsorbed on montmorillonite did not have the ability to catalyze the reduction of water by $MV^{+\cdot}$, as does the cluster incorporated into Bovin Serum Albumin[95] or the enzyme hydrogenase.[2] Far from catalyzing hydrogen evolution, the presence of the cluster hindered water reduction. The larger the amount of cluster used, the smaller was the amount of hydrogen produced. The most efficient case was the blank experiment in which no cluster was present. Therefore, we turned our attention to the study of this blank system, in which hydrogen was produced by the irradiation of $Ru(bpy)_3^{2+}$, MV^{2+} and TEOA in the presence of a clay mineral without any other catalysts.

Figure 26 shows the dependence of the amount of hydrogen evolved on the concentration of the clay montmorillonite (curve A) and on the concentration of the electron relay MV^{2+} (curve B) used. In both cases, bell shape curves were obtained. One can see from curve A of figure 26, that only traces of hydrogen were found in the absence of clay. The yield of hydrogen increased with the increase of the clay concentration up to a maximum of 5.6 μmol/L in 20 hours of irradiation, at a clay concentration of 3.3 g per litre of solution. When the clay concentration was increased to 5.0 g per litre, the activity was reduced by a factor of 3. Similarly, the yield of H_2 increased with the concentration of MV^{2+} (see curve B), until a maximum was reached. At higher MV^{2+} concentration, the yield decreased.

The maxima in both cases corresponded to the same conditions, in which the concentration of MV^{2+} was 5.0×10^{-3}M and the clay concentration was 3.3 g/L. In other words, the optimum conditions were those in which the ratio of MV^{2+} to clay was 1.5

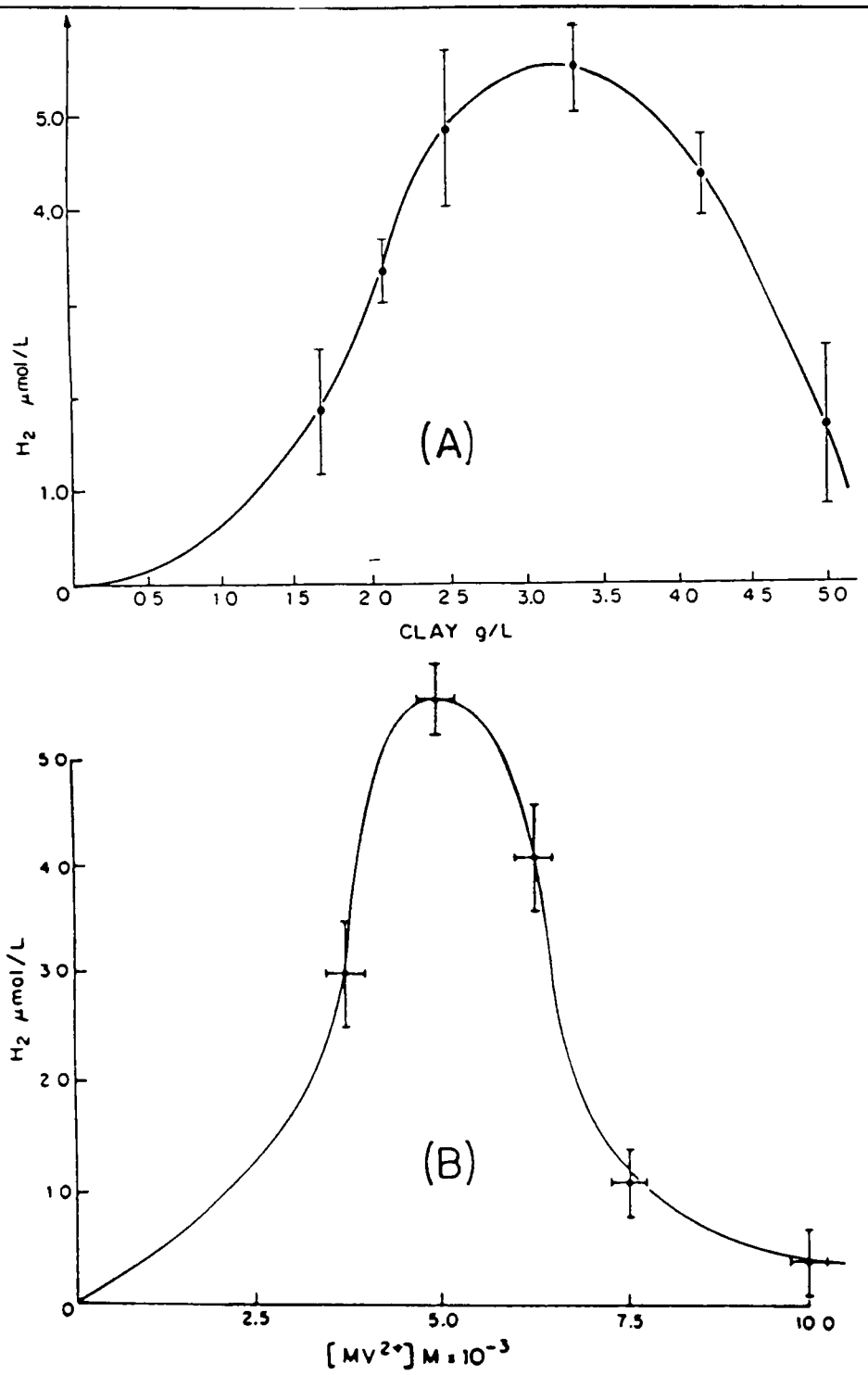

Figure 26: Amount of hydrogen evolved at pH 7.0 after 20 hours of illumination under argon of a system containing TEOA (1.0 x 10^{-1}M) and $Ru(bpy)_3^{2+}$ (5.0 x 10^{-4}M). A) Dependence on concentration of clay with $[MV^{2+}]$ = 5.0 x 10^{-5}M B) Dependence on the concentration of MV^{2+} with [Clay] = 3.3 g/L.

mmol MV^{2+}/g of clay. This is a surprisingly high value, three times higher than the typical cation exchange capacity of montmorillonite.[134] Under optimum conditions the ratio of MV^{2+} to $Ru(bpy)_3^{2+}$ was 10 to 1. As we will see later this value will be important in the interpretation of the dependence of hydrogen production on the concentration of MV^{2+}.

The production of hydrogen was also followed as a function of the concentration of clay and MV^{2+}, when their ratio was kept constant at a value close to the optimum value. (Table 7) Since the concentration of $Ru(bpy)_3^{2+}$ was kept constant, the hydrogen production should increase with an increase in the MV^{2+} concentration. However, the observed hydrogen production depended only slightly upon the quantity of MV^{2+} used in the experiment.

Table 7: Hydrogen production as a function of $[MV^{2+}]$ and [Clay] at a constant ratio MV^{2+}/clay.

$[MV^{2+}]$ $(10^{-3}M)$	[Clay] (g/L)	H_2 (μmol/L)
2.50	1.50	3.9 + 0.5
5.00	3.00	5.4 + 0.6
7.50	4.50	4.3 + 0.7
10.00	6.00	6.3 + 0.7

H_2 production after 20 hours of illumination at pH 7.0 under argon of a system containing $Ru(bpy)_3^{2+}$ ($5.0 \times 10^{-4}M$), TEOA ($1.0 \times 10^{-1}M$), and a MV^{2+}/montmorillonite ratio of 1.67 mmol/g.

The amount of hydrogen produced was directly proportional to the time of irradiation, at least for the first 24 hours.* It was also found that the H_2 production was independent of the cation with which the montmorillonite was saturated prior to its use. In

* Correlation coefficient = 0.96 for 10 points with a slope of 185 nmol/L/hr.

table 8, the amounts of hydrogen evolved using samples of nine different homoionic clays (see section 5.1.4) are shown. No synergistic effect between methylviologen and the interlayer cation was found. The order of magnitude of the hydrogen production was the same as the one observed with the clay, in which the natural distribution of interlayer cations was present. This is consistent, as we will see later, with the ability of MV^{2+} and $Ru(bpy)_3^{2+}$ to displace completely the inorganic cations from the clay interlayer spaces.[135 136]

Table 8: Effect of the associated metal cation on hydrogen evolution in the presence of homoionic clays.

Clay associated metal cation	H_2 (μmol/L)
Cu^{2+}	5.6 ± 0.8
Ni^{2+}	4.8 ± 0.7
Sr^{2+}	4.6 ± 0.7
Zn^{2+}	4.3 ± 0.7
Ca^{2+}	3.8 ± 0.7
Cd^{2+}	2.9 ± 0.7
Mg^{2+}	2.9 ± 0.7
NH_4^+	2.4 ± 0.7
Natural	3.9 ± 0.5

H_2 production after 20 hours illumination under argon at pH 7.0 of a system containing MV^{2+} (2.5×10^{-3}M), $Ru(bpy)_3^{2+}$ (5.0×10^{-4}M), TEOA (1.0×10^{-1}M) and homoionic montmorillonite (1.5 g/L).

Hydrogen evolution was also observed in the presence of two other smectites, namely hectorite and nontronite. In table 9 the efficiency of those two clays is compared with that of montmorillonite. The conditions of the measurements were those for optimum hydrogen production according to figure 26, that is a MV^{2+}/clay ratio of 1.5 mmol per gram and a ratio of $MV^{2+}/Ru(bpy)_3^{2+}$ of 10 to 1. The table also includes the iron con-

tent of the three clays expressed as % Fe_2O_3. There was no correlation between hydrogen evolution efficiency and the clay iron content.

Table 9. Hydrogen production with different clays at pH 7.0

Clay	Fe_2O_3	H_2 (μmol/L)
Nontronite	32.3 %	9.0 ± 0.8
Montmorillonite	4.17 %	5.0 ± 0.6
Hectorite	0.25 %	5.7 ± 0.8

H_2 produced in the presence of the clay at pH 7.0 after 20 hours of illumination under argon, [Clay] = 3.3 g/L, $[Ru(bpy)_3^{2+}] = 5.0 \times 10^{-4}$, $[MV^{2+}] = 5.0 \times 10^{-3}$M, [TEOA] = 1.0×10^{-1}M. Note that in each case the amount of H_2 evolved in the absence of clay was subtracted. (see table 10)

A complete series of blank experiments was performed, in which one of the system components was omitted. (Table 10) Little or no hydrogen was evolved unless all the components of the reaction mixture were present. Also, if the system was not irradiated, but only stirred in the dark for 20 hours, no hydrogen was produced, showing that the reaction was driven by visible light.

Table 10: Results of the blank experiments (pH 7.0).

$[Ru(bpy)_3^{2+}]$ (10^{-4}M)	$[MV^{2+}]$ (10^{-3}M)	[Clay] g/L	[TEOA] (10^{-1}M)	H_2* (μmol/L)
5.0	5.0	3.3	1.0	5.6 ± 0.6
---	5.0	3.3	1.0	--------
5.0	---	3.3	1.0	--------
5.0	5.0	---	1.0	0.6 ± 0.4
5.0	5.0	3.3	---	0.6 ± 0.4

*Hydrogen evolved after 20 hours of illumination under argon.

6.1.2 Hydrogen Evolution at pH 5.3.

The replacement of the pH 7.0 buffer by a pH 4.0 buffer and the sacrificial donor TEOA by ethylenediamine tetraacetic acid (EDTA) lowers the pH of the mixture to 5.3 (see section 5.2.2). The pH did not go down to 4.0 because EDTA (the disodium salt was used) itself acted as a buffer (pk_1 = 2.0, pk_2 = 2.7, pk_3 = 6.2 and pk_4 = 10.3). The first effect of this reduced pH was to increase the rate of hydrogen evolution. The amount of H_2 production in 20 hours of illumination in the presence of montmorillonite at pH 5.3 was 27 μmol/L compared to only 5.6 μmol/L at pH 7.0. The importance of hydrogen produced in the blank experiment, when no clay was used, was also increased, accounting for approximately 40% of the evolved hydrogen (10 μmol/L) compared to only 10% (0.6 μmol/L) at pH 7.0. But, even after correcting for the blanks, the amount of hydrogen evolved at pH 5.3 was still more than three times the amount evolved at pH 7.0. (17 μmol/L vs 5.0 μmol/L)

This is attributed to the increase in the driving force of the reduction of water by $MV^{+\cdot}$. Methylviologen has a pH independent redox potential of -0.445 V.[2] The redox potential needed to reduce water at pH 5.3 is only -0.313 V compared to -0.414 V at pH 7.0. Attributing the increased hydrogen evolution to the increase in the thermodynamic driving force also accounts for the increase in the yield of hydrogen in the blank experiment.

The dependence of the rate of hydrogen evolution on the concentration of MV^{2+} at pH 5.3 was studied (See figure 27). Similarly to the pH 7 experiment, a bell shape curve was obtained. Note that the maximum efficiency was found at the same concentration of MV^{2+} as at pH 7.0. Lowering the pH of the reaction mixture has no effect on the optimum conditions of hydrogen evolution, namely the ratio of MV^{2+} to clay of 1.5 mmol/g and the ratio of MV^{2+} to $Ru(bpy)_3^{2+}$ of 10 to 1. This is taken as an evidence that lowering the pH does not affect the reaction mechanism.

The yields of hydrogen in the optimum conditions, at pH 5.3, in the presence of the clays montmorillonite and hectorite, after 4 and 20 hours of irradiation are compared in table 11. The rate of hydrogen evolution was approximately proportional to the time of irradiation within experimental error. Comparing these results with those of table 9 shows that lowering the pH had a dramatic effect on the relative yield of hydrogen. At pH 7.0 both clays produced approximately the same amount of hydrogen, while at pH 5.3 the efficiency of hectorite was much lower than that of montmorillonite.

If the porphyrin $ZnTMPyP^{4+}$ (see figure 23) was used in place of $Ru(bpy)_3^{2+}$ as photosensitizer, similar yields of hydrogen were found. With a concentration of 4.0 x 10^{-4}M of porphyrin and 3.3 g/L of montmorillonite, 4.8 μmol/L of hydrogen were produced in 4 hours of illumination at pH 5.3 under argon. In this case the blank experiment, in which no clay was used, gave 1.1 μmol/L of hydrogen. After subtraction of this blank 3.7 μmol/L of hydrogen were obtained, due to the presence of the clay with the porphyrin compared to 3.8 μmol/L when $Ru(bpy)_3^{2+}$ was used. (see table 11)

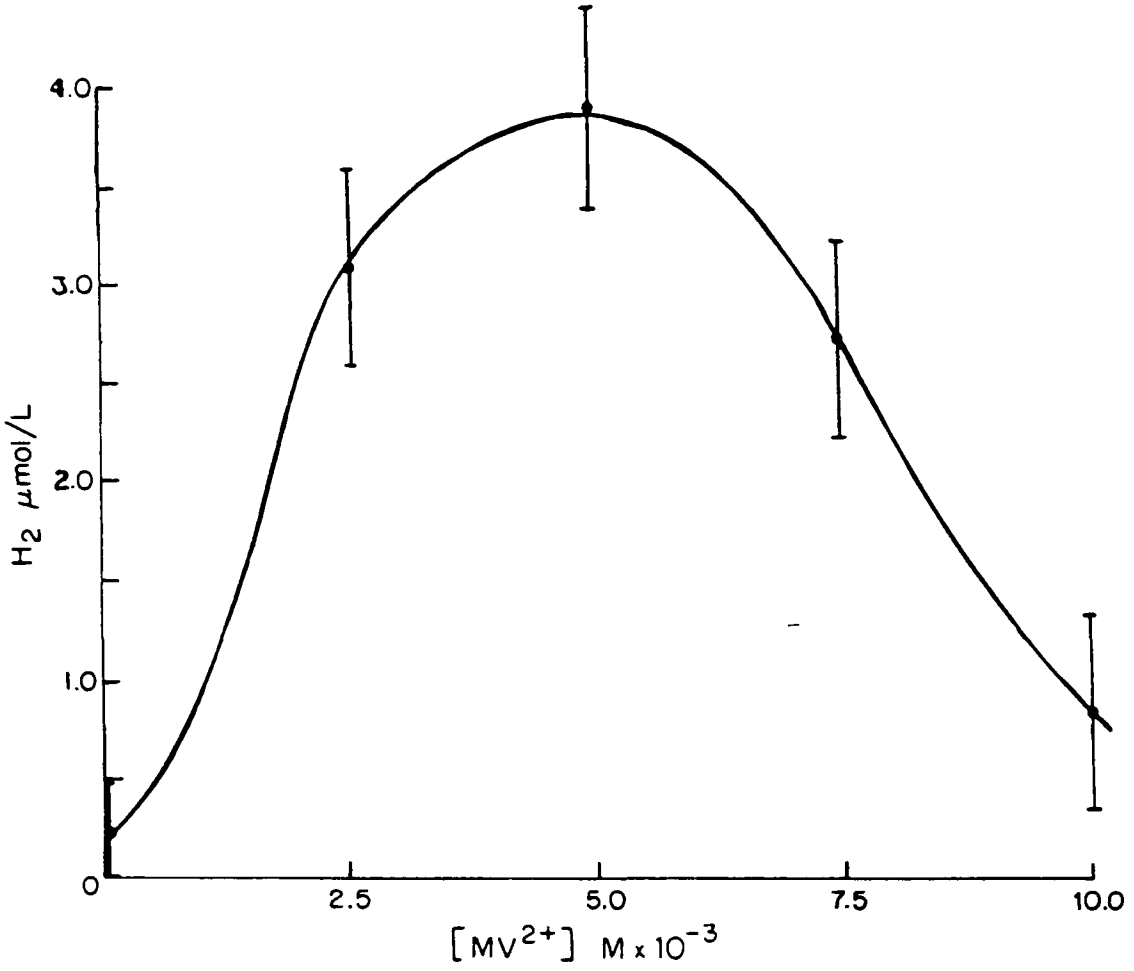

Figure 27: Hydrogen produced as a function of $[MV^{2+}]$ at pH 5.3 after 4 hours of illumination under argon. $[Ru(bpy)_3^{2+}]$= 5.0 x 10^{-4}M, [EDTA]= 1.0 x 10^{-1}M and [clay]= 3.3 g/L. The amounts of H_2 evolved in the absence of the clay were subtracted from each point.

Table 11: Hydrogen production with different clays at pH 5.3

Clay	H_2 µmol/L (4 hrs)	H_2 µmol/L (20 hrs)
Montmorillonite	3.8 ± 0.7	17 ± 1.0
Hectorite	0.5 ± 0.3	4.3 ± 1.0

One further experiment was done using the concentration of reagents found to be optimum for the photoproduction of $MV^{+\cdot}$ by irradiation of $ZnTMPyP^{4+}$ [28] (see section 5.2.2). In that case 7.9 μmol/L of hydrogen were produced in a system containing 2.0 x 10^{-5}M $ZnTMPyP^{4+}$, after 20 hours of illumination, for a turnover with respect to the porphyrin of 79%. This is the highest turnover with respect to the photosensitizer ever obtained. With $Ru(bpy)_3^{2+}$, even after 20 hours of illumination at pH 5.3 in the presence of montmorillonite, the turnover was only about 10%, while at pH 7.0 the turnover after 20 hours was only about 2%. Since the production of H_2 is seen to be linear with time, at least for the first 24 hours, we could achieve a turnover larger than 1 providing the illumination period be long enough. But, since we never tried periods of illumination longer than 24 hours, we cannot say that we have a catalytic system. Hydrogen evolution may not be linear with time for longer irradiation periods.

6.1.3 Dependence of the Yield of H_2 on the Method of Preparation of the Reaction Mixture.

The amount of hydrogen evolved was found to be dependent on the method used in the preparation of the reaction mixtures. In particular the order in which the photosensitizer $Ru(bpy)_3^{2+}$ and the electron relay MV^{2+} were added to be clay suspension had a dramatic effect on the yield of hydrogen. This dependence is illustrated by the results shown in table 12

In the optimum conditions, when $Ru(bpy)_3^{2+}$ was added immediately after MV^{2+}, 7.5 μmol/L of hydrogen were produced. In the absence of clay 3.0 μmol/L of H_2 were evolved. But if $Ru(bpy)_3^{2+}$ was added to the clay suspension 15 minutes after MV^{2+} the yield fell to 4.5 μmol/L and if $Ru(bpy)_3^{2+}$ was added 15 minutes before MV^{2+} then the yield fell to only 1.5 μmol/L. This effect was not observed when $ZnTMPyP^{4+}$ was used instead of $Ru(bpy)_3^{2+}$. With this photosensitizer the yield of H_2 varied only slightly with the order of addition of the reagents.

Table 12: Dependence of the H_2 yield on the method of preparation of the reaction mixtures at pH 5.3.

Conditions	H_2 (μmol/L)
Clay + MV^{2+} + $Ru(bpy)_3^{2+}$	7.5 ± 0.8
MV^{2+} + $Ru(bpy)_3^{2+}$ (no clay)	3.0 ± 0.6
Clay + MV^{2+} + 15 minutes + $Ru(bpy)_3^{2+}$	4.5 ± 0.6
Clay + $Ru(bpy)_3^{2+}$ + 15 minutes + MV^{2+}	1.5 ± 0.5
Clay + MV^{2+} + $ZnTMPyP^{4+}$	4.8 ± 0.6
MV^{2+} + $ZnTMPyP^{4+}$ (no clay)	1.1 ± 0.2
Clay + MV^{2+} + 15 minutes + $ZnTMPyP^{4+}$	6.1 ± 0.7
Clay + $ZnTMPyP^{4+}$ + 15 minutes + MV^{2+}	4.4 ± 0.6

Amounts of H_2 produced after 4 hours of illumination under argon in the presence of 3.3 g/L of montmorillonite. (see text)

The results of a further series of experiment on the effect of the method of preparation of the reaction mixtures are listed in table 13. Under optimum conditions, 5.6 μmol/L of hydrogen were produced. In the absence of clay, only traces of hydrogen were found. When a sample of montmorillonite that had been previously exchanged with MV^{2+} was used instead of the usual clay exchanged with an inorganic cation, no hydrogen was produced. Finally, when sodium dithionate was added to the system to reduce MV^{2+} to $MV^{+\cdot}$ chemically, according to equation 32

$$Na_2S_2O_4 + 8MV^{2+} + 4H_2O \rightarrow Na_2S_2O_8 + 8MV^{+\cdot} + 8H^+ \qquad [32]$$

Table 13: Dependence of the yield of H_2 on the method of preparation of the reaction mixtures at pH 7.0.

Conditions	H_2 (μmol/L)
Clay + MV^{2+} + $Ru(bpy)_3^{2+}$	5.6 ± 0.6
MV^{2+} + $Ru(bpy)_3^{2+}$ (no clay)	0.6 ± 0.4
MV^{2+} - exchanged clay + $Ru(bpy)_3^{2+}$	0
Clay + MV^{2+} + $Na_2S_2O_4$	0

Amounts of H_2 after 20 hours of illumination under argon in the presence of 3.3 g/L of montmorillonite. (see text)

no hydrogen was produced. The function of the clay is not simply the catalysis of water reduction by $MV^{+\cdot}$. The evolution of hydrogen requires the simultaneous presence of both the photosensitizer and MV^{2+} on the clay surfaces.

6.1.4 Evolution of Hydrogen with Colloidal Clay Suspensions.

In all the results reported so far the clay suspensions were flocculated by the addition of the MV^{2+} and $Ru(bpy)_3^{2+}$ solutions. (see section 2.3) To ensure that the clay suspensions did not flocculate it was necessary to reduce the concentration of these two cations in the system. (see section 5.2.2) No hydrogen was detected when such a system was irradiated. If any was produced, it was below the detection limit of the apparatus used for hydrogen analysis. (see section 5.2.3)

Some of these mixtures were submitted to ultrasound. In those cases, hydrogen was detected, but it was attributed entirely to the sonication of the samples. As can be seen from table 14, illumination of the systems after sonication did not result in any increase

in the amount of hydrogen produced. The production of H· and OH· radicals by the action of ultrasound had no effect on the yield of hydrogen. (see discussion)

Table 14: Hydrogen evolution vs. sonication.

Conditions	H_2 (μmol/L)
1 hr. irradiation	0
1 hr. irrad. 1 min. sonication	3.8 ± 0.4
1 hr. irrad. 1 min. sonic 1 hr. irrad.	3.8 ± 0.4
4 min. sonic. 1 hr. in the dark	18 ± 2
4 min. sonic. 1 hr. irradiation	19 ± 2

6.2 Study of the Adsorption of MV^{2+}, $Ru(bpy)_3^{2+}$ and $ZnTMPyP^{4+}$ by Clay Minerals.

6.2.1 Amount of Cation Adsorbed.

Table 15: Formula of the Clays. (< 2.0 μm Ca^{2+} saturated fractions)

Clay	Calculated Formula	Calculated CEC meq/g
Nontronite	$\left[(Si_{3.48}Al_{0.52})^{IV}(Al_{0.13}Fe^{3+}_{1.87}Mg_{0.04})^{VI}O_{10}(OH)_2\right]_2Ca_{0.44}$	0.96
Montmorillonite	$\left[(Si_{3.94}Al_{0.06})^{IV}(Al_{1.58}Fe^{3+}_{0.20}Mg_{0.20})^{VI}O_{10}(OH)_2\right]_2Ca_{0.32}$	0.83
Hectorite*	$\left[(Si_{3.99}Al_{0.01})^{IV}(Al_{0.07}Fe^{3+}_{0.02}Mg_{2.71}Li_{0.04})^{VI}O_{10}(OH)_2\right]_2Ca_{0.28}$	0.67

* Estimated after correction for $CaCO_3$ impurities (see section 5.1.4 d)

The formula of the three clays used in this work, along with their cation exchange capacities (CEC), as calculated from their elemental analysis (see table 5), are listed in table 15.

Table 16: Adsorption by < 2.0 μm Ca^{2+}-Montmorillonite.

Cation	Amount adsorbed (meq/g)	Basal Spacings Measured (Å)	Literature (Å)
Na^+	------	10.7	10.6[131]
$Ru(bpy)_3^{2+}$	0.83 ± 0.04	17.4	18.0[137]
MV^{2+}	0.89 ± 0.04	12.6	12.4[134]
$ZnTMPyP^{4+}$	0.84 ± 0.05	13.4	----

The amounts of MV^{2+}, $ZnTMPyP^{4+}$ and $Ru(bpy)_3^{2+}$ adsorbed by 1.0 gram of montmorillonite are shown in table 16. For all three cations these amounts were found to be equivalent, within experimental error, to the full extent of the cation exchange capacity of the clay, as calculated from the clay elemental composition. For $Ru(bpy)_3^{2+}$ and MV^{2+}, this is in agreement with previous reports on the adsorption of these two cations by montmorillonite.[135 136]

The observed increase in the basal spacings of oriented thin films of montmorillonite exchanged with the three cations, as measured by X-ray diffraction shows that the cations were intercalated in between the layers of the clay. The measured values of the basal spacings agree well with those reported in the literature.

The amounts of MV^{2+} and $Ru(bpy)_3^{2+}$ adsorbed by 1.0 gram of < 2.0 μm Ca^{2+}-hectorite are shown in table 17, along with the basal spacings of oriented films of this clay intercalated with the two cations. Once again they were found to be adsorbed by the clay to the full extent of its calculated cation exchange capacity. Adsorption of these

Table 17: Adsorption by < 2.0 μm Ca^{2+}-Hectorite.

Cation	Amount adsorbed (meq/g)	Basal Spacings (A)
MV^{2+}	0.72 0.05	12.7
$Ru(bpy)_3^{2+}$	0.66 0.05	17.4

two cations increased the basal spacings of hectorite, indicating that they were intercalated. The values of the basal spacings were in good agreement with those of MV^{2+} and $Ru(bpy)_3^{2+}$ intercalated in montmorillonite.

6.2.2 Competitive Adsorption of $Ru(bpy)_3^{2+}$ and MV^{2+} or of $ZnTMPyP^{4+}$ and MV^{2+} by Montmorillonite.

The results of the study of the competitive adsorption of MV^{2+} and $Ru(bpy)_3^{2+}$ by montmorillonite, when the two cations were added to the clay suspension simultaneously (see section 5.3.2), are shown in figure 28. The results of a similar study of competitive adsorption of MV^{2+} and $ZnTMPyP^{4+}$ by montmorillonite are shown in figure 29. In the case of $Ru(bpy)_3^{2+}$ and MV^{2+} (figure 28), a quasi-equal distribution of the cationic species between the two phases was observed. At low $Ru(bpy)_3^{2+}/(MV^{2+} + Ru(bpy)_3^{2+})$ ratios, no preferential adsorption was found. The clay and the water phases contain the same molar ratio in $Ru(bpy)_3^{2+}$ vs. the total concentration of charged organic species. At high $Ru(bpy)_3^{2+}$ concentration a slight preferential adsorption of MV^{2+} was observed.

The situation was different in the case of the simultaneous addition of $ZnTMPyP^{4+}$ and MV^{2+} (figure 29). Except at very low $ZnTMPyP^{4+}/MV^{2+}$ ratios, the clay displayed a large preference for the adsorption of MV^{2+}. For example when the molar fraction of

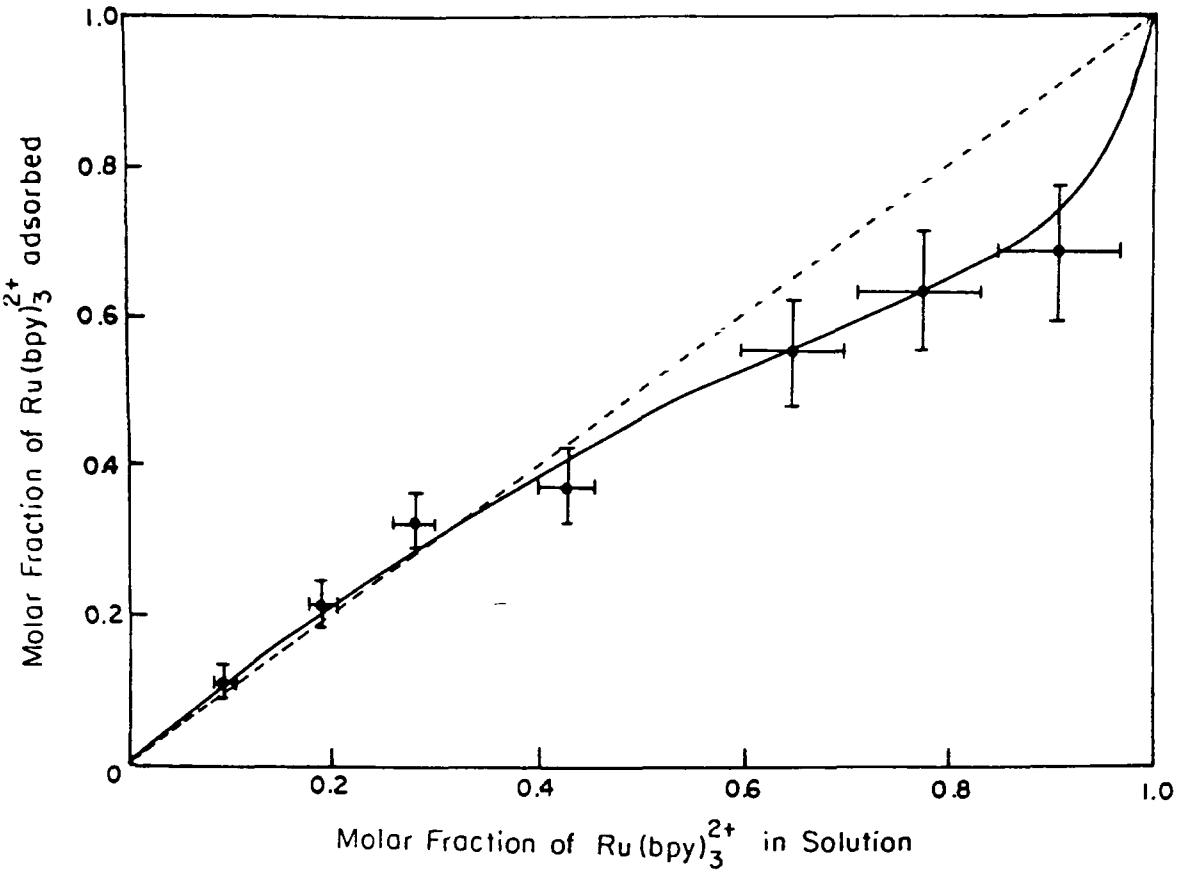

Figure 28: Molar fraction of $Ru(bpy)_3^{2+}$ adsorbed. on clay $[Ru(bpy)_3^{2+}]ads/([Ru(bpy)_3^{2+}]ads + [MV^{2+}]ads)$ as a function of the molar fraction of $Ru(bpy)_3^{2+}$ in solution. (see text)

$ZnTMPyP^{4+}$ in solution was 0.80, the molar fraction of $ZnTMPyP^{4+}$ adsorbed by the clay was only 0.20. In figures 29, 31 and 33, the composition of the adsorbed and solution phases are expressed as the fraction $[ZnTMPyP^{4+}]/[(ZnTMPyP^{4+}] + [MV^{2+}])$ with all the quantities in mole of cations. It turns out that it makes very little difference whether the fractions are expressed as molar fraction of cation or as fraction of cation in number of equivalents, to account for the different charge of the two cations. In both cases, the shape of the adsorption curves are very similar. Using equivalents only shifts the curves upward.

The results were very different when the two cations were not added to the clay suspension simultaneously. Figure 30 shows the results of a study of the competitive

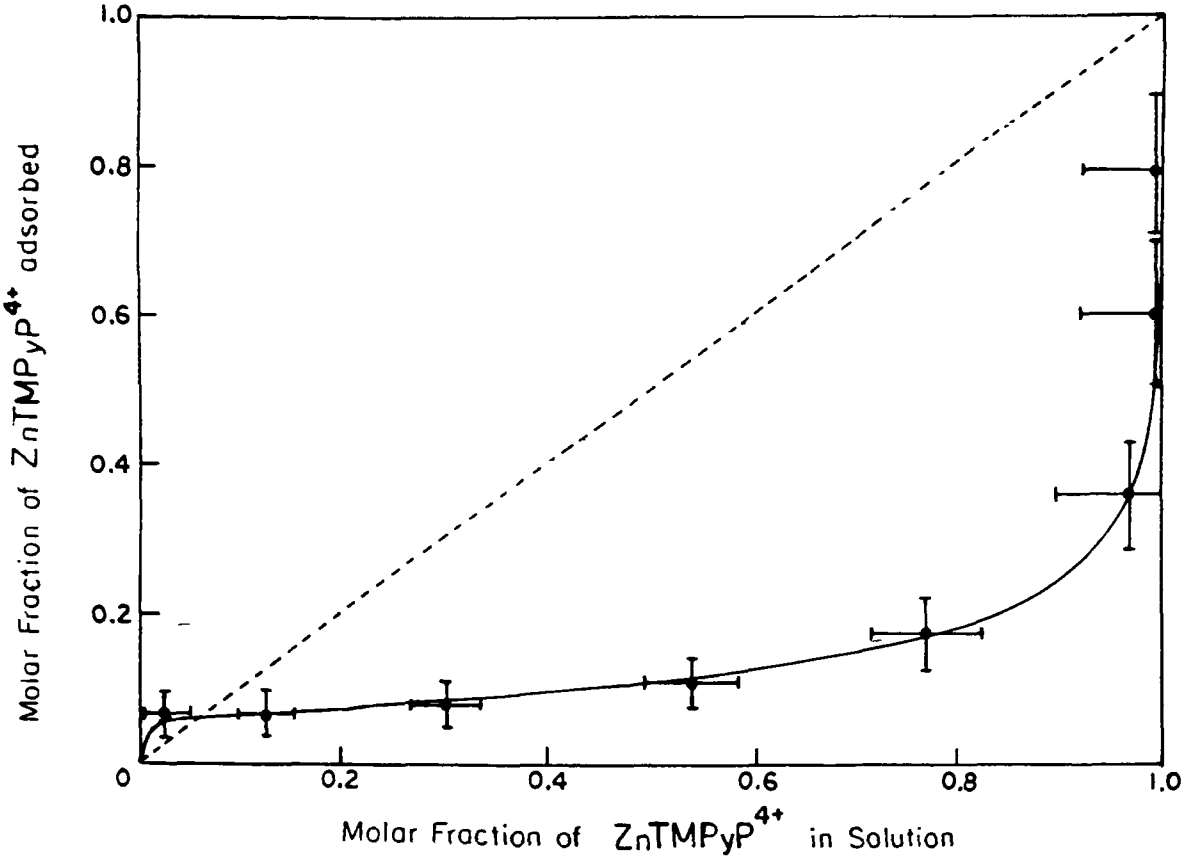

Figure 29. Molar fraction of $ZnTMPyP^{4+}$ adsorbed. $[ZnTMPyP^{4+}]ads/([ZnTMPyP^{4+}ads] + [MV^{2+}]ads)$ on clay as a function of the molar fraction of $ZnTMPyP^{4+}$ in solution. (see text)

adsorption of $Ru(bpy)_3^{2+}$ and MV^{2+} by suspensions of montmorillonite when there was a delay of 30 minutes between the addition of the two cations (see section 5.3.2 b)). When a solution of MV^{2+} was added first (curve A), a large preference for this cation was found. Even for large $Ru(bpy)_3^{2+}/MV^{2+}$ ratios only about 20% of the adsorbed cations were $Ru(bpy)_3^{2+}$. In other words, $Ru(bpy)_3^{2+}$ could only displace a small fraction of the MV^{2+} pre-adsorbed by the clay. When $Ru(bpy)_3^{2+}$ was added first (curve B), MV^{2+} could displace a large fraction of the pre-adsorbed $Ru(bpy)_3^{2+}$, up to about 60%.

Figure 31 shows the results of a similar study on the competitive adsorption of $ZnTMPyP^{4+}$ and MV^{2+} by montmorillonite. Once again the clay adsorbed preferentially the first cation added to the suspension. In both cases, the second cation added could dis-

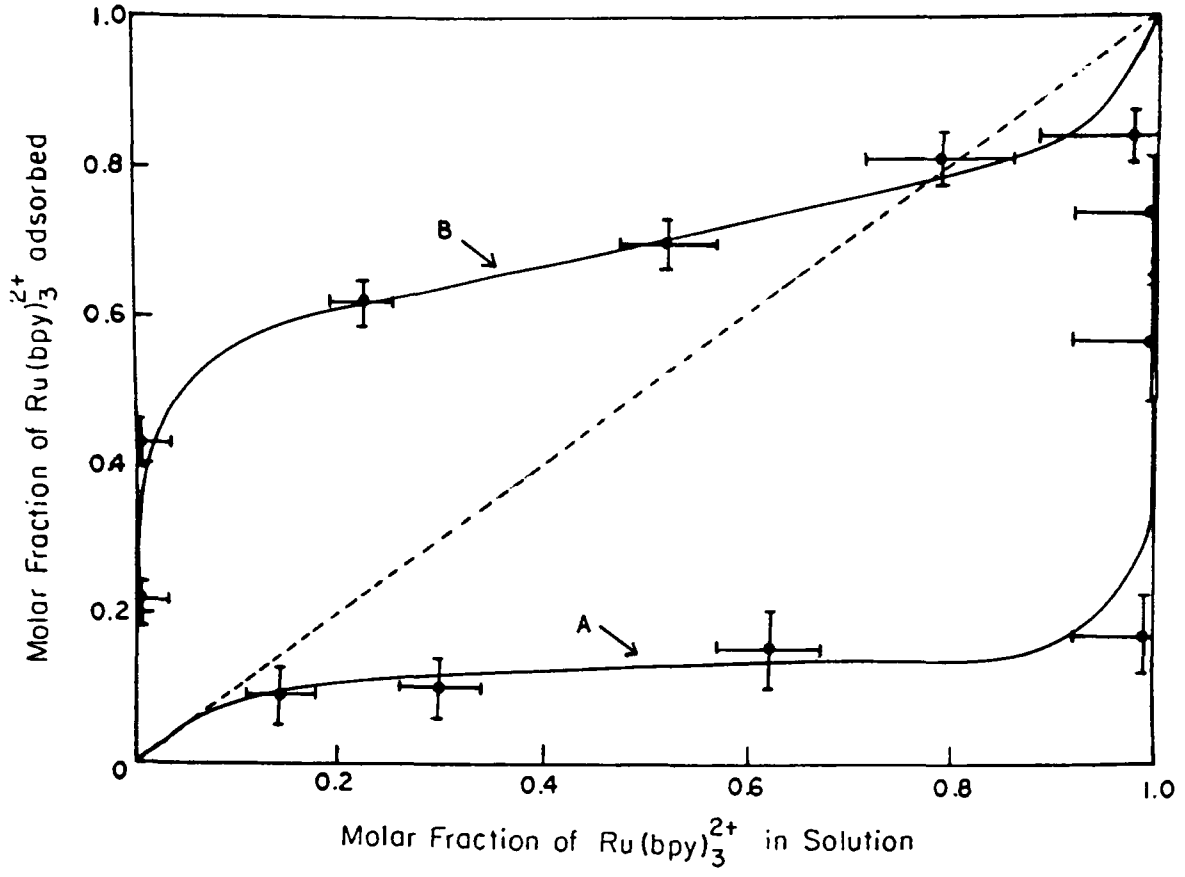

Figure 30: Molar fraction of $Ru(bpy)_3^{2+}$ adsorbed on clay. as a function of the molar fraction of $Ru(bpy)_3^{2+}$ in solution a) MV^{2+} added 30 minutes before $Ru(bpy)_3^{2+}$, b) $Ru(bpy)_3^{2+}$ added 30 minutes before MV^{2+}.

place only approximately 20% of the preadsorbed one. Further, curve A was similar to the one found when both cations were added simultaneously (see figure 29). It appears to make little difference whether or not MV^{2+} was added first or if the two cations were added simultaneously.

In the last type of competitive adsorption studies, whose results are shown in figure 32 and 33, the ability of one cation to replace the other one from the clay was studied for the cases where a solution of one cation was added to a clay previously saturated with the other one. Figure 32 shows the results of adding a solution of $Ru(bpy)_3^{2+}$ to a suspension of homoionic MV^{2+}-montmorillonite (curve A) and of adding a solution of MV^{2+} to a suspension of homoionic $Ru(bpy)_3^{2+}$-montmorillonite (curve B). $Ru(bpy)_3^{2+}$ could dis-

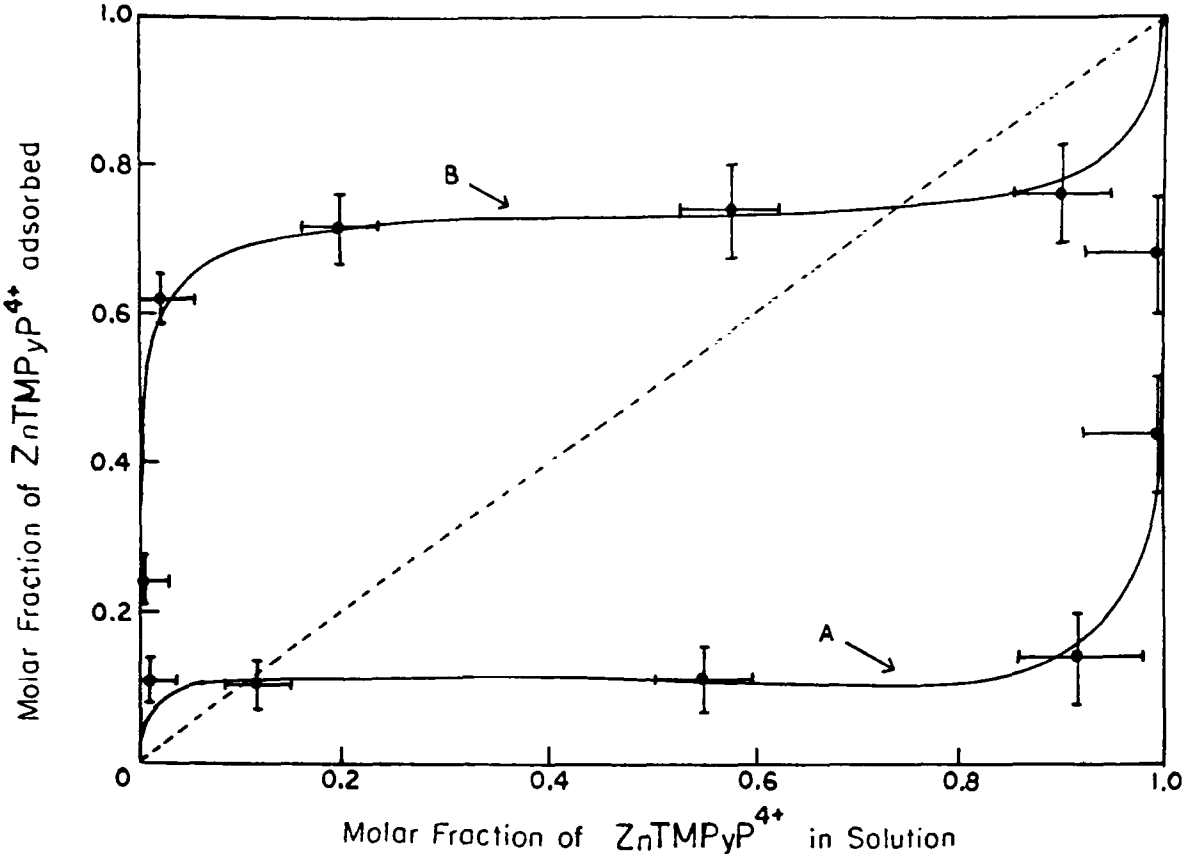

Figure 31: Molar fraction of $ZnTMPyP^{4+}$ adsorbed on clay. as a function of the molar fraction of $ZnTMPyP^{4+}$ in solution a) MV^{2+} added 30 minutes before $ZnTMPyP^{4+}$ b) $ZnTMPyP^{4+}$ added 30 minutes before MV^{2+}.

place only a limited fraction of the MV^{2+} (curve A). Even with a $Ru(bpy)_3^{2+}/MV^{2+}$ ratio equal to 10 only 22% of the MV^{2+} was displaced. The composition of the two phases was similar only at very low $Ru(bpy)_3^{2+}/MV^{2+}$ ratios.

Curve A of figure 32 is almost identical to curve A of figure 30. Using a pre-exchanged clay sample or simply waiting 30 minutes between the addition of the two cations made very little difference in this case. However, when a MV^{2+} solution was added to homoionic $Ru(bpy)_3^{2+}$-montmorillonite (curve B of figure 32) practically no $Ru(bpy)_3^{2+}$ was replaced by MV^{2+}. When the two cations were added to a Ca^{2+}-montmorillonite suspension at 30 minute interval, about 60% of the adsorbed cations were MV^{2+} (see curve B figure 30).

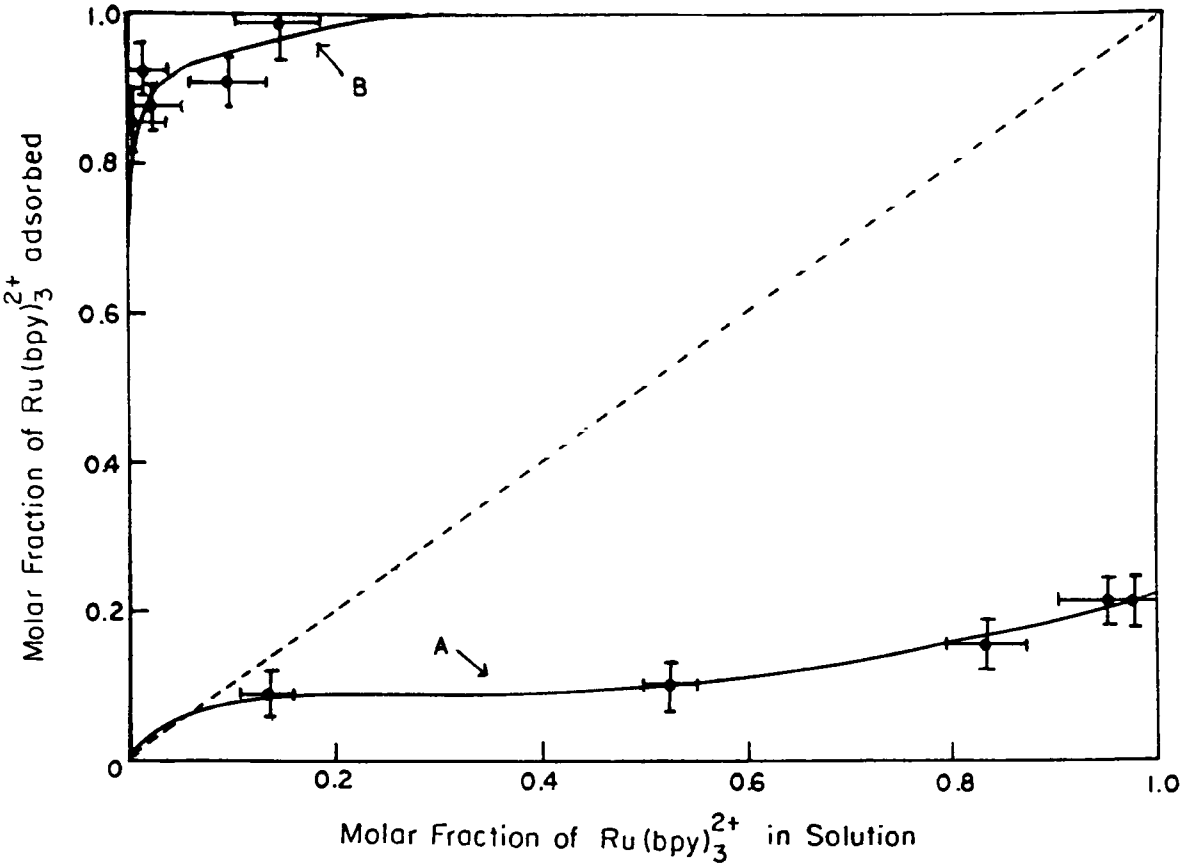

Figure 32: Molar fraction of $Ru(bpy)_3^{2+}$ adsorbed on clay. a) on which MV^{2+} has been previously adsorbed and b) on which $Ru(bpy)_3^{2+}$ has been previously adsorbed, as a function of molar fraction of $Ru(bpy)_3^{2+}$ in solution.

Figure 33 shows the results of the study of the ability of $ZnTMPyP^{4+}$ to displace MV^{2+} from montmorillonite (curve A) and of the ability of MV^{2+} to displace $ZnTMPyP^{4+}$ from montmorillonite (curve B). The results are the same as in figure 32. $ZnTMPyP^{4+}$ could only displace a small fraction of the pre-adsorbed MV^{2+}, less than 20% of the total (curve A), while practically no $ZnTMPyP^{4+}$ was displaced by MV^{2+}. (curve B) Further, curves A of figure 31 and 33 are very similar.

In summary, the clay adsorbed preferentially the first cation added, and even a large excess of the other one could only replace a small fraction of the first incorporated one. This fraction was usually around 20% of the total amount of cation adsorbed by the clay. When MV^{2+} was added first, or when the two cations were added simultaneously, the

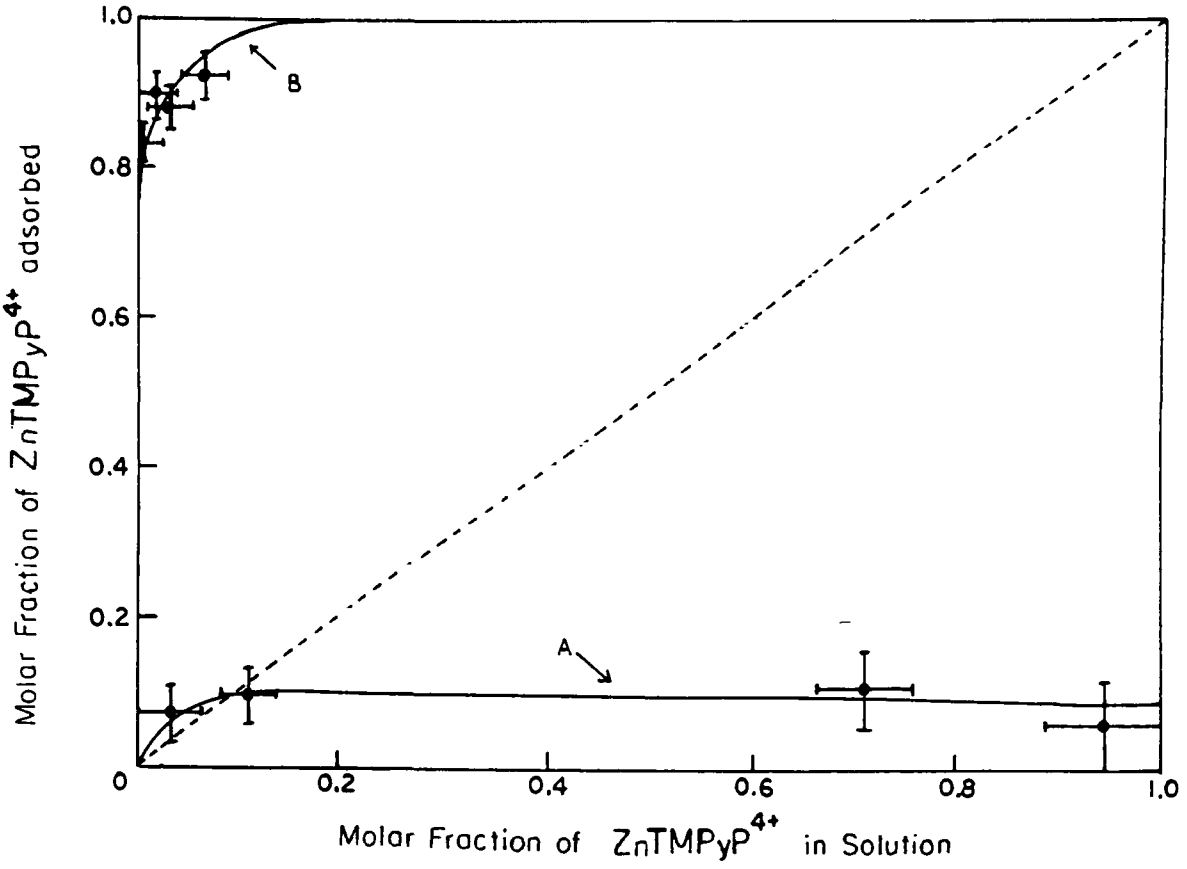

Figure 33: Molar fraction of $ZnTMPyP^{4+}$ adsorbed on clay as a function of molar fraction of $ZnTMPyP^{4+}$ in solution. a) on which MV^{2+} has been previously adsorbed and b) on which $ZnTMPyP^{4+}$ has been previously adsorbed.

composition of the solution and adsorbed phases were similar at a low $Ru(bpy)_3^{2+}/MV^{2+}$ ratio (see figure 28 and curves A of figures 30 and 32). This is important since in the optimum conditions for hydrogen evolution the ratio of $Ru(bpy)_3^{2+}$ to MV^{2+} was 1 to 10 (see figures 26 and 27). Further, under optimum conditions, the ratio of $Ru(bpy)_3^{2+}$ to clay was only 0.15 mmol/g or about 1/3 of the clay exchange capacity, so that according to curve B of figure 30, when $Ru(bpy)_3^{2+}$ was added first, it was fully adsorbed by the clay. This will be used to account for the dependence of the yield of hydrogen on the order of addition of the reagents shown in table 12.

CHAPTER VII

DISCUSSION.

7.1 Reaction on the Clay Surfaces.

The first conclusion that can be drawn from the results reported in chapter 6 is that the reaction leading to photoproduction of hydrogen takes place between species adsorbed on the clay surfaces.

This is shown by the observed increase in the amount of hydrogen produced upon the addition of the clay mineral to the reaction mixtures. Table 10 shows that, at pH 7.0, ten times more hydrogen was evolved when montmorillonite was present than when no clay was used. Similar increases in the amounts of hydrogen were observed upon the addition of nontronite or hectorite to the $Ru(bpy)_3^{2+}$ and MV^{2+} system (see table 9). At pH 5.3, the addition of montmorillonite resulted in an increase in the amount of hydrogen evolved after 4 hours of illumination from 3.0 to 7.5 μmol/L, when $Ru(bpy)_3^{2+}$ was used as photosensitizer, and from 1.1 to 4.8 μmol/L when $ZnTMPyP^{4+}$ was used as photosensitizer. The presence of the clay mineral definitely promoted hydrogen evolution.

Table 8 shows that the cation with which the montmorillonite was initially saturated had very little effect on the amount of hydrogen produced. It is known that inorganic cations, such as those of table 8 are totally displaced from the clay surface by MV^{2+} [135] or $Ru(bpy)_3^{2+}$.[136] This was confirmed by the results shown in tables 16 and 17, which show that both MV^{2+} and $Ru(bpy)_3^{2+}$ were adsorbed by hectorite and montmorillonite to the full extent of the clays cation exchange capacities (CEC) as calculated from the clay formulas (see table 15). The cations originally saturating the clays had lit-

tle effect on the hydrogen yield since they were displaced from the clay phase. Therefore they would not affect a reaction between MV^{2+} and $Ru(bpy)_3^{2+}$ taking place on the clay surfaces. This is what was observed (see table 8).

Locating the electron transfer reaction between MV^{2+} and $Ru(bpy)_3^{2+}$ on the clay surfaces also accounts for the observed effect of the iron-sulfur cluster $[n\text{-}Bu_4N]_2[Fe_4S_4(SPh)_4]$ on the yield of hydrogen (see table 6). The adsorption of this compound, in particular of its $n\text{-}Bu_4N^+$ cations, could interfere with the adsorption of the $Ru(bpy)_3^{2+}$ and MV^{2+} cations by occupying some of the adsorption sites.

7.2 Proposed Mechanism of Hydrogen Evolution.

The observed dependence of the amount of hydrogen produced on the concentration of the clay and on the concentration of the electron relay, MV^{2+}, are consistent with the following hypothesis. The reduction of water comes about via a visible light driven reaction taking place between $Ru(bpy)_3^{2+}$ and MV^{2+} coadsorbed on the external surfaces of the clay. Intercalated cations do not react to give hydrogen, it is only those found on the outside surfaces of the clay particles that are effective in the photoreduction of water.

This hypothesis can be used to account for the dependence of the hydrogen yield on the concentration of MV^{2+}, as well as the effect on changing the order of addition of MV^{2+} and $Ru(bpy)_3^{2+}$, providing that $Ru(bpy)_3^{2+}$ cannot displace clay intercalated MV^{2+} and that MV^{2+} cannot displace clay intercalated $Ru(bpy)_3^{2+}$. We will first show that this is the case by looking at the results of the competitive adsorption measurements of these two cations by montmorillonite.

7.2.1 Adsorption of MV^{2+}, $Ru(bpy)_3^{2+}$ and $ZnTMPyP^{4+}$ by Montmorillonite or Hectorite.

The three cations, MV^{2+}, $Ru(bpy)_3^{2+}$ and $ZnTMPyP^{4+}$ were adsorbed by the clays to the full extent of the clays calculated CEC (tables 15, 16 and 17). In fact, the interactions of the three cations with the clays are very strong, in agreement with the observation that large organic and inorganic cations are more strongly held by clays than are small inorganic cations.[49]

In particular, the interaction of methylviologen (which is a widely used herbicide called paraquat) with soils, including clay minerals, has been studied extensively.[138 139 140] Its enthalpy of adsorption by Na^+-montmorillonite measured by microcalorimetry was -48 kJ/mole. The cation was found to be completely adsorbed by the clay, in an amount equivalent to the clay CEC, in less than 30 minutes.[138] The adsorption isotherm was of the H-type, which indicated a strong preference for the MV^{2+} adsorbate; no free MV^{2+} was found in solution until at least 90% of the clay cation exchange capacity was saturated with MV^{2+}.[135]

Further, MV^{2+} was very difficult to desorb from clays. Only about 5% of the adsorbed cations could be displaced from montmorillonite by 1 M $BaCl_2$.[135] A five fold excess of a dilute chloride salt solutions of Al^{3+}, Ca^{2+}, Mg^{2+} or K^+ could not displace more than 15% of the adsorbed methylviologen from montmorillonite. A similar treatment of vermiculite, an other 2:1 smectite derived from talc (like hectorite, see chapter 2) released up to 70% of the adsorbed MV^{2+}.[141]

$Ru(bpy)_3^{2+}$ is also very strongly held by clay minerals. A hundred fold excess of the anionic micelles SDS could not displace any measurable amounts of $Ru(bpy)_3^{2+}$ from the interlayer spaces of montmorillonite.[64]

From the basal spacings measured on oriented films of the two clays intercalated with MV^{2+} and $Ru(bpy)_3^{2+}$ (table 16 and 17), and from the value of the thickness of a clay layer (9.6 Å[138]), one can calculate interlamellar distances of 3.0 and 7.8 Å for the intercalated methylviologen and $Ru(bpy)_3^{2+}$ cations. These relatively small distances, considering the size of the two cations[142 143] impose a strained adsorption geometry. We propose the geometry shown in figure 34.

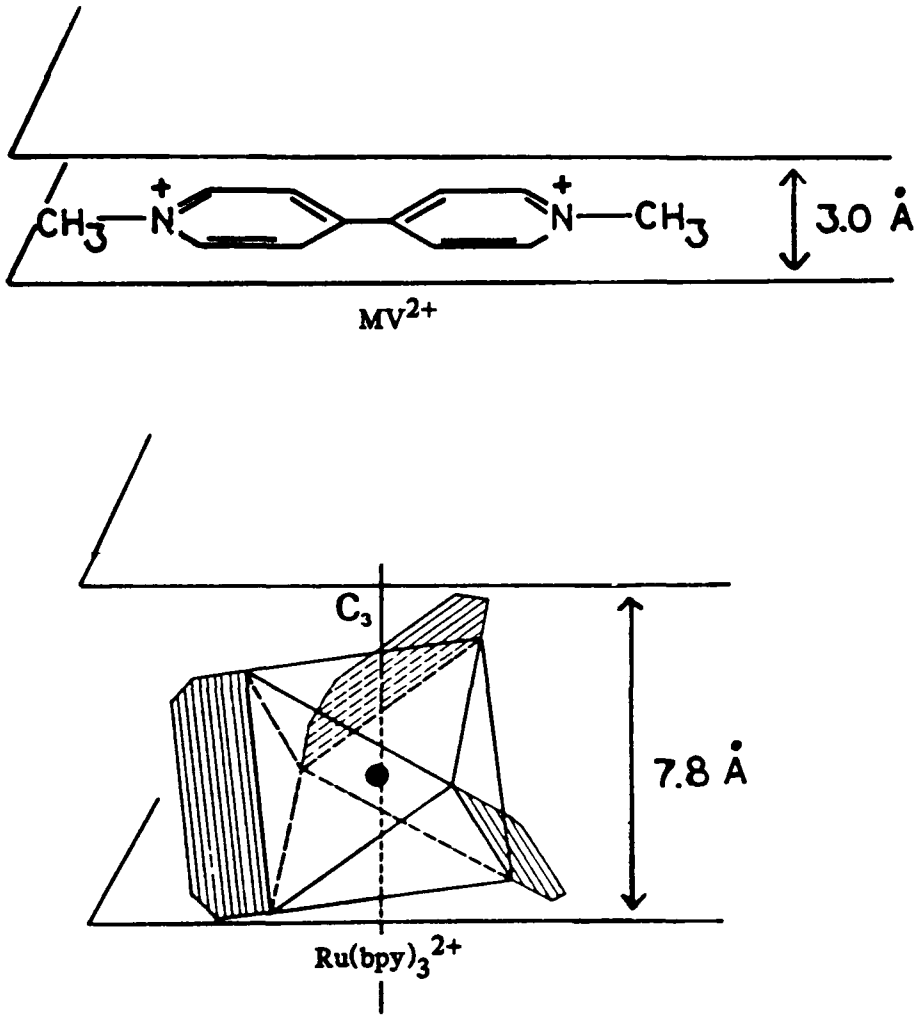

Figure 34: Proposed geometry of MV^{2+} and $Ru(bpy)_3^{2+}$ intercalated in montmorillonite or hectorite.

To fit in an interlayer spacing of only 3.0 Å, MV^{2+} could be adsorbed in a planar configuration with both of its rings parallel to the clay layers. In fact, 3.0 Å is less than the van der Waals thickness of a pyridinium ring. For example, MV^{2+} intercalated into layered metal phosphorus trichalcogenides such as $MnPS_3$, $CdPS_3$ or $FePS_3$ is known to adopt a planar configuration. Yet in those intercalation complexes, the gap between the MPS_3 layers is 3.3 Å.[144] This is not an unknown phenomenon. The interlayer spacings of adsorbed organic molecules are not always compatible with the nominal van der Waals dimensions of the molecules. For instance Greene-Kelly[145] has quoted a spacing of 0.53 nm for aromatic molecules oriented perpendicular to the expanded interlamellar surfaces of montmorillonite, although the nominal width of the hexagonal aromatic structure from van der Waals dimensions is 0.67 nm.[146] The discrepancy may be explained partly by the keying of the molecules into the lattice holes of the clay surfaces and partly by uncertainties in the van der Waals radii of atoms.

Moreover, methylviologen intercalated in montmorillonite has been shown by IR spectroscopy to be adsorbed flat to the clay surfaces.[134] This was not the case for MV^{2+} in vermiculite, where the pyridinium rings were adsorbed at an angle of 35-37° to the clay layers with keying of the molecules into lattice holes. This planar configuration of the adsorbate was used to explain the difference in the enthalpy of adsorption of MV^{2+} and the related cation diquat (1,1'-ethylene 2,2'-bipyridinium, see figure 35). Diquat has a dihedral angle of 19.7°.[147] The lower enthalpy of adsorption, -32 kJ/mole as opposed to -48 kJ/mole for MV^{2+}, may represent the additional energy required to flatten the diquat molecule puckered by its ethylenic bridge.[139]

$Ru(bpy)_3^{2+}$ on the other hand, which is a distorted octahedral cation[142] could be adsorbed as shown in figure 34, in order to fit in an interlayer spacing of only 7.8 Å. The geometry of this adsorbed cation has been studied by IR and XPS spectroscopy in the interlamellar spaces of hectorite.[148] It was shown that the planes of the three bipyridyl

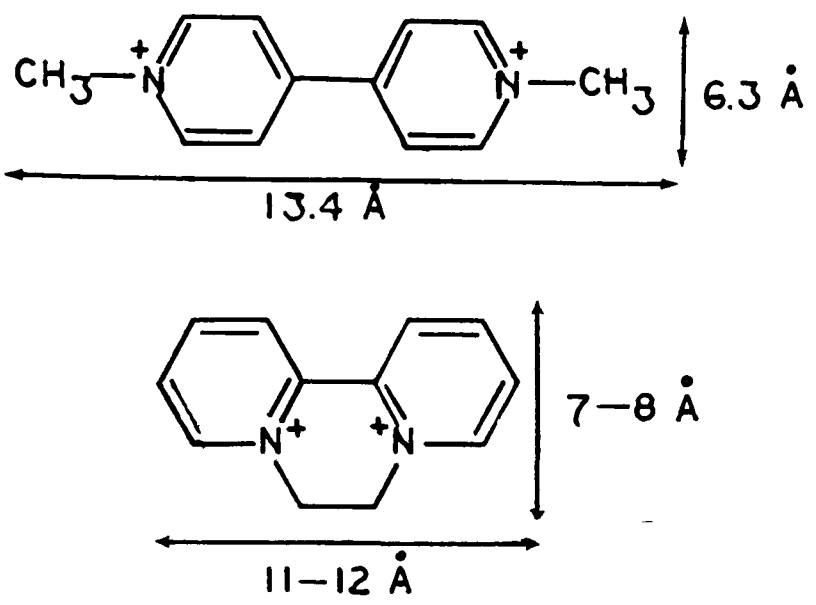

Figure 35: Structure and surface area of MV^{2+} and diquat in planar configurations.

ligands of the cation made an angle of 60^{0} with the plane of the clay layers, that two of the triangular faces of $Ru(bpy)_3^{2+}$ were parallel to the clay layers and that the cation pseudo threefold axes of symmetry was perpendicular to the clay layers.

An interesting effect of the intercalation of larger organic cations is their ability to alter the clay swelling ability[49] (see section 2.5). In particular, methylviologen has been found to destroy the swelling ability of montmorillonite. Knight and Denny[149] found that fully saturated MV^{2+}-montmorillonite complexes could not be expanded by ethylene glycol, although some expansion was evident for partially saturated complexes. The intercalation of MV^{2+} collapsed the lamellae of montmorillonite, the water molecules associated with the inorganic cations being expulsed. This collapse was not observed in wet vermiculite methylviologen complexes. There, the basal spacings of a wet film were 14.5 Å, they decreased to 12.7 Å when the film was dried. In MV^{2+}-montmorillonite complexes, drying the films only changed the basal spacings from 12.6 to 12.5 Å.[138 139]

This difference between the two clays was attributed to the energy needed to displace adsorbed water molecules. In vermiculite the surface charge comes mainly from isomorphous substitutions in the tetrahedral sheets of the clay (see section 2.2). Due to the proximity of the negative charge sites to the adsorption sites, the hydration forces operating in vermiculite are larger than in montmorillonite, where the charge is due mainly to octahedral substitution. The adsorption energy of MV^{2+} by the clay is enough to displace water from montmorillonite but not from vermiculite.

Still, even in the collapsed clay, the water was not fully displaced. Considering the surface covered by one planar MV^{2+} cation (see figure 35) and the number of cations adsorbed by 1.0 g of clay (see table 16), one can calculate that even for a montmorillonite completely saturated by MV^{2+} the cation covers only about 60% of the available surface (assuming monolayer coverage and taking the surface area of the clay to be 750 m^2/g). $Ru(bpy)_3^{2+}$ covers a larger fraction of the surface, but its larger interlayer spacings could allow for more than one partial layer of adsorbed water molecules.

Finally, the collapse of the clay layers upon intercalation of methylviologen is the process to which we will attribute the increase in the intensity of the fluorescence of MV^{2+} in the presence of a clay suspension. (see chapters 8, 9 and 10)

7.2.2 Competitive Adsorption of Two Cations.

When MV^{2+} and $Ru(bpy)_3^{2+}$ were added simultaneously to the clay, no preferential adsorption was found (see figure 28), except at high $Ru(bpy)_3^{2+}$ molar fractions where a small preferential adsorption of MV^{2+} was observed. The result is in agreement with the strong interaction between the clay and the two cations discussed in the previous section. The small preference for MV^{2+} at high $Ru(bpy)_3^{2+}$ molar fraction can be attributed to the collapse of the clay layer induced by the intercalation of methylviologen.[138 139] The resulting interlayer spacings of 3.0 Å are too small to allow the entry of $Ru(bpy)_3^{2+}$ cations.

$ZnTMPyP^{4+}$ was expected to interact strongly with the clay surface because of it 4+ charge. Still a preference for MV^{2+} was observed (figure 29). In fact the results of the competitive adsorption of MV^{2+} and $ZnTMPyP^{4+}$ by montmorillonite, when the two cations were added together were very similar to those obtained when MV^{2+} was added 30 minutes before $ZnTMPyP^{4+}$ (figure 31 curve A). Further MV^{2+} is known to be adsorbed very rapidly by clay minerals.[138] Therefore we attributed the strong preferential adsorption of MV^{2+} (figure 29) to the speed of intercalation. The MV^{2+} being adsorbed more rapidly, it occupied the majority of the interlayer sites before $ZnTMPyP^{4+}$ could be intercalated.

It made very little difference on the amounts of the two cations that were adsorbed by montmorillonite, whether $Ru(bpy)_3^{2+}$ was added to a clay suspension 30 minutes after MV^{2+}, or $Ru(bpy)_3^{2+}$ was added to a suspension of montmorillonite that had been previously completely exchanged with MV^{2+} (see curves A of figures 30 and 32). Two conclusions can be drawn from these two curves. First, since the two curves were very similar, adsorption of MV^{2+} by montmorillonite was complete within 30 minutes. It made no difference whether $Ru(bpy)_3^{2+}$ was added 30 minutes after MV^{2+} or several hours later. This confirms the rapidity of the intercalation of MV^{2+} in montmorillonite.[138] Second, $Ru(bpy)_3^{2+}$ could only displace a limited fraction of the pre-adsorbed MV^{2+}. Even a ten fold excess of $Ru(bpy)_3^{2+}$ displaced a maximum of only 22% of the pre-adsorbed MV^{2+}.

The fraction of MV^{2+} that could not be displaced from montmorillonite, 78% of the adsorbed cation, was in agreement with the reported strong adsorption capacity (SAC) of montmorillonite for MV^{2+}, 76% of the clay CEC.[140] The SAC is defined as the fraction of the clay CEC below which MV^{2+} can no longer be detected in solution after centrifugation of the clay mineral. We propose that the SAC value corresponds to the fraction of the adsorbed MV^{2+} that was intercalated between two layers of montmorillonite. The remainder, the 22% that could be displaced by $Ru(bpy)_3^{2+}$, is assumed to be MV^{2+} cations

that were adsorbed on the external surfaces of the clay particles. This proposal is supported by the fraction of the surface area in a montmorillonite suspension that was reported to be external surface area in the literature. Tennakoon et al[66] has reported that 30% of the surface area of a Na^+ exchanged montmorillonite were outside surfaces and that those external surfaces accounted for 33% of the clay cation adsorption capacity. Finally, as it will be seen in chapter 11, "the interlayer CEC" of montmorillonite, defined as the quantity of cation that can be intercalated by 1.0 gram of clay, measured by X-ray diffraction, was found to be of the order of 80% of the total CEC measured by cation exchange.

The reason why $Ru(bpy)_3^{2+}$ could not displace intercalated MV^{2+} could be due to the collapse of the clay layer caused by the intercalation of this cation (see previous section). Methylviologen intercalated montmorillonite was characterized by a stable interlayer spacing of 3.0 Å. The clay could not swell to accommodate $Ru(bpy)_3^{2+}$ cations which required a spacing of 7.8 Å. The $Ru(bpy)_3^{2+}$ cations could only compete with MV^{2+} for the external adsorption sites. In fact it appears that the clay had a preference for $Ru(bpy)_3^{2+}$ over MV^{2+} in those outside sites. For low $Ru(bpy)_3^{2+}$ molar fractions, both figures 30 and 32 (curves A) show that the ratio of MV^{2+} and $Ru(bpy)_3^{2+}$ adsorbed were similar to the molar fraction of the two cations in solution. Since the interlayer spaces contained almost exclusively MV^{2+}, the ratio of $Ru(bpy)_3^{2+}$ to MV^{2+} on the external surfaces must have exceeded the ratio of $Ru(bpy)_3^{2+}$ to MV^{2+} in solution.*

This can be used to explain the results shown in curve B of figure 32. When MV^{2+} was added to a suspension of montmorillonite that had been previously completely exchanged with $Ru(bpy)_3^{2+}$, MV^{2+} was not able to displace any significant amount of pre-adsorbed $Ru(bpy)_3^{2+}$ from the clay. Not only was MV^{2+} unable to replace intercalated $Ru(bpy)_3^{2+}$, it also had great difficulty displacing $Ru(bpy)_3^{2+}$ from the external surfac-

* The first point of curve A of figure 32 shows that the fraction $[Ru(bpy)_3^{2+}]/([Ru(bpy)_3^{2+}]+[MV^{2+}])$ in solution is 0.14. Taking the fraction of externally adsorbed cations to be 22% of the clay CEC and assuming that all the $Ru(bpy)_3^{2+}$ adsorbed were adsorbed on the external surfaces, the fraction $[Ru(bpy)_3^{2+}]/([Ru(bpy)_3^{2+}]+[MV^{2+}])$ on the external surfaces was 0.4.

es of the clay. As for the difference between the results of figure 30 B from those of figure 32 B, they can be attributed to the speed of adsorption of the two cations. Even after a delay of 30 minutes, adsorption of $Ru(bpy)_3^{2+}$ was not complete, so that MV^{2+} could occupy a larger fraction of the sites, up to 60%, than it would if the delay between the addition of $Ru(bpy)_3^{2+}$ and MV^{2+} had been longer.

The two curves of figure 31 are symmetric. In both cases the second cation added could only replace about 20% of the first one whether it was MV^{2+} or $ZnTMPyP^{4+}$. Again this shows that only the cations adsorbed on the external surfaces of the clay could be desorbed by the addition of the other cation. Finally, figure 33 shows that the clay had a preference for $ZnTMPyP^{4+}$ on its outside surface. MV^{2+} could not displace the externally adsorbed porphyrin. This was expected, since the 4+ charge of the porphyrin should make its interaction with the clay surface very strong.

7.2.3 Dependence of the Yield of Hydrogen on the Concentrations of MV^{2+} and Clay.

The result of the study of the competitive adsorption of MV^{2+} and $Ru(bpy)_3^{2+}$ by montmorillonite can be used to interpret the dependence of the amount of hydrogen evolved on the concentration of the electron relay, MV^{2+}, and of the clay used (figure 26). It can also show why the optimum efficiency was found at a concentration of MV^{2+} of 5.0×10^{-3} M when the concentration of clay was 3.3 g/L.

What is the effect of changing the order of addition of MV^{2+} and $Ru(bpy)_3^{2+}$? The conditions used for the experiment of Table 12 were those that gave the maximum amount of hydrogen according to figure 26. That is, the ratio $MV^{2+}/Ru(bpy)_3^{2+}$ was 10 and the ratio MV^{2+}/clay was 1.5 mmol/g. In other words, the ratio $Ru(bpy)_3^{2+}$/clay was 0.15 mmol/g, which was only 36% of the total amount of $Ru(bpy)_3^{2+}$ the clay could adsorb (see Table 17). Therefore, when $Ru(bpy)_3^{2+}$ was added 15 minutes before MV^{2+} it

was fully intercalated in the clay, as shown by figure 30 (curve B). MV^{2+} which could not replace pre-adsorbed $Ru(bpy)_3^{2+}$ will then occupied the remaining interlayer sites and all the external adsorption sites. No $Ru(bpy)_3^{2+}$ was adsorbed on the clay outside surfaces. In this case, Table 12 shows that only 1.5 μmol/L of hydrogen were produced, which was only half the amount obtained when no clay was used. When $Ru(bpy)_3^{2+}$ was added first, the presence of the clay actually hindered the photogeneration of hydrogen. This is understandable since we proposed that evolution of hydrogen results from the reaction of excited $Ru(bpy)_3^{2+}$ with MV^{2+} on the clay external surfaces. We have shown that in this case there was almost no $Ru(bpy)_3^{2+}$ adsorbed on the clay outside surfaces, only MV^{2+}. The presence of the clay in this case reduced the amount of contact between the two reagents.

A possible interpretation for the fact that intercalated cations do not react to give hydrogen could be the ability of the clay to segregate MV^{2+} from $Ru(bpy)_3^{2+}$. To explain the very inefficient quenching of excited $Ru(bpy)_3^{2+}$ by MV^{2+} in a suspension of hectorite compared to the quenching in water (k_q in Na-hectorite = 1.1 x $10^6 M^{-1}s^{-1}$, k_q in H_2O = 3.0 x $10^8 M^{-1}s^{-1}$), Bard and his group[150] proposed that $Ru(bpy)_3^{2+}$ and MV^{2+} were segregated by the clay. That is to say, in one particular interlayer space only one cationic species and not a homogeneous mixture of the two cation was found. This implies that there was very little contact between the two intercalated cations. As will seen in chapter 11, we have confirmed the existence of this segregation by X-ray diffraction measurements.

When MV^{2+} was added 15 minutes before $Ru(bpy)_3^{2+}$ the amount of hydrogen produced was 4.5 μmol/L (see Table 12). The maximum yield, 7.5 μmol/L was obtained when $Ru(bpy)_3^{2+}$ was added immediately after MV^{2+}. In both cases, since MV^{2+} was added in approximately three fold excess of the clay cation exchange capacity and since adsorption of MV^{2+} was very rapid, the clay interlayer spaces were practically saturated

by MV^{2+} prior to the addition of $Ru(bpy)_3^{2+}$. Since $Ru(bpy)_3^{2+}$ was capable of displacing pre-adsorbed MV^{2+} from the clay outside surfaces, there was a competition between the photosensitizer and the excess of MV^{2+} for those outside surface sites. This was the situation in which photogeneration of hydrogen was the most efficient.

When a solution of $Ru(bpy)_3^{2+}$ was added to a clay that had been pre-exchanged with MV^{2+}, no hydrogen was produced (Table 13). Unlike the previous system, here there was no excess of MV^{2+} in solution. $Ru(bpy)_3^{2+}$ displaced all the surface adsorbed methylviologen since there was no MV^{2+} in solution to compete for those sites, and the clay adsorbed $Ru(bpy)_3^{2+}$ preferentially in those sites. As a result, the clay interlayer spaces were saturated with MV^{2+} while the surface sites were saturated with $Ru(bpy)_3^{2+}$. There was very little contact between the adsorbed cations.

To recapitulate, in the first case the external surfaces of the clay were saturated with MV^{2+}, while $Ru(bpy)_3^{2+}$ and some MV^{2+} were intercalated. Only a small amount of hydrogen was produced. In the third case MV^{2+} was intercalated, while the external surfaces were saturated with $Ru(bpy)_3^{2+}$. No hydrogen was produced. It is only in the second case when both MV^{2+} and $Ru(bpy)_3^{2+}$ were coadsorbed on the clay external surfaces that the presence of the montmorillonite significantly enhanced the rate of hydrogen evolution.

When $ZnTMPyP^{4+}$ was used instead of $Ru(bpy)_3^{2+}$ as photosensitizer, the yield of hydrogen was much less dependent on the order of addition of MV^{2+} and $ZnTMPyP^{4+}$. This could be attributed to two factors. First, the relative amounts of the two cations adsorbed were similar whether MV^{2+} was added first or the two cations were added simultaneously (see figure 29 and 31). The relative amount of cations adsorbed by montmorillonite was not as sensitive to the order of addition of the two cations. Second, we are not aware of any report of segregation of $ZnTMPyP^{4+}$ and MV^{2+} by clay minerals. There may still be a significant amount of contact between the cations even in the clay interlay-

er spaces, so that with the porphyrin, hydrogen evolution may not be limited to a reaction of surface adsorbed cations, but could also come from electron transfer between intercalated cations.

The results of the competitive adsorption measurements of MV^{2+} and $Ru(bpy)_3^{2+}$ could account for the dependence of the rate of hydrogen evolution on the concentration of MV^{2+} observed in figures 26 and 27. The ratio $MV^{2+}/Ru(bpy)_3^{2+}$ at the maximum of the two figures was 10. At such a low molar fraction of $Ru(bpy)_3^{2+}$ figures 28, 30 and 32 show that the relative amounts of the two cations adsorbed by the clay were similar to the relative amounts of the two cations in solution. In other words, one $Ru(bpy)_3^{2+}$ cation was adsorbed for each ten MV^{2+} cations adsorbed. It has been established that about 22% of the cations adsorbed by montmorillonite were located on the external surfaces of the clay.[38] Further, since $Ru(bpy)_3^{2+}$ was the second cationic species added during the preparation of the reaction mixtures, the results of the competitive adsorption study show that it was almost exclusively adsorbed on the clay external surfaces. Therefore, under the conditions of optimum hydrogen evolution, $Ru(bpy)_3^{2+}$, which accounts for approximately 10% of the cations adsorbed by the clay, was found only on the external surfaces. Since those surfaces adsorbed approximately 20% of the total number of cations adsorbed, in the optimum conditions the ratio of MV^{2+} and $Ru(bpy)_3^{2+}$ on the external surfaces was about 1 to 1.* In fact the amounts of $Ru(bpy)_3^{2+}$ and MV^{2+} adsorbed by the clay were measured in an actual water photoreduction reaction mixture, 0.11 meq/g of $Ru(bpy)_3^{2+}$ were adsorbed out of a total of 0.90 meq/g which correspond to the expected value (10%).

*More precise calculation based on the numbers above afforded a ratio $MV^{2+}/Ru(bpy)_3^{2+}$ adsorbed on the external surfaces of 1.4. The same amount of $Ru(bpy)_3^{2+}$ and MV^{2+} were coadsorbed on the external surfaces of the clay when the ratio between the total amounts of MV^{2+} and $Ru(bpy)_3^{2+}$ was 8. Given the precision of our measurements and the assumptions made in the calculation, the agreement between the observed maxima of the curves in figures 26 and 27 and the calculated number is excellent.

The bell shape curves found in figures 26 and 27 could then be attributed to variations of the ratio of MV^{2+} and $Ru(bpy)_3^{2+}$ adsorbed on the external clay surfaces. When the concentration of MV^{2+} was increased by a factor of 2, the ratio MV^{2+} to $Ru(bpy)_2^{3+}$ on the external surfaces was close to 3 to 1 and, more importantly, the amount of $Ru(bpy)_3^{2+}$ adsorbed by the clay was reduced by half. The yield of hydrogen fell accordingly. When the concentration of MV^{2+} was decreased, the outside surfaces became saturated with $Ru(bpy)_3^{2+}$, with very little coadsorbed MV^{2+} and although the absolute amount of $Ru(bpy)_3^{2+}$ adsorbed increased, the yield of hydrogen fell because the quenching of excited $Ru(bpy)_3^{2+}$ by MV^{2+} became very inefficient.

The dependence of the rate of hydrogen evolution on the clay concentration was also studied (see figure 32). At low clay concentrations the rate of hydrogen evolution first increased with an increase of the clay concentration since the amount of cation adsorbed also increased. The ratio of MV^{2+} to $Ru(bpy)_3^{2+}$ adsorbed did not change since the total concentrations of MV^{2+} and $Ru(bpy)_3^{2+}$ were kept constant. However, when more clay was added, a larger fraction of the adsorbed $Ru(bpy)_3^{2+}$ was screened by other clay particles. The decrease of light intensity reaching the $Ru(bpy)_3^{2+}$ cations became more important than the increase in the number of $Ru(bpy)_3^{2+}$ adsorbed by the clay. Accordingly, the yield of hydrogen fell at high clay concentration.

7.3 Function of the Clay Mineral.

The ways by which a solid support could affect the evolution of hydrogen were described in chapter 3. First, the clay could provide a surface on which adsorbed H atoms could be produced or sites in which electrons could be accumulated. The clay could also promote electron transfer between excited $Ru(bpy)_3^{2+}$ and MV^{2+}. Finally, the clay could prevent charge recombination.

7.3.1 Catalysis of Water Reduction.

The clay could possibly act as a catalyst for the reduction of water by $MV^{+\cdot}$, fulfilling the function of colloidal platinum[23] or the enzyme hydrogenase.[26] In other words the clay could provide sites in which electrons can be accumulated or surfaces on which H atoms could be produced.

But taking into account one of the results listed in table 13, which shows that no hydrogen was produced when MV^{2+} was reduced to $MV^{+\cdot}$ chemically, by the addition of $Na_2S_2O_4$, in the presence of montmorillonite, one sees that the function of the clay was not simply the catalysis of water reduction by $MV^{+\cdot}$. In the absence of visible light irradiation, no hydrogen was evolved even when $Ru(bpy)_3^{2+}$ was added to the system. Not only was the simultaneous presence of $Ru(bpy)_3^{2+}$ and MV^{2+} on the surface needed, but also visible light irradiation.

This was a very surprising result. After all, even if the function of the clay was not the catalysis of water reduction, but the promotion of charge separation, this leads to more efficient production of $MV^{+\cdot}$! The quantitative reduction of MV^{2+} by $Na_2S_2O_4$ should still give the same amount of hydrogen. It should not make any difference whether $MV^{+\cdot}$ is produced photochemically or via a chemical reaction.

One possibility is that clay mediated photoproduction of hydrogen does not involve reduction of water by $MV^{+\cdot}$, but proceeds via a mechanism other than that of figure 6. The production of $MV^{+\cdot}$, as indicated by the purple color of the reaction mixture, would then be only a side reaction that does not produce hydrogen.[151] However, this cannot be the case since hydrogen was not produced in the absence of MV^{2+} (Table 10).

An alternative interpretation may lie in the variation of the positive charges of the coadsorbed MV^{2+} and $Ru(bpy)_3^{2+}$ cations. When MV^{2+} was reduced with $Na_2S_2O_4$ before its addition to the clay suspension, the clay adsorbed $MV^{+\cdot}$ and not MV^{2+}. In a

reaction mixture where MV^{2+} was reduced prior to its addition to the clay 0.90 mmol/g of methylviologen was adsorbed, while only 0.45 mmol/g of MV^{2+} was adsorbed when the cation was not reduced (i.e. 0.89 meq of MV^{2+} per gram of clay). This is normal since a clay adsorbs the fixed number of equivalents of a cation that it needs to cancel its surface charge. Twice as many methylviologen cations were adsorbed when they were reduced from 2+ to 1+. It means that each time an adsorbed $MV^{+\cdot}$ cation was oxidized to MV^{2+}, as it must be to reduce water (see equation [11]), an adsorbed $MV^{+\cdot}$ cation had to be desorbed in order to accommodate the extra positive charge of the oxidized methylviologen. Or, since two electrons were needed to produce a molecule of hydrogen, two $MV^{+\cdot}$ had to react, giving two MV^{2+} cations, one of which was desorbed. Extra energy was needed to overcome the strong adsorption energy of MV^{2+}[139] (ΔH_{ad}= -48 kJ/mole). In the photochemical transfer of electrons between MV^{2+} and excited $Ru(bpy)_3^{2+}$ no such desorption was required. The electron transfer produced adsorbed $Ru(bpy)_3^{3+}$ and $MV^{+\cdot}$. The total charge was still 4+. When $MV^{+\cdot}$ was oxidized to give hydrogen, $Ru(bpy)_3^{3+}$ was reduced by the sacrificial donor. In fact, the reduction of $Ru(bpy)_3^{3+}$ to $Ru(bpy)_3^{2+}$ could help to drive the oxidation of $MV^{+\cdot}$ to MV^{2+}.

7.3.2 Increase in Local Concentrations of the Reacting Cations.

The most likely and also the simplest interpretation for the increase in hydrogen production in the presence of clays, is the increase in the local concentrations of the cations due to their adsorption in a small volume on the clay surfaces. The probability of the quenching of excited $Ru(bpy)_3^{2+}$ by MV^{2+} is therefore increased, leading to more efficient charge separation (see section 3.2). In the case of clay minerals the cations were very strongly adsorbed. If the totality of the cations adsorbed on the outside clay surfaces were located in a thin layer of about 10 A thickness ($Ru(bpy)_3^{2+}$ has a diameter of about 8 Å), and if we assumed that the external surface area of the clay was 150 m^2/g (20% of

the total surface area 750 m^2/g), then about 0.1 meq/g of either $Ru(bpy)_3^{2+}$ or MV^{2+} adsorbed in this volume, which was of the order of 0.15 cm^3, corresponded to a local concentration of the two cations on the external surfaces of the order of 0.3 M.* This is an increase in concentration of the cations of several order of magnitude compared to the bulk concentrations. This can easily account for the ten fold increase in the rate of hydrogen evolution observed in the presence of the clay minerals!

This fixation on the clay surface, of the photosensitizer and of the electron relay in close proximity gave a result similar to what was obtained by the preparation of a complex in which a photosensitizer and an electron relay moieties were linked by chemical bonds. For example, evolution of hydrogen has been recently reported upon the irradiation of a viologen linked porphyrin[152] in the presence of a platinum catalyst. Light induced charge separation was also observed in chlorophyll linked to a quinone.[153]

7.3.3 Acidity of the Clay Surfaces.

Another property of clay minerals, which may play a role in the promotion of water reduction is their surface acidity.[39 42] Intercalated molecules are highly polarized by the clay surface charges. The dissociation constant of water intercalated in montmorillonite, for example, was estimated to be of the order of 10^{-7}.[64] The observed increase in the amount of hydrogen evolved in the presence of clays could be due to this higher local acidity.

*If the same calculation was done using the external surface area of Na^+-montmorillonite determined by Tennakoon et al[66] of 228 m^2/g, the local concentration of cations turned out to be 0.2 M. The argument is still valid.

7.3.4 Possible Involvement of the Clay Minerals in the Electron Transfer Process.

Aside from variations in local concentrations of the adsorbed cations or the acidity of the clay surfaces, another possible effect of clays on water photoreduction could be its involvement in the electron transfer process between $^{*}Ru(bpy)_2^{3+}$ and MV^{2+}.

The clay could act as an electron relay between $^{*}Ru(bpy)_3^{2+}$ and MV^{2+}, thereby contributing to forward electron transfer. We have determined that the cations involved in the evolution of hydrogen were adsorbed on the clay external surfaces. If we assumed that the approximately 0.2 meq/g of cation thus adsorbed were evenly distributed on the 150 m^2/g of external surface area and that the adsorbed cations were fixed on these surfaces, the average distance between them was 16 Å‡ (intercalated $Ru(bpy)_2^{3+}$ can be considered as practically immobile since its diffusion coefficient D_o was of the order of $10^{-12}cm^2s^{-1}$ in the interlayer spaces.[154]). This is more than the sum of the radii of the two cations, which is approximately 10 Å. Milasavljevic and Thomas[79] have shown that the radius of the active sphere for the quenching of the luminescence of $Ru(bpy)_2^{3+}$ by MV^{2+} in a cellulose matrix was 20 Å and that electron transfer took place via a tunneling process. Further, as was discussed in section 2.5, clay minerals can act as either electron acceptors or donors.[41 46] The acceptor or donor sites are structural atoms that exist in more than one oxidation state, in particular iron atoms. But iron cannot act as an electron relay between $^{*}Ru(bpy)_3^{2+}$ and MV^{2+} because the redox potential of the $Fe^{3+/2+}$ couple is not comprise between the redox potentials of the $Ru(bpy)_3^{3+/2+*}$ (-0.86 V) and the $MV^{2+/+\cdot}$ (-0.445 V) couples. In water the redox potential of $Fe^{3+/2+}$ is 0.77 V and in the montmorillonite octahedral sheets it was estimated to be 0.84 V.[154]

‡If the external surface area was taken as 228 m^2/g as measured by Tennakoon et al[66] the average distance turned out to be 19 Å.

Another possibility is that the structural iron could reduce $Ru(bpy)_3^{3+}$ to $Ru(bpy)_3^{2+}$, thereby hindering back electron transfer. The reduction of this cation by cellulose[79] and by montmorillonite[92] has been reported. In montmorillonite this reaction was recently shown to proceed via equation 33.[154]

$$Ru(bpy)_3^{3+} + Fe(II)_{lattice} \longrightarrow Ru(bpy)_3^{2+} + Fe(III)_{lattice} \qquad [33]$$

If this is the explanation for the effect of clay minerals on water reduction then there should be a relation between the yield of H_2 and the iron content of the clays. Tables 9 and 11 show that no clear correlation between the clay iron content and the amount of hydrogen produced was found. At pH 5.3, more hydrogen was found in the presence of montmorillonite than in the presence of hectorite (nontronite is not stable at this pH). At pH 7.0 we did observe slightly more hydrogen with iron rich nontronite than with montmorillonite (see table 5), but hectorite, with practically no structural iron, gave about the same amount as montmorillonite.

7.4 Hydrogen Production in Colloidal Clay Suspensions.

The absence of hydrogen production in the experiments in which colloidal suspensions of montmorillonite were illuminated (see table 17) can be attributed to one of two factors. First, to ensure that the clay suspensions did not flocculate it was necessary to reduce the concentrations of $Ru(bpy)_3^{2+}$ and MV^{2+} used in the system (see section 5.2.2). Thus the amount of hydrogen evolved, if any, may have been too small to be measurable (the detection limit of the hydrogen analysis system used was of the order of 0.3 μmol/L, see section 5.2.3). Or, since the total amount of cations added was below the adsorption capacity of the clay used, all the $Ru(bpy)_3^{2+}$ and MV^{2+} cations added were intercalated in the clay, leaving no cations on the external surfaces where, as we have shown, the hydrogen producing reaction took place.

When the systems were sonicated, Table 17 shows that the hydrogen gas was due to the ultrasound and not to the irradiation of the mixtures. Sonication of water containing dissolved gases leads to the production of H· and OH· radicals by the process of acoustic cavitation.[156] The observed hydrogen came from the recombination of these H· radicals. Irradiation of the mixtures had no detectable effect on the yield of hydrogen.

7.5 Conclusion.

The three cations used in this study, MV^{2+}, $Ru(bpy)_3^{2+}$ and $ZnTMPyP^{4+}$, were intercalated in the interlayer spaces of the smectite clays hectorite and montmorillonite. All three cations were adsorbed to the full extent of the clays cation exchange capacities.

The results of the competitive adsorption studies of two cations by montmorillonite showed that an intercalated cation could not be replaced by another. Only a limited fraction of the pre-adsorbed cations, about 20 % of the total, could be desorbed from the clay by the addition of a second cation. This was assumed to be the fraction of cations adsorbed on the clay external surfaces.

The hydrogen evolution reaction was shown to be a light driven reaction taking place between $Ru(bpy)_3^{2+}$ and MV^{2+} coadsorbed on those clay external surfaces only. Intercalated cations did not react to give hydrogen. The optimum conditions for hydrogen evolution corresponded to the case for which the ratio of $Ru(bpy)_3^{2+}$ to MV^{2+} adsorbed on the external surfaces was approximately one. The dependence of the efficiency of hydrogen evolution on the concentration of MV^{2+} was attributed to the variation of this ratio, combined with the total amount of $Ru(bpy)_3^{2+}$ adsorbed by the clay. The dependence of the efficiency of hydrogen evolution on the clay concentration was attributed to an increase of the opacity of the system with the increase of the clay concentration.

The simplest interpretation of water reduction promotion by clay minerals was the increase in the local concentrations of the reacting cations, $Ru(bpy)_3^{2+}$ and MV^{2+}, that resulted from their adsorption on the clay external surfaces. But we could not completely exclude other possibilities such as the acidity of the clay surfaces or the involvement of structural iron in the reduction of photogenerated $Ru(bpy)_3^{3+}$.

Part 2

FLUORESCENCE OF CLAY-INTERCALATED METHYLVIOLOGEN.

CHAPTER VIII

FLUORESCENCE SPECTROSCOPY IN THE STUDY OF COLLOIDAL SYSTEMS.

8.1 Introduction.

The absorption of a light photon causes an electronic transition. An electron from the highest occupied molecular orbital is promoted to an unoccupied higher orbital. According to the Franck-Condon principle, since electronic motions are much faster than nuclear motions, electronic transitions occur most favorably when the nuclear structure of the ground and initially excited states are similar.[157] Because light absorption is extremely fast, (10^{15} s^{-1}) molecular positions are unchanged in the excited state. In other words "vertical transitions" are preferred. (see figure 36) Excitation occurs to different vibrational levels of the excited state.[157 158] Since in condensed media vibrational relaxation is very fast, the singlet excited state, S_1, relaxes rapidly to its lowest vibrational level.

Being an excited state, S_1 is only meta-stable. The molecule will seek to return to a ground state. This can occur by several competing routes. The energy dissipating processes can basically be divided into two classes, photochemical processes and photophysical processes.[157 159]

The photochemical processes are those in which the energy of the photon absorbed is used to drive a chemical reaction. For example, when the energy of the light quantum absorbed in the excitation process is large enough to cause the breaking of a chemical bond, dissociation can occur. Or the energy absorbed can cause the photoionization of the chromophore. The energy of the excited state can also be dissipated by photochemical bimole-

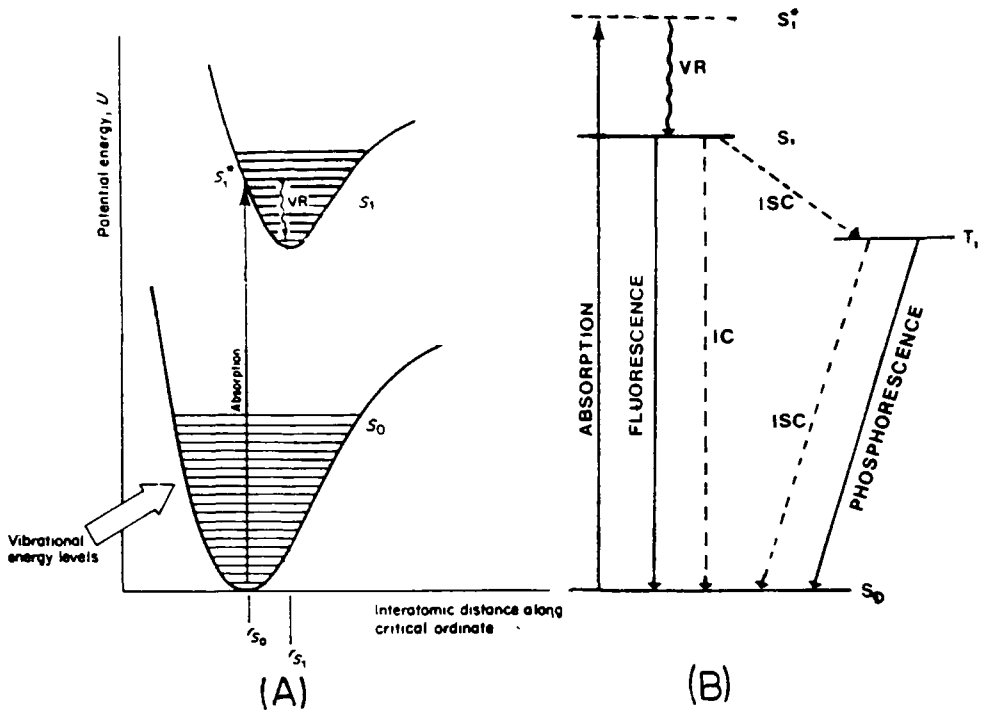

Figure 36: Representation of an electronic transition produced by light absorption. A) Vertical or Franck-Condon allowed transition from S_0 to S_1^* and vibrational relaxation to S_1. B) Some of the photophysical processes involved in light absorption and light emission.

cular processes. An example is the quenching of $^*Ru(bpy)_3^{2+}$ by electron transfer to MV^{2+} that was observed to lead to the production of hydrogen in part 1 of this thesis.

In the second class, the photophysical processes, no net chemical reaction takes place. Some of these photophysical deactivation processes are shown in figure 36. The energy can be dissipated as heat in radiationless transitions. Two of the most common radiationless processes are shown in figure 36. Internal conversion (IC) is a transition between S_1 and the ground state S_0. (i.e. a transition between two singlet states or two triplet states) Intersystem crossing (ISC) is a transition between S_1 and the triplet excited state T_1. (i.e. between a singlet and a triplet state)

Figure 36 also shows two radiative processes, in which light is emitted. Light emission by a spin-allowed transition between S_1 and S_0 is called fluorescence. Light emission by a spin forbidden transition between T_1 and S_0 is called phosphorescence.[160] [161] Because it is a forbidden transition, phosphorescence usually occurs at a much slower rate (see table 18) and it is not often observed at ambient temperatures.

Deactivation of the excited state can also occur via bimolecular photophysical processes. Quenching by the solvent, self quenching or quenching by other molecules such as oxygen are bimolecular processes by which an excited state can return to the ground state. Sometimes, the distinction between photochemical and photophysical processes is not clear. An example is the quenching of excited $Ru(bpy)_3^{2+}$ by 9-anthracenecarboxylic acid shown in figure 18. (see chapter 3) Energy transfer produces the triplet excited state of 9-anthracenecarboxylic acid, which reacts with MV^{2+} to give $MV^{\cdot+}$.[77]

All of these deactivation processes are in competition with one another. The intensity of the fluorescence emitted by a particular molecule will depend on the relative efficiency of the various processes. The efficiency of fluorescence is measured by its quantum yield Φ_f, defined as the number of light quanta emitted per light quanta absorbed. It may be shown to be related to the rate constants of the various deactivation processes (equation 34).

$$\Phi_f = k_f/(k_f + \Sigma k) \qquad [34]$$

k_f is the rate constant of fluorescence and Σk is the sum of the rate constants for all the other possible deactivation processes. Φ_f will be large when k_f is much greater than Σk. Table 18 shows the range of rate constants typically found for some of the processes discussed here.

Fluorescence is a very sensitive technique, more so than the absorption spectrophotometric methods, since the absolute emitted radiation is measured, as opposed to the differ-

Table 18: Average rate constants of some photophysical processes.

Step	Process	rate constant (sec^{-1})
Excitation	$S_o + h\nu \rightarrow S_i$	10^{15}
Internal conversion (IC)	$S_i \rightarrow S_1$	10^{11}-10^{14}
Fluorescence (F)	$S_1 \rightarrow S_o + h\nu_f$	10^{6} -10^{11}
Intersystem crossing(ISC)	$S_1 \rightarrow T$	10^{8} -10^{11}
Internal conversion (IC)	$S_1 \rightarrow S_o$	10^{7} -10^{9}
Internal conversion (IC)	$T_j \rightarrow T_1$	10^{11}-10^{14}
Phosphorescence (P)	$T_1 \rightarrow S_o + h\nu_p$	10^{-2}-10^{3}
Intersystem crossing(ISC)	$T_1 \rightarrow S_o$	10^{-2}-10^{3}

ence between the incident and transmitted beams.[159] Further, the fluorescence spectrum and the fluorescence intensity have been shown to be very sensitive to both the environment of the fluorescing molecules, and the efficiency of the deactivation processes. Information on them can therefore be inferred from their effect on the fluorescence of a particular molecule.[161] This technique, called fluorescence probing has proven very useful in many cases, including in the study of colloidal systems.

The fluorescent probes used in this technique can be separated into two groups. In systems where a fluorescent molecule is naturally present, one can use it as an intrinsic probe. In most cases however it is necessary to add a fluorophore to the system. These are called extrinsic probes.

This section of the thesis describes some of the fluorescence properties of MV^{2+}. The fluorescence of this cation has not been observed in water. However, we have observed the fluorescence of MV^{2+} for the first time. We found that in clay minerals MV^{2+} fluoresces with a reasonable efficiency.[182] As such methylviologen has the potential to become a very useful new probe for the study of clay colloidal suspensions. The

fluorescence of clay intercalated MV^{2+} was studied by three related fluorescent techniques, the fluorescence spectra, the anisotropy of the fluorescence and lifetime of the singlet excited state.

8.2 Fluorescence Spectrum.

One of the advantages of fluorescence spectroscopy over other spectroscopic techniques is that the observed spectral intensity is a function of two spectral variables, the excitation wavelength, λ_{ex} and the emission wavelength, λ_{em}. Two different types of fluorescence spectra can therefore be measured. If λ_{ex} is held constant and λ_{em} is scanned, a fluorescence emission spectrum results. If λ_{em} is held constant and λ_{ex} is scanned a fluorescence excitation spectrum results.

The excitation spectrum should be nearly identical to the absorption spectrum of the fluorophore. When there is more than one chromophoric species present, the shape of the excitation spectrum will be the same as that of the absorption band which gives rise to the observed fluorescence. That is, when the excitation and the absorption spectra do not agree, then the excitation spectrum gives the absorption spectrum of the emitting species.

As mentioned in the previous section, the relative efficiencies of the various energy dissipating processes will control the intensity of the emitted light (I_f). This intensity is found to be proportional to the quantum yield of fluorescence, (Φ_f) and to the concentration of the sample.

$$I_f = I_o(1 - 10^{-\epsilon cl})\Phi_f \qquad [35]$$

ϵ, c and l are the molar absorptivity, the concentration of the sample and the path length respectively and I_o is the intensity of the excitation radiation. For low values of ϵcl (i.e. low optical density) equation 35 reduces to

$$I_f = I_o(2.3\epsilon cl)\Phi_f \qquad [36]$$

and the fluorescence intensity is linearly proportional to the concentration of the sample. In practice one tries to work at low concentration to be able to use equation 36. Otherwise inner filter and geometry effects need to be considered.

It is difficult to measure the absolute quantum yield of fluorescence.[159] However it has been measured for certain standards, allowing the measurement of the relative quantum yield of a substance (equation 37).

$$\Phi_f = (I_f \epsilon_s c_s / I_{fs} \epsilon c) \Phi_{fs} \qquad [37]$$

I_{fs}, ϵ_s and c_s are the fluorescence intensity, molar absorptivity and concentration of a standard compound whose absolute quantum yield Φ_{fs} is known.

The fluorescence spectrum and the fluorescence intensity of an absorbed probe can give information about the local polarity, the mobility and the accessibility to quenchers or to the solvent of an adsorbed chromophore.[161 162]

In inorganic colloids the probe $Ru(bpy)_3^{2+}$ has been the most widely used chromophore, especially for the study of clay suspensions. In water $Ru(bpy)_3^{2+}$ emits light at 607 nm with a quantum yield of 0.042 and a lifetime of 620 nsec[17] (see section 1.4). In inorganic colloids its spectrum provided information on the chromophore's mobility. For example, the shift of the spectrum of $Ru(bpy)_3^{2+}$ adsorbed on polymerized SiO_2 from the one found in water to the one found in ethylene glycol/water glass at 77 K (see figure 37 A) was attributed to a rigid adsorption site.[164] The comparison of the spectra of $Ru(bpy)_3^{2+}$ adsorbed on montmorillonite or kaolin, in ethylene glycol/water glass showed that $Ru(bpy)_3^{2+}$ retained more mobility in montmorillonite (see figure 37 B). This was attributed to the fact that $Ru(bpy)_3^{2+}$ in montmorillonite was intercalated and therefore, isolated from the ethylene glycol/water matrix, while on kaolin, a non-expandable clay (see section 2.2), it could only be adsorbed on the clay external surfaces.[64]

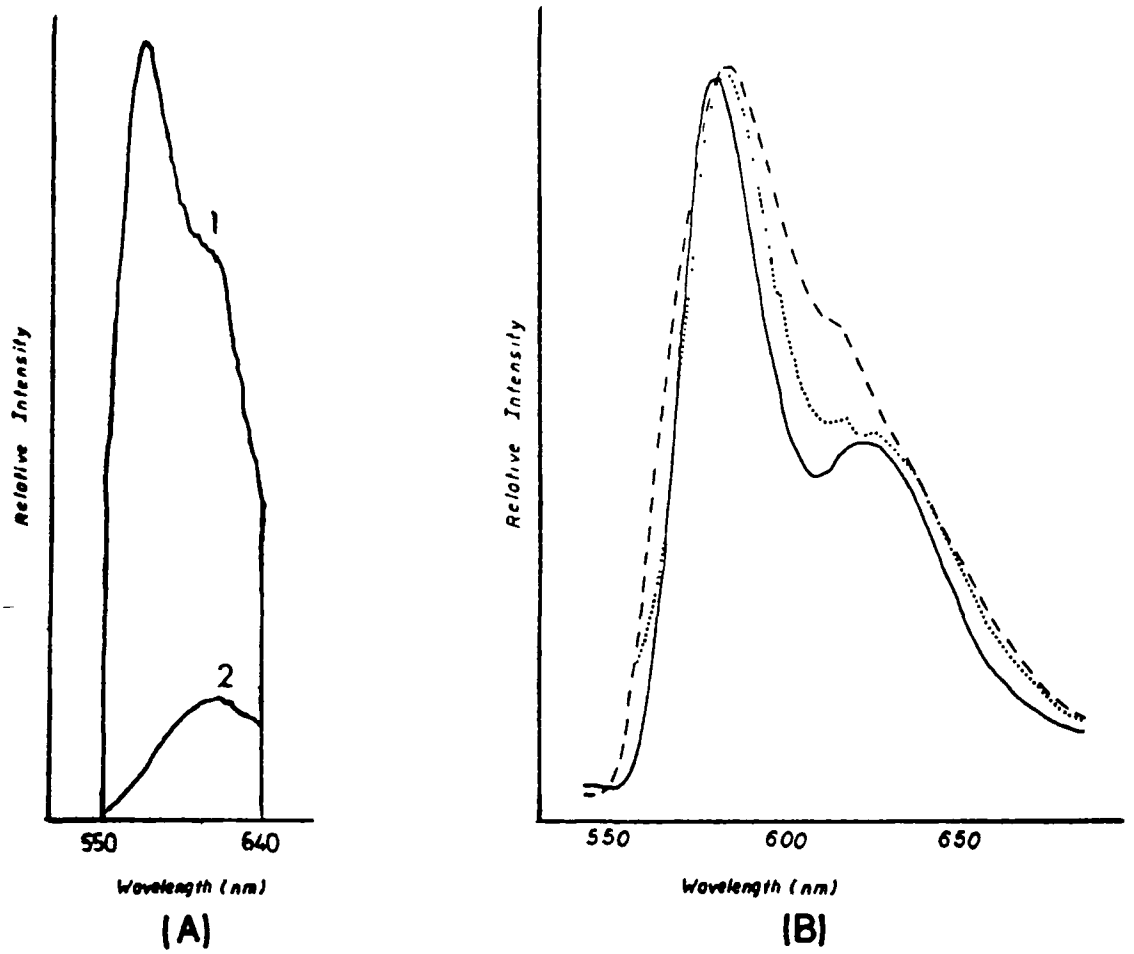

Figure 37: Emission spectra of $Ru(bpy)_3^{2+}$ A 1) adsorbed on polymerized silica and 2) in water (Reproduced with permission from reference 164). B) (—) in an ethylene glycol/water glass at 77 K, (····) adsorbed on kaolin in ethylene glycol/water glass at 77 K, (----) adsorbed on montmorillonite in ethylene glycol/water glass at 77 K (Reproduced with permission from reference 64). Note the spectra of part A and B are not on the same scale.

The spectrum can also be used to determine the site of adsorption of a chromophore. For example the magnitude of the blue shift of the emission maximum of $Ru(bpy)_3^{2+}$ in clays has been correlated with the clay particle size.[165] It has been proposed that intercalation induced a larger spectral shift, since the externally adsorbed $Ru(bpy)_3^{2+}$ was more exposed to the solvent. Since the ratio of internal to external surfaces decreased with particle size, this could explain the smaller spectral shifts found in the presence of smaller particles.

The same distinction between intercalated and surface adsorbed cations was used to account for the increase in luminescence intensity of $Ru(bpy)_3^{2+}$ adsorbed on laponite, with increase in either clay concentration or salt concentration. Laponite is a synthetic clay having a structure similar to hectorite. In dilute solution, laponite was completely dispersed and all the $Ru(bpy)_3^{2+}$ was adsorbed on outside surfaces. As the clay concentration increased or in the presence of salt, aggregation of the layers occurred, forming clay stacks into which $Ru(bpy)_3^{2+}$ could be intercalated (see section 2.3). These intercalated cations were assumed to be more luminescent than those adsorbed on the outside surfaces.[166]

8.3 Fluorescence Polarization.

Another steady state fluorescence measurement that can be made on a probe intercalated in clay minerals is the fluorescence anisotropy, r, given by equation 38:

$$r = (I_{||} - I_{\perp})/(I_{||} + 2I_{\perp}) \qquad [38]$$

$I_{||}$ and $I_{\perp}$ are the fluorescence intensities observed through a polarizer oriented parallel and perpendicular to the plane of polarization of the excitation beam.[167] The measurement involves the excitation of fluorescence with plane polarized light, usually in the vertical direction, and the observation of the emitted light at right angles to the excitation propagation direction, through a polarizer oriented parallel and perpendicular to the plane of polarization of the excitation beam. The anisotropy is a measure of the extent to which the emitted light retains the polarization of the excitation light. It gives information on the flexibility of the probe and the ordering or structure of its adsorption sites.

Theoretically, the maximum value of r is 0.4 in a solution system. The observed value of r can be reduced by different effects. It will depend on the angle between the

absorption and the emission oscillator in the chromophore.[168] It will be reduced by dynamic processes like rotational flexibility of the probe and the fluidity of its adsorption site. This is what makes fluorescence anisotropy such a useful technique in the study of supramolecular assemblies.

For a rotating fluorescent sphere in an isotropic environment, the observed r value obeys the Perrin equation.[168 169]

$$r_0/r = 1 + 3\tau/\rho \qquad [39]$$

r_0 is the value of r when the emitting molecules maintain their orientations between excitation and emission (i.e. in a very viscous solvent), is the fluorescence lifetime and the rotation relaxation time, given by equation 40.[170]

$$\rho = 3V\eta/RT \qquad [40]$$

V is the molar volume of the fluorophore, η is the viscosity, R is the gas constant and T is the temperature. The quantity r_0/r is called the degree of depolarization of the fluorescence.

Fluorescence anisotropy uses the fluorescence lifetime as a clock of the probe mobility. A particular orientation of the probe is selectively excited by using polarized light. The extent to which the emitted light is depolarized will show how much the angle between the emission oscillator at the time of emission and the absorption oscillator at the time of excitation differs from the angle between the absorption and emission oscillators at the time of excitation. The degree of depolarization is a measure of the fraction of the probes that change their orientations in the time τ, the delay between light absorption and emission.

Some examples of the use of fluorescence anisotropy follow. Combining equations 39 and 40 gives

$$r_0/r = 1 + RT\tau/\eta V \qquad [41]$$

This suggests that anisotropy measurements may be related to either the viscosity or the volume of the probe. For example the degree of depolarization has been used to obtain values of the microviscosity of probes in a variety of micellar systems.[168] However, it has now been shown that in anisotropic systems, such as micelles, the estimation of the microviscosity of the system is inappropriate. Rather one discusses the anisotropy in terms of the fluidity of the system. Fluidity can have both dynamic and structural connotations.

The effective volume of a rotating probe V can also be estimated from fluorescence anisotropy measurements. For example the volume of the inverted micelle AOT (sodium diidootyl sulfosuccinate) as a function of its water content has been measured in this way.[171 172]

In inorganic colloids, only r is usually measured, and the result is then used directly as an indication of the probe fluidity by comparing it with the corresponding value in a rigid matrix. For example, pyrene adsorbed on TiO_2 had a polarization value of 0.26, which was attributed to a rigid adsorption site.[173] The degrees of polarization of the light emitted by $Ru(bpy)_3^{2+}$ in ethylene glycol and adsorbed on kaolin and montmorillonite were 0, 0.10 and 0.11 at 298 K and 0.20, 0.15 and 0.11 at 77 K respectively. This was in agreement with the interpretation of the luminescence spectra (see section 8.2, figure 37 B). At low temperatures $Ru(bpy)_3^{2+}$ intercalated in montmorillonite exhibited more flexibility then $Ru(bpy)_3^{2+}$ adsorbed on the outside surfaces of kaolin.[64] $Ru(bpy)_3^{2+}$ adsorbed on porous vycor glass had a similar flexibility as clay adsorbed $Ru(bpy)_3^{2+}$. Its degree of polarization was 0.12.[174 175]

Since clay suspensions are turbid, the effect of light scattering by the clay particles must be considered. In biological systems this problem has been treated by Teale.[176] Light scattering of the excitation beam or emission beam can cause a partial depolarization, leading to a reduction of the observed anisotropy. In membranes a numerical relationship was found between r_{obs} and the absorbance[177] (used as a measured of light scattering).

$$r_{obs} = -KAr' + r' \qquad [42]$$

r_{obs} is the observed anisotropy, r' the extrapolated anisotropy to infinite dilution where A, the absorbance, is zero and K is a proportionality constant.

8.4 Fluorescence or Singlet Lifetimes.

The singlet lifetime τ_s, is the mean lifetime of the excited singlet state. The probability of finding a given molecule that has been excited at time zero still in the excited state at time t is $e^{-t/\tau}s$. τ_s is the reciprocal of the sum of the rate constants of deactivation.

$$\tau_s = 1/(k_f + \Sigma k) \qquad [43]$$

This is distinguished from the radiative lifetime τ_r, which is

$$\tau_r = 1/k_f \qquad [44]$$

The equation relating the fluorescence intensity and the singlet lifetime in most cases is

$$I = I_0 e^{-t/\tau_s} \qquad [45]$$

where I and I_0 are the fluorescence intensities at time t and at time zero.[160 161] The singlet lifetime can therefore be obtained by measuring the fluorescence intensity as a function of time. In practice the technique consists of exciting a fluorescent molecule with a short light pulse at a suitable wavelength and monitoring the intensity of the emitted light, at a fixed observation wavelength, as a function of the time after excitation. The decay curve is then fit to a kinetic decay law, which describes the physical processes by which the excited state is deactivated. In many cases this is an exponential function from which the lifetime of the fluorescent excited state species can be calculated.

The singlet lifetime of many organic molecules is in the nanosecond region. In table 18 the average rate constants of the photophysical processes described in section 8.1 are compared. As mentioned previously, the efficiency of fluorescence, the quantum yield, will depend on the relative values of these rate constants for a specific molecule (see equation 34). Measuring the singlet lifetime can therefore give information on the kinetic parameters. Combining equations 34, 43 and 44 gives:

$$\tau_r = \tau_s/\Phi_f \qquad [46]$$

Measuring the lifetime and the fluorescence quantum yield can therefore be used to get k_f and then using equation 34, Σk etc.

If there is more than one fluorescing species the decay of the fluorescence intensity may not be satisfactorily fit by a single exponential function as in equation 45, but rather by a sum of two or more exponentials, from which more than one decay time can be determined. The pre-exponential factors will be proportional to the relative fluorescence contribution and the concentration of the different fluorescing species. For example the decay of the intensity of the light emitted by $Ru(bpy)_3^{2+}$ adsorbed on kaolin, montmorillonite[64] and hectorite[150] were fit to the sum of two exponentials. The fast decay time had values of 100, 32 and 62 nsec respectively and accounted for 50, 62 and 60% of the excited molecules. The slow decay time had values of 715, 415 and 350 nsec respectively and accounted for the remaining luminescence. In water the decay of $Ru(bpy)_3^{2+}$ luminescence is single exponential with a lifetime of 620 nsec.[17] These results have been attributed to the existence of two distinct adsorption sites for this cation in the different clays.

Valuable information can also be gained by comparing the lifetimes of an adsorbed probe with its lifetime in solution. The decay of the fluorescence of pyrene on TiO_2 for example was double exponential.[173] 70% of the excited states were quenched very effi-

ciently by the support, their lifetimes was only 5 nsec. The remaining 30% had a lifetime of 290 nsec, longer than the solution lifetime of 200 nsec. Apparently pyrene was initially adsorbed in a limited number of sites where quenching was very efficient. Only when these sites were filled was pyrene adsorbed in other sites where the excited molecule was protected from quenching by the support.[173]

Quenching by the support was also observed when $Ru(bpy)_3^{2+}$ was adsorbed on clays. The shorter lifetime of $Ru(bpy)_3^{2+}$ phosphorescence in clays was attributed to quenching by impurities present in the clay lattice, in particular structural iron. In water, Fe^{3+} is known to quench excited $Ru(bpy)_3^{2+}$ by electron transfer.[178 179 180] According to van Damme et al[181] the decay of $Ru(bpy)_3^{2+}$ luminescence in clay minerals was multiexponential. Since only one type of adsorbed $Ru(bpy)_3^{2+}$ was detected by UV-Visible spectroscopy, steady-state fluorescence, IR spectroscopy or X.p.s., they attributed this multiexponential decay to a range of surface environments. These environments did not perturb the electronic properties of the probe molecule but they modified its fluorescence lifetime. They suggested that a key factor was the number of neighboring iron atoms, which could quench the essentially immobile adsorbed cation. As is discussed in the next chapter, the iron content of the clay had a dramatic effect on the fluorescence of intercalated MV^{2+}.[182]

Instead of quenching luminescence some supports have the effect of increasing the fluorescence lifetime of adsorbed probe. This was the case for $Ru(bpy)_3^{2+}$ adsorbed on polymerized silica, where it had a lifetime of 2 μsec.[164] $Ru(bpy)_3^{2+}$ was proposed to be adsorbed in a very rigid site where it was protected from quenching by the solvent.

Finally, besides looking at the effect of the support on the lifetime of an adsorbed probe one can look at the effect of adding an external quencher. This provides information on the accessibility of the probe and therefore of the adsorption site. For example, quenching of $^*Ru(bpy)_3^{2+}$ in hectorite by MV^{2+} was much less efficient than the quench-

ing of $^{*}Ru(bpy)_3^{2+}$ by MV^{2+} in water. This was attributed to the segregation of these two cations by clays[150] (see chapter 11). Excited $Ru(bpy)_3^{2+}$ was thus shielded from MV^{2+} by the clay.

In the next two chapters we present and discuss the results of the study of the fluorescence of MV^{2+} intercalated in montmorillonite and hectorite by these three fluorescent techniques.

CHAPTER IX

RESULTS.

9.1 Experimental

9.1.1 UV-Visible Spectra.

The UV-Visible spectra of $Ru(bpy)_3^{2+}$ and MV^{2+} adsorbed on < 2.0 μm Ca^{2+}-exchanged fractions of the clays hectorite and montmorillonite were recorded on a Varian DMS 90 UV-Visible spectrophotometer. Some spectra were taken on a Cary 219 spectrophotometer.

Suspensions of the clays exchanged with one of the two cations were prepared, such that the cation concentration was 5.00 x 10^{-5}M and the clay concentration 0.50 g/L. Spectra were recorded with a blank in the reference cell containing 0.50 g/L of clay but no cations. In the same way the spectrum of MV^{2+} adsorbed in micelles of Sodium DodecylSulphonate (SDS) in which the micelle concentration was 1.0 x 10^{-4}M and the concentration of MV^{2+} was 5.0 x 10^{-6}M, was taken. The effect of the cation to clay ratio on the absorption spectrum was studied. Clay suspensions were prepared in which the concentration of methylviologen was kept constant while the concentration of the clay was increased in order to decrease the ratio MV^{2+}/clay. The absorption spectra were recorded in each case using the corresponding suspension of clay with no adsorbed methylviologen as the reference, as described above.

9.1.2 Fluorescence Measurements.

The fluorescence spectra of MV^{2+} in montmorillonite, hectorite, nontronite and water were recorded on a Perkin Elmer Model 44A spectrophotofluorimeter equipped with a DCSU-2 corrected spectra Unit in the laboratory of Dr. A. Szabo at the Division of Biological Sciences of the National Research Council of Canada in Ottawa. Fluorescence anisotropy was measured on the same instrument using the appropriate polarizers. The instrument used to measure the fluorescence lifetime is described in detail in reference 133.

The samples were prepared by simply mixing volumes of a stock solution of MV^{2+} with volumes of stock suspensions of the clays 0.400 g/L. One measurement was done on the fluorescence of MV^{2+} (5.0×10^{-6}M) in SDS micelles (1×10^{-4}M).

9.2 UV-Visible Absorption Spectrum of Clay Intercalated Methylviologen.

The absorption spectrum of the MV^{2+} in water is shown in figure 38. It was identical to the one previously reported.[130] The absorption maximum, λ_{max} was at 257.5 nm, where ϵ = 20,800 $M^{-1}cm^{-1}$ (lit. $\lambda_{257.5\ nm}$ ϵ = 20,100 $M^{-1}cm^{-1}$ [130]). Also shown in figure 38 is the absorption spectrum of MV^{2+} in montmorillonite. We noted a red shift of λ_{max} from 257.5 nm to approximately 280 nm. This was in agreement with previous reports of the spectrum of MV^{2+} intercalated into montmorillonite.[183] A red shift was also found when MV^{2+} was intercalated in hectorite.

The effect of the MV^{2+}/clay ratio on the absorption spectrum of intercalated MV^{2+} was studied. In this thesis, the ratio MV^{2+}/clay is expressed as a fraction of the clay cation exchange capacity (CEC). In chapter 6 it was shown that MV^{2+} was fully adsorbed by both clays to the full extent of their CEC (see tables 16 and 17). The ratio MV^{2+}/clay is therefore expressed as the fraction of the clay exchangeable cations that have

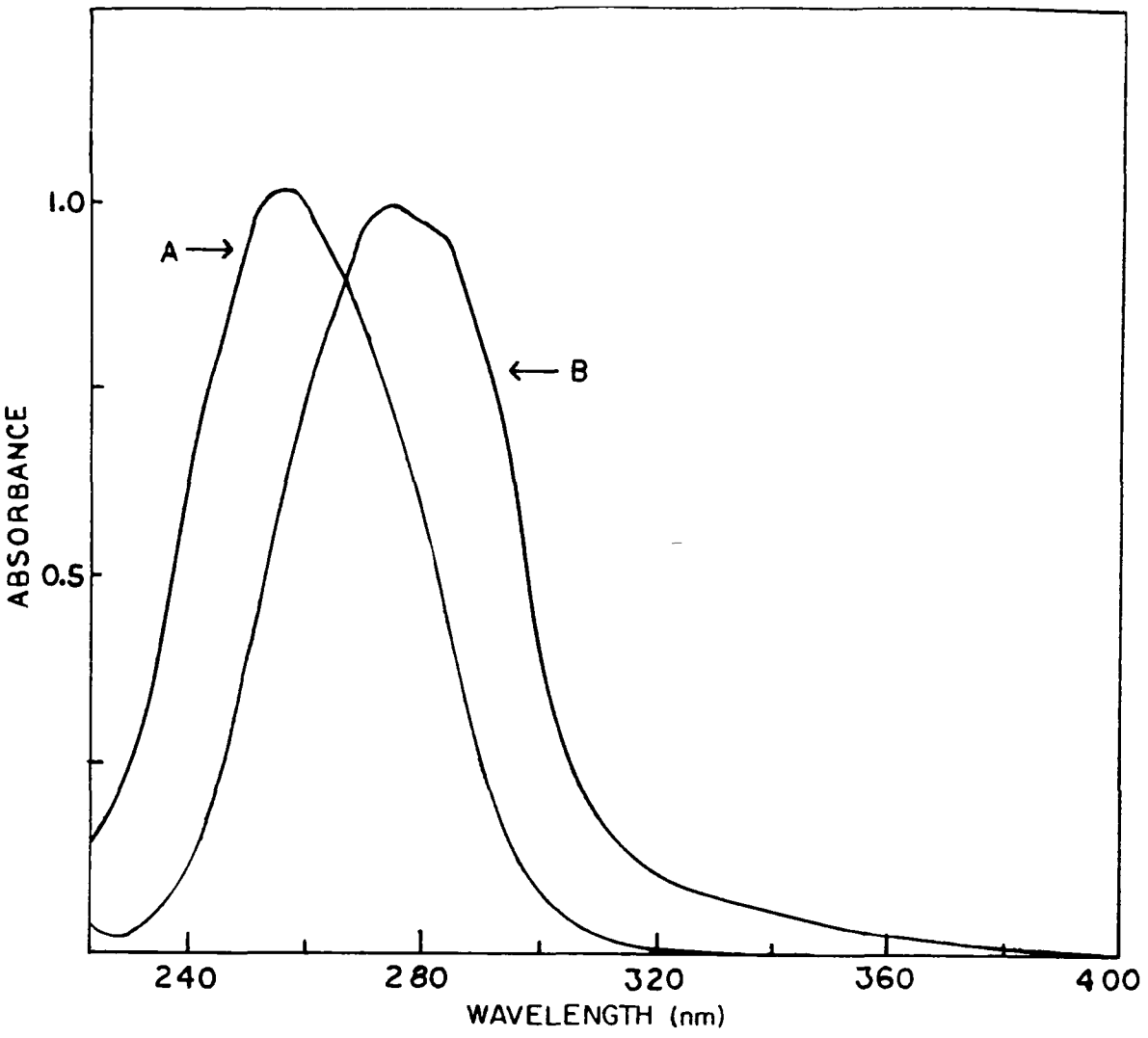

Figure 38: Absorption spectra of MV^{2+}. A) in water B) in a suspension of montmorillonite, $[MV^{2+}] = 5.0 \times 10^{-5}M$ and [clay] = 0.50 g/L. (MV^{2+}/clay = 22.5% CEC, see text)

been displaced by MV^{2+}, assuming the complete adsorption of the MV^{2+} present. For example, in the spectrum shown in figure 38, the concentration of the clay was 0.50 g/L and the concentration of MV^{2+} was $5.0 \times 10^{-5}M$. This corresponds to a ratio of MV^{2+}/clay of 5.0×10^{-5} mol/0.50 g, or 1.0×10^{-4} mole of MV^{2+} per gram of montmorillonite. Table 16 shows that one gram of montmorillonite could adsorb up to 0.89 meq

of MV^{2+}. Therefore with complete adsorption, MV^{2+} accounted for 2.0 x 10^{-4} eq./g/8.9 x 10^{-4} eq./g = 0.225 or 22.5% of the clay CEC.

Figure 39 shows the absorption spectra of MV^{2+} adsorbed in montmorillonite and hectorite for different ratios MV^{2+}/clay, for the cases where this ratio was larger than 100% CEC. In these cases both free and bound MV^{2+} cations were present simultaneously. In both clays, a gradual shift of λ_{max} was noted, from 257.5 nm in water to approximately 280 nm in montmorillonite and 275 nm in hectorite, as the cation to clay ratio decreased. Isosbestic points were observed at 268 nm in montmorillonite and at 273 nm in hectorite.

The absorption spectra for the mixtures in which the ratio MV^{2+}/clay was less than 100% of the CEC are shown in figures 40 and 41. The first observation made was that in both clays the intensity of the band appeared to increase with the decrease in the cation to clay ratio. In hectorite, ϵ changed from 25,000 $M^{-1}cm^{-1}$ at 90% CEC to 32,000 $M^{-1}cm^{-1}$ at 5.6% CEC, while in montmorillonite it increased from 18,000 $M^{-1}cm^{-1}$ at 90% CEC up to 34,000 $M^{-1}cm^{-1}$ at 2.2% CEC. Note that in montmorillonite this variation was not regular, at 45% CEC, ϵ was larger than at 30% CEC. There was no change in the shape of the band or shift in their maxima. Further the absorbance of the mixtures did not reach zero at 400 nm, where MV^{2+} did not absorb light, especially in the case where the ratio of cation to the clay was large (see figures 40 and 41).

The variation in ϵ was not large considering the experimental error. With $[MV^{2+}]$ = 2.0 x 10^{-6}M, the observed variation of ϵ from 25,000 to 32,000 $M^{-1}cm^{-1}$ corresponded to a variation of the absorbance of 0.050 to 0.064, which was not large if one considers the turbidity of the clay suspensions. This turbidity could be estimated by measuring the absorbance of the blank (i.e. no MV^{2+}). For example in hectorite and montmorillonite at 14% and 15% CEC the concentrations of the clays were 0.040 and 0.030 g/L respectively. The absorbancies at 270 nm with respect to water of these two suspensions were 0.138 and 0.178.

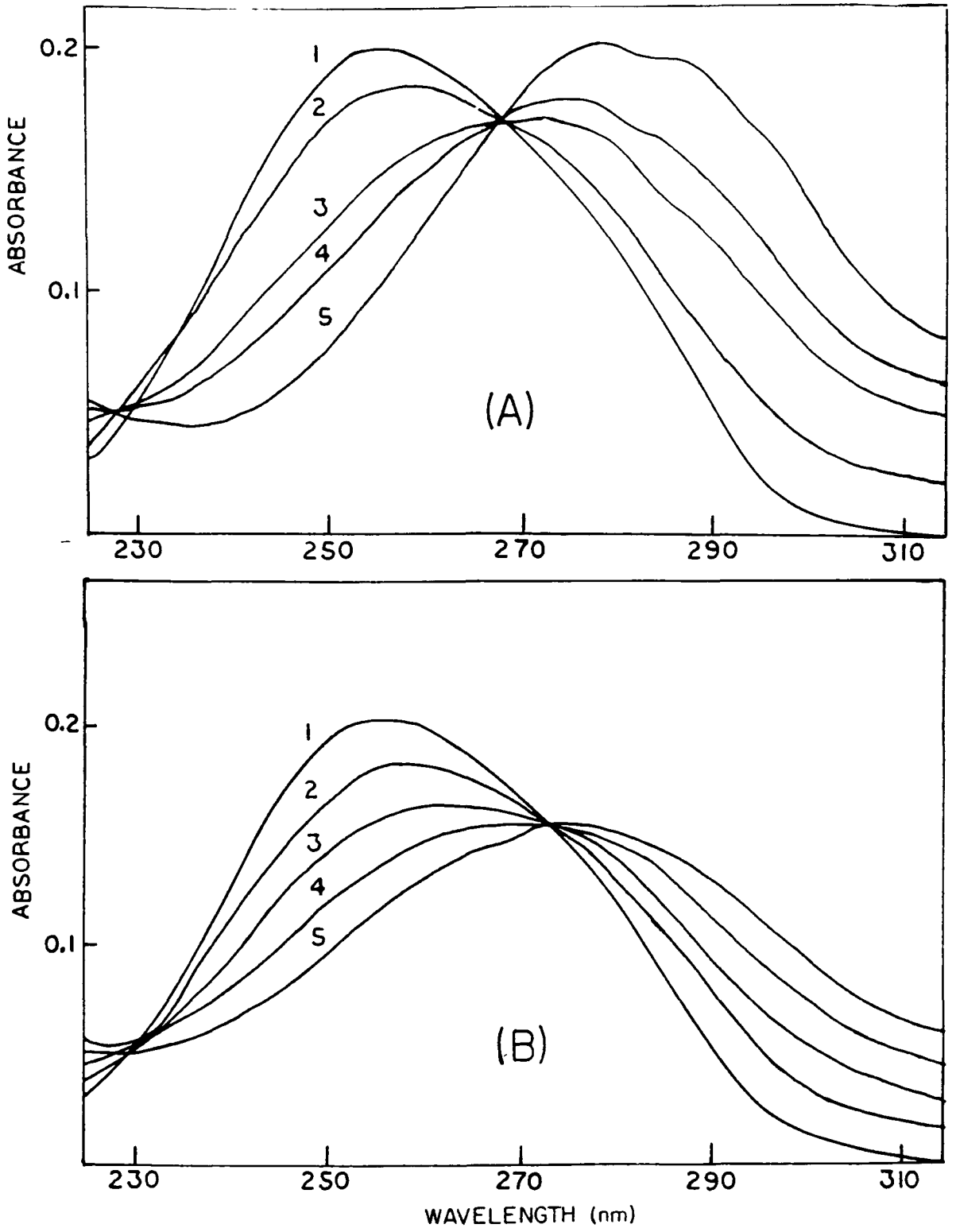

Figure 39. Absorption spectra of MV^{2+} in clays vs. MV^{2+}/clay ratio for the ratios larger than 100% CEC. (A) in montmorillonite, MV^{2+}/Mont. = 1) in water, 2) 550% CEC, 3) 190% CEC, 4) 140% CEC and 5) 100% CEC. (B) in hectorite, MV^{2+}/Hect. = 1) in water, 2) 570% CEC, 3) 290% CEC, 4) 200% CEC and 5) 150% CEC. In all cases the concentration of MV^{2+} was constant (1.0×10^{-5}M).

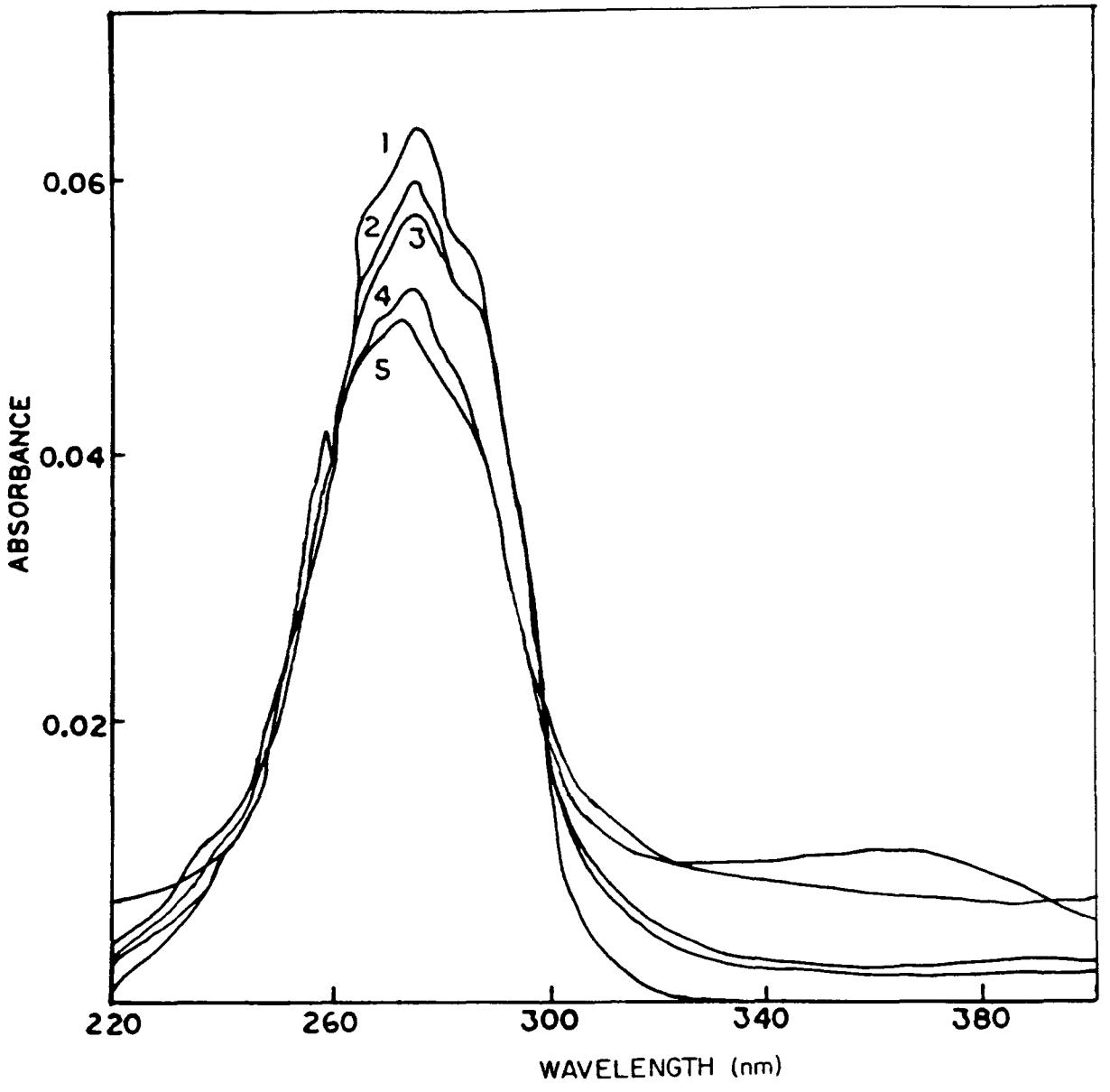

Figure 40: Absorption spectra of MV^{2+} adsorbed on hectorite vs. MV^{2+}/clay ratio. for the ratios less than 100% CEC. [MV^{2+}] was constant at 2.0 x 10^{-6}M, MV^{2+}/Hect. = 1) 5.6% CEC, 2) 14% CEC, 3) 28% CEC, 4) 56% CEC and 5) 92% CEC.

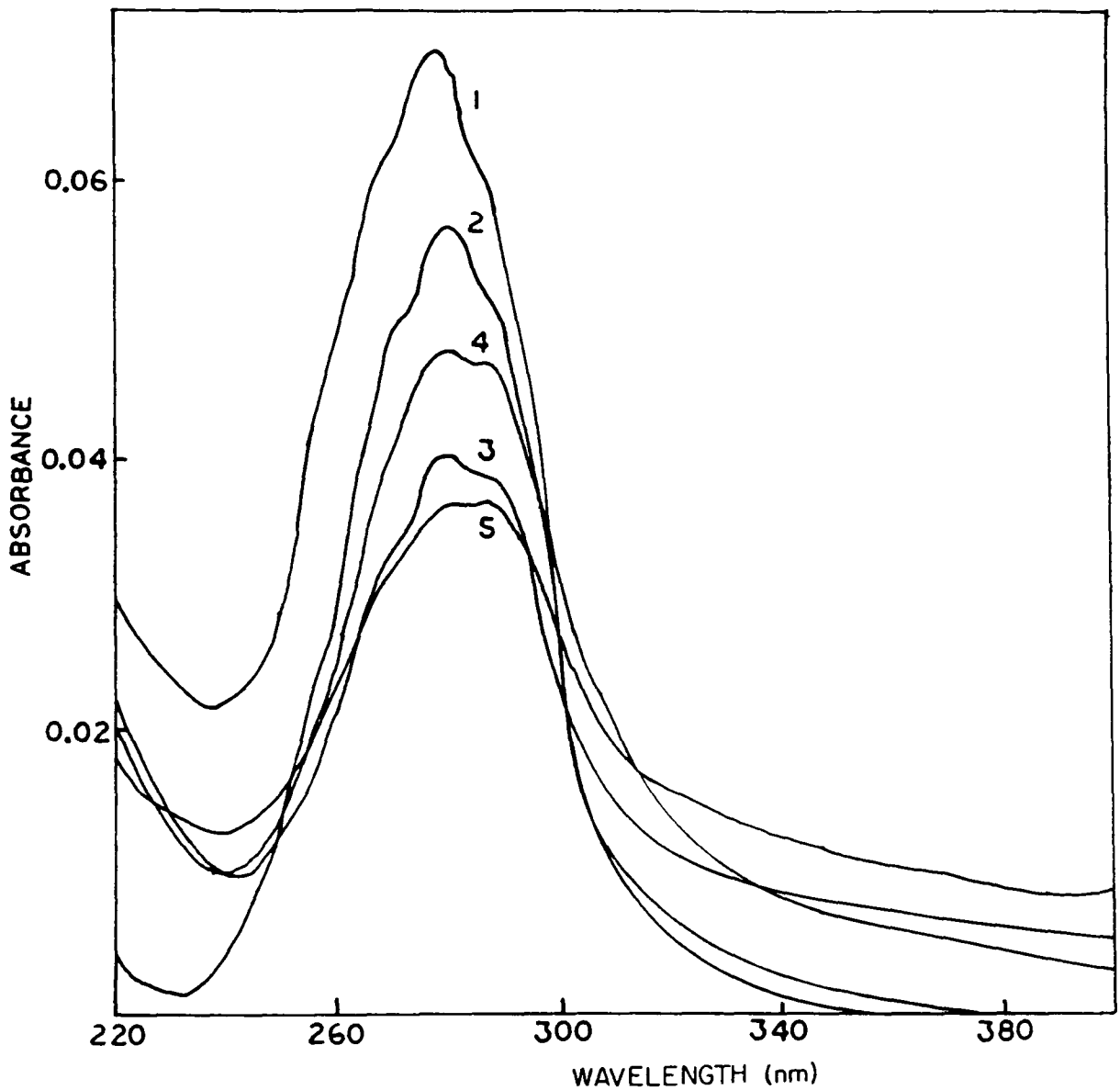

Figure 41: Absorption spectra of MV^{2+} in montmorillonite vs. MV^{2+}/clay ratio. for the case where this ratio was less than 100%, in all cases the concentration of MV^{2+} was kept constant at 2.0×10^{-6}M, MV^{2+}/Mont. = 1) 2.2% CEC, 2) 15% CEC, 3) 30% CEC, 4) 45% CEC and 5) 90% CEC.

An estimate of the relative value of ε in the two clays could be obtained from the comparison of two similar situations. The extinction coefficients were 28,000 $M^{-1}cm^{-1}$ at 280 nm (curve 2 of figure 41), at 15% CEC in montmorillonite and 30,000 $M^{-1}cm^{-1}$ at 275 nm (curve 2 of figure 40) at 14% CEC in hectorite.

Finally, the absorption spectrum of MV^{2+} (5.0×10^{-6}M) bound to the micelle SDS (1.0×10^{-4}M) was recorded. λ_{max} shifts to 265 nm but the molar extinction coefficient remained the same as in water, 20,000 $M^{-1}cm^{-1}$.[130]

9.3 UV-Visible Absorption Spectrum of $Ru(bpy)_3^{2+}$ Intercalated in Hectorite and Montmorillonite.

The absorption spectra of $Ru(bpy)_3^{2+}$ intercalated in hectorite and montmorillonite were measured. Figure 42 shows the metal to ligand charge transfer band (MLCT) of this complex in water, montmorillonite and hectorite. In agreement with previous reports λ_{max} shifted from 452 nm in water to about 470 nm in the clays.[150] In hectorite the molar extinction coefficient at 470 nm, 20,400 $M^{-1}cm^{-1}$, was also in agreement with the value reported in the literature. In montmorillonite it was lower than expected, only 15,100 $M^{-1}cm^{-1}$.

The spectra of $Ru(bpy)_3^{2+}$ in montmorillonite and hectorite were also measured at different values of the $Ru(bpy)_3^{2+}$/clay ratio. Once again some small variations of intensity were found at the various ratios. In hectorite when the ratio $Ru(bpy)_3^{2+}$/clay varied from 10% to 90 %CEC, ε decreased irregularly from 20,400 to 16,700 $M^{-1}cm^{-1}$. In montmorillonite the change was smaller, ε was 15,100 $M^{-1}cm^{-1}$ at 8% CEC and decreased irregularly to 13,000 $M^{-1}cm^{-1}$ at 85% CEC. The average in hectorite was 18,200 $M^{-1}cm^{-1}$ at 467 nm and in montmorillonite it was 14,200 $M^{-1}cm^{-1}$ at 474 nm. There was no visible change in the band shape or shift in λ_{max} with changes in the $Ru(bpy)_3^{2+}$/clay ratio.

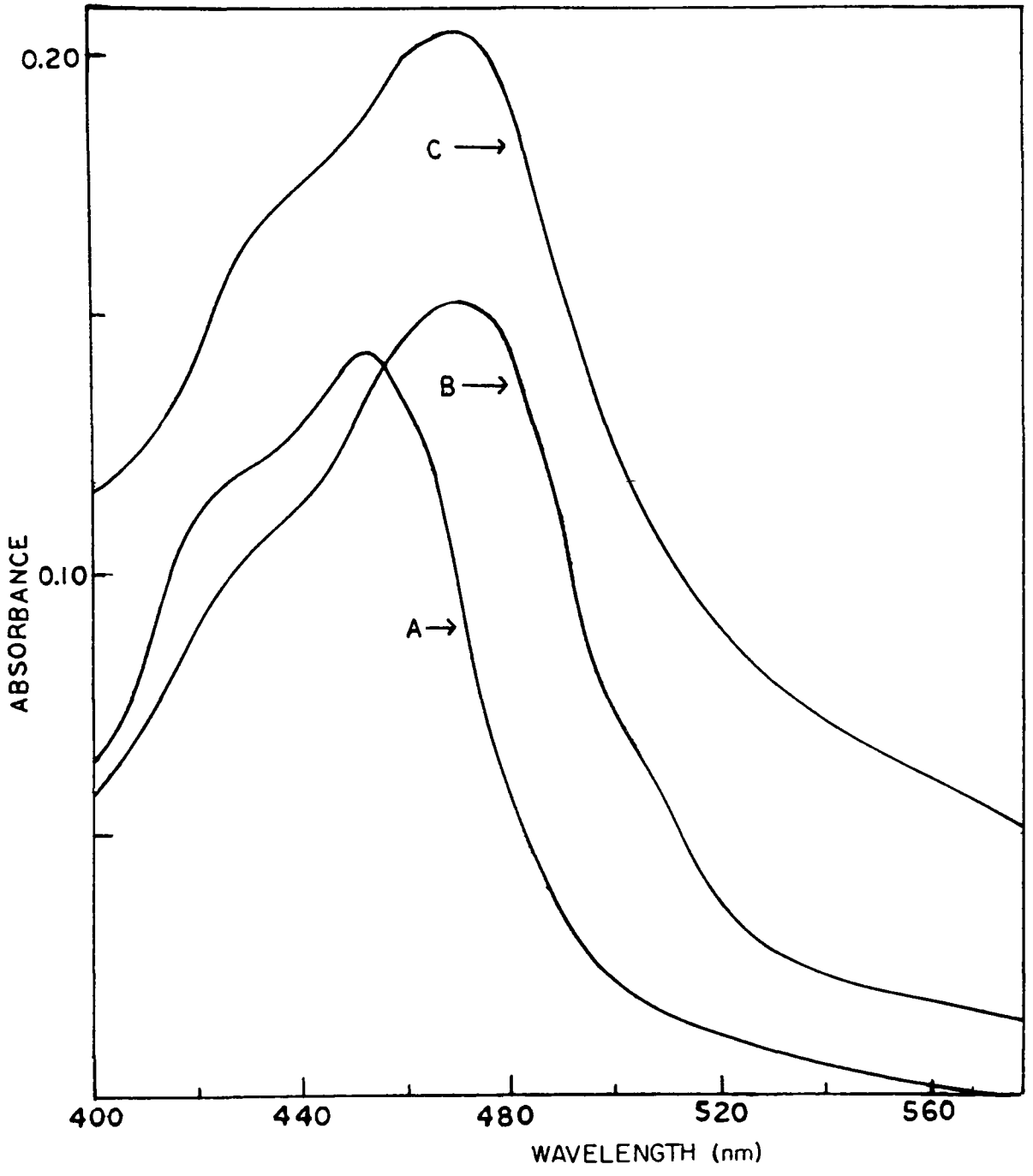

Figure 42: Absorption spectra of $Ru(bpy)_3^{2+}$. (1.0×10^{-5}M) in A) water B) montmorillonite (0.30 g/L, 8.0% CEC) and C) hectorite (0.30 g/L, 10% CEC).

9.4 Fluorescence of Clay Intercalated Methylviologen.

9.4.1 Fluorescence Spectra.

To the best of our knowledge, the fluorescence of MV^{2+} has not been previously reported under any conditions. The emission of light, near 500 nm, found in solutions of this cation has now been attributed to a fluorescent impurity.[185] No emission in the 300 to 400 nm region has ever been observed. In fact this cation was reported to be non-fluorescent in water.[184]

Despite this, a study of the effect of the presence of clay minerals on the fluorescence of MV^{2+} was undertaken. When MV^{2+} was intercalated in montmorillonite or hectorite a distinct fluorescence could readily be observed.[182]

In figure 43, the emission spectrum of MV^{2+} in montmorillonite is shown. The emission maximum was at 330 nm and the quantum yield, measured using NATA (N-acetyl-L-tryptophanamide)[161] as standard was 0.014. The fluorescence of MV^{2+} in water at the same concentration was barely detectable, the maximum occurred at 345 nm and the quantum yield was estimated to be less than 0.001. To check that the fluorescence in water or clays was not due to an impurity the MV^{2+} cation was purified by two successive recrystallizations from methanol. It had no effect on the observed light emission.

The fluorescence of MV^{2+} was also measured in two other clays minerals, hectorite and nontronite. The intensity of fluorescence observed was seen to depend on the iron content of the clay. Table 19 shows that in hectorite, which contained almost no iron, the intensity was 10 time greater than that in montmorillonite, while no fluorescence could be detected in the presence of the iron rich clay nontronite. Finally, negligible fluorescence was observed when MV^{2+} (5.0×10^{-6}M) was adsorbed into SDS (1.0×10^{-4}M) micelles.

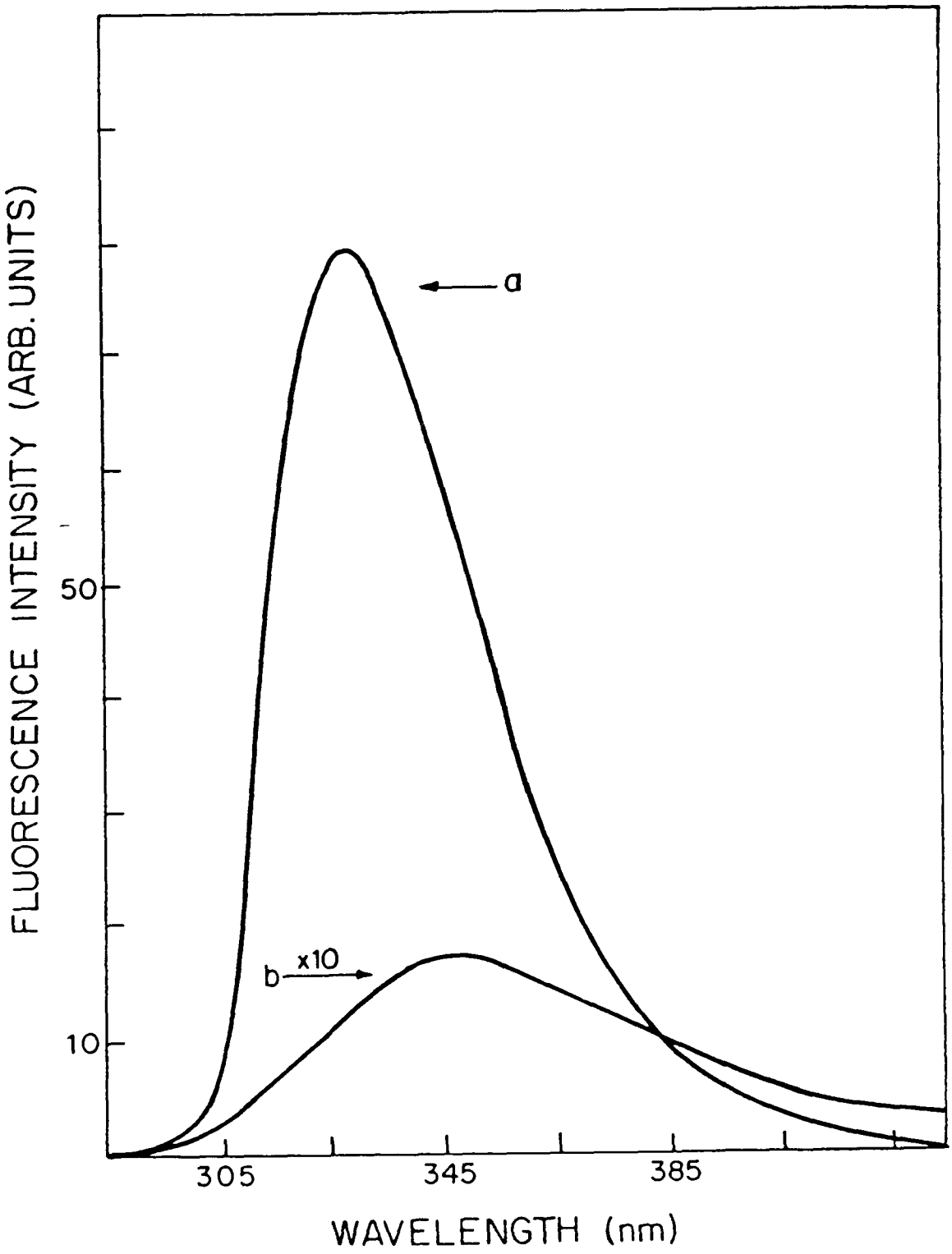

Figure 43: Corrected fluorescence spectra (λ_{ex} = 285 nm) of MV^{2+}, 5 x 10^{-6}M. a) Adsorbed on montmorillonite (0.25 g/L, 4.5% CEC) and b) in water at room temperature and pH 7. The spectrum (b) in aqueous solution was recorded at a sensitivity which was 10 x greater than for spectrum (a).

Table 19. Fluorescence intensity of MV^{2+} in smectites of different iron content.

Clay	$\%Fe_2O_3$	MV^{2+}/clay (%CEC)	Fluor. Int. Arb. Unit
Hectorite	0.37	5.6	640
Montmorillonite	4.17	4.5	43
Nontronite	32.3	4.2	--

Fluorescence intensity at 330 nm following excitation at 285 nm of a solution 5.0×10^{-6}M in MV^{2+} in the presence of 0.25 g/L of the clay.

The fluorescence emission and excitation spectra of MV^{2+} intercalated in hectorite and montmorillonite are compared in figures 44 and 45. Except for the fact that the intensity in hectorite was more than ten times larger than in montmorillonite, the two emission spectra are very similar. The emission maxima were at 330 nm and 326 nm in montmorillonite and hectorite respectively.

The two excitation spectra were also similar in shape. Their maxima were 274 nm in hectorite and 275 nm in montmorillonite. Again the intensity was more than ten times larger in hectorite. Further, comparison with figures 40 (curve 1) and 41 (curve 1) showed that the two excitation spectra were also very similar in shape to the corresponding absorption spectra. In hectorite the excitation spectrum was also recorded for two different emission wavelengths (see figure 46) and at several values of the MV^{2+}/clay ratio (see figure 47). In all cases the spectra had the same shape and only the intensity varied. All these results indicated that there was either one fluorescing species, or that all the fluorescing species had the same spectra.

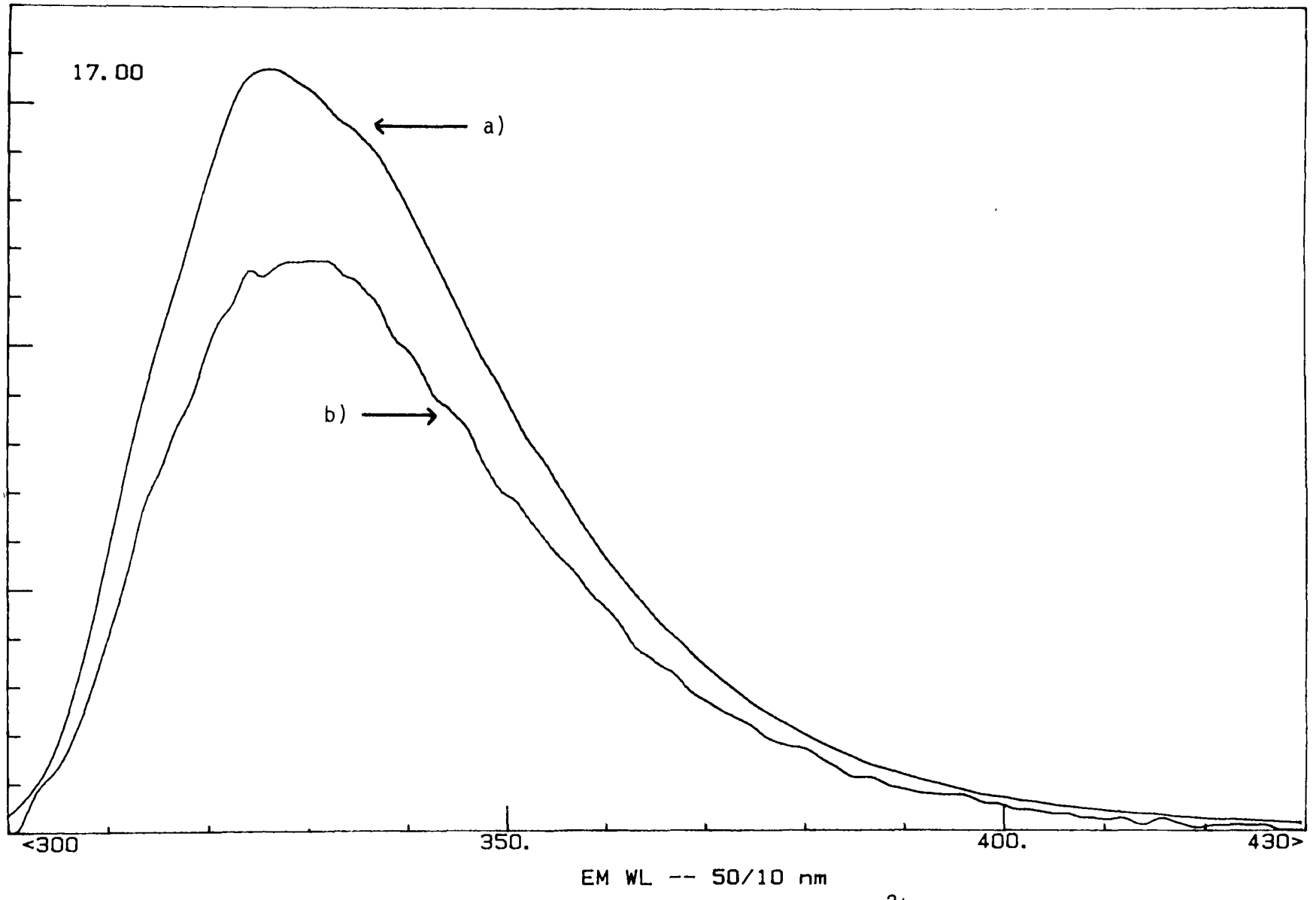

Figure 44: Corrected fluorescence emission spectra (λ_{ex} = 270 nm) of MV^{2+} (1.0×10^{-6} M) intercalated in a) hectorite (0.050 g/L, 5.6% CEC); b) montmorillonite (0.100 g/L, 2.2% CEC). The spectrum b) was recorded at a sensitivity which was 10 x greater than that for spectrum a).

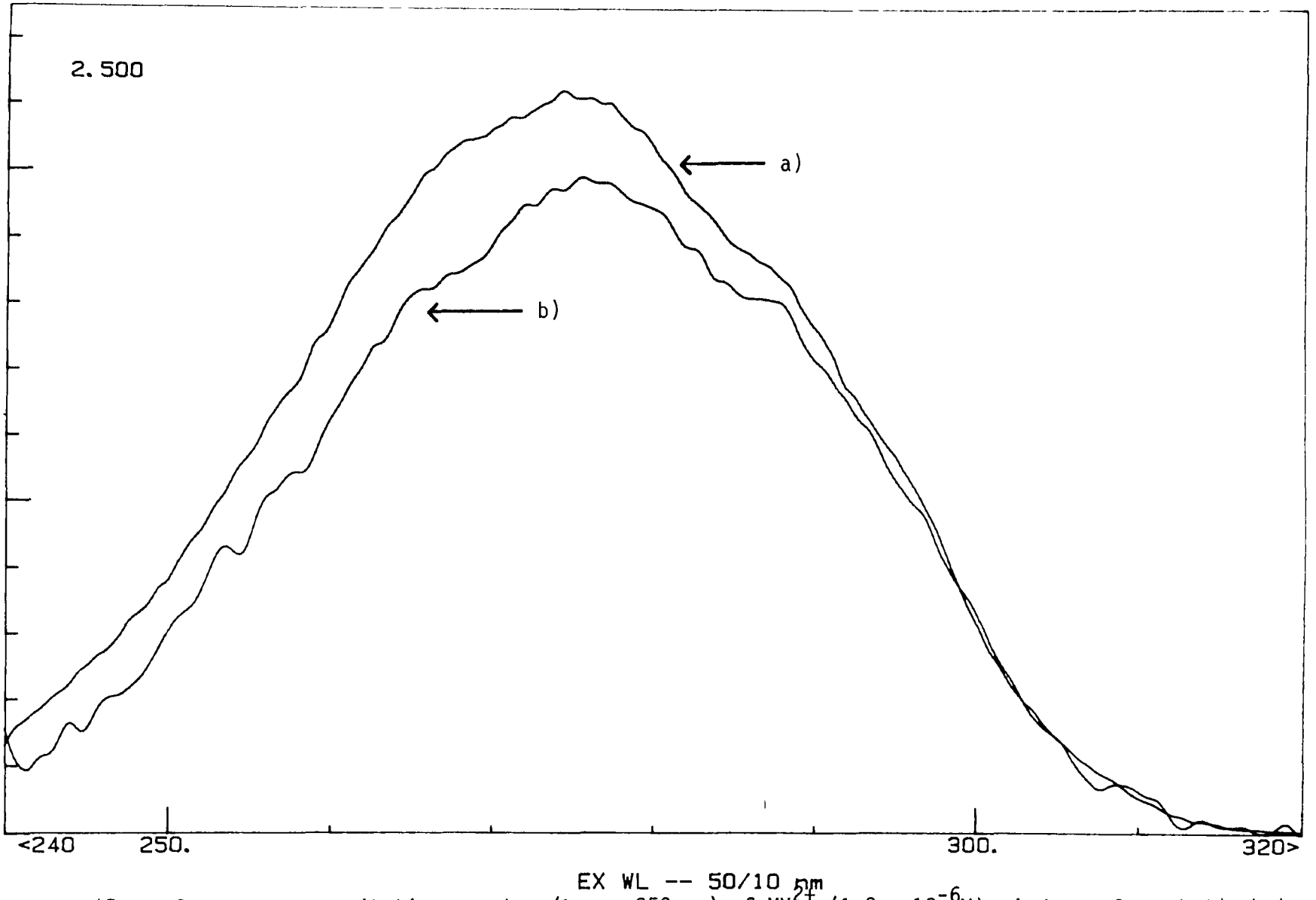

Figure 45: Fluorescence excitation spectra (λ_{em} = 350 nm) of MV^{2+} (1.0×10^{-6} M), intercalated in (a) hectorite (0.050 g/L, 5.6% CEC); (b) montmorillonite (0.100 g/L, 2.2% CEC). The spectrum (b) was recorded at a sensitivity which was 10 x greater than that for spectrum (a).

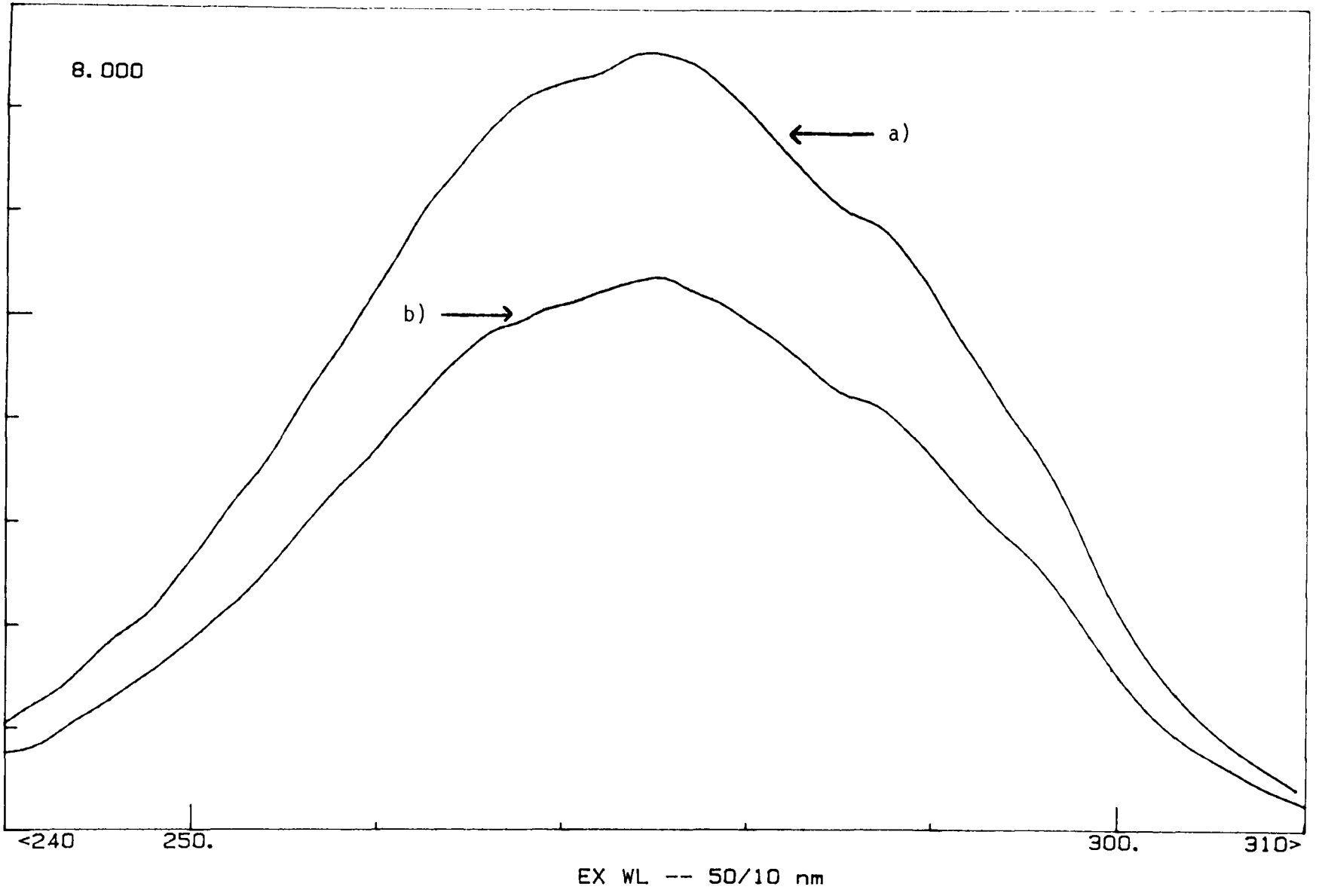

Figure 46: Fluorescence excitation spectra of MV^{2+} (2.0×10^{-6}M), intercalated in hectorite (0.050 g/L, 2.8% CEC) for two different emission wavelenghts, a) 325 nm and b) 350 nm.

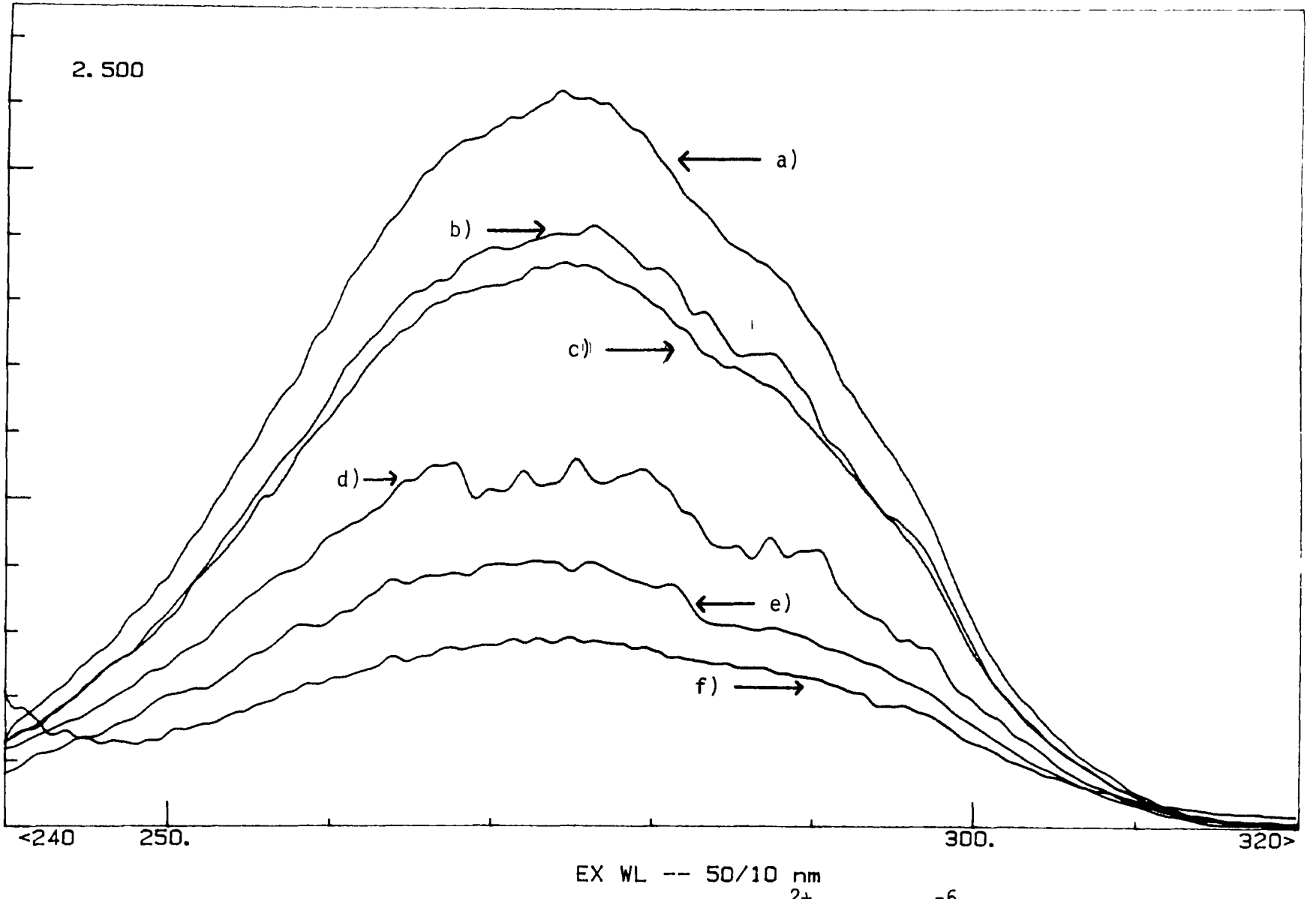

Figure 47: Fluorescence excitation spectra (λ_{em} = 350 nm) of MV^{2+} (1.0×10^{-6}M), intercalated in hectorite for different MV^{2+}/clay ratios, a) 5.6% CEC, b) 13.9% CEC, c) 27.7% CEC, d) 46.3% CEC, e) 92.6% CEC and f) 185% CEC.

9.4.2 Fluorescence Intensity as a Function of the MV^{2+} to Clay Ratio.

The fluorescence of MV^{2+} intercalated into hectorite and montmorillonite was measured as a function of the cation to clay ratio. As seen in figures 48 and 49, in both clays the intensity of the emitted light was observed to depend on this ratio.

Table 20: Variation of the fluorescence intensity with the ratio MV^{2+}/clay in montmorillonite.

MV^{2+}/clay (%CEC)	clay/MV^{2+} (g/mole)	Fluor. Int. Arb. Unit
0.28	8.0×10^{-5}	58 ± 10*
0.37	6.0×10^{-5}	49 ± 10
0.55	4.0×10^{-5}	57 ± 10
1.1**	2.0×10^{-5}	58 ± 5
1.9	1.2×10^{-5}	65 ± 5
2.2	1.0×10^{-5}	73 ± 5
4.5	0.5×10^{-5}	81 ± 5

* The large error margin on the fluorescence intensity was due to the need to reduce [MV^{2+}] so as not to have to increase [clay] and render the mixture too opaque. ** First point of figure 48.

In montmorillonite the intensity of fluorescence increased as the ratio increased from 1.1% CEC to 15% CEC. With further increase in the ratio, the intensity decreased nearly linearly. In hectorite the fluorescence intensity was largest at the lower ratios. With an increase in the ratio, it fell rapidly at first and then more slowly.

The variation of the intensity was further studied at very low MV^{2+}/clay ratios in montmorillonite. The decrease in intensity was observed to level off at MV^{2+}/clay ratios of less than 1% CEC. (see table 20)

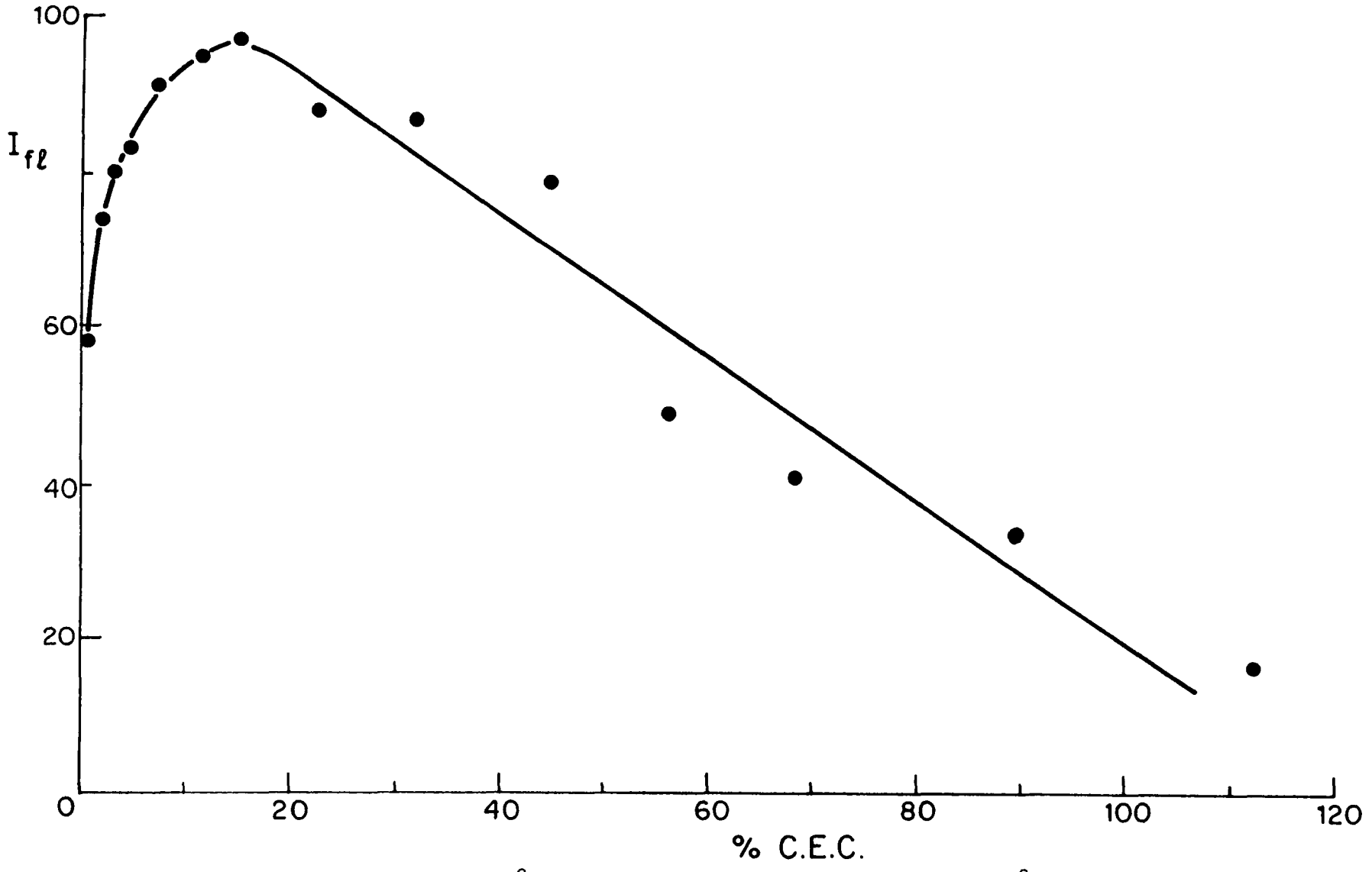

Figure 48: Fluorescence intensity of MV^{2+} intercalated in montmorillonite vs. MV^{2+}/clay ratio. λ_{ex} = 270 nm λ_{em} = 330 nm, the concentration of methylviologen was constant at 1.0×10^{-6}M and the clay concentration was varied from 0.200 to 0.002 g/L.

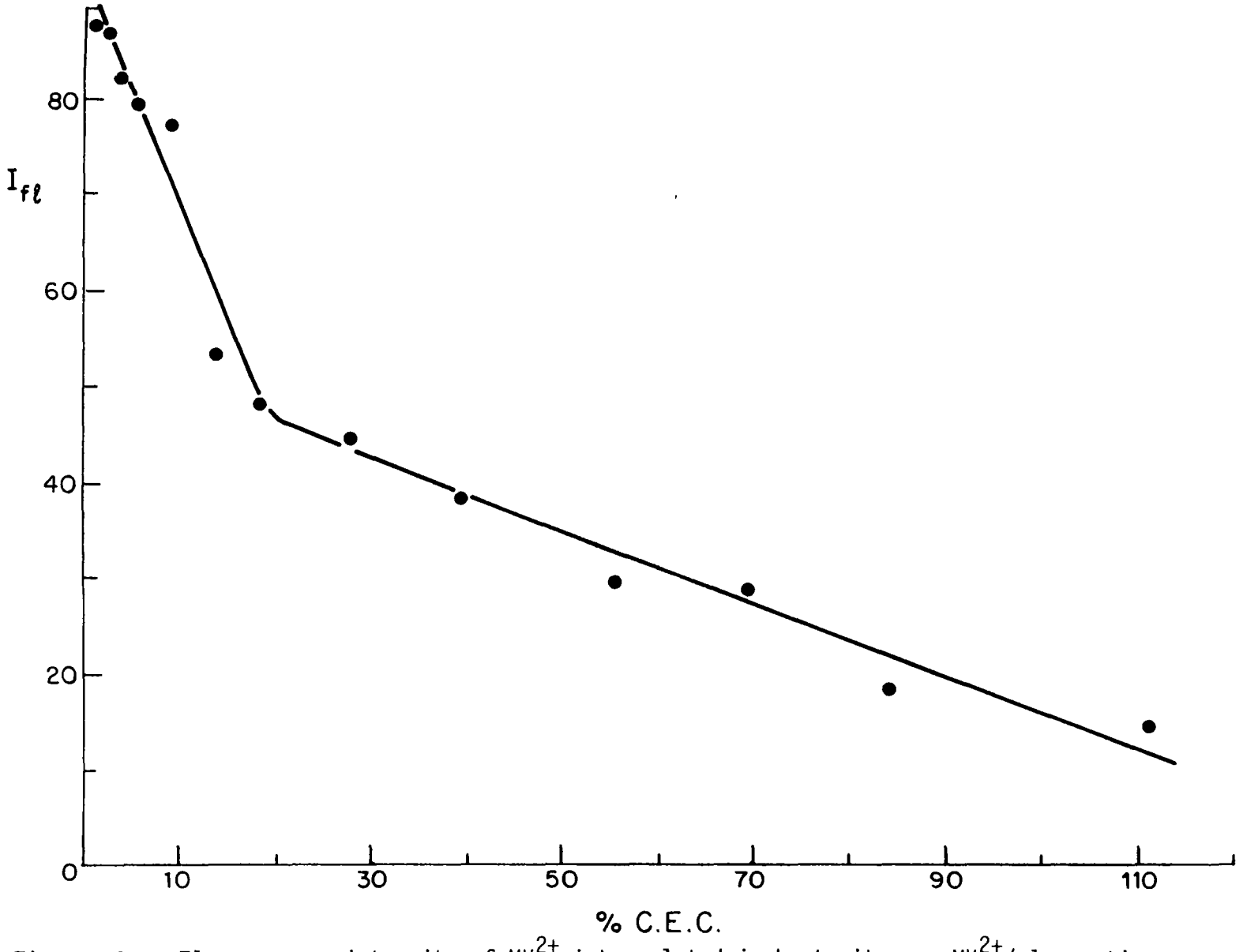

Figure 49: Fluorescence intensity of MV^{2+} intercalated in hectorite vs. MV^{2+}/clay ratio. λ_{ex} = 270 nm, λ_{em} = 330 nm, the concentration of **methylviologen was constant at** 1.0×10^{-6} M and the clay concentration was varied from 0.200 to 0.0025 g/L.

9.4.3 Fluorescence Anisotropy.

The anisotropy of the fluorescence of MV^{2+} intercalated in hectorite was studied. In practice when one measures the anisotropy one must correct for the response of the instrument, which is different for vertically and horizontally polarized light. This instrument correction factor, G, is given by equation 47.

$$G = I_{HV}/I_{HH} \qquad [47]$$

I_{HH} is the intensity when both polarizer are oriented horizontally and I_{HV} is the intensity when excitation is with horizontally polarizer light and the emission is observed through a vertically oriented polarizer. G should be the same for all samples at a given set of excitation and emission wavelengths. The value of the anisotropy is given by a modified equation 38.[161]

$$r = [I_{VV} - (I_{VH}G)]/[I_{VV} + (I_{VH}G)] \qquad [48]$$

I_{VV} is the intensity when both polarizers are oriented vertically and I_{VH} is the intensity when the emitted light is measured through an horizontally oriented polarizer.

The value of G was observed to vary with the MV^{2+}/clay ratios, going from 1.07 at 6.9% CEC to 1.33 at 93% CEC. This was thought to be due to light scattering. The anisotropy was therefore measured as a function of the absorbance at 270 nm of the blank (no MV^{2+}) clay suspensions, to obtain r' via equation 42.[176 177] (see section 8.3) The value of G (0.91) used in the calculation of r_{obs} was the one obtained using NATA in water. NATA was used because it had similar excitation and emission wavelengths, its emission was not polarized and it did not scatter light.

The expected decrease in the observed anisotropy, predicted by Teale[176] was not found. Within experimental error the value of r', the anisotropy obtained by extrapola-

tion to zero turbidity (see equation 42), was the same as the average of the values of r_{obs}. The values of the anisotropy given in the remainder of this section refer to this average of the r_{obs}.

Table 21: Anisotropy as a function of the MV^{2+}/clay ratio.

MV^{2+}/clay (%CEC)	Anisotropy r
3.9	0.068 ± 0.005
6.9	0.065 ± 0.005
14	0.071 ± 0.005
28	0.087 ± 0.005
57	0.114 ± 0.005
69	0.115 ± 0.010
83	0.120 ± 0.010
93	0.121 ± 0.010
99	0.110 ± 0.010

Excitation 270 nm, emission 330 nm, $[MV^{2+}] = 5.0 \times 10^{-6}$M, G = 0.91 measured with a sample of NATA in water.

The fluorescence anisotropy was measured as a function of the ratio MV^{2+}/clay. The results are shown in table 21 and are plotted in figure 50. The anisotropy was found to increase as the ratio increased, until a plateau was reached at approximately 50% CEC. The same variation was found for MV^{2+} intercalated in montmorillonite. In fact the anisotropy variation was larger in montmorillonite. It went from 0.08 at 3.1% up to 0.19 at 90% CEC. Because of the much lower intensity of the fluorescence, a complete study was not done in montmorillonite.

The anisotropy of the fluorescence of MV^{2+} in hectorite was also studied as a function of the temperature. It was difficult to obtain reproducible results because of the samples' turbidity. The anisotropy was found to be temperature independent between 2 and

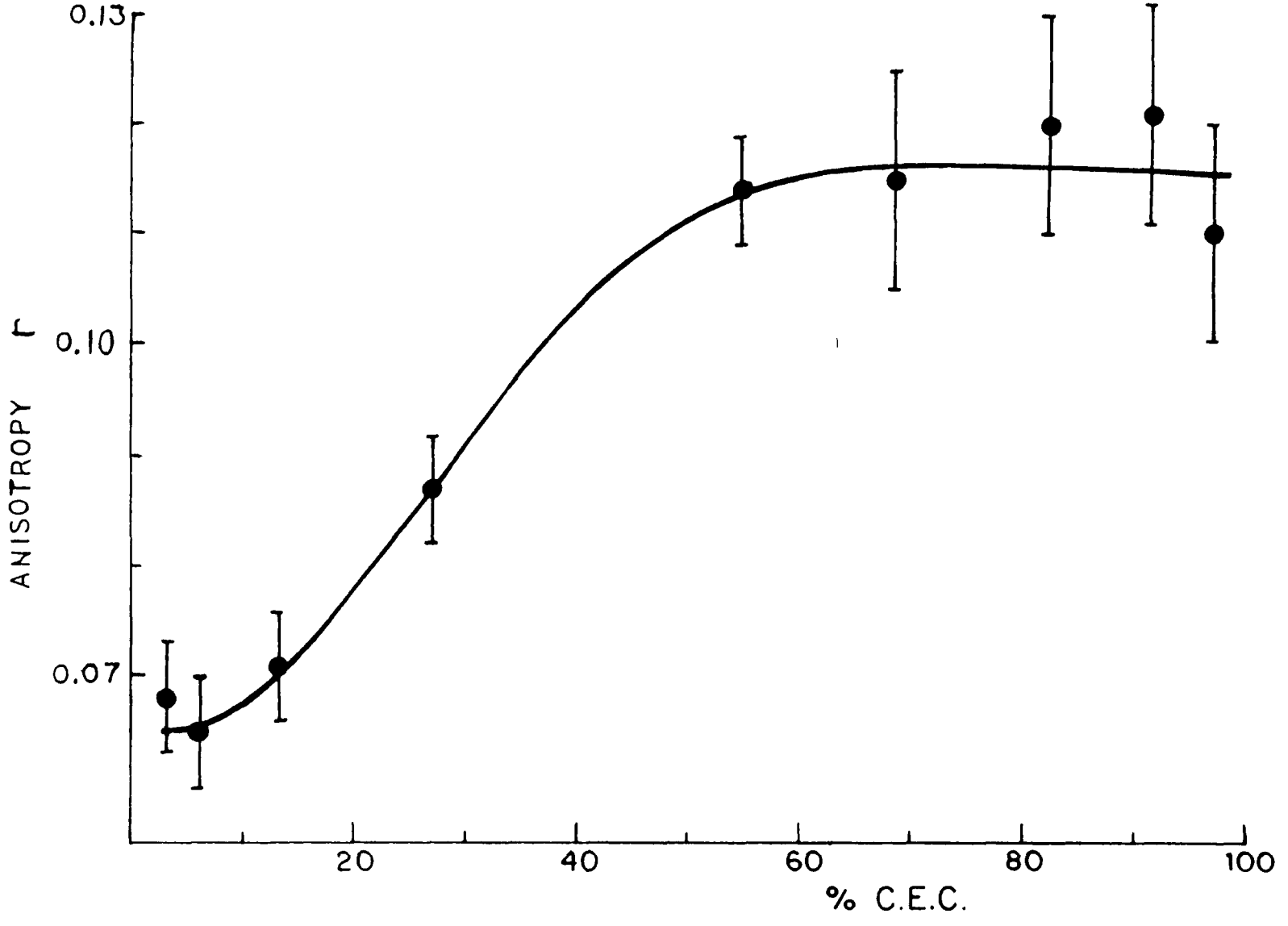

Figure 50: Fluorescence anisotropy as a function of the MV^{2+}/hectorite ratio. λ_{ex} = 270 nm, λ_{em} = 330 nm, the concentration of methylviologen was constant at 5.0×10^{-6} M and the clay concentration was varied from 0.360 to 0.014 g/L.

60°C within the error limits of the measurements (±10%). Finally it was observed that, at large MV^{2+}/clay ratio, the value of the anisotropy decreased as the sample aged. For example at 69% CEC, r decreased from 0.145 immediately after preparation to 0.115 3 hours after preparation, where it stabilized. At low MV^{2+}/clay ratio this was not the case. At 6.9% CEC for example r was time independent.

9.4.4 Fluorescence Lifetimes.

The fluorescence decay time of MV^{2+} intercalated into the two clays was measured at different values of the MV^{2+}/clay ratio. The results are summarized in tables 22 and 23. In figure 51 A, curve 1) is a typical example of the log of the fluorescence decay of MV^{2+} in hectorite and curve 2) is a typical instrument response function measured at the excitation wavelength used. In figure 51 B and C the residual plots for the best fit exponential functions are shown.

In montmorillonite, the best fit of the fluorescence decay was obtained with a sum of three exponential components (see figure 51). Except for the result at a MV^{2+}/clay ratio of 11.2% CEC, which was not consistent with the others, the three lifetimes were found to be independent of the cation to clay ratio. Even more surprisingly the relative contributions, F_i, of the exponentials to the total fluorescence intensity were also independent of the MV^{2+}/clay ratio.

All three lifetimes were shorter than one nanosecond. The longest was 0.95 nsec and its contribution to the fluorescence intensity was 0.41.* The second was shorter, 0.37 nsec, but it made a larger contribution to the fluorescence, 0.50. Finally the third was extremely short, 0.078 nsec and it contribution to the fluorescence was only 0.10.

* The results at MV^{2+}/clay ratio of 11.2% CEC were not used in the calculation of the average lifetimes or contributions.

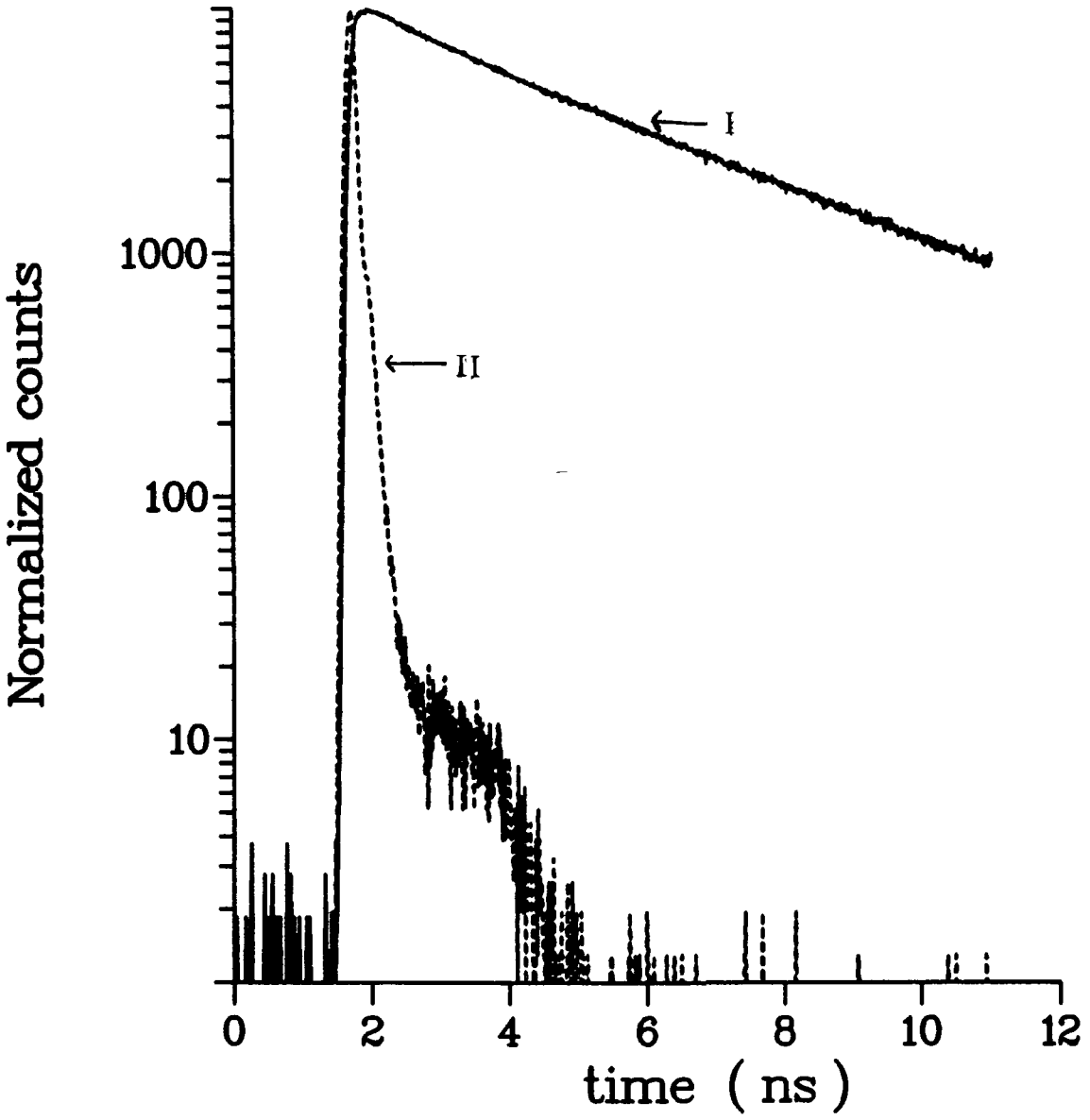

Figure 51A Log plot of I) fluorescence decay profile of MV^{2+} (1.0×10^{-6}M) in hectorite, (0.020 g/L) CEC = 27.8%, λ_{em} = 340 nm; II) instrument response function measured at 295 nm with a glycogen scatter. Channel width 10.8 ps.

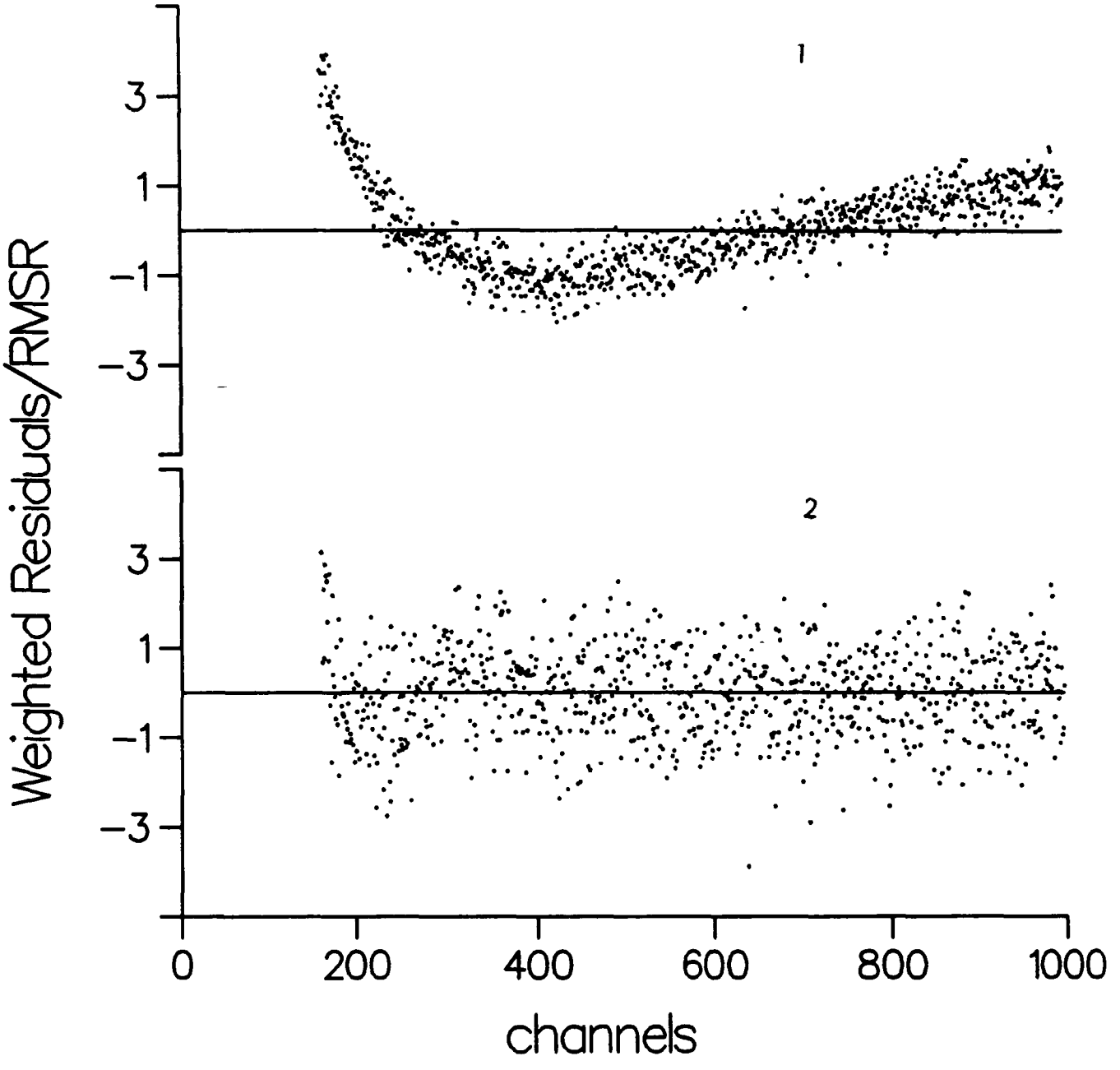

Figure 51B Plot of weighted residuals after iterative convolution of data for MV^{2+} in hectorite (27.8% CEC) for the "best fits" for 1) single exponential, 2) double exponential decay function.

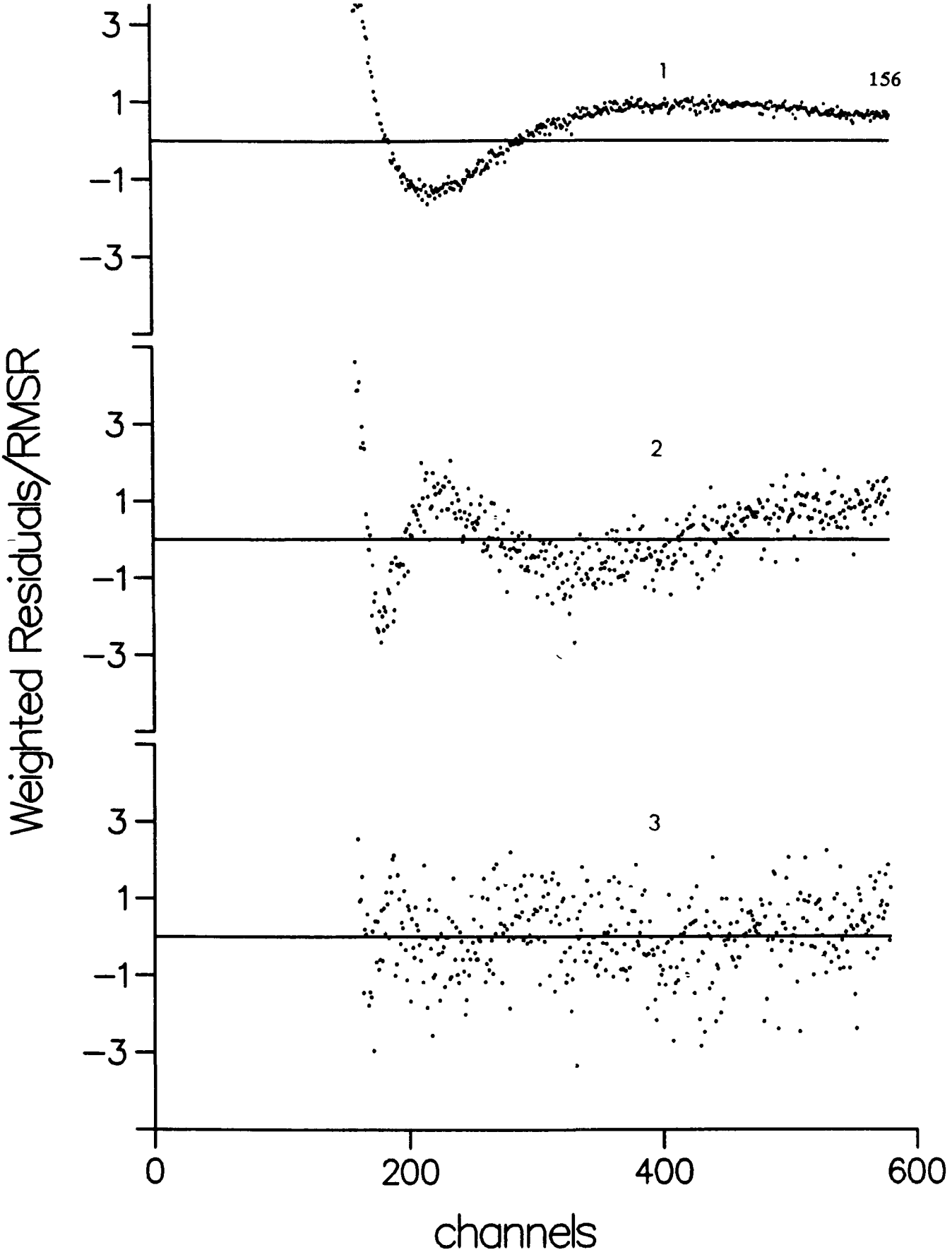

Figure 51C Plot of weighted residuals after iterative convolution of data for MV^{2+} in montmorillonite (22.4% CEC) for the "best fits" for 1) single exponential, 2) double exponential and 3) triple exponential decay function.

Table 22: The "best fit" decay lifetimes of fluorescence of MV^{2+} intercalated in montmorillonite.

MV^{2+}/clay (%CEC)	τ_1 nsec (F_1)	τ_2 nsec (F_2)	τ_3 nsec (F_3)
3.1	0.93 (0.41)	0.37 (0.50)	0.083 (0.10)
5.6	0.91 (0.43)	0.37 (0.48)	0.084 (0.10)
11.2	1.02 (0.32)	0.45 (0.52)	0.135 (0.15)
22.4	0.94 (0.41)	0.37 (0.50)	0.071 (0.10)
45	0.94 (0.42)	0.35 (0.49)	0.064 (0.09)
64	0.95 (0.40)	0.37 (0.50)	0.077 (0.10)
90	0.95 (0.38)	0.37 (0.50)	0.089 (0.12)

λ_{ex} = 295 nm, λ_{em} = 340 nm. Δt = 0.0108 nsec/ch, τ is the lifetime and F the relative contribution to the fluorescence intensity, given by $\alpha_i\tau_i/\Sigma\alpha\tau$, where α_i are the pre-exponential factors. Errors were for $\tau_1 \pm 0.01$, $\tau_2 \pm 0.01$, $\tau_3 \pm 0.005$ and $F_i \pm 0.01$

Table 23: The "best fit" decay lifetimes of fluorescence of MV^{2+} intercalated in hectorite.

MV^{2+}/clay (%CEC)	τ_1 nsec (F_1)	τ_2 nsec (F_2)	τ_3 nsec (F_3)
3.9	4.37 (0.90)	1.38 (0.10)	-----
9.9	4.26 (0.92)	1.19 (0.08)	-----
17.4	4.12 (0.93)	1.00 (0.07)	-----
28	4.06 (0.93)	1.07 (0.07)	-----
56	3.80 (0.91)	1.00 (0.09)	-----
93	3.50 (0.$^{-5}$)	1.12 (0.11)	0.023 (0.01)

λ_{ex} = 295 nm, λ_{em} = 340 nm. Δt = 0.0108 nsec/ch, τ is the lifetime and F the relative contribution to the fluorescence intensity. Errors were for $\tau_i \pm 0.01$ and $F_i \pm 0.01$.

In hectorite, the best fit of the fluorescence decay was obtained with a sum of two exponential components, (see figures 51 and 52) except at the ratio MV^{2+}/clay of 93% CEC, where three exponentials were required. Here the lifetimes were not independent of the MV^{2+}/clay ratio. The first lifetime decreased from 4.37 nsec at 3.9% CEC to 3.50 nsec at 93% CEC. (see table 23) The second lifetime also decreased, but not as regularly with increase of the MV^{2+}/clay ratio. At the ratio of 93% CEC a third lifetime was found, 0.023 nsec, It had a very small contribution to the fluorescence intensity of only 0.01. Also, in hectorite the decay parameters were highly correlated.

CHAPTER X

DISCUSSION.

10.1 The Fluorescence of MV^{2+} in Water.

Recently, MV^{2+} was reported to form fluorescent ion pairs with a variety of anions.[187 188] These complexes were found to have excitation and emission spectra that were independent of the anion present. Their emission spectra were centered around 520 nm and their excitation spectra were centered around 400 nm. This green fluorescence was not observed when the MV^{2+} cation was excited to its singlet excited state by illumination at 280 nm.[189 190]

It has now been shown conclusively that this emission was due to a strongly fluorescent impurity, and not to the MV^{2+} cation.[185 189] This was shown first of all by the fact that the intensity of the emission was dependent on the history of the MV^{2+} sample. In particular a freshly prepared solution did not emit.[190] Further, such a freshly prepared solution of MV^{2+} began to emit green light after exposure to ultraviolet light. Further, the emission has now been observed in the absence of added anions.[185] The emission was therefore attributed to an impurity, formed by the decay of MV^{2+} upon its irradiation with ultraviolet light.[190]

Emission from the singlet state of MV^{2+} was recently reinvestigated.[195] The authors concluded that the quantum yield of fluorescence of this cation had to be less than 10^{-4}, since they were not able to detect any fluorescence. To the best of our knowledge no fluorescence attributed to the transition from the singlet excited state of the MV^{2+} has ever been reported. In aqueous solution, this cation is considered to be non-fluorescent.[184 186]

Yet, as shown in figure 43, we were able to detect a very weak fluorescence of MV^{2+} in water. This barely detectable emission persisted even after two recrystallizations of the cation from hot methanol, showing that it was probably not due to an impurity. By comparison with the fluorescence of clay intercalated MV^{2+}, the quantum yield, which was too low to be measured reliably, was estimated to be approximately 3×10^{-4}. [182]

In our hands, the fluorescence in water was extremely weak, if it was detectable at all. As shown in figure 43, we found that the fluorescence of MV^{2+} was significantly enhanced when it was in the presence of clay minerals. In this chapter, this emission is described and we attempt to show how intercalation of MV^{2+} may lead to such a dramatic increase of the fluorescence.

10.2 Fluorescence of Clay Intercalated Methylviologen.

An enhancement of the fluorescence of MV^{2+} was observed when the cation was in the presence of two expandable clay minerals, montmorillonite and hectorite. The emission spectra were similar in shape in both clays. The emission maxima were 330 and 327 nm, respectively, in montmorillonite and hectorite.

In hectorite, the fluorescence intensity was more than ten time higher than in montmorillonite. This was attributed to the presence of larger amounts of structural iron in montmorillonite than in hectorite. Table 19 showed that the intensity of the fluorescence of MV^{2+} in the presence of three clay minerals, hectorite, montmorillonite and nontronite correlated well with the iron content of the clays. The lower intensity found in montmorillonite bound MV^{2+} and the absence of fluorescence in the presence of iron rich nontronite was therefore attributed to quenching of the excited MV^{2+} cations by structural iron. This was in accord with what was found when the effect of the clay iron content on the intensity of the light emitted by intercalated $Ru(bpy)_3^{2+}$ was studied.[150 181]

The excitation spectra were similar in shape in both clays. They were also found to be superimposable on the absorption spectra of MV^{2+} in the two clays. Further, all spectral evidence showed that all the adsorbed MV^{2+} cations have the same absorption spectrum and the same fluorescence spectrum.

The absorption spectra of MV^{2+} bound to montmorillonite and hectorite (figures 38 to 41) can be discussed in the following terms. The red shift was reported previously for MV^{2+} in montmorillonite.[138 183] It was attributed to either a charge transfer complex between the cation and the clay or to conformational changes induced by the intercalation of the cation. Charge transfer processes with aromatic nuclei are known to cause shifts in the ultraviolet spectra of molecules. The shift in MV^{2+} clay complexes were analogous to the shifts observed for several ion pairs formed by the association of MV^{2+} with anions.[192] Furthermore, attributing the observed shift of the absorbance maximum of clay bound MV^{2+} to a charge transfer process between the siloxane surface and the bipyridyl nuclei, allowed a similar interpretation of the analogous shift of the MLCT band of clay adsorbed $Ru(bpy)_3^{2+}$ (see figure 42).

Alternatively, the shift could be due to a change in configuration of the adsorbed cation. In aqueous solution, MV^{2+} can rotate about the single bond joining its two pyridinium rings. But in the clay interlayer spaces, as we saw in chapter 7, MV^{2+} was constrained into a planar configuration.[134 138 139] The position of λ_{max} in the presence of clay minerals was similar to the absorption maximum found for solid $MVCl_2$, 285 nm,[193] and it is known that in solid $MVCl_2$, the MV^{2+} cation adopts a planar configuration.[143] Further, although it has a more rigid conformation, diquat in water is not planar.[147] When it was intercalated into clays, diquat assumed a flatten configuration.[138 139] Its absorbance maximum was also shifted to the red by intercalation, but by a smaller amount than MV^{2+}. The red absorbance shift has also been reported to be much smaller when MV^{2+} was intercalated into vermiculite.[138] This was attributed to a greater

conformational flexibility of the cation in the interlayer spaces of this clay. As we saw in chapter 7, the intercalation of MV^{2+} in vermiculite did not cause the collapse of the clay. The interlayer spacings of a wet MV^{2+} vermiculite complex were 5 Å compared to 3 Å for MV^{2+} in montmorillonite.

All the UV-Visible results showed that all the adsorbed MV^{2+} cations have the same absorption spectrum. The presence of isosbestic points in the spectra of MV^{2+} for the cases in which the MV^{2+}/clay ratios are larger than 100% CEC (see figure 39) is indicative that there are only two spectral species, one for free MV^{2+} and one for bound MV^{2+}. Figures 40 and 41 show that the spectrum of bound MV^{2+} did not change with the ratio MV^{2+}/clay, when this ratio was less than 100% CEC. The shape and the position of the band were independent of the MV^{2+}/clay ratio in both clays. The apparent increase in the intensity of the bands was attributed not to the presence of more than one species having distinct absorption spectra, but to differences in size and shape of the clay particles between the reference and the sample clay suspensions. The presence of the MV^{2+} cation in the sample affected the clay suspension in such a way that a suspension of Ca^{2+} exchanged clay was not a proper blank for recording the absorption spectrum of MV^{2+} exchanged clay. A study of MV^{2+} exchanged montmorillonite by scanning electron microscopy (see chapter 12) showed that the presence of the organic cation had an effect on the configuration of the clay particles. Therefore, the increase in the intensity of the absorption band of clay intercalated MV^{2+} was assumed to be due to alteration of the properties of the clay suspension, resulting in changes in the light scattering power or the degree of aggregation of the clay particles. Some evidence that this was indeed the case was provided by the observation that the absorbance of the mixtures, especially at high ratios did not go to zero at 400 nm, where MV^{2+} did not absorb light.

Similarly, the independence of the excitation spectra on the emission wavelength and the MV^{2+}/clay ratio, shown in figures 46 and 47, showed that either there was only one fluorescing species, or that all fluorescing species have the same fluorescence spectrum.

10.3 Origin of the Fluorescence of Intercalated Methylviologen.

The observed enhancement of the fluorescence of intercalated MV^{2+} may originate from several phenomena.

One is a reduction of the quenching by the chloride counter ions. Intercalated MV^{2+} cation would be shielded from the counter ion by the clay layers. MV^{2+} and 4,4'-bipyridine were nonfluorescent in aqueous solution. Yet their derivatives 1,1',2,2',6,6'-hexamethyl-4,4'-bipyridine dication and 2,2',6,6'-tetramethyl-4,4'-bipyridine were fluorescent.[190] This was attributed to shielding of the cations from deactivation by interaction with the counter anions, due to steric hindrance resulting from the presence of the methyl groups.[190] Adsorption of the cation was expected to isolate MV^{2+} from the chloride counter ion much more efficiently. Such a protection of an adsorbed chromophore was invoked to account for the low efficiency of the quenching of excited $Ru(bpy)_3^{2+}$ by oxygen when $Ru(bpy)_3^{2+}$ was adsorbed on polymerized SiO_2.[164] An argument against reduced quenching by the counter ion as the main reason for the increase in fluorescence was that in such dilute solutions (10^{-6}M) quenching by the chloride was not expected to be so efficient as to preclude the detection of any fluorescence.

Some entropy was lost upon intercalation of MV^{2+}, especially since it caused the collapse of the clay stacks.[138] Its apparent diffusion coefficient, the sum of contributions from the lateral diffusion and from electron exchange (hopping) between adjacent sites was estimated to be 9.0×10^{-12} cm^2/s.[140] Essentially the cations were immobile in the clay on a nanosecond time scale. This would preclude diffusional self-quenching of the MV^{2+} cations and could account for part of the increase in fluorescence. But, once again, because of the low concentration, reduced self quenching was not expected to be a major factor.

As mentioned in the previous section, the intercalation of MV^{2+} had an effect on the configuration of the cation. In water MV^{2+} is not planar, and there is some rotation-

al freedom around the single bond linking the two pyridinium rings. Intercalated MV^{2+} has been shown to adopt a planar configuration.[138 139] The interlayer spacings of intercalated MV^{2+} were only 3.0 Å (see tables 16 and 17). Rotation around the single bond linking the two pyridinium rings would therefore be restricted. We propose that this reduced rotational flexibility reduces the efficiency of the nonradiative deactivation processes. The importance of the conformational flexibility of MV^{2+} in fluorescence deactivation processes was shown principally by the fact that the conformationally rigid viologen derivative, diquat (1,1'-ethylene-2,2'-bipyridinium dichloride, see figure 35) was fluorescent in water.[184] In diquat, rotations around the single bond linking the two pyridinium rings are blocked by the ion's ethylene bridge,[147] and the cation fluorescence can be observed in water.[184] In intercalated MV^{2+}, these rotations are blocked by the clay layers, and the cation fluorescence can be observed in clay suspensions. Another argument for this explanation was our observation that MV^{2+} adsorbed in the micelle SDS did not fluoresce. Unlike in clays, MV^{2+} adsorbed on the surface of SDS retained much of its conformational flexibility. This was supported by the smaller red shift of the MV^{2+} absorption maximum observed when the cation was adsorbed in the micelle compared to clays, from 257.5 to only 265 nm. MV^{2+} did not adopt a rigid planar configuration in the micelle and therefore it did not fluoresce.

Alternatively, the absence of fluorescence when MV^{2+} in the SDS micelle could be due to the fact that since the cation was adsorbed on the outside surface, it was still exposed to the solvent, and MV^{2+} was non-fluorescent in water because of solvent quenching. Reduced quenching by water was used for example, to account for the increase of the fluorescence of 2-p-toluidinyl-6-naphthalene sulfonate when it was bound to proteins.[191] The fluorescence in clay minerals may be due to a shielding of MV^{2+} from quenching by the solvent. Such a protection from quenching by the solvent was invoked to account for the very long lifetime of the phosphorescence of $Ru(bpy)_3^{2+}$ in polymer-

ized silica.[164] The intercalation of MV^{2+} would remove the cation from a water environment since, as we saw in chapter 7, intercalation of MV^{2+} in montmorillonite resulted in the displacement of most of the interlayer water. Even if some water molecules remained in the interlayer spaces of the clay, the immobilization of the cation and of these adsorbed water molecules could still result in a reduction of the efficiency of the quenching.

10.4 Effect of the MV^{2+}/clay Ratio on the Fluorescence of Clay Intercalated Methylviologen.

The intensity and the lifetime of the fluorescence of MV^{2+} intercalated in clays were studied as a function of the cation to clay ratio.

The most surprising results obtained in the study of the lifetime of the fluorescence was the independence of the decay time on the cation to clay ratio. In montmorillonite the decay of the fluorescence of adsorbed MV^{2+} was fit to the sum of three exponentials (see table 22). In hectorite, except at a ratio of 93% CEC the decay of the fluorescence intensity was best fit to a sum of two exponentials (see table 23). In both clays, the lifetimes, τ_i and the relative contributions to the fluorescence intensity, F_i, did not change with the cation to clay ratio. Therefore, we do not believe that the decay times represent distinct adsorption sites for MV^{2+} in the clays. If we assume that there were two or three fluorescing species in hectorite and montmorillonite respectively, then the fact that the relative contributions to the fluorescence intensity were constant with variation of the %CEC would require that they all had the same binding constant with the clays. Then their relative populations would remain constant, irrespective of the MV^{2+}/clay ratio. We do not consider that this was likely.

Hence, the postulation of several fluorescing species cannot be used to explain the variation of the fluorescence intensity with the %CEC shown in figures 48 and 49. If the relative populations of the sites were independent of the cation to clay ratio, so too would the intensity of the fluorescence.

According to equation 46, the quantum yield of fluorescence is directly proportional to the lifetime, if the lifetime is constant, then Φ_f must be constant. Further since we found that the relative contributions to the fluorescence were independent of the %CEC then, according to equation 36, the only way I_f could vary when Φ_f did not, was a variation of the concentration of the fluorescing species. In order to interpret the variation of the fluorescence intensity shown in figures 48 and 49, we have to take into account non-fluorescent component, whose concentration was not constant.

The results in hectorite, (figure 49) showed that the intensity was highest at low CEC. With increased %CEC, the intensity fell, rapidly at first and then more slowly. There appeared be a break in the curve at near 20% CEC. It is suggested that there were two factors that could account for this decrease. The first was self-quenching of the fluorescence of adsorbed MV^{2+}, and the second was that with an increase in the %CEC there was a gradual increase of the population of a non-fluorescent binding site.

At low %CEC self-quenching was inefficient because of the large distance between the adsorbed cations. For example in hectorite at a ratio of 3% CEC the average distance between two MV^{2+} was almost 70 Å, while at 100% CEC it was less than 15 Å.* The variation of the average distance between two adsorbed MV^{2+} cations in hectorite as a function of the cation to clay ratio is shown in figure 52. In the first case (curve A) all the MV^{2+} were assumed to be intercalated, with no cations on the clay external surfaces, while in the second case (curve B) a uniform distribution of the cations on both the inter-

* The average distance between the center of two cations assuming a uniform distribution of the cations on the surfaces, taking 750 m^2/g as the surface area of the clay, 150 m^2/g as the external surface area of the clay and 0.72 meq/g as 100% CEC. (see figure 52)

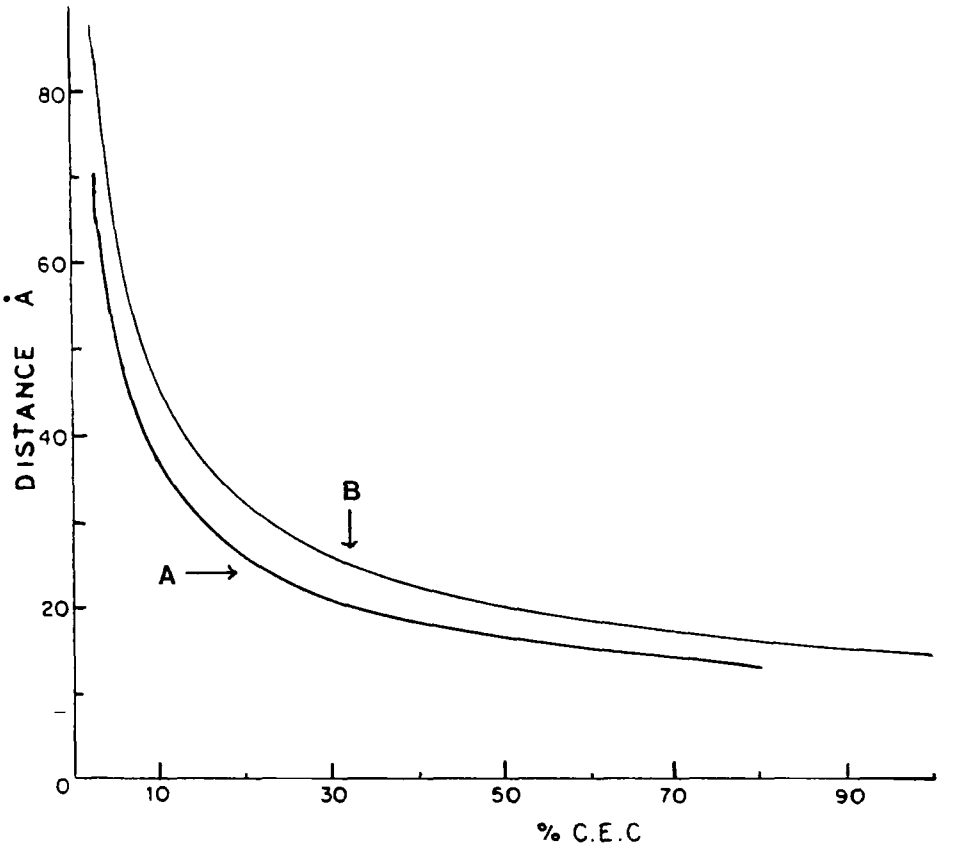

Figure 52: Average distance between two adsorbed MV^{2+} in hectorite as a function of the CEC. A) Calculated assuming that all of the cations were intercalated. B) Calculated assuming that the cation were evenly distributed in the interlayer and on the external surfaces of the clay. (the external surfaces were assumed to account for 20% of the total surface area of the clay, 150 m^2/g out of 750 m^2 /g.)

nal and external surfaces was assumed. Both curves are similar in shape. The "real" situation was probably a gradual change from curve A at low %CEC to curve B at large %CEC. Notice the similarity of these curves to the one shown in figure 49 for the variation of the fluorescence intensity of MV^{2+} in hectorite as a function of the %CEC. The decrease of the fluorescence intensity with increase in the cation to clay ratio could therefore be attributed to self-quenching of the intercalated cation. Since the average distance decreased much more rapidly at low %CEC, this explanation account for the break in the curve of figure 49.

The decrease of the fluorescence intensity could also be due to the existence of a non-fluorescent site. In chapter 7 we postulated that at 100% CEC approximately 20% of

the adsorbed MV^{2+} cations were adsorbed on the clay external surfaces, while the remaining 80% were intercalated. Since surface adsorbed MV^{2+} were not isolated from the solvent and retained some rotational flexibility, they were expected to be non-fluorescent. The decrease in the fluorescence intensity may therefore be due to an increasing proportion of externally adsorbed non-fluorescent cation with increasing cation to clay ratio. But, in chapter 7 we have established that the intercalation of MV^{2+} was preferred, by far, over its surface adsorption. If the observed decrease in the fluorescence intensity was due only to an increasing fraction of surface adsorbed cations, then it would be expected that the curvature would be reversed from the one found in figure 49. The proportion of surface adsorbed cation would be expected to increase slowly at first (or not at all) at low %CEC, and then more rapidly at high %CEC. The fluorescence intensity variation in hectorite was the reverse of this, at low %CEC it decreased rapidly, while at high %CEC the decrease was slower.

This was for the case in which the ratio of external to internal surface area did not change with the %CEC. Increase in the population of adsorbed cation on the clay external surface alone cannot explain the results of figure 49. But there may be change in the structure of the clay with variation of the cation to clay ratio. For example, since the concentration of MV^{2+} used for the measurements was constant, at low ratio MV^{2+}/clay, high concentrations of clay were required. At these higher concentration of clay the degree of aggregation of the clay is known to be larger.[166] The ratio of internal to external surface area was high. The cation has therefore a greater probability of being intercalated as opposed to be only adsorbed on the external surfaces. As the ratio MV^{2+}/clay increased more and more of the MV^{2+} was adsorbed on the outside surfaces of the clay since the decrease of the clay concentration led to a greater dispersion of the clay and therefore to larger ratio of external to internal surface area. This could explain why the decrease in fluorescence intensity was largest at low %CEC.

In montmorillonite the results were different. (see figure 48) A likely interpretation for the decrease of fluorescence intensity at ratios less then 15% CEC is the static quenching by structural iron of a fraction of the adsorbed MV^{2+}. The MV^{2+} cations were initially adsorbed in a non-fluorescent site, possibly in close proximity to an iron atom in the clay tetrahedral sheet (see section 2.2). Iron is in much higher concentration in montmorillonite than in hectorite (see table 19). The low but constant fluorescence found at less than 1% CEC (see table 20) was due to the fraction of the cation not quenched by the iron. As the MV^{2+}/clay ratio increased, these iron sites became saturated and the fraction of adsorbed MV^{2+} not quenched increased giving rise to the observed increase in the fluorescence intensity. A maximum was reached at 15% CEC, presumably at the point at which the other factors, self-quenching and increasing fraction of the cation adsorbed on the external surfaces became more important. The intensity then started to fall.

The fluorescence decay results support the above interpretation. Since a MV^{2+} molecule bound very close to an Fe atom would be non-fluorescent, it would not be detected in the fluorescence decay experiment either. Because there was no variation in the decay or fractional fluorescence with the %CEC, the three components may correspond to MV^{2+} cation intercalated in the lattice that vary only in their relationship to structural iron. For example, the long lifetime component would correspond to a 40% fraction of MV^{2+} which was furthest removed from Fe sites. The short decay component would represent 10% of the population which was quite close to an iron atom. The intermediate component then would represent 50% of the MV^{2+} cations which were at intermediate positions. In other words the different lifetimes could be a function of the number of iron quenchers in a particular radius around the adsorbed cations.[181]

The above interpretation suggest that a distribution function would better account for the decay behavior. While the fluorescence decay data was fit to three discrete exponential components they may not represent discrete fluorescing species. Rather the fit

may only be a mathematical fit of population distribution function. Evidence for the presence of a distribution function rather than distinct species was suggested by inspection of the correlation matrix of the decay parameters. The decay parameters were highly correlated. This can be considered to be evidence that the data represented fit a distribution function.

10.5 The Anisotropy of the Fluorescence of Clay Intercalated Methylviologen.

The variation of the anisotropy of the fluorescence of MV^{2+} intercalated in hectorite as a function of MV^{2+}/clay ratio is shown in figure 50. Clearly there were two states of flexibility in the clay. At low ratio the cations had more rotational flexibility. As the ratio increased, the anisotropy increased until a plateau was reached at about 50% CEC. This correlated well with the collapse of the clay layer that is known to occur upon the intercalation of MV^{2+}.[138 139] (see chapter 7) At low %CEC, the clay layers could be assumed not to have collapsed since there was insufficient intercalated MV^{2+}. In this case the cations retained a greater degree of rotational flexibility. On the other hand, at high MV^{2+}/clay ratios, the energy gained by the adsorption of MV^{2+} was large enough to dehydrate the clay surface. (see section 7.2.1) The basal spacings of the clay were reduced to only 12.6 Å,[139] greatly curtailing the rotational flexibility of the cations, hence the larger anisotropy. Support for this interpretation came from the observation that montmorillonite saturated with MV^{2+} (i.e. at ratio of 100% CEC) could not be expanded with ethylene glycol, but some expansion was observed for the partially saturated complex.[149]

The same variation in anisotropy was found in montmorillonite intercalated with MV^{2+}. In fact the anisotropy at high MV^{2+}/clay ratio was larger in montmorillonite than in hectorite, 0.19 at 90% CEC compared to 0.12 at 93% CEC. The increase in anisotropy with the %CEC can be attributed to the same phenomena, the collapse of the clay

layers. The anisotropy was higher in montmorillonite either because MV^{2+} had a stronger interaction with this clay or because the clay CEC was larger. At 90% CEC in montmorillonite there was actually more MV^{2+} adsorbed in the clay than at 93% CEC in hectorite (see table 16 and 17).

Another factor that must be considered in accounting for the increase in the anisotropy with increased %CEC was the ordering of the intercalated cations. As was seen in the previous section, the average distance between the cations decreased with increase in the %CEC. In order to "fit" in the clay interlayer space, the cation have to be highly ordered. At low %CEC, MV^{2+} was diluted in the clay interlayer spaces. In this situation the structure would be less ordered and the MV^{2+} may have more fluidity. Considering the length of a MV^{2+} cation (13.4 Å, see figure 35), with an average distance between them of less than 15 Å at 100% CEC, at high %CEC a cation may not be able to move independently. This increased order would account for the observed increase of the anisotropy with the MV^{2+} to clay ratio.

Further support for this explanation came from the observation that the anisotropy was time dependent at high % CEC. Immediately after the intercalation the anisotropy was larger because the cation did not yet have the time to form an organized structure. The cations were disorganized and there was interference with their respective motions. In time, the cations organized themselves in the most efficient packing and the anisotropy was observed to stabilize at a lower value than immediately after the preparation of the mixture.

10.6 Conclusion.

The intercalation of MV^{2+} in clay minerals resulted in a dramatic increase in the quantum yield of fluorescence of this cation. This was attributed to the adsorption of

MV^{2+} in a rigid planar configuration which hindered rotational deactivation processes, and/or to the shielding of the intercalated cation from quenching by the solvent. The increase of the fluorescence anisotropy with the cation to clay ratio was attributed to the collapse of the clay layers induced by the intercalation of MV^{2+} as well as to a restricted fluidity resulting from an increase in the degree of ordering of the intercalated cation. The decay of the fluorescence intensity could be fit to the sum of either two exponentials in hectorite or three exponentials in montmorillonite. This was attributed to a distribution of environments of the adsorbed cations in the clay interlayer spaces. Because both the lifetimes and the relative contributions of the exponential components were independent of the cation to clay ratio, non-fluorescent components were postulated to account for the variation of the intensity with this ratio. The intensity decrease for cation/clay higher than 15% CEC variation was attributed to the self-quenching of the intercalated cations. In montmorillonite a second non-fluorescent component, was postulated to account for the decrease of the intensity at low cation to clay ratio. Plausibly, this non-fluorescent site consists in Fe(III) substituted sites in the tetrahedral sheets of the clays. These sites are highly negatively charged and could adsorb MV^{2+} preferentially. The presence of non-fluorescent surface adsorbed MV^{2+}, combined with the variation of the degree of aggregation of the clay could also contribute to the observed intensity results.

Part 3

X-RAY DIFFRACTION AND SCANNING ELECTRON MICROSCOPY OF CLAYS MINERALS EXCHANGED WITH MV^{2+} AND $RU(BPY)_3^{2+}$.

CHAPTER 11 Application of X-ray Diffraction to the Analysis of Interlayering in Clay Minerals.

CHAPTER 12 Scanning Electron Microscopy of MV^{2+} and $Ru(bpy)_3^{2+}$ Clay Aggregates.

CHAPTER XI

APPLICATION OF X-RAY DIFFRACTION TO THE ANALYSIS OF INTERLAYERING IN CLAY MINERALS.

11.1 Introduction.

X-rays are electromagnetic radiations characterized by wavelengths between 0.1 and 45 Å. They are generated when electrons collide with the atoms of an obstacle.[194] The energy lost by the electrons in these collisions is emitted as X-ray photons. The wavelengths of these photons are a function of the amount of energy lost by the electrons during the encounters. This gives rise to a continuous spectrum of X-ray radiation. When the energy of the bombarding electrons is varied to a critical level, which depends on the composition of the target, they have sufficient energy to penetrate to the interior of the atoms and dislodge electrons from the innermost shells. Electrons from higher levels fall in to fill the vacancies, emitting X-ray photons having a characteristic wavelength, which depends on the difference between the energy levels involved in the transition. This gives rise to a characteristic or line spectrum.[194]

The simplest way to describe X-ray diffraction is to picture the phenomenon as the reflection of a part of the incident beam by lattice planes, as described by W. L. Bragg.[194] The "reflected" rays combine to form a diffracted beam only if they differ in phase by a whole number of wavelengths, that is, if the path length difference is equal

to a multiple of the wavelength of the X-ray used. It can be shown that this condition is met only when equation 49 is satisfied.

$$n\lambda = 2d\sin\theta \qquad [49]$$

Where λ is the wavelength of the X-rays, d the spacing between the lattice planes and θ the angle of incidence of the X-ray beam.

X-rays are useful in the determination of crystal structures because their wavelengths are similar to the distance between atoms in crystals.[194 195] Equation 49 shows that diffraction does not occur if $n\lambda > 2d$. On the other hand if $n\lambda << 2d$, θ becomes too small to be measurable. Since crystals are repetitive arrangements of atoms, they diffract X-rays in the same way as ruled gratings diffract visible light. Measuring the angle θ at which diffraction occurs allows the calculation of the lattice spacings d, from which the lattice dimension can be deduced.

X-ray diffraction is not limited to the study of perfectly ordered single crystals. Debye and Scherrer have developed a very useful method for the study of powder samples.[194] Powders are composed of many small crystals called "crystallites". In an ideal sample all possible orientations of the crystallites, and therefore of the crystal lattice planes are simultaneously present. When X-rays strike the sample, the Bragg condition for reflection is simultaneously satisfied by all of the types of lattice planes present in the sample. The sample is placed at the center of a cylindrical film whose axis is normal to the X-ray beam. When this beam strikes the sample the diffraction cones formed are recorded as arcs on the cylindrical film. The positions of these arc allows the calculation of the separation between the reflecting planes, from which the lattice dimensions can be deduced.[194 195]

11.2 X-ray Diffraction by Clay Minerals.

X-ray diffraction by clay minerals is used mostly as an analytical tool for the identification of minerals.[132] [197] X-ray diffraction patterns of powder clay minerals are sometimes recorded by the Debye-Scherrer method, but usually only the one dimensional diffraction of X-ray by oriented thin films of clay are measured.

It is easy to prepare an oriented mount of a clay for X-ray analysis.[132] When a suspension of clay in water is left undisturbed, sedimentation takes place. The clay platelets naturally deposit on the bottom of the flask, with the clay layers parallel to each other. To prepare an oriented clay film, a clay suspension is placed on a glass slide and the water is allowed to evaporate. To get good diffraction patterns the films must have a certain thickness. For clay minerals, the best results are obtained with films having thicknesses of between 0.07 to 0.12 mm.[197] For a film surface area of about 5 $\mathring{A}^2$, this corresponds to approximately 40 mg of clay. The preparation of oriented mounts for clay minerals has been discussed by Gibbs.[198]

In an oriented film, order is found in only one direction, the direction normal to the basal plane (i.e. normal to the plane of the clay layers, the c-axis), the direction that coincides with the stacking sequence of the layers. The observed X-ray diffraction pattern is only due to the lattice plane spacings along that direction. The Bragg equation (equation 49) will only be satisfied for value of d corresponding to the clay basal spacings. This makes the interpretation of the results much simpler, but of course this method provides only one dimensional structural information.

The X-ray diffraction data of clay films presented in this chapter were obtained using an automated X-ray diffractometer in the laboratory of Dr. H. Kodama at the Land Resource Research Institute, of Agriculture Canada Central Experimental Farm in Ottawa. A diffractometer consists of an X-ray generator, a goniometer for measuring diffraction

angles and a number of electronic circuits for determining the intensity of diffraction at any angle. The apparatus is shown schematically in figure 53. The X-ray beam originates from a fixed point, labeled F, and strikes a large flat sample, S, at an incident angle of Θ. The diffracted beam is then recorded by a counter at C. This counter is mounted so as to sweep an arc (see goniometer arc). The circle formed by extending this arc passes through point F and has the sample at its center. In practice the intensities of the diffracted X-rays are recorded as a function of the angle Θ. The sample is rotated about the goniometer axis to sweep all the values of Θ. At the same time the counter is moved along the goniometer arc so that the angle between FS and SC is 2Θ[194] A diffraction peak is detected when the sample passes through a value of Θ for which equation 49 is satisfied. The intensity of diffraction is plotted as a function of the angle 2Θ, allowing the calculation of the d_{001} distances in the oriented clay films.

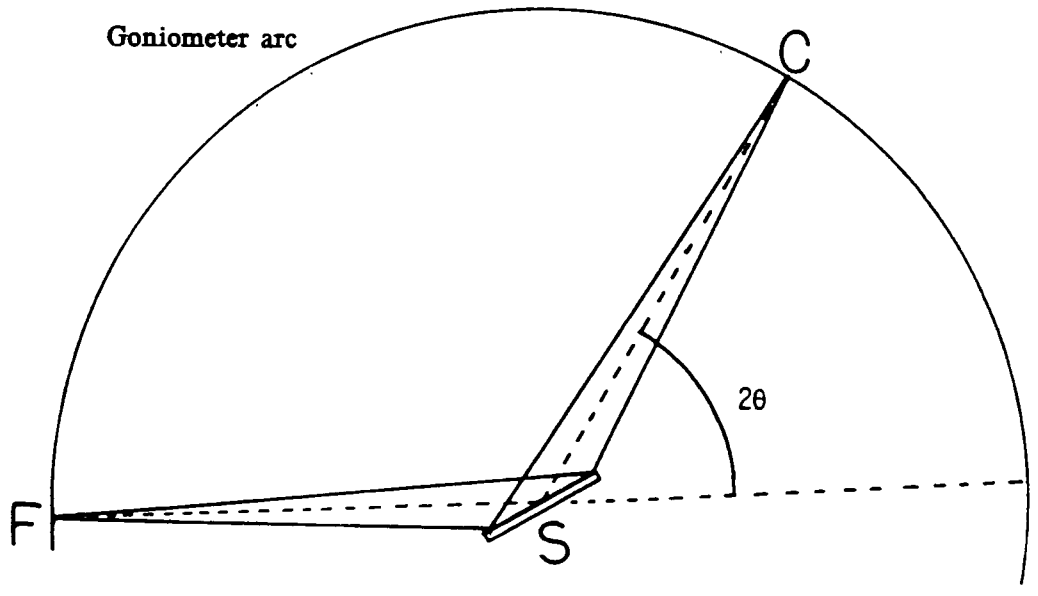

Figure 53: Schematic representation of a diffractometer X-ray optical system.

This method is well suited to the study of clay films, since the large flat samples which it requires can easily be made from clayey materials. Diffractometers have better resolving power than Debye-Scherrer cameras. Further, it is easier to compare the relative intensities of peaks recorded by a counter than it is for those recorded onto a photographic film. But diffractometers require large amounts of samples. The Debye-Scherrer method is useful when a very limited amount of sample is available. It is also better for low intensity lines.

11.3 Experimental.

11.3.1 The Measurements of Basal Spacings.

Oriented thin films of MV^{2+}, $Ru(bpy)_3^{2+}$ and $ZnTMPyP^{4+}$ exchanged montmorillonite were prepared as followed: a suspension of < 2.0 μm Ca^{+}-montmorillonite was prepared (30 mg in 6 ml water). A solution of MV^{2+}, $Ru(bpy)_3^{2+}$ or $ZnTMPyP^{4+}$ was added such that the total amount of cation was about twice the amount the clay could adsorb. After a night of stirring, the solid was isolated by centrifugation and washed several times with water. The clay was then resuspended in water (5 ml) and stirred overnight. This suspension was then placed, drop by drop, on a glass slide (6 cm^2) and the water was allowed to evaporate depositing a thin oriented film of the clay on the glass.[132] It was necessary to repeat this last operation one or two times since the glass slide could not contain the 5 ml of suspension at once. The same preparation was done with $Ru(bpy)_3^{2+}$ and MV^{2+} hectorite suspensions, using < 2.0 μm Ca^{2+} hectorite as the starting clay material. The oriented films had weights that varied between 20 and 35 mg.

The oriented films were examined by an X-ray diffraction method to measure the changes in d_{001}-spacings of the clays. The diffraction patterns were recorded on a Scintag computer automated X-ray diffractometer using Co radiation in the laboratory of Dr. H.

Kodama. The clay films were dried over P_2O_5 prior to measurement of their basal spacings.

11.3.2 Study of Ions Segregation by Clays.

The ability of the two clays, hectorite and montmorillonite, to segregate the two cations MV^{2+} and $Ru(bpy)_3^{2+}$ was investigated by X-ray diffraction.

In the first case, oriented films were prepared in the same way as in the previous section, except that the suspensions of < 2.0 μm Ca^{2+} hectorite or montmorillonite were saturated with mixed solutions of both MV^{2+} and $Ru(bpy)_3^{2+}$. Three montmorillonite and one hectorite films were prepared. UV-Visible measurements done on the supernatant, after addition of the mixed solutions, showed that the montmorillonite films contained 0.22, 0.43 and 0.67 meq of $Ru(bpy)_3^{2+}$ and 0.67, 0.46 and 0.25 meq of MV^{2+} per gram of clay, while the hectorite film contained 0.35 meq of $Ru(bpy)_3^{2+}$ and 0.43 meq of MV^{2+} per gram of clay.

In a second series of experiments, two oriented films of hectorite were prepared in the following way: a solution of $Ru(bpy)_3^{2+}$ or MV^{2+}, containing enough cations to account for approximately 50% of the amount the clay could adsorb, was added to a clay suspension, followed 30 minutes later by a solution of the other cation of equal concentration. UV-Visible measurement on the supernatant showed that the two films contained 0.40 and 0.35 meq of $Ru(bpy)_3^{2+}$ and 0.35 and 0.39 meq of MV^{2+} per gram of clay.

In a third series of measurements, suspensions of MV^{2+} and $Ru(bpy)_3^{2+}$ exchanged montmorillonite were prepared. (see section 5.3.2 c). Volumes of the two suspensions were mixed to prepare oriented films containing 22.7, 46.9 and 72.2% $Ru(bpy)_3^{2+}$ and 77.3, 53.1 and 27.8% MV^{2+} respectively.

11.4 Results

11.4.1 X-ray Diffraction Patterns of MV^{2+} or $Ru(bpy)_3^{2+}$ Intercalated Clays.

Oriented thin films of montmorillonite and hectorite saturated with MV^{2+} or $Ru(bpy)_3^{2+}$ were prepared as described in the previous section and their X-ray diffraction patterns were measured. The results are shown in figures 54 to 57. The clay basal spacings shown in tables 16 and 17 were calculated from these patterns (see section 6.2.1).

Figures 54 and 55 show the X-ray diffraction patterns of oriented films of montmorillonite exchanged with MV^{2+} and $Ru(bpy)_3^{2+}$ respectively. On these figures, the intensity of the diffracted X-rays, in counts per second, is plotted on the vertical axis, against the value of 2θ, twice the angle of incidence on the horizontal axis. The values of the lattice plane spacings d_{001}, as calculated from equation 49 (using the wavelength of the X-rays used Co Kα, λ = 1.7902 A[194]) are included for each peak, along with the peak intensity.

From the four main peaks of figure 54, a value of d_{001} = 12.6 Å for MV^{2+} intercalated in montmorillonite was calculated. In the case of $Ru(bpy)_3^{2+}$ intercalated in montmorillonite (figure 55) six 001 reflections were seen, from which a value of d_{001} = 17.4 Å was calculated. Figures 56 and 57 show the X-ray diffraction patterns of films of hectorite saturated with the two cations MV^{2+} and $Ru(bpy)_3^{2+}$. The result for MV^{2+} intercalated clay (figure 56) shows three 001 reflections from which a value of d_{001} = 12.7 Å was calculated. In the case of $Ru(bpy)_3^{2+}$ intercalated hectorite (figure 57) seven 001 reflections were seen. The average value of d_{001} was 17.6 Å. Note that in some of these spectra, there are some small peaks around 4 Å. They are attributed to impurities.

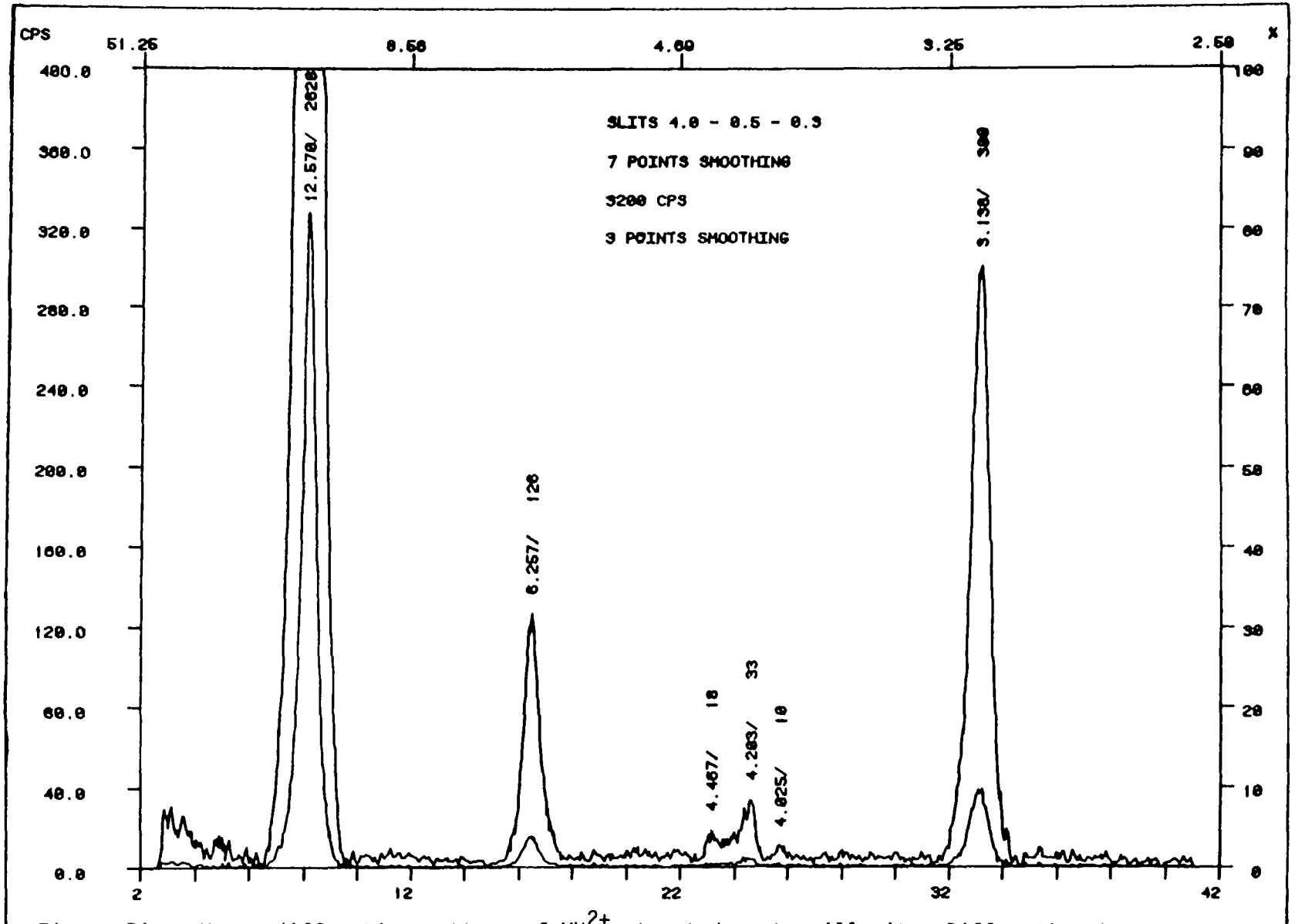

Figure 54: X-ray diffraction pattern of MV^{2+} saturated montmorillonite. Diffraction intensity in CPS vs. 2θ recorded at 0% humidity.(0.89 meq of MV^{2+} per gram of clay)

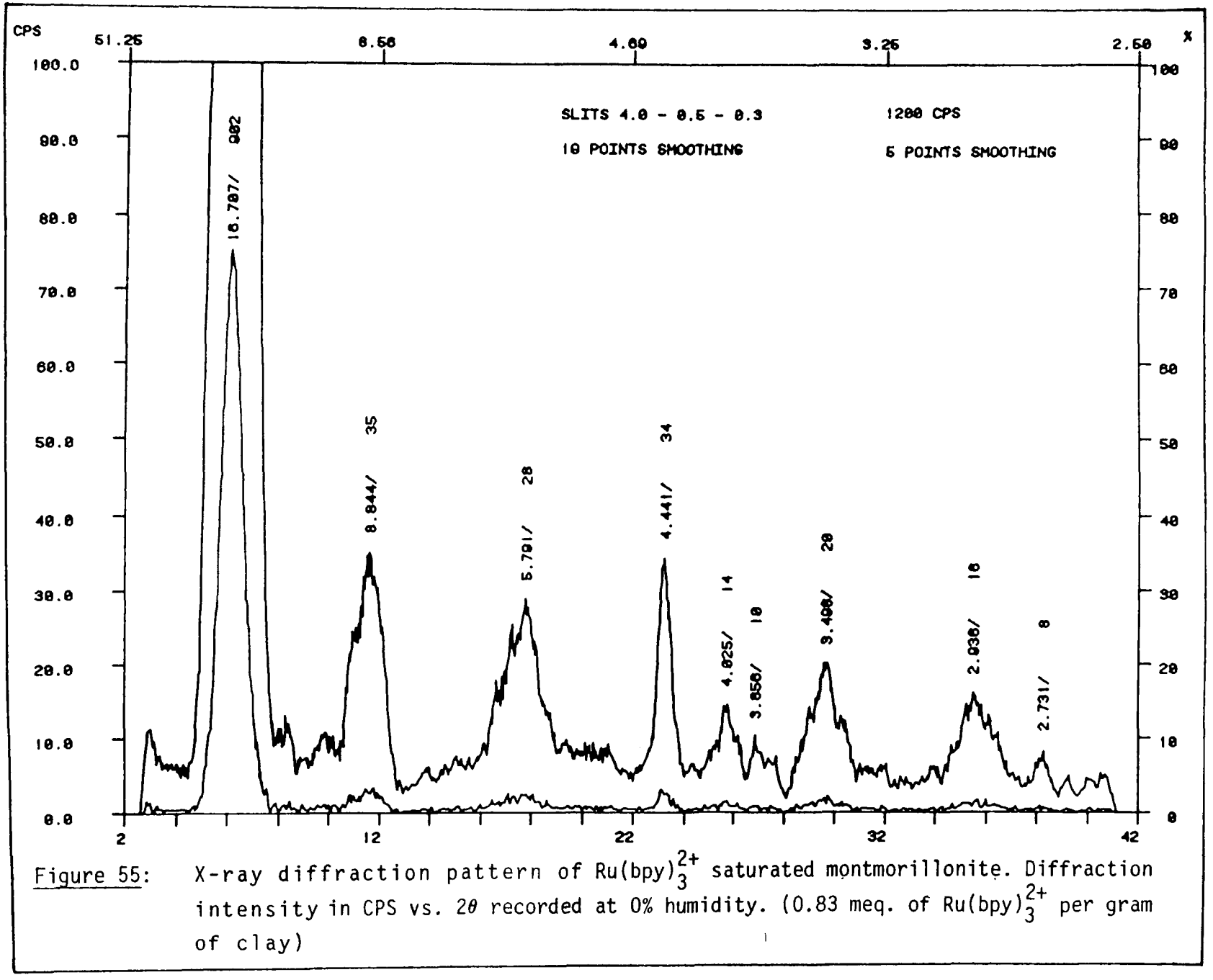

Figure 55: X-ray diffraction pattern of $Ru(bpy)_3^{2+}$ saturated montmorillonite. Diffraction intensity in CPS vs. 2θ recorded at 0% humidity. (0.83 meq. of $Ru(bpy)_3^{2+}$ per gram of clay)

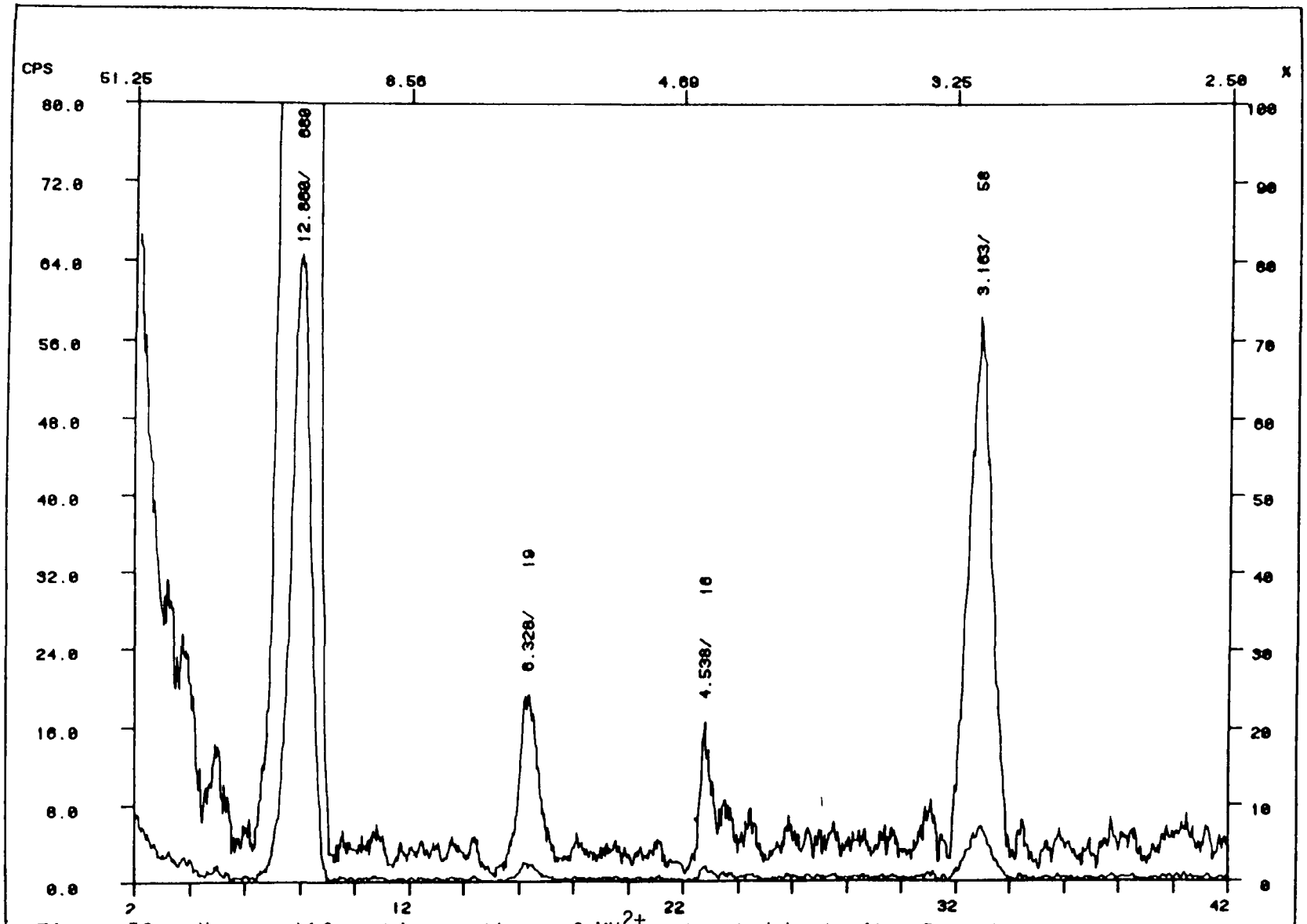

Figure 56: X-ray difraction pattern of MV^{2+} saturated hectorite. Recorded at 0% humidity. (0.72 meq of MV^{2+} per gram of clay)

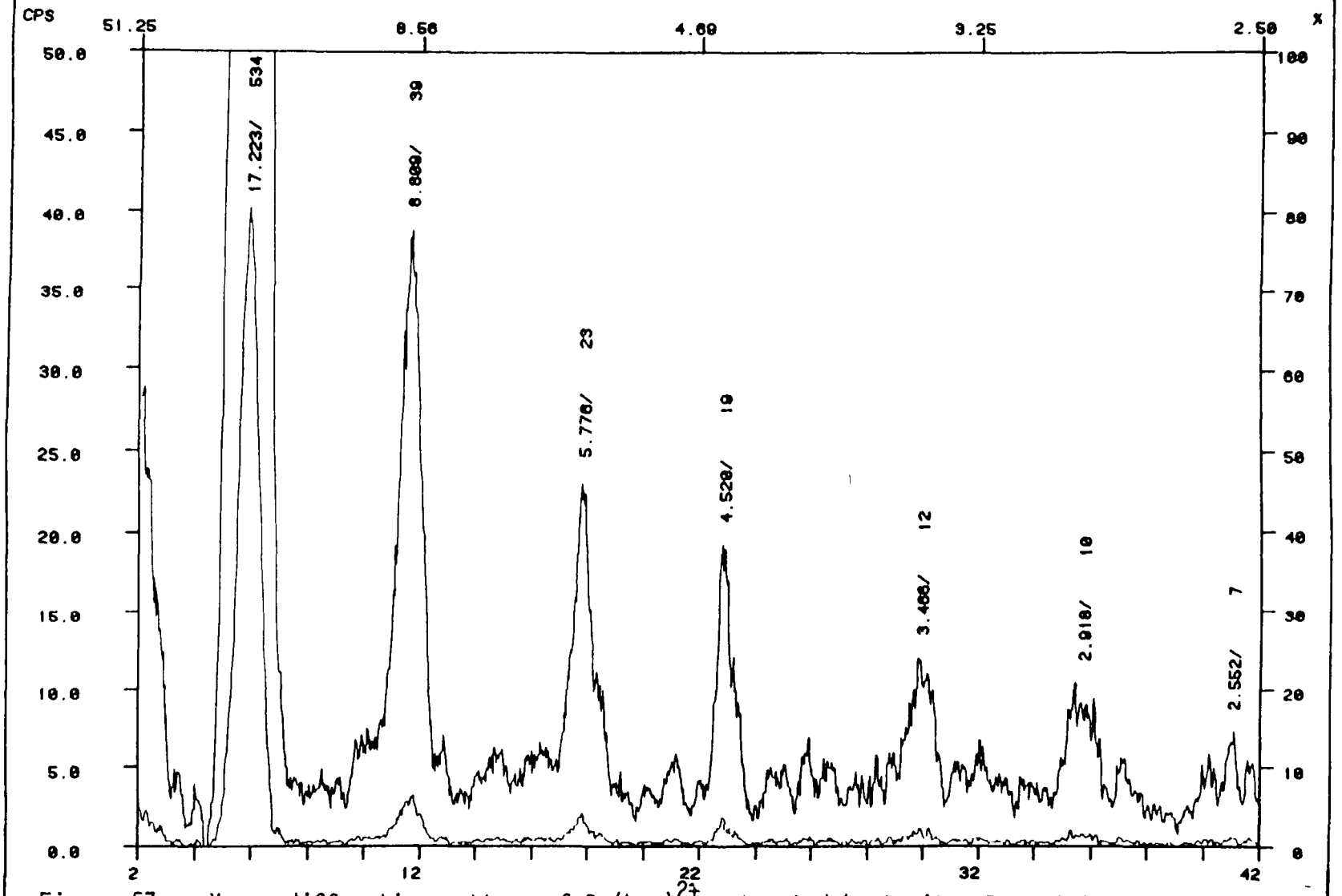

Figure 57: X-ray diffraction pattern of $Ru(bpy)_3^{2+}$ saturated hectorite. Recorded at 0% humidity. (0.66 meq of $Ru(bpy)_3^{2+}$ per gram of clay)

11.4.2 X-ray Diffraction by Clay Film Intercalated with a Mixture of the two Cations.

In order to explain the low efficiency of the quenching of excited $Ru(bpy)_3^{2+}$ by MV^{2+} in an hectorite suspension, Ghosh and Bard[150] postulated that the clay could segregate these two cations in its interlayer spaces. If this segregation exists, an oriented film containing a mixture of the two cations would contain two types of clay layers, having distinct basal spacings. This would be detectable by X-ray diffraction. Such mixtures were prepared and examined by X-ray diffraction.

Figure 58 shows the X-ray diffraction pattern of an oriented film of montmorillonite containing a mixture of $Ru(bpy)_3^{2+}$ (47%) and MV^{2+} (53%) intercalated cations, prepared by mixing a suspension of MV^{2+} saturated clay with a suspension of $Ru(bpy)_3^{2+}$ saturated clay (see previous section). The result was the superimposition of figures 54 and 55. All of the major peaks could be attributed to 001 reflections from two distinct clay phases, having basal spacings of 12.6 and 17.4 Å respectively. When the ratio of the two cations was changed from approximately 1:1 to about 3:1 or 1:3, similar results were obtained except for changes in the relative intensities of the two sets of 001 reflections. This superimposition of two patterns is characteristic of a mechanical mixture of two constituents[194 199] (see next section).

Figures 59 to 62 show that this was not the case when mixtures of the two cations in the smectites were prepared by adding a premixed solution of the two cations to a water suspension of the clays. Two sets of peaks were still seen, but they were shifted to positions intermediate to those expected for the layer thicknesses of the two constituents, 12.6 and 17.4 Å. When the ratio of the two cations was approximately one (figure 59 and 60, in montmorillonite and hectorite respectively) two set of peaks were observed Their positions were close to those expected for a d_{001} value of 12.6 Å and 17.4 Å.

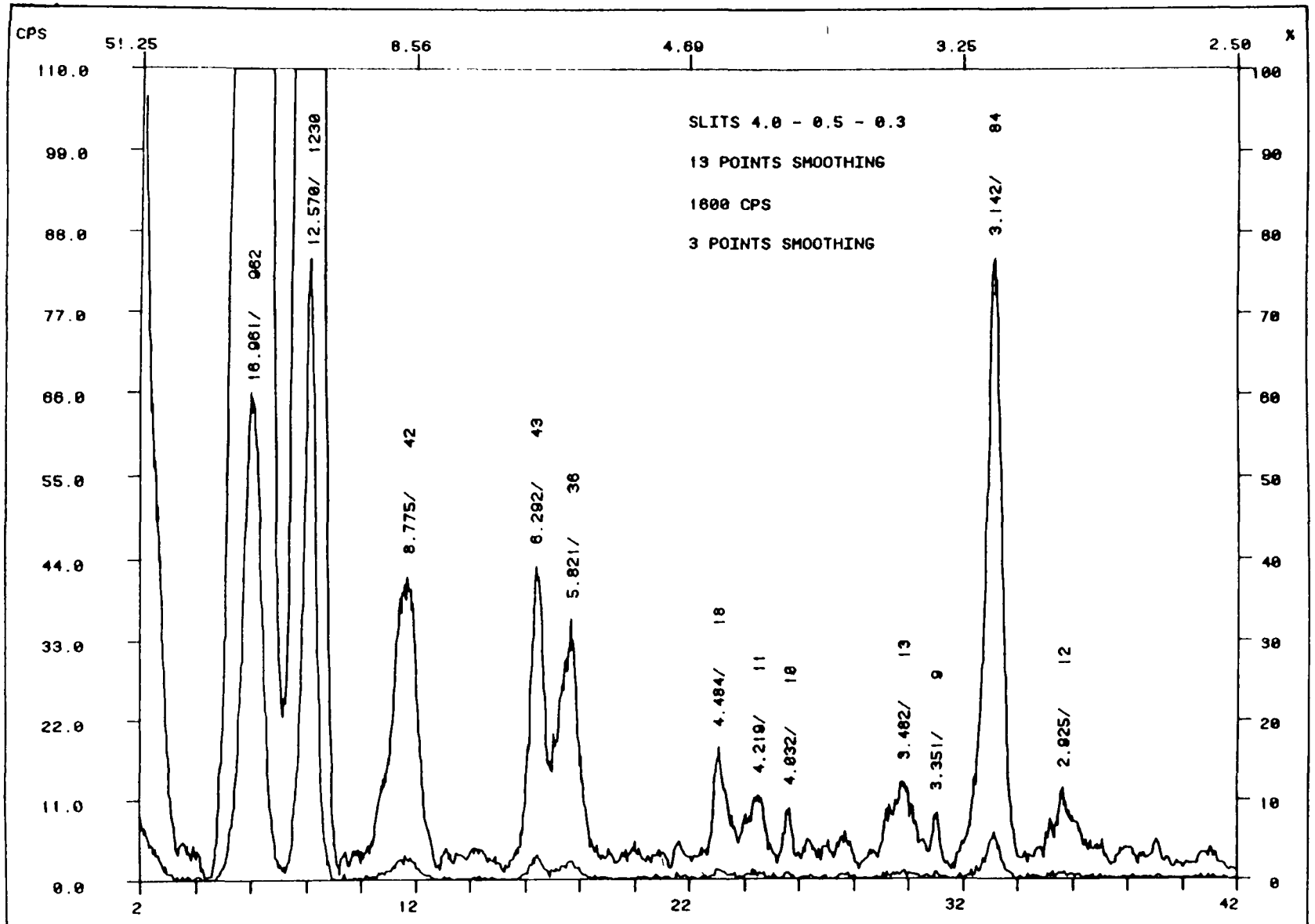

Figure 58: X-ray diffraction pattern of a montmorillonite film containing a 53:47 mixture of MV^{2+} and $Ru(bpy)_3^{2+}$ prepared by mixing MV^{2+} and $Ru(bpy)_3^{2+}$ saturated clay suspensions. (recorded at 0% humidity)

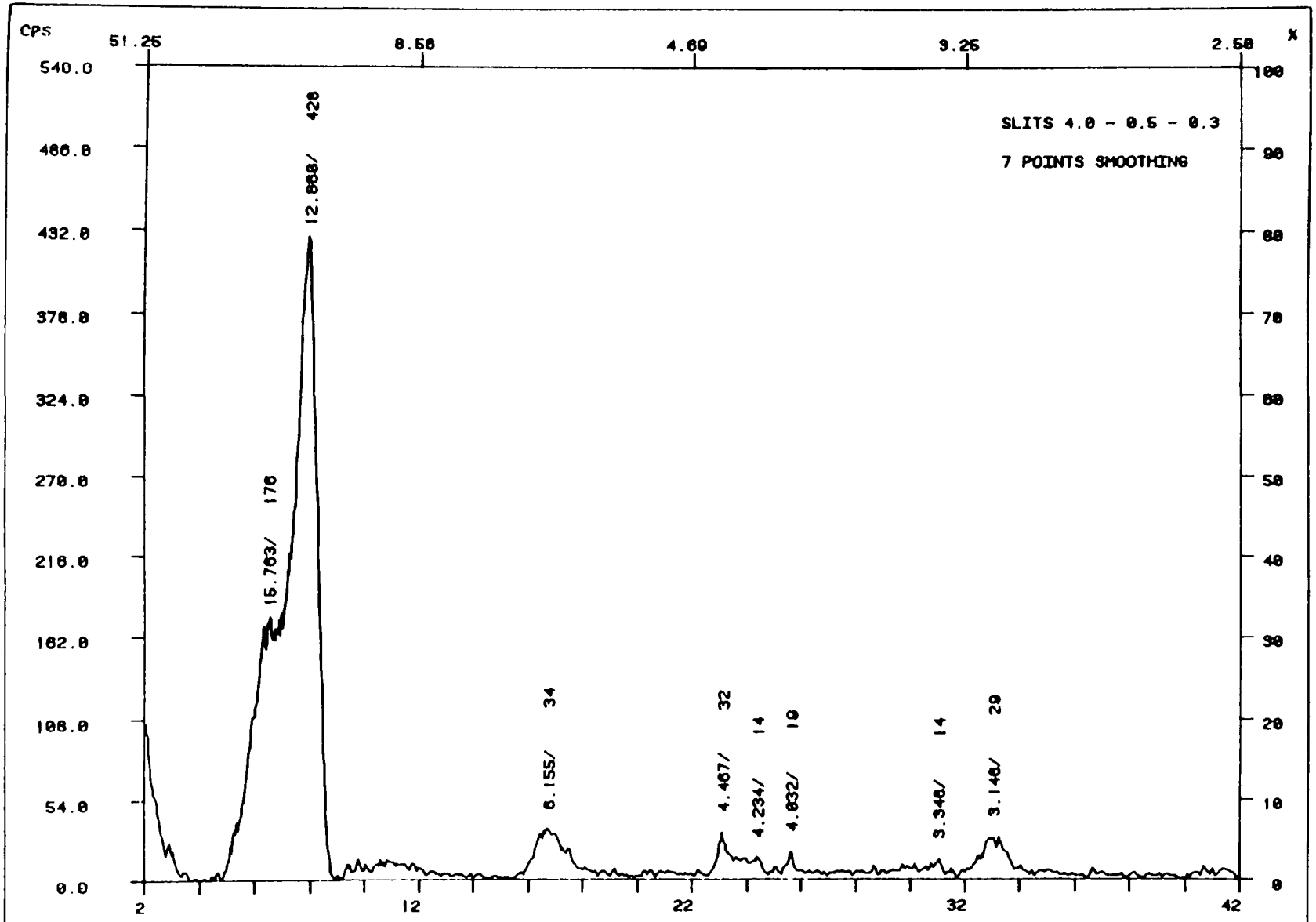

Figure 59: X-ray diffraction pattern of an oriented film of montmorillonite containing a 52:48 mixture of MV^{2+} and $Ru(bpy)_3^{2+}$ prepared from a premixed solution of the two cations. (recorded at 0% humidity)

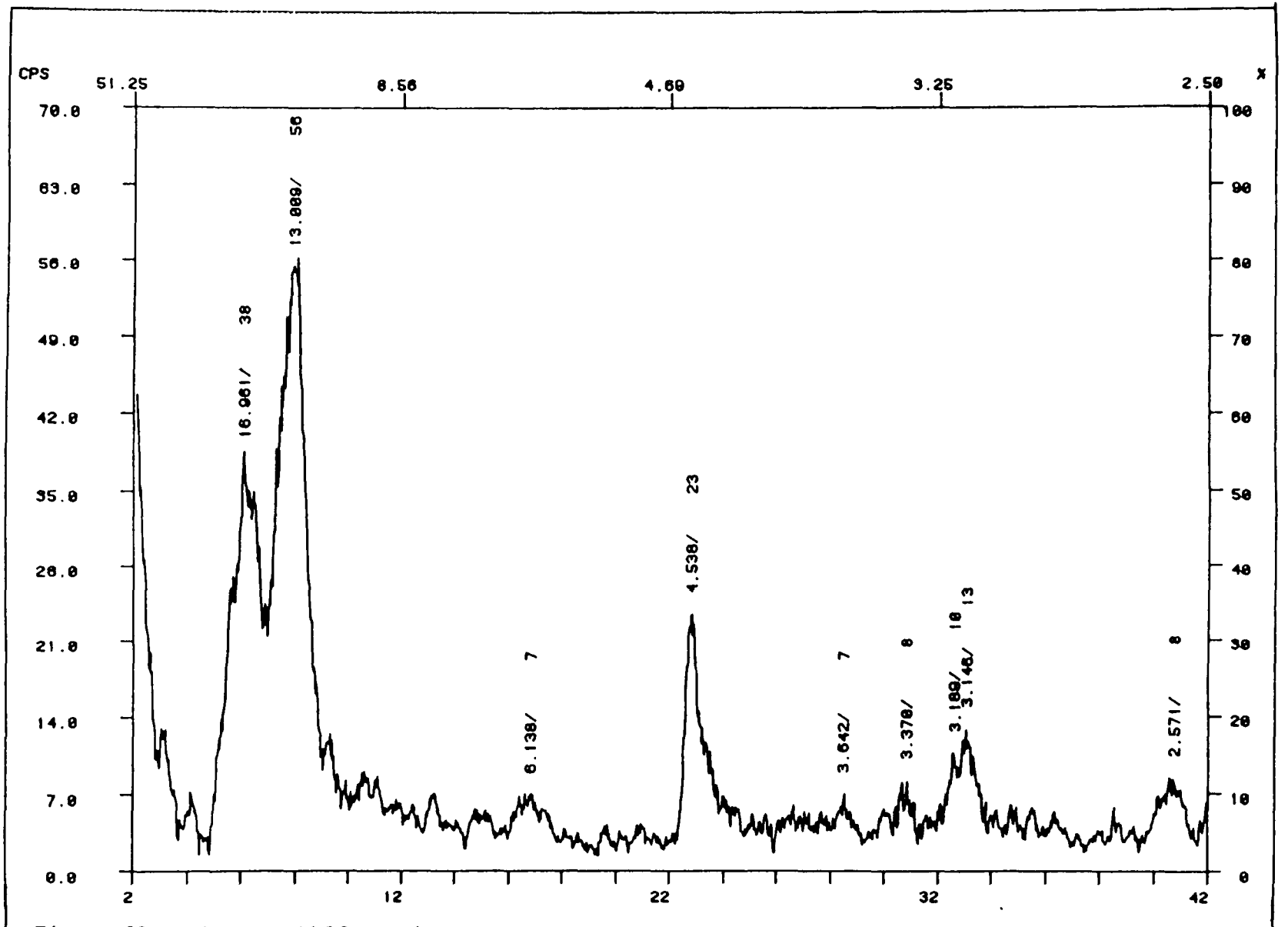

Figure 60: X-ray diffraction pattern of an oriented film of hectorite containing a 55:45 mixture of MV^{2+} and $Ru(bpy)_3^{2+}$ prepared from a premixed solution of the two cations. (recorded at 0% humidity)

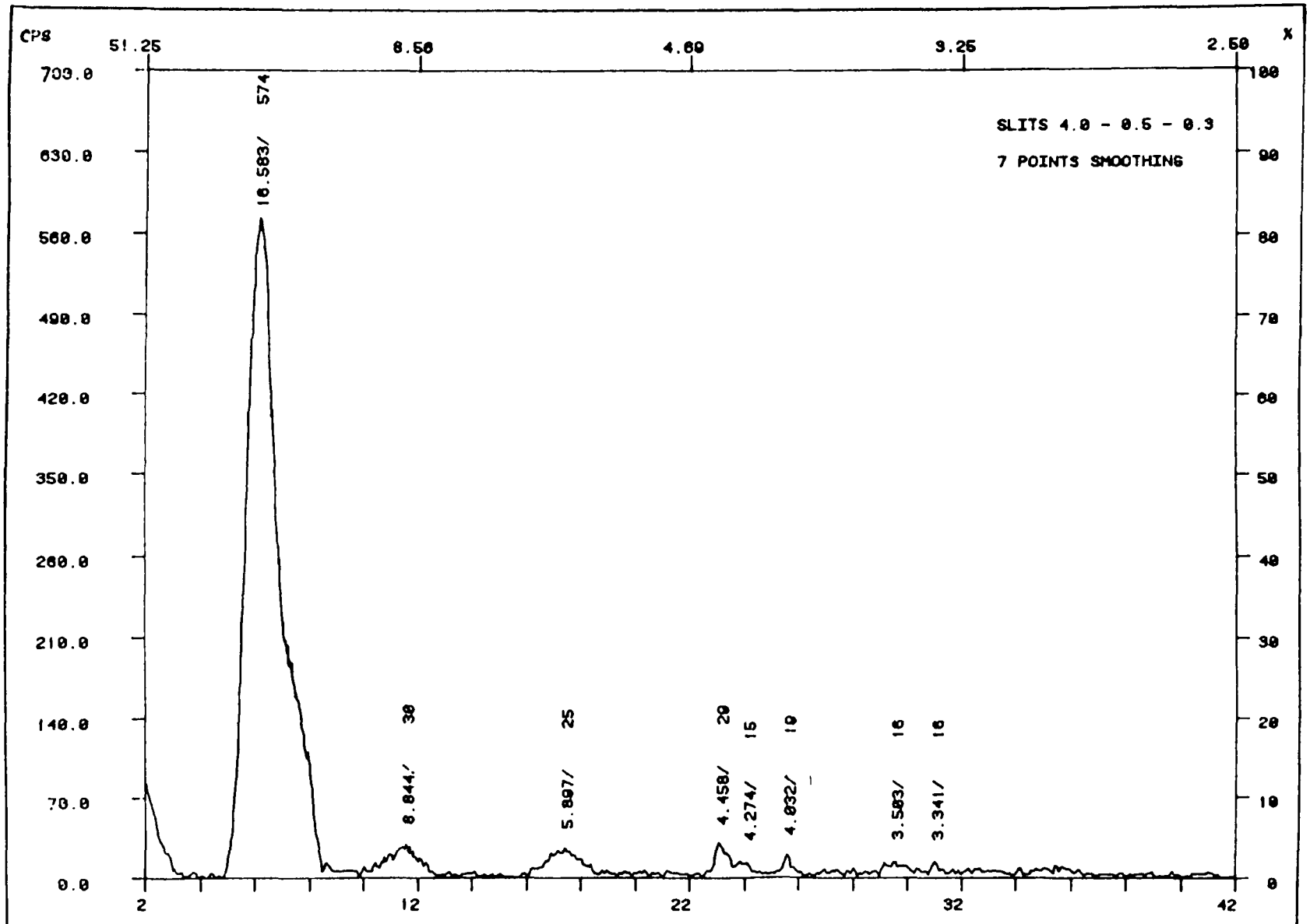

Figure 61: X-ray diffraction pattern of an oriented film of montmorillonite containing a 27:73 mixture of MV^{2+} and $Ru(bpy)_3^{2+}$ prepared from a premixed solution of the two cations. (recorded at 0% humidity)

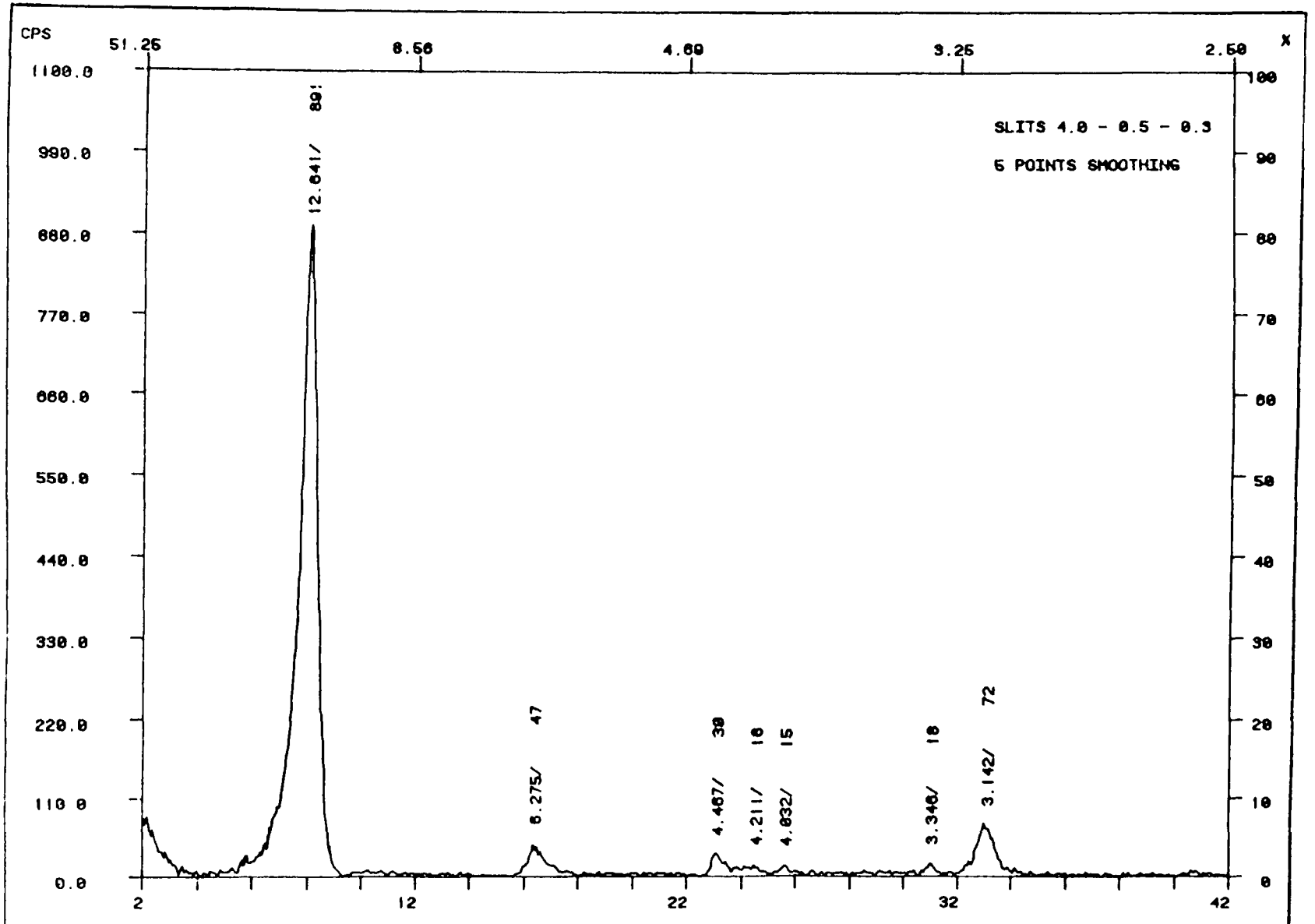

Figure 62: X-ray diffraction pattern of an oriented film of montmorillonite containing a 75:25 mixture of MV^{2+} and $Ru(bpy)_3^{2+}$ prepared from a premixed solution of the two cations. (recorded at 0% humidity)

When the ratio of $Ru(bpy)_3^{2+}$ to MV^{2+} was increased to 7:3 (figure 61) or decreased to 1:3, (figure 62) the main peaks (the 001 reflections) merged into a single one, although shoulders were still visible. For the higher reflections, two sets of peaks were again found, giving d_{001} values slightly larger than 12.6 Å and slightly smaller than 17.4 Å.

Finally, figures 63 and 64 show the X-ray diffraction patterns of hectorite films containing an approximate 1 to 1 ratio of the two cations MV^{2+} and $Ru(bpy)_3^{2+}$. They were prepared by adding a solution of one of the cations to a water suspension of the clay. Its concentration was such that it replaced about 50% of the inorganic exchangeable cations. Thirty minutes later a solution of the second cation was added to the clay suspension. The two patterns were practically identical, and they were very similar to the one shown in figure 60. Two sets of peaks were observed. One set corresponded to a basal spacing close to that of MV^{2+} exchanged hectorite (see figure 56), and the other to a basal spacing close to that of $Ru(bpy)_3^{2+}$ intercalated hectorite (see figure 57).

The presence of peaks in positions intermediate between those of the pure constituents of a mixture was indicative of the interstratification of two types of layers having different thicknesses.[200]

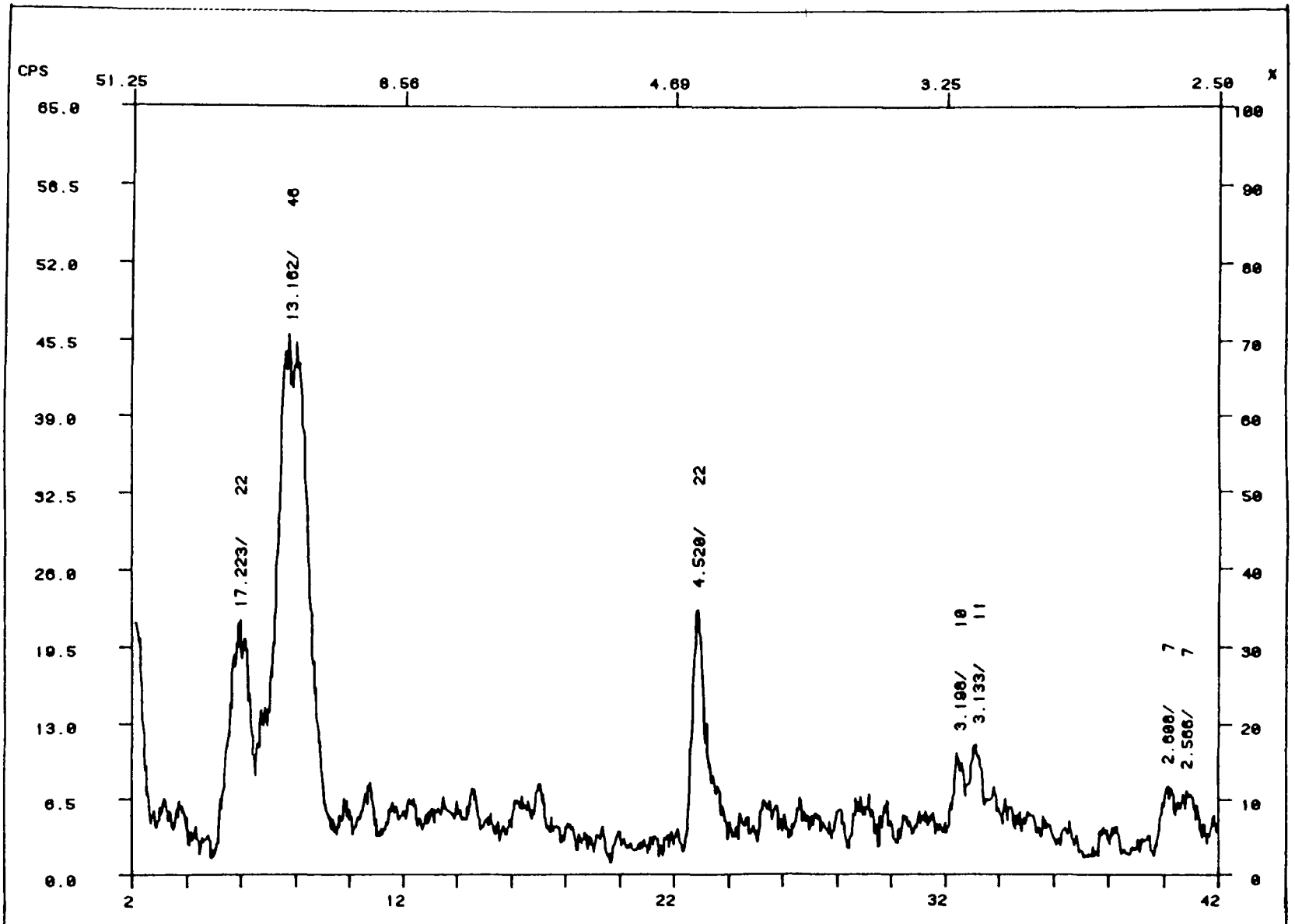

Figure 63: X-ray diffraction pattern of an oriented film of hectorite containing a 53:47 ratio of MV^{2+} to $Ru(bpy)_3^{2+}$ prepared by adding a solution of $Ru(bpy)_3^{2+}$ to MV^{2+} exchanged clay. (recorded at 0% humidity)

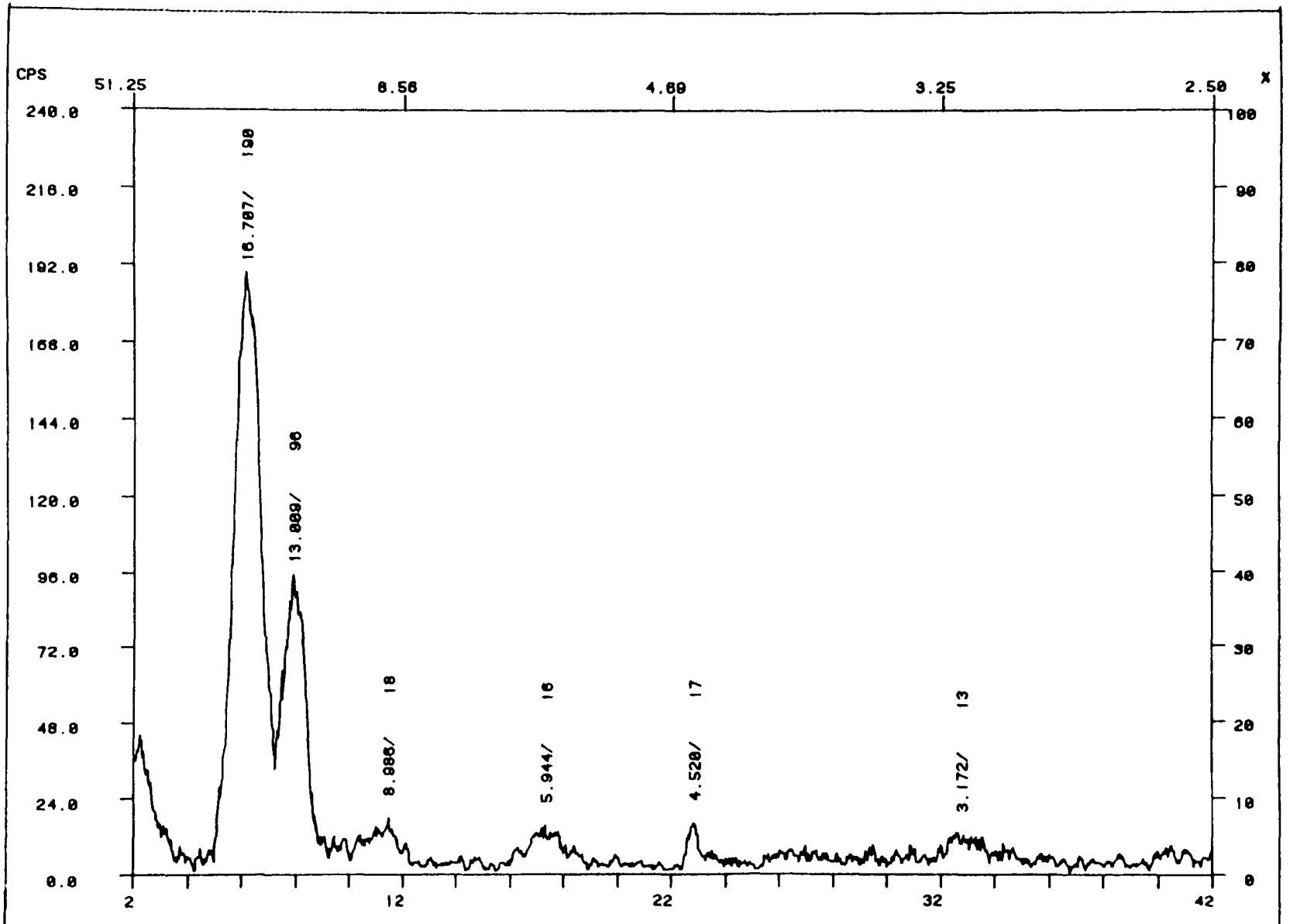

Figure 64: X-ray diffraction pattern of an oriented film of hectorite containing a 47:53 ratio of MV^{2+} to $Ru(bpy)_3^{2+}$ prepared by adding a solution of MV^{2+} to $Ru(bpy)_3^{2+}$ exchanged clay. (recorded at 0% humidity)

11.5 Discussion.

The basal spacings of MV^{2+} and $Ru(bpy)_3^{2+}$ intercalated montmorillonite and hectorite, as measured by the X-ray diffraction patterns given in figures 54 to 57, were discussed in detail in chapter 7. (see section 7.2.1). Those diffraction patterns can be used as reference in the comparison of the different patterns shown in figures 58 to 64.

First, a few terms that will appear in the following discussion are defined. The expression "segregation of MV^{2+} and $Ru(bpy)_3^{2+}$ by clay minerals" means that the clay has the ability to adsorb preferentially one of the two cations in a given interlayer space. That is, in a segregated mixture, a given interlayer space contains only one species of cation. This results in the creation of two types of layers. The layers which contain only MV^{2+} intercalated cations have a basal spacing of 12.6 Å and the layers which contain only $Ru(bpy)_3^{2+}$ cations have a basal spacing of 17.4 Å. It is the opposite of an "homogeneous mixture", in which the composition of the substance is completely uniform. In that case a given interlayer space contains both cations in a ratio equal to their bulk ratio, and there is only one type of clay layer. In the case of segregation, two types of layers are present. These layers can either be "interstratified", that is, stacked together in one crystallite or not. Further, the interstratification can be random or ordered.

Figures 58 to 64 show that segregation was present. The mixtures were not homogeneous. In the case of a completely uniform distribution of the two cations in the clay interlayer spaces every interlayer space would contain some $Ru(bpy)_3^{2+}$. Table 16 shows that the basal spacing of $Ru(bpy)_3^{2+}$ intercalated montmorillonite was 17.4 Å as opposed to only 12.6 Å for MV^{2+} intercalated montmorillonite. In an homogeneous mixture, the $Ru(bpy)_3^{2+}$ ions would act as props, keeping the clay layers 7.8 Å apart so that only one d_{001} spacing would be present, that of clay intercalated $Ru(bpy)_3^{2+}$. Further, the X-ray spectra would be the same regardless of the ratio of the two cations in the mixture.[199]

Of course there could be deviation from the "ideal" case, at very low $Ru(bpy)_3^{2+}/MV^{2+}$ ratios or if the mixture were only partially homogeneous.

There are examples in the literature where such homogeneous mixtures of two interlayer cations were used to account for constant basal spacings. It was found that montmorillonite exchanged with a mixture of Cu^{2+} and tetrapropylammonium or tetramethylammonium cations had constant basal spacings equal to those of the clay exchanged with only the organic cations,[201] if the organic cations accounted for at least 55% of the exchangeable cations. Montmorillonite whose surface charge was reduced by reaction with Li^+ also displayed a constant basal spacing when it was exchanged with tetramethylammonium, provided the charge of the clay was reduced by less then 40%.[200] These observations were attributed to an uniform distribution of the organic cations in the clay interlayer spaces.

Clearly, this was not the case in our study. The X-ray diffraction pattern shown in figure 58 was the superimposed sum of the patterns shown in figures 54 and 55. Changing the ratio of the two cations in the mixture did not affect the position of the peaks. It only changed their relative intensities according to the mixing ratios of the two components. This was characteristic of a mixture in which two phases were present.[194] Not only was there segregation of the two cations, but the two types of clay layers thus formed were not interstratified. Two types of clay particles (or at least crystallites) were observed, one type containing only $Ru(bpy)_3^{2+}$ and one type containing only MV^{2+}. The pattern consisted in two sets of peaks, corresponding to the 001 reflections of $Ru(bpy)_3^{2+}$ and MV^{2+} intercalated montmorillonite,[199] as if the two constituents had been recorded separately.

This was not surprising considering that the mixtures were prepared by mixing two suspensions of MV^{2+} and $Ru(bpy)_3^{2+}$ saturated clay. The mixing of the two cations would involve the desorption of a cation from its original adsorption site, followed by the

displacement of another cation from another particle. This would require a lot of energy. The interactions of both these cations with the clay surfaces are strong[136 138 139] (see chapter 7). Further, the results of the competitive adsorption of these two cations by montmorillonite (chapter 6) showed that they cannot displace each other from an interlayer adsorption site. Also, intercalation of methylviologen is known to cause the collapse of the clay layers.[138 139] In order to replace MV^{2+}, $Ru(bpy)_3^{2+}$ would have to expel the MV^{2+} cation and then force the clay layers apart. Therefore the cations, remained separated into two distinct clay phases. Entropy was not enough of a driving force to lead to a more homogeneous mixing of the two cations.

Two sets of peaks were observed when the mixtures were prepared from homogeneous premixed solutions of the two cations (figures 59 to 62). Although the adsorbed cations were not homogeneously mixed, there was some degree of mixing. Since the peaks were shifted toward each other, there was not a complete separation of the two types of layers. This peak migration to positions in between those of the pure constituents, was indicative of the random interstratification of two the types of layer.

The two cations were segregated, forming two types of layers having distinct thicknesses, and the two types of layers were stacked together in a given crystallite. These types of mixtures have been extensively studied. The problem of the interstratification of two types of layers can be divided into two parts, ordered and random interstratification.

The results shown in figures 59 to 64 show that the interstratification was not ordered. In the discussion below, a layer intercalated with only MV^{2+} characterized by a thickness of 12.6 Å will be called layer A, and a layer intercalated with $Ru(bpy)_3^{2+}$ characterized by thickness of 17.4 Å, layer B. Ordered interstratification is characterized by the presence of a "superlattice".[202 203] For example, if the ordering is a simple sequence ABABABAB etc, in a mixture where the ratio of A to B is approximately one, as was the case in figures 59 and 60, the repeating unit in the staking sequence is AB. The

X-ray pattern should show a thickness of 12.6 + 17.4 = 30 Å. We did not observe such a "superlattice".

The other type, random interstratification, in which the occurrence of the two types of layers in a stack is random, has also been extensively studied.[204-211] Reynolds has recently reviewed the subject.[207] Numerous procedures have been developed to interpret the X-ray diffraction patterns of such mixtures in terms of their composition and degree of interstratification. The interpretation below is based on the work of Hendricks and Teller in 1942.[204] They looked at the X-ray interference for layer lattices in which the phase shifts between consecutive layers did not follow a strictly periodic arrangement. They derived an equation for the calculation of the X-ray diffraction intensity in such systems.

Later, MacEwan developed a method to calculate the expected X-ray diffraction patterns of oriented clay film mixtures as a function of the thicknesses of the two constituent layers.[205 206] This method is based on the calculation of a mixing function, ϕ, for the two types of layers (equation 50).

$$\phi(r^*) = 2N/a\Sigma n\sigma(R_n)\cos 2\pi r^* R_n \qquad [50]$$

Where a is the thickness of the sample, N is the number of layers per crystallite, σ is the total probability of occurrence of the given spacing R_n and $r^* = 2\sin\theta/\lambda$ where θ is the angle of incidence of the X-ray beam and λ the wavelength of the X-rays used.[206] The mixing function does not give the actual X-ray diffraction curve. The curve calculated by equation 50 must be multiplied by $|F|^2\Xi$, where F is the layer structure factor, a measure of the scattering power of a given layers and Ξ is a geometrical factor. F varies with wavelength and with the orientation and direction of the polarization of the incident and out going radiation, relative to the plan of the layers. It can be calculated by adding the scatterings from all the atoms within the layers.[204 207]

Using this method, Ruiz-Amil et al[212] have published a wide series of curves of the expected results of X-ray diffraction patterns for a large number of two component systems. This method was also extended to three component systems.[213] The random interstratification of two layers was characterized by so-called nonrational peaks.[200] The position of these peaks could not be obtained directly from the values of the two layers thicknesses. For example, for a completely random 1:1 mixture of layers having thicknesses of 15 and 10 Å, the calculation showed the occurrence of peaks at d = 13.3 Å and d = 6.67 Å.[206]

In general it was found that completely random interstratification was characterized by one set of nonrational peaks, with a d_{001} value in between the values of the two layers thicknesses. When two sets of nonrational peaks were found, one having a d_{001} value close to the thickness of layer A and one having a d_{001} value close to the thickness of layer B, this indicated the presence of zonal structures. If P_A and P_B were the probability of finding layers A or B in a given stack and if P_{AA} and P_{BB}, were the probability that a layer A was followed by another layer A or B, then in zonal structures, $P_{AA} > P_A$ and $P_{BB} > P_B$. Some zones in the crystallites contain mostly one type of layer and some that contain mostly the other type of layer. One example of such a zonal structure was provided by hectorite partially exchanged with tris-bipyridyl metal complexes.[136]

This was what we observed in the X-ray patterns shown in figures 59 to 64. We compared our results with the curves published by Ruiz-Amil et al[212] for the expected X-ray diffraction patterns for the random interstratification of two types of clay layers having thicknesses of 12.5 and 17.5 Å. Since we knew the mixtures compositions, we could determine P_A and P_B. They were equal to the molar fractions of the two cations in the mixtures (layer A is MV^{2+} intercalated clay while layer B is $Ru(bpy)_3^{2+}$ intercalated clay). The values of r^* (see equation 50) were calculated from the values of the average d_{001} distances given by the two sets of nonrational peaks of figures 59 to 64. The com-

parison with the curves of Ruiz-Amil et al[212] allowed the estimation of the value of P_{AA}. The results are summarized in table 24.

Table 24: Estimation of P_{AA} by the Method of MacEwan.[212]

X-ray Pattern	P_A	P_B	r^* $\mathring{A}^{-1}$		P_{AA}
Figure 59	0.52	0.48	7.93	5.96	0.80 ± 0.05
60	0.55	0.45	7.92	5.77	0.85 ± 0.05
61	0.27	0.73	7.93	5.78	0.80 ± 0.05
62	0.75	0.25	7.52	5.73	0.70 ± 0.05
63	0.53	0.47	7.75	5.76	0.75 ± 0.05
64	0.47	0.53	7.78	5.67	0.75 ± 0.05

$r^* = 100 \times 2\sin\theta/\lambda = 100/d_{001}$ where d_{001} are the basal spacings calculated from the two sets of nonrational peaks in the patterns of figures 59 to 64. (see text for the definitions of P_A, P_B and P_{AA})

With the exception of the mixture in which the ratio $MV^{2+}/Ru(bpy)_3^{2+} = 3$ (figure 62), the values of P_{AA} were consistently larger than the values of P_A. In fact, P_{AA} was similar in all cases. The fact the $P_{AA} > P_A$ implied that the layers of one type had a tendency to cluster together in regions or zones of the crystallites, giving rise to zonal structures. For example, in the cases for which $P_A = 0.5$, if we assumed that a crystallite was made up of ten clay layers, 5 of type A and 5 of type B, the stacking sequence had to be for example AAABBBBBAA|AA... to obtained a value of P_{AA} of approximately 0.8 The tendency of formation of zonal structure was even more important in the case where $P_A = 0.27$ (figure 61). The stacking sequence had to be for example AAABBBBBBB|AA... for which $P_{AA} = 0.67$.

In the case where $P_A = 0.75$ (figure 62), P_A was approximately equal to P_{AA}, and the tendency towards the formation of zonal structures was much less important. This

was in agreement with the observation that the second set of nonrational peaks appeared only as small shoulders on the main peaks.

The following discussion will deal with the two main questions coming from the X-ray results. Why is there segregation between the two organic cations? Why does the interstratification of the two types of layers favor stacking of the same type of layers in a given region of the clay particles?

When there was a delay of 30 minutes between the addition of the two cations the results were the similar whether MV^{2+} or $Ru(bpy)_3^{2+}$ was added first (figures 63 and 64). They were also similar to the case in which two cations were added together (figure 60). In these cases, a preferential adsorption of the organic cations in certain interlayer spaces was observed. The segregation of organic and inorganic cations by clay minerals has been observed before. For example, X-ray basal spacings measurements done on montmorillonite exchanged with mixtures of copper and tetramethylammonium or tetrapropylammonium cations have shown that the mixtures of the two cations were not homogeneous.[199 201] The distribution of tetramethylammonium cations in the interlayer spaces of charge reduced montmorillonite was not homogeneous either.[200] In fact, Traynor et al[136] proposed segregation between sodium and tris-bipyridyl metal complex cations, including $Ru(bpy)_3^{2+}$, in the interlayer spaces of hectorite, to account for the nonrational peaks found in their X-ray diffraction patterns.

The interpretation most often given to account for this segregation is the nonhomogeneous charge density of the surfaces of smectite clays. It has been shown that the surface charge density in clays is not uniform.[214] Some interlayer spaces have higher charge densities, with closely spaced exchangeable cations and other have lower charge density with more widely spaced cations. The transition between monolayer and bilayer coverage in clay minerals exchanged with alkylammonium cations was studied by X-ray.[214] It showed that certain interlayer spaces were more highly charged than others. For example,

in a New Zealand bentonite, 59% of the interlayer spaces had a charge density of 0.30, 18% of 0.35 and 20% of 0.40 eq./$(Si,Al)_4O_{10}$.[214] This method also allowed the measurement of the interlayer CEC of a clay. It was found to be of the order of 80% of the total CEC measured by cation exchange.

The segregation was assumed to be due to a preference of the organic cations for those interlayer spaces with higher charge density. The first cation added displaced preferentially the inorganic cations from those sites. Since the two organic cations could not displace each other from the clay interlayer adsorption sites, (see chapter 6 and 7) the second cation added filled the remaining sites, the interlayer spaces of low charge density. The formation of zonal structures could then be attributed to a clustering of the interlayer spaces of high layer charge densities in certain zone of the clay particles.

This interpretation could be extended to the cases where the two cations were added simultaneously (figures 59 to 62). One could assume either a similar preference of one of the two organic cations for these higher charge density interlayer spaces, or a faster adsorption of one of them, filling most of the preferred sites before the other can be adsorbed.

An alternative interpretation for the segregation, is the collapse of the clay layers to 12.6 Å that is known to occur upon intercalation of MV^{2+}.[138 139] As discussed in chapter 7, this collapse was attributed to the strong interaction of the clay and the organic cation. When we studied the anisotropy of the fluorescence of clay intercalated MV^{2+} as a function of the MV^{2+}/clay ratio (see figure 50) we attributed the increase to this collapse. It was assumed that the collapse was complete only for a ratio larger than 50% CEC. A given interlayer space had to contain a minimum amount of MV^{2+} before it collapsed. Since it was the preferred situation, we can assume that MV^{2+} was preferentially adsorbed in certain interlayer spaces causing them to collapse. Once the layers had collapsed, no $Ru(bpy)_3^{2+}$ could be intercalated since the cation was too large to fit between

the clay layers. The collapsed layers contained only MV^{2+} cations and others contained only $Ru(bpy)_3^{2+}$. This is similar to the argument that segregation of inorganic and alkylammonium cations in clay minerals was due to the favored adsorption of the large organic cation in the interlayer spaces that had already been expanded by the previous adsorption of an organic cation.[215] Here the large $Ru(bpy)_3^{2+}$ ions were preferentially adsorbed in the interlayer spaces that had not been collapsed by adsorption of MV^{2+}.

The zonal structures in this case could be attributed to the aggregation of the clay particles upon addition of the organic cations. As will be seen in chapter 12, addition of MV^{2+} or $Ru(bpy)_3^{2+}$ caused aggregation of the clay. Possibly the clay exchanged with one cationic species aggregated preferentially, forming particles in which most of the interlayer cations were of one species.

11.6 Conclusion.

When the sample preparation involved the mixing of suspensions of MV^{2+} and $Ru(bpy)_3^{2+}$ homoionic montmorillonites, the two cations remained completely separated. There was a physical mixture of two distinct clay phases and the X-ray diffraction pattern was the superimposed sum of those of the two pure constituents.

Even when the mixtures were prepared from homogeneous premixed solutions of MV^{2+} and $Ru(bpy)_3^{2+}$, the X-ray patterns showed that there was not an homogeneous mixture of the two cations in the clay interlayer spaces. The X-ray results were interpreted by assuming the segregation of the two cations and the clustering of the two types of layers thus formed in regions of the crystallites to form zonal structures. The fact that intercalated MV^{2+} and $Ru(bpy)_3^{2+}$ did not react to give hydrogen (see chapter 7) could be attributed to this segregation.

The segregation could be attributed to either a property of the clay, namely the non-homogeneous charge density of the surface of smectites,[214] or to properties of the cations like size and hydration energy, in particular their ability to cause the collapse of the clay layers.[217]

CHAPTER XII

SCANNING ELECTRON MICROSCOPY OF MV^{2+} AND $RU(BPY)_3^{2+}$ CLAY AGGREGATES.

12.1 Introduction.

The fundamental principles on which scanning electron microscopy (SEM) is based were first recognized in Germany in the 1930,[216] von Ardenne actually built such a microscope in 1938,[217] but it was not until after World War II that progress in electronics allowed the construction of a practical apparatus. The modern scanning electron microscope has been available since about 1965. It was developed in the Cambridge University Engineering Department beginning around 1950 by the group of C. W. Oatley.[217] The first SEM sold commercially was custom built by one of Oatley's students, in 1958 for the Pulp and Paper Research Institute of Canada and in 1964, DuPont Company of Canada bought the prototype of the first commercial SEM.[217]

Figure 65 shows schematically a typical SEM column. At the top there is a source of electrons. They are accelerated by a potential to form the primary electron beam. This beam is focused by electromagnetic lenses to a fine spot of less than 10 nm in diameter and deflected by the two scan coils so that the surface of the specimen can be scanned point by point and line by line. When the beam strikes the sample several phenomena occur. The electrons can be backscattered, or they can ionize the specimen causing the emission of either secondary or Auger electrons or the emission of X-ray radiation. All of these phenomena can be measured and used to form an image of the sample.

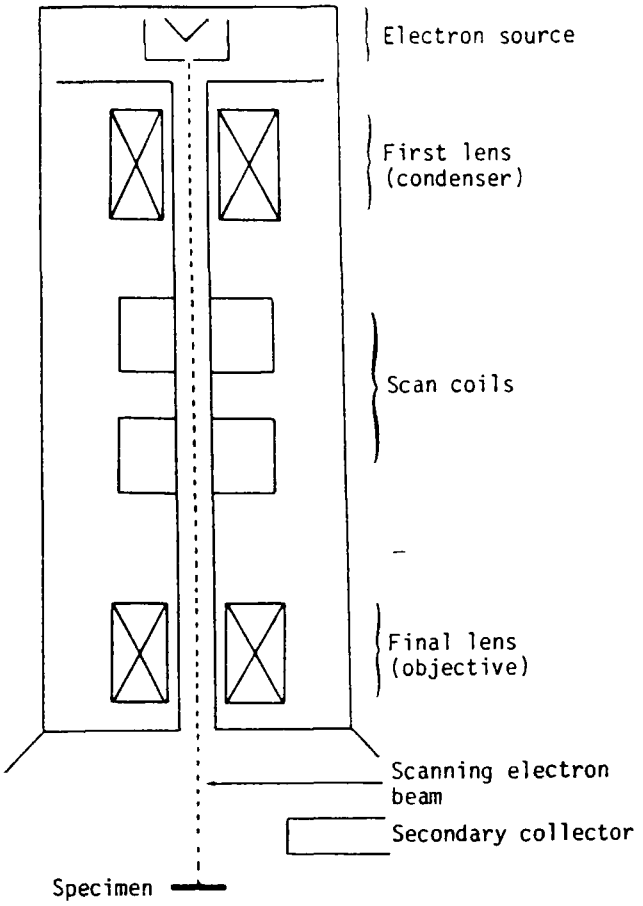

Figure 65: Schematic representation of a typical SEM column. (see text)

In most cases, only the secondary electrons are detected. Since they have much lower energy than the primary electrons, they can only escape from the sample if they are produced close to its surfaces. In other words, the image is produced by the surface of the specimen, in a manner similar to the image produced by the reflection of light on a surface.[218] This makes SEM particularly useful for looking at the topography of rough surfaces. The other three processes can also be used if the microscope is equipped with the appropriate detectors. Since the energy of the backscattered electrons, the Auger electrons or the X-rays emitted by a sample are dependent on its composition, their detection can provide information on the specimen composition.

The major advantage of SEM over light microscopes, aside from its resolution of about 10 nm as compared to 500 nm for a light microscope, is its depth of focus, which is more than 300 times better than that of a light microscope. Further, in SEM, as already mentioned, the image is mostly formed by electrons produced close to the samples surface, so it closely resembles the normal image.[218]

Theoretically the depth of focus of a transmission electron microscope (TEM) is the same as that of a SEM, but in a TEM the image is formed using electrons transmitted through the sample. It can only be applied directly to samples that are transparent to electrons. In most cases the samples are opaque to electrons and one must use either very thin sections of the specimen or replica of the surfaces.[219] This is often difficult and time consuming. In SEM, one has only to place the sample on a suitable mount, and if it does not conduct electricity, to coat it with gold. The only limitation is the need for a vacuum.[216]

However, SEM can not replace the other two microscopic techniques. Despite the problem of sample preparation, TEM continues to be used because of it better resolution, 2 Å as opposed to 100 Å for SEM, while light microscopy remains the only technique that provides color photographs.[216] Color SEM images can be produced by the use of filters,[220] but they do not give the true colors of the samples.

12.2 The Use of SEM in Clay Mineralogy.

In recent years, scanning electron microscopy has proven to be a powerful tool of the descriptive mineralogist.[221] This is due to its ability to produce photomicrographs with an apparent three dimensional quality that comes from its great depth of focus, and because SEM can be used to determine the chemical composition of the specimens. In clay mineralogy, scanning electron microscopy is used either as an analytical tool for the identification of a given clay or to look at the morphology of clay minerals.[222]

Since the SEM characterization of the major clay minerals groups (i.e. kaolin, chlorite, smectite, illite) is well established,[222] [223] the presence of a given clay species in a sample can be shown by SEM. In some cases SEM even allows a distinction between minerals that cannot be distinguished by other methods. For example, Tompkins[224] has shown, by SEM, that a sample of regular chlorite/smectite (corrensite) was actually made up of two clays having different morphology but the same X-ray diffraction pattern.

In the study of clay morphology, SEM can give some information on a variety of clay characteristics. It has been used to look at the configuration of clays particles (i.e. size and shapes). However, the method of preparation of the sample has been shown to have a dramatic effect on the particles shapes.[222] A natural rock sample of kaolinite was seen to be made up of the small plates characteristic of this type of clay,[223] [225] but if the specimen was prepared by spray-drying a suspension of the clay, spherical aggregates having radii of up to 10 μm were formed.[222] The texture of clay minerals can also be investigated by SEM. Smectites for example are easily identified by their characteristic crinkly, ridged, honeycomb-like texture which is sometimes called the typical "corn flake" or "maple and oak leaf" texture of expanding clay minerals.[222] [225] The relationship between the clay particles such as interlocking, interpenetration and aggregation features is also accessible to SEM. For example, SEM showed very clearly the face to face arrangements of the platelets of Li-montmorillonite.[226] Finally, scanning electron microscopy can also be used to look at the way in which clay minerals were formed in nature. SEM has been used to look at such processes as the smectite to illite conversion series,[227] the formation of kaolinite,[228] and the formation of montmorillonite.[229] In all these studies the change in the morphology of the samples was monitored by SEM.

Most of the SEM work done on clay minerals has been done on samples of natural rocks, but in some cases samples prepared by evaporation of dilute suspensions of clay were studied.[230] These gave different results, since one could see isolated particles. They

did not give information on texture or fabric, but only on the configuration of the clay particles. We looked at isolated particles of montmorillonite prepared in this way by scanning electron microscopy. In particular we were interested by the effect of replacing the inorganic exchangeable cations by either MV^{2+} or $Ru(bpy)_3^{2+}$ on the configuration of the particles.

12.3 Experimental.

We studied suspensions of montmorillonite exchanged with various amounts of MV^{2+} or $Ru(bpy)_3^{2+}$ by scanning electron microscopy. The samples were prepared in the following way: solutions of MV^{2+} or $Ru(bpy)_3^{2+}$ were added to suspensions of the clays in water such that 0, 25, 50, 80 and 100% of the clay exchangeable cations were replaced by MV^{2+} or $Ru(bpy)_3^{2+}$. The suspensions were diluted with water to a concentration of 0.005 g/L. A few drops of each suspension were placed on a smooth clean quartz slide (1 cm^2) and the water was allowed to evaporate overnight. Gold was sputtered on the samples and pictures of each samples were taken at different magnification with a scanning electron microscope.

The samples in which 50% of the exchangeable cations were replaced by MV^{2+} or $Ru(bpy)_3^{2+}$ were divided into three fractions prior to the final dilution. One fraction was then diluted as described above. A second was diluted and then placed in an ultrasound bath for 3 hours. The third fraction was centrifuged, the sediment was washed several times with water, to remove all nonadsorbed cations. The clay was resuspended in water and diluted to a concentration of 0.005 g/L like the other samples.

The SEM measurement were taken by Dr. T. Wrzesniewska on a Nanobabs 7 scanning electron microscopy from SEMCO in the department of chemistry of the university of Ottawa. The energy of the electron source was 30 keV.

12.4 Results.

Figure 66 shows the configuration of the particles of homoionic < 2.0 μm Ca^{2+} montmorillonite. Irregular shaped platelets were found. This result was similar to what was reported by Mingelgrin and Tsetkov[230] for a sample of bentonite. This clay was used as the starting material for all other samples.

Replacement of some of the calcium exchangeable cations by either MV^{2+} or $Ru(bpy)_3^{2+}$ had a dramatic effect on the configuration of the particles. The SEM micrographs of montmorillonite exchanged with methylviologen are shown in figure 67. Figures 67 A, B and C show the case in which approximately 25% of the calcium ions were exchanged by MV^{2+}. In the general view (figure 67 A) one can see that two types of particle configuration were present: platelets, similar to those seen in figure 66, which are shown at a higher magnification in figure 67 B, and a new type of particle, spherical globules, which are shown at higher magnification in figure 67 C.

When 80% of the calcium cations were replaced by MV^{2+}, fewer, but larger, particles were formed. Again, both configurations, platelets and globules, were found, the globules being the more numerous. Only a few platelets could be seen. Figure 67 D shows a close up of a larger spherical particle. One clearly sees that it was formed by the aggregation of platelets. When all of the calcium was replaced by MV^{2+} the spherical particles were not found, only platelets. (see figures 67 E and F)

When the exchangeable calcium ions were replaced by $Ru(bpy)_3^{2+}$ similar observations were made. Figures 68 A and B show that the same two types of particle configurations were found in a sample in which approximately 25% of the Ca^{2+} have been replaced by $Ru(bpy)_3^{2+}$. This was also the case for a sample in which about 80% of the calcium ions were replaced by $Ru(bpy)_3^{2+}$ (see figures 68 C and D). In both cases the two types of particles, spherical globules and platelets, coexist. Spherical particles were also found in the clay saturated with $Ru(bpy)_3^{2+}$ (see figures 68 E and F).

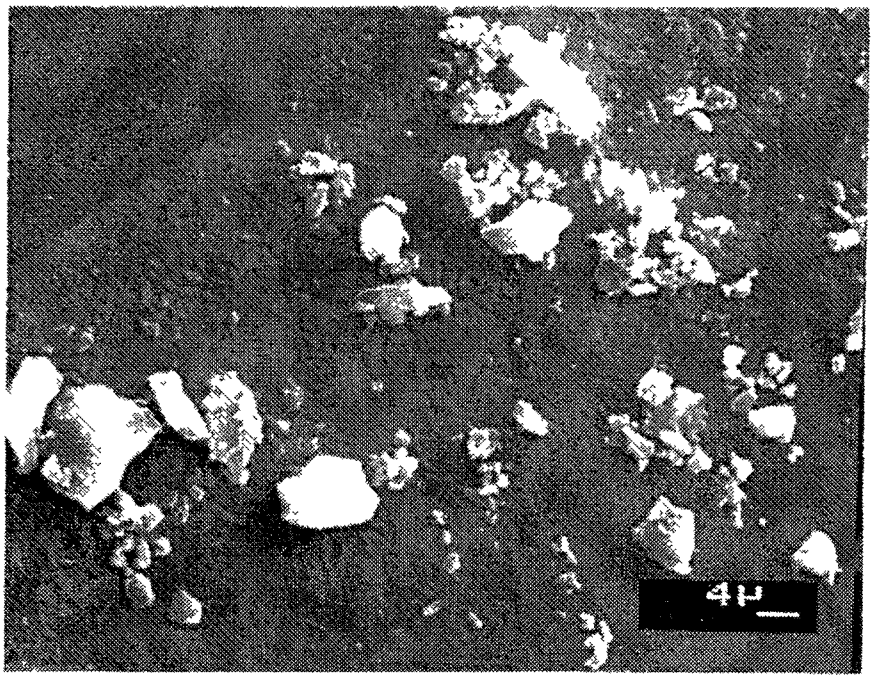

Figure 66: SEM micrograph of homoionic Ca^{2+} < 0.2 μm montmorillonite.

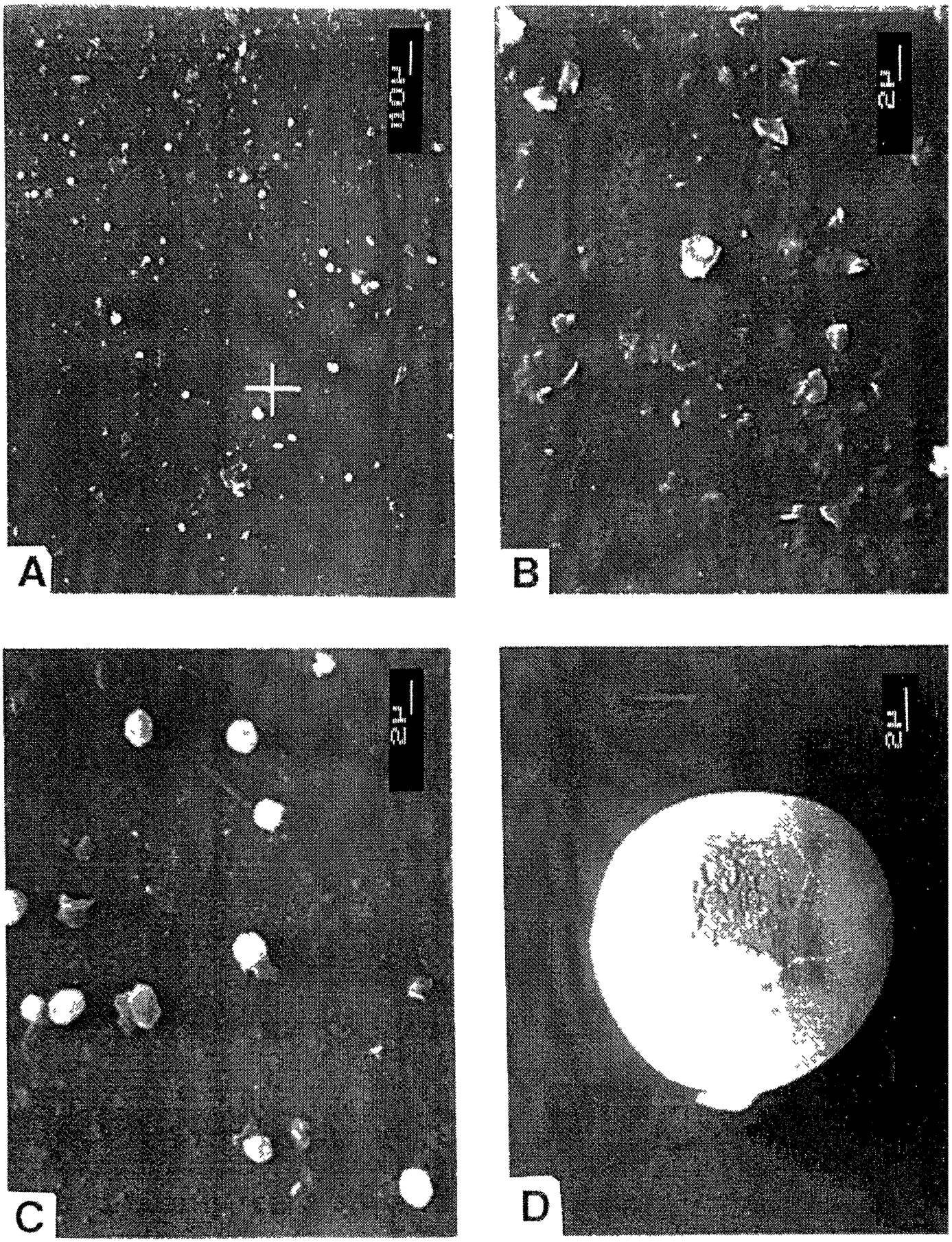
A
100µ
B
2µ
C
2µ
D
2µ

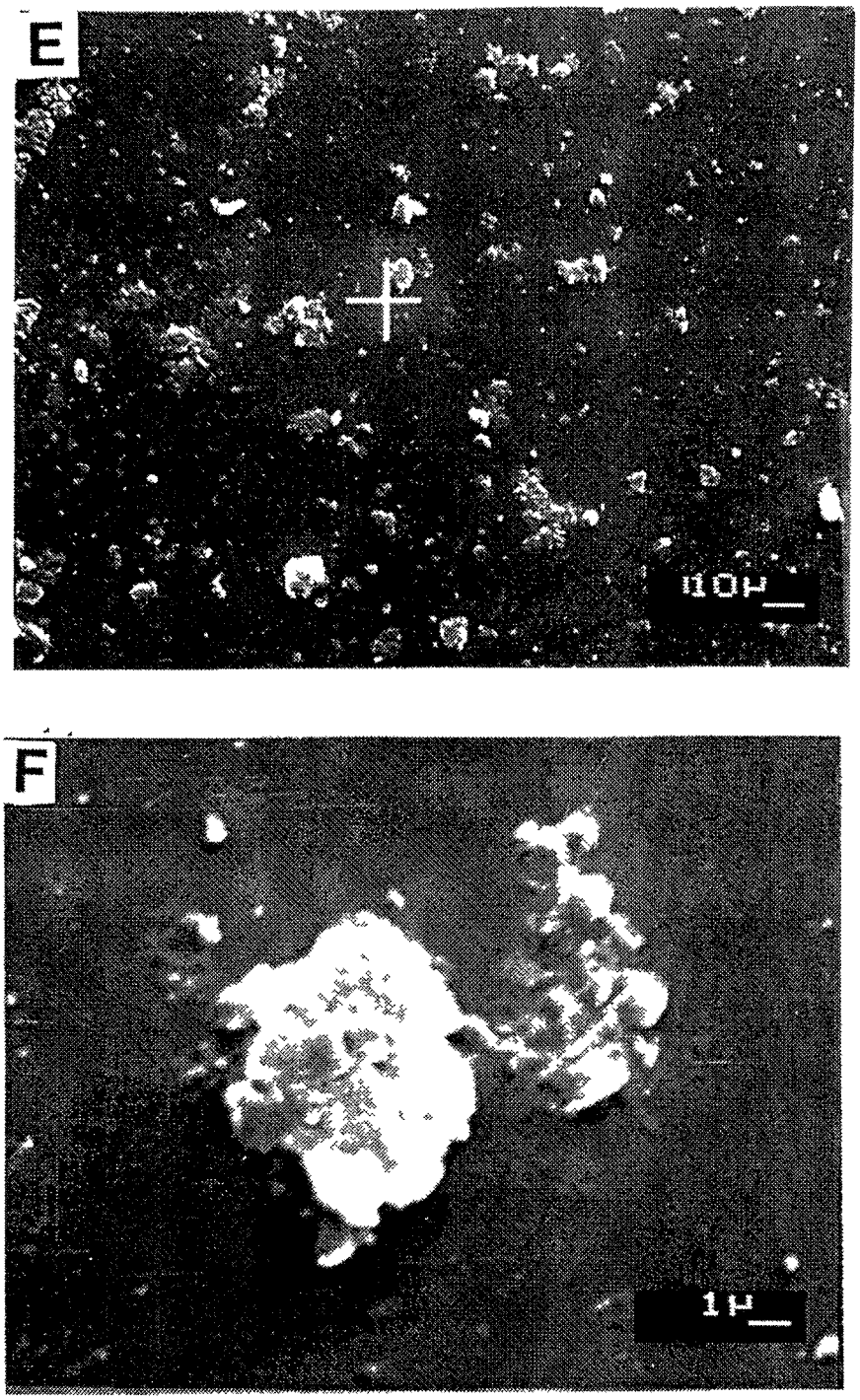

Figure 67. SEM micrographs of montmorillonite exchanged with MV^{2+}. A) General view of a clay sample in which approximately 25% of the exchangeable calcium ions have been replaced by MV^{2+}, showing two types of particle configurations B) Higher magnification of sample A showing the platelets C) Higher magnification of sample A showing the spherical particles D) Close up of one large spherical particle form when 80% of the calcium was replaced by MV^{2+} E) and F) Micrograms of montmorillonite saturated with MV^{2+} showing only platelets and no globules

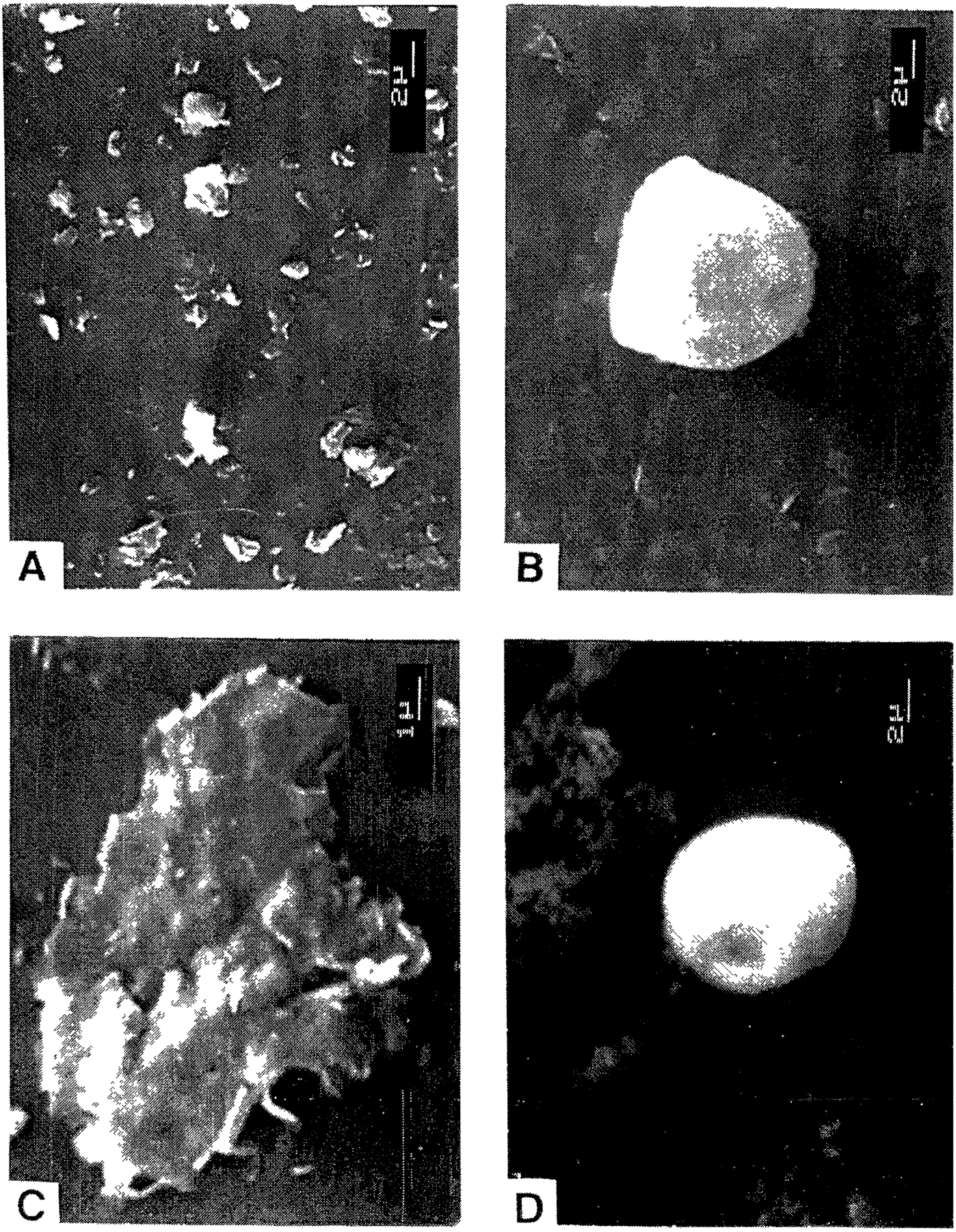
A
2μ
B
2μ
C
1μ
D
1μ

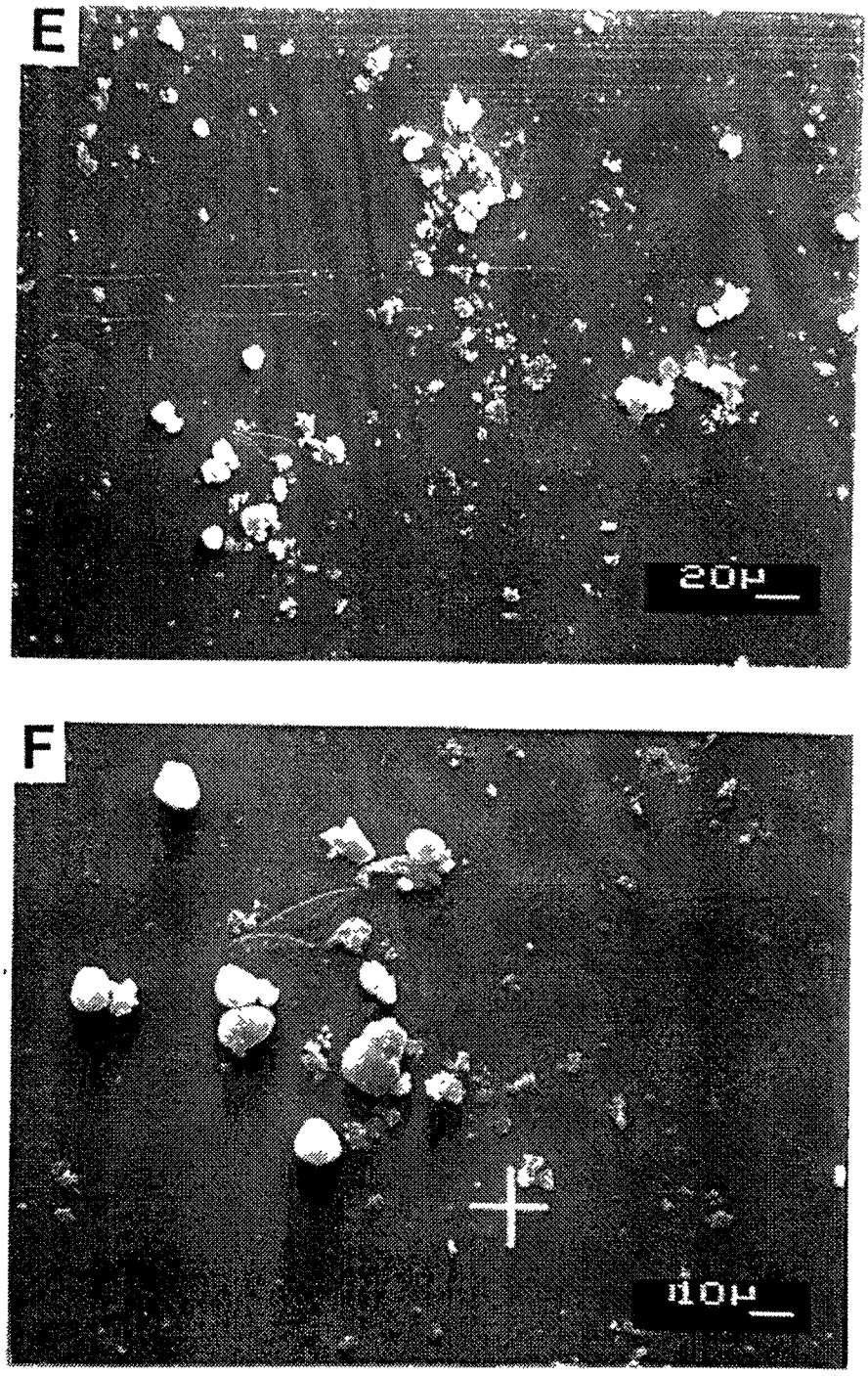

Figure 68: SEM micrographs of montmorillonite exchanged with $Ru(bpy)_3^{2+}$. A) and B) The two types of particles found in a sample of clay in which approximately 25% of the exchangeable calcium ions have been replaced by $Ru(bpy)_3^{2+}$, C) and D) The two types of particles found in a sample of the clay in which 80% of the exchangeable calcium ions have been replaced by $Ru(bpy)_3^{2+}$, E) General view of a clay saturated with $Ru(bpy)_3^{2+}$, showing the two types of particles configurations and F) higher magnification of sample E showing spherical particles.

The effect of changing the sample preparation method was studied. Samples of montmorillonite, in which approximately 50% of the exchangeable cations were replaced by either MV^{2+} or $Ru(bpy)_3^{2+}$, were prepared in three different ways. The results are shown in figures 69 and 70.

In the first case, the samples were prepared in the same way as for figures 67 and 68 . The results were generally similar. Two distinct configurations were found, platelets and spheres. However as can be seen in figure 69 A and B, there were large, thin particles and rolls not observed before. In the second case, the clay suspension was centrifuged and the clay was washed with water to eliminate the $CaCl_2$ formed when Ca^{2+} was displaced by MV^{2+}. Figures 69 C and D show the results. Again platelets, globules and rolls were found. In fact figure 69 C shows an incompletely formed globule. The only difference was in the appearance of particle clusters (see figure 69 D). These clusters disappeared when the sample was submitted to ultrasound, indicating that they were due to incomplete redispersion of the clay in water after the centrifugation. Under higher magnification these clusters resembled the "corn flake" texture typical of smectites.[224]

When the clay was exchanged with $Ru(bpy)_3^{2+}$ the same general results were found. Globules, platelets and rolls coexist in all three samples. Figures 70 A, B and C show general views of the three cases. One can observe a cluster of particles in figure 70 B, in the case of the specimen that was centrifuged and wash with distilled water. The average particle size was much smaller in the specimen submitted to ultrasound (figure 70 C). The important point was that the globules did not completely disappear even, after sonication of the sample (figure 70 D).

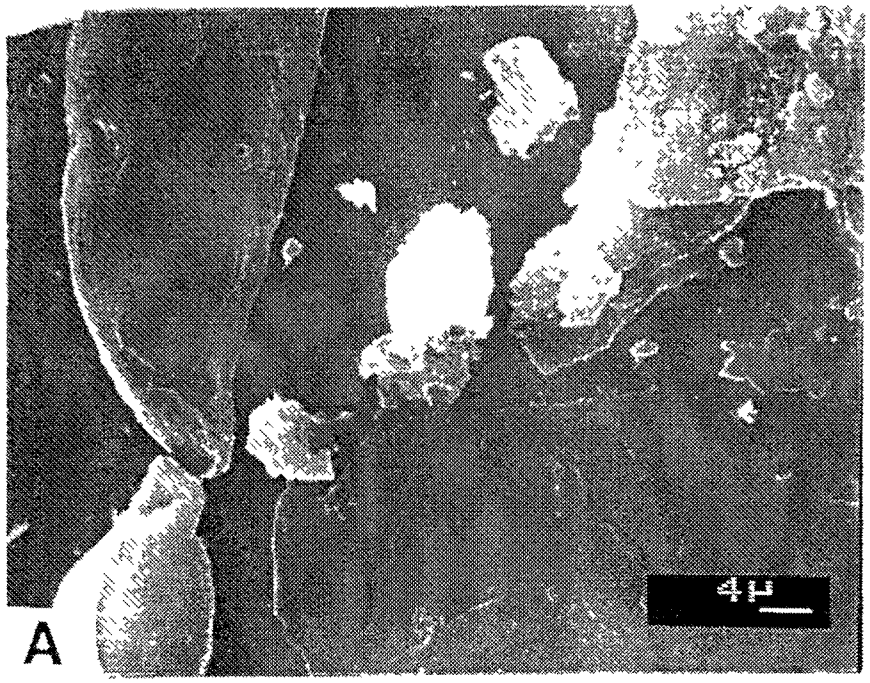
4μ
A

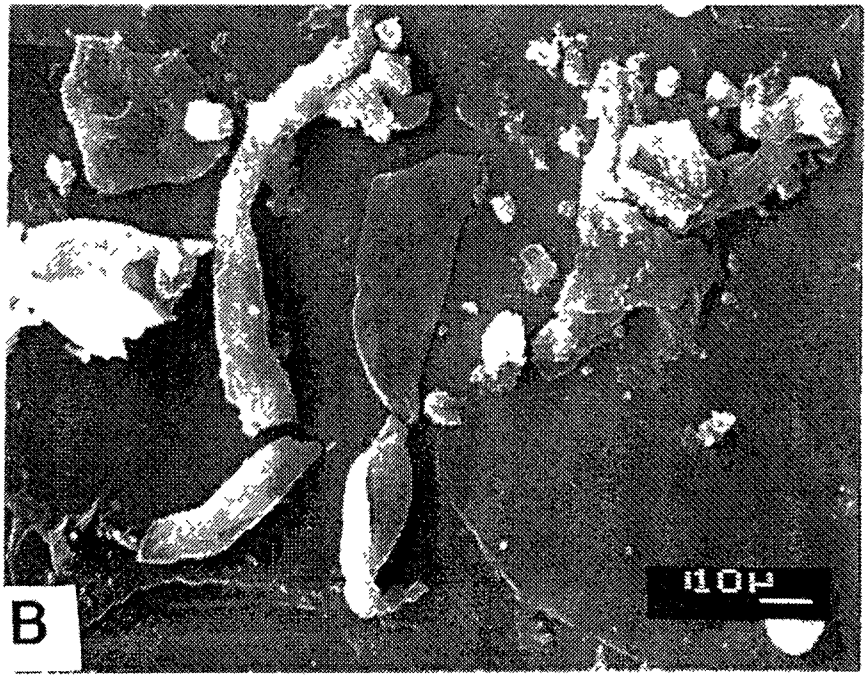
10μ
B

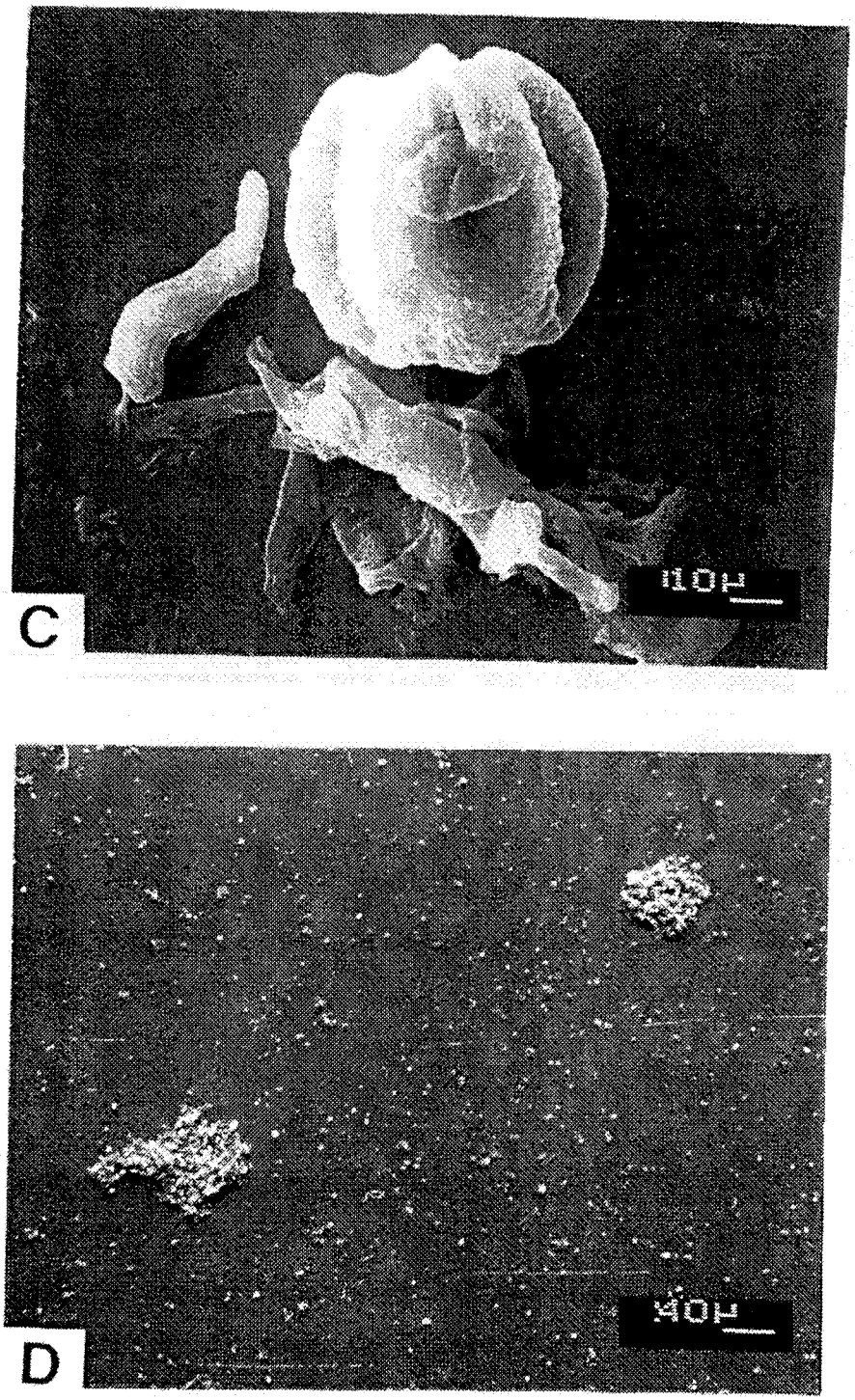

Figure 69. SEM micrographs of montmorillonite exchanged with MV^{2+} showing the effect of the method of preparation.. A) and B) View of large thin plates and rolls formed by a sample of montmorillonite in which 50% of the calcium ions were replaced by MV^{2+}, C) and D) samples of montmorillonite in which the excess salts was removed by washing with distilled water, showing a half formed globule and a cluster of particles.

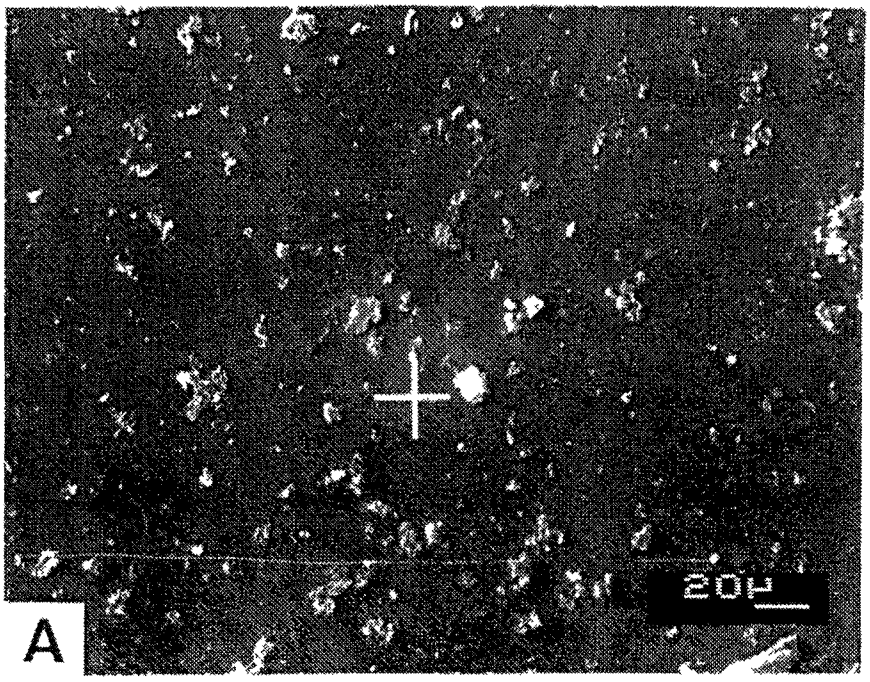
20μ
A

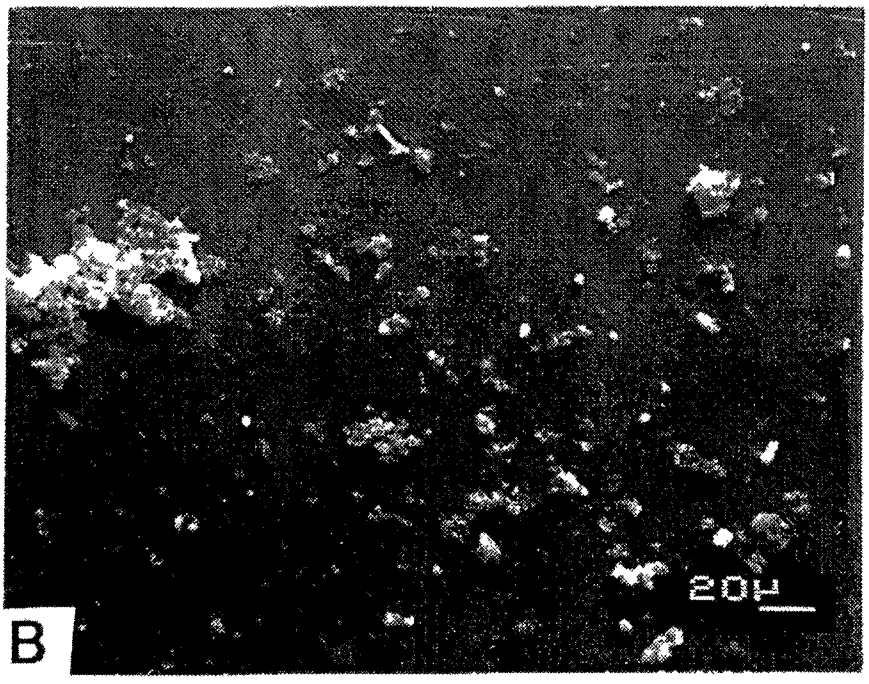
20μ
B

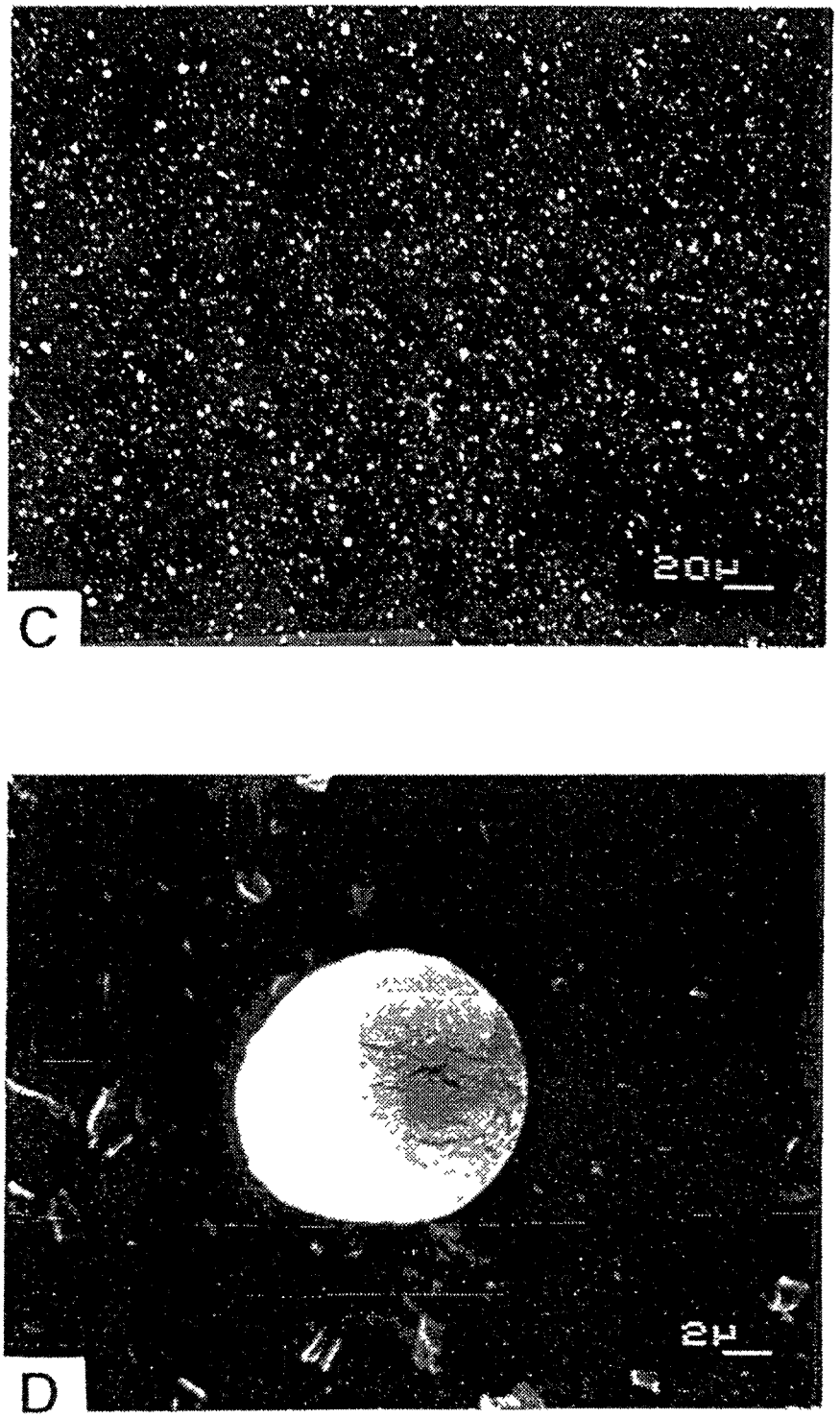

Figure 70. SEM micrographs of montmorillonite exchanged with $Ru(bpy)_3^{2+}$ showing the effect of the method of preparation. General view of a sample of montmorillonite in which about 50% of the exchangeable calcium cations were replaced by $Ru(bpy)_3^{2+}$, A) prepared as in figure 68, B) washed to removed excess $CaCl_2$, C) sonicated, D) view of a spherical particle that remained after sonication of the sample. (close up of C)

12.5 Discussion.

The intercalation of MV^{2+} or $Ru(bpy)_3^{2+}$ in montmorillonite caused some of the clay platelets to aggregate and form spherical globules (figures 66 to 70).

A possible interpretation is that the spheres were formed during the preparation of the samples. The spherical aggregates observed by Bohor and Hughes[224] in a spray-dried sample of kaolinite were attributed to the method of preparation of the sample. Spray-drying was also observed to results in the formation of spherical bentonite particles having a mean diameter of 7 μm.[230] However, we cannot attribute the spheroids found here to the method of preparation of the samples. First, the suspensions were not spray-dried. Second, the same method of preparation was used for homoionic Ca^{2+} montmorillonite (figure 66), and spherical globules were not observed in that sample.

The globules had therefore to be formed in the suspensions, by the aggregation of clay platelets taking place upon the addition of the solutions of either MV^{2+} or $Ru(bpy)_3^{2+}$. In accordance with the observations of segregation of organic and inorganic cations by clay minerals, that was discussed in chapter 11, we know that some clay particles (or at least clay crystallites) contained mostly Ca^{2+}. Since, in homoionic Ca^{2+} montmorillonite only platelets were observed, we can attribute the globules to the aggregation of those clay particles that contained the MV^{2+} or $Ru(bpy)_3^{2+}$ cations. The large thin plates and the rolls seen in figure 69 A and B are assumed to be intermediate situations between the platelets and the fully formed globules.

Several reports of spherical clay particles exist in the literature.[231-234] Two plausible interpretation of there occurrence have been suggested. The presence of spherical particles could be due to the relics of the previous structure of the material from which the clay was formed. For example, the bubbles found in a sample of bentonite formed from volcanic ash, were assumed to have retained the original morphology of the volcanic ash.[234] Obviously this was not the reason for the globule observed in figures 67 to 70.

Most often, spherical clay particles are attributed to the mechanism by which the clay was formed. For example, Tomura et al[231] report the synthesis of spherical kaolinite particles having diameters of up to 0.6 μm. Their formation was explained by assuming that kaolinite was formed around a small noncrystalline aluminosilicate "seed" particle. The spherical particles of montmorillonite reported by Glasmann,[232] and the large (10 to 20 μm) globular clusters of endellite (hydrated halloysite), made up of tubular structures radiating from the center, reported by Diamond and Bloor[233] were similarly attributed to the growth of the particles around "seeds" from the solution phase. Growth habits were also invoked to explain the formation of a rare form of chlorite, the "cabbagehead" configuration.[223]

The addition of organic cations to clay suspensions is known to cause the aggregation of the clay particles. We assume therefore that the globular particles seen here were due to the aggregation of those clay platelets containing the organic cations. This aggregation took place around seeds, perhaps provided by the first few particles that adsorbed the organic cations. The presence or absence of calcium chloride in the solution had very little effect on this aggregation, since washing the clay with distilled water did not change the configuration of the clay (see figures 69 C and D and 70 B). The aggregates, once formed, were very stable since submitting the suspensions to ultrasound did not completely destroy them (figures 70 C and D).

12.6 Conclusion.

Scanning electron microscopy showed that the intercalation of MV^{2+} or $Ru(bpy)_3^{2+}$ in montmorillonite had an effect of the configuration of the clay particles. The spherical aggregates observed by SEM were attributed to the aggregation of the clay particles which took place in the suspension upon the addition of the solution of MV^{2+} or $Ru(bpy)_3^{2+}$.

This aggregation led to the growth of spherical particles around a center in a manner analogous to what has been previously observed in the formation of spherical clay particles from solution. They were not due to the method of preparation of the suspension. The seed around which aggregation took place may be one of those first few clay platelets to be saturated with the MV^{2+} or $Ru(bpy)_3^{2+}$ cations.

REFERENCES

1. M. Gratzel, "Energy Resources through Photochemistry and Catalysis", Academic Press, New York, (1983).
2. J. R. Darwent, chapter 2 of A. Harriman and M. A. West "Photogeneration of Hydrogen", Academic Press, New York (1982).
3. G. H. Stine, "The Space Enterprise", Ace Books New York (1980).
4. Y. Hamakawa, J. Phys. C *42*, C4-1131 (1981).
5. H. B. Gray, A. W. Maverick, Science, *214*, 1201 (1981).
6. C. Kutal, J. Chem. Educ. *60*, 882 (1983).
7. J. R. Bolton, S. J. Strickler and J. S. Conolly, Nature, *316*, 495 (1985).
8. P. R. Ryason, Surv. Prog. Chem. *9*, 89 (1980).
9. V. Balzani, L. Moggi, M. F. Manfrin, F. Bolletta and M. Gleria, Science, *189*, 852 (1975).
10. M. D. Archer, Chem. Br. 991 (1984).
11. M. Calvin, Photochem. Photobiol. *37*, 349 (1983).
12. J. H. Fendler, J. Phys. Chem. *89*, 2730 (1985).
13. K. Kalyanasundaram and M. Gratzel, Photochem. Photobiol *40*, 807 (1984).
14. R. J. Ross and T-L. Hsioo, J. Appl. Phys. *48*, 4783 (1977).
15. D. O. Hall, Chapter 2 of "Solar Power and Fuels", ed J. R. Botton, Academic Press Inc, New York (1977).
16. B. V. Koryakin, T. S. Dzhabiew and A. E. Shilov, Dokl. Akad. Nauk. SSSR, *233*, 620 (1977).
17. K. Kalyanasundaram, Coord. Chem. Rev. *46*, 159 (1982).

18. V. Balzani, F. Bolletta, M. T. Gandolpi and M. Maestri, Top. Curr. Chem. *75*, 1 (1978).

19. D. G. Whitten, P. J. DeLaive, T. J. Meyer and B. P. Sullivan, J. Am. Chem. Soc. *101*, 4007 (1979).

20. J. Kiwi and M. Gratzel, Nature *281*, 657 (1979).

21. K. Mandal and M. Z. Hoffman, J. Phys. Chem. *88*, 5632 (1984).

22. J. Kiwi, K. Kalyanasundaram and M. Gratzel, Struc. Bonding, *49*, 39 (1982).

23. A. Moradpour, E. Amouyal, P. Keller and H. B. Kagan, Nouv. J. Chim. *2*, 547 (1978).

24. K. Kalyanasundaram, J. Kiwi and M. Gratzel, Helv. Chim. Acta. *61*, 2720 (1978).

25. M. O. Delcourt and N. Keghouche, Nouv. J. Chim, *9*, 235 (1985).

26. I. Okura and N. Kim-Thuan, J. Chem. Soc. Chem. Commun. 84 (1980).

27. M. C. Richoux, Chapter 3 of reference 2

28. A. Harriman, G. Porter and M. C. Richoux, J. Chem. Soc. Faraday. trans. 2 *77*, 833 (1981).

29. M. Rougee, T. Ebbeson, F. Ghetti and R. V. Benasson, J. Phys. Chem. *86*, 4404 (1982).

30. K. Kalyanasundaram and M. Gratzel, Angew, Chem. Int. Ed. Engl. *18*, 701 (1979).

31. E. Borgarello, J. Kiwi, E. Pelizzetti, M. Visca and M. Gratzel, Nature *289*, 158 (1981).

32. J. Kiwi, E. Borgarello, E. Pelizzetti, M. Visca and M. Gratzel, chapter 7 of reference 2

33. C. N. Satterfield, "Heterogeneous Catalysis in Practice", McGraw-Hill New York (1980).

34. P. A. Brugger, P. Cuendet and M. Gratzel, J. Am. Chem. Soc. *103*, 2923 (1981).

35. A. J. Frank and K. Honda, J. Phys. Chem. *86*, 1933 (1982).

36. Ch. Leygraf, M. Hendewerk and G. A. Somerjai, J. Phys. Chem. *86*, 4484 (1982).

37. G. Villemure, C. Detellier and H. Kodama, Can. J. Chem. *63*, 1139 (1985).

38. C. Detellier and G. Villemure, Inorg. Chim. Acta L-19 (1984).

39. J. M. Thomas, chapter 3 of "Intercalation Chemistry," Academic Press (1982).

40. G. Bram, E. d'Incan and A. Loupy, Nouv. J. Chim. *6*, 689 (1982).

41. D. H. Solomon, B. C. Loft and J. D. Swift, Clay Miner. *7*, 399 (1968).

42. J. M. Adams, S. E. Davis, S. H. Graham and J. M. Thomas, J. Catal. *78*, 197 (1982).

43. A. McKillop and D. W. Young, Synthesis 401 (1979).

44. L. D. Rollmann, J. Catal. *47*, 113 (1977).

45. E. Keiman, Y. Mazur, J. Am. Chem. Soc. *99*, 3861 (1977).

46. D. H. Solomon, Clays Clay Miner. *16*, 31 (1968).

47. D. T. B. Tennakoon, J. M. Thomas, M. J. Tricker and J. O. Williams, J. Chem. Soc. Dalton Trans. 2207 (1974).

48. C. Breen, J. M. Adams, C. Riekel, Clays Clay Miner. *33*, 275 (1985).

49. S. B. Hendricks, J. Phys. Chem. *45*, 65 (1941).

50. A. G. Cairns-Smith, "Genetic Takeover and the Mineral Origins of Life", Cambridge University Press, Cambridge (1982).

51. M. Paecht-Horowitz, J. Berger, and A. Katchalsky, Nature *228*, 636 (1970).

52. M. Paecht-Horowitz, Origin of Life, 289 (1978).

53. B. Velde, "Clays and Clay Minerals in Natural and Synthetic Systems", Developments in Sedimentology, Vol.*21*, Elsevier Scientific Publishing Company, Amsterdam (1977).

54. H. van Olphen, "An Introduction to Clay Colloid Chemistry", Wiley Interscience Publ., 2ed., New York (1977).

55. C. E. Weaver and L. D. Pollard, "The Chemistry of Clay Minerals", Developments in Sedimentology Vol.*15* Elsevier Scientific Publ. Co. Amsterdam (1973).

56. R. M. Barrer and D. L. Jones, J. Chem. Soc. A 1531 (1970).

57. G. H. Posner, Angew. Chem. Int. Ed. Engl. *17*, 487 (1978).

58. Z. Cohen, E Keinan, Y. Mazur and T. H. Varkary, J. Org. Chem. *40*, 2141 (1975).

59. J. R. Durland and H. Adkins, J. Am. Chem. Soc. *61*, 429 (1939).

60. C. D. Chang and A. J. Silverstri, J. Catal. *47*, 249 (1977).

61. E. G. Derouane, "Catalysis by Zeolite", Elsevier Scientific Publishing Company, New York (1980).

62. J. M. Parera and N. S. Figoli, J. Catal. *14*, 303 (1969).

63. T. J. Pinnavaia, R. Raythatta, J. G. S. Lee, L. J. Halloran and J. F. Hoffman, J. Am. Chem. Soc. *101*, 6891 (1979).

64. R. A. DellaGuardia and J. K. Thomas, J. Phys. Chem. *87*, 990 (1983).

65. B. K. G. Theng, Clays Clay Miner. *19*, 383 (1971).

66. D. T. B. Tennakoon, J. M. Thomas, M. J. Tricker and J. O. Williams, J. Chem. Soc. Dalton Trans. 2211 (1974).

67. A. Bylina, J. M. Adams, S. H. Graham and J. M. Thomas, J. Chem. Soc. Chem. Commun. 1003 (1980).

68. J. A. Ballentine, M. Davies, H. Purnell, M. Rayanakorn, J. M. Thomas and K. J. Williams, J. Chem. Soc. Chem. Commun. 8 (1981).

69. J. A. Ballentine, R. P. Galvin, R. M. O'Neil, H. Purnell, M. Rayanakorn and J. M. Thomas, J. Chem. Soc. Chem. Commun. 695 (1981).

70. J. A. Ballentine, M Davies, H. Purnell, M. Rayanakorn, J. M. Thomas and K. J. Williams, J. Chem. Soc. Chem. Commun. 427 (1981).

71. J. M. Adams, S. E. Davis and S. H. Graham, J. Chem. Soc. Chem. Commun. 930 (1978).

72. J. M. Adams, S. E. Davis and S. H. Graham, J. Chem. Soc. Chem. Commun. 527 (1979).

73. S. Suib and K. A. Carrodo, Inorg. Chem. *24*, 863 (1985).

74. T. J. Pinnavaia, M. S. Tzou and S. D. Landou, J. Am. Chem. Soc. *107*, 4783 (1985).

75. E. P. Giannelis and T. J. Pinnavaia, Inorg. Chem. *24*, 2115 (1985).

76. P. A. Brugger and M. Gratzel, J. Am. Chem. Soc. *102*, 2461 (1980).

77. O. Johansen, A. W. H. Mau and W. H. F. Sasse, Chem. Phys. Lett. *94*, 113 (1983).

78. M. S. Tunuli and J. H. Fendler, J. Am. Chem Soc. *103*, 2507 (1981).

79. B. H. Milosarlzevic and J. K. Thomas, J. Phys. Chem. *89*, 1830 (1985).

80. M. Kaneko, J. Motoyoshu and A. Yamada, Nature *285*, 468 (1980).

81. N. J. Turro, M. Gratzel and A. M. Braun, Angew Chem. Int. Ed. Engl. *19*, 675 (1980).

82. S. S. Atik and J. K. Thomas, J. Am. Chem. Soc. *103*, 4367 (1981).

83. R. E. Sassoon and J. Rabbani, Isr. J. Chem. *22*, 138 (1982).

84. T. Ohsako, T. Sakamoto and T. Matsuo, J. Phys. Chem. *89*, 222 (1985).

85. R. E. Sassoon, J. Am. Chem. Soc. *107*, 6133 (1985).

86. D. Meyerstein, J. Rabani, M. S. Matterson and D. Meisel, J. Phys. Chem. *82*, 1879 (1978).

87. I. Willner, J. M. Yang, C. Laane, J. W. Ottros and M. Calvin, J. Phys. Chem. *85*, 3277 (1981).

88. H. Nijs, M. I. Cruz, J. J. Fripiat and H. van Damme, Nouv. J. Chim. *6*, 551 (1982).

89. H. Nijs, H. van Damme, F. Berzaya, A. Habti and J. J. Fripiat, J. Mol. Catal. *21*, 223 (1983).

90. H. Nijs, J. J. Fripiat and H. van Damme, J. Phys. Chem. *87*, 1279 (1983).

91. F. R. F. Fan, H. Y. Liu and A. J. Bard, J. Phys. Chem. *89*, 4418 (1985).

92. D. Ege, P. K. Ghosh, J. R. White, J. F. Equey and A. J. Bard, J. Am. Chem. Soc. *107*, 5644 (1985).

93. O. Enea and A. J. Bard, J. Phys. Chem. *90*, 301 (1986).

94. N. Kakuta, K. H. Park, M. F. Finlayson, A. Ueno, A. J. Bard, A. Campsion, M. A. Fox, S. E. Webber and J. M. White, J. Phys. Chem. *89*, 732 (1985).

95. I. Okura, S. Nakamura, and M. Kalayoshi, Bull. Chem. Soc. Jpn. *54*, 3794 (1981).

96. R. H. Holm, Acc. Chem. Res. *10*, 427 (1977).

97. M. C. W. Evans, "Iron-Sulfur Proteins", John Wiley and sons, New York (1982).

98. K. S. Hagen, J. G. Reynolds and R. H. Holm, J. Am. Chem. Soc. *103*, 4054 (1981).

99. I. Okura, S. Aono and S. Kusunoki, Inorg. Chim. Acta *71*, 77 (1983).

100. T. Tsukilava, K. Fukuyama, M. Nakamura, Y. Katsube, N. Tanaka, M. Kakudo, K. Wada, T. Hase and H. Matsubara, J. Biochem. *90*, 1763 (1981).

101. T. E. Wolff, J. M. Berg, K. O. Hadgson, R. B. Frenkel and R. H. Holm, J. Am. Chem. Soc. *101*, 4140 (1979).

102. D. I. Arnon and R. K. Chain, Proc. Nat. Acad Sci. USA *74*, 3377 (1977).

103. R. Maskiewiez and B. H. J. Bielski, Biochim. Biophys. Acta *680*, 297 (1982).

104. G. Christou, R. V. Hageman and R. H. Holm, J. Am. Chem. Soc. *102*, 7600 (1980).

105. G. Christou and C. D. Garner, J. Chem. Soc. Dalton Trans. 1094 (1979)

106. J. G. Reynolds and R. H. Holm, Inorg Chem. *19*, 3275 (1980).

107. M. Millar, J. F. Lee, S. A. Koch and R. Fika, Inorg. Chem. *21*, 4105 (1982).

108. B. A. Averill, T. Herskovitz, R. Holm and J. A. Ibers, J. Am. Chem. Soc. *95*, 3523 (1973).

109. R. W. Lane, J. A. Ibers, R. B. Frankel, G. C. Papaefthymiou and R. H. Holm, J. Am. Chem. Soc. *99*, 84 (1977).

110. J. J. Mayerle, S. E. Denmark, B. V. DePamphilis, J. A. Ibers and R. H. Holm, J. Am. Chem. Soc. *97*, 1032 (1975).

111. T. Nagano, K. Yashikawa and M. Hirobe, Tetrahedron Lett. *21*, 297 (1980).

112. T. Itoh, T. Nozano and M. Hirobe, Tetrahedron Lett. *21*, 1343 (1980).

113. M. Tezuka, T. Yajima and A. Tsuchija, J. Am. Chem. Soc. *104*, 6834 (1982).

114. K. Tanaka, Y. Hozumi and T. Tanaka, Chem. Lett. 1203 (1982).

115. K. Tanaka, M. Tanaka and T. Tanaka, Chem. Lett. 895 (1981).

116. I. Okura and N. K. Thuan, J. Mol. Catal. *5*, 311 (1979).

117. I. Okura, N. Kaji, S. Aono and T. Kita, Inorg. Chim. Acta *86*, L-79 (1984).

118. I. Okura, N. Kaji, S. Aono, T Kita and A. Yamada, Inorg. Chem. *24*, 451 (1985).

119. I. Okura, S. Aono, M. Takeuchi and S. Kusunoki, Nouv. J. Chim. *6*, 221 (1982).

120. I. Okura, M. Kabayashi, N. K. Thuan, S. Nakamira and K. I. Nakamura, J. Mol. Catal. *8*, 385 (1980).

121. Y. Okuno and O. Yonemitsu, Chem. Lett. 959 (1980).

122. R. G. Bowman and R. L. Burwell Jr, J. Am. Chem. Soc. *101*, 2877 (1979).

123. L. Que Jr, R. H. Holm and L. E. Mortenson, J. Am. Chem. Soc. *97*, 463 (1975).

124. R. H. Holm, W. D. Phillips, B. A. Averill, J. J. Mayerle and T. Herskovitz, J. Am. Chem. Soc. *96*, 2109 (1974).

125. K. Kalyanasundaram, Inorg. Chem. *23*, 2453 (1984).

126. J. E. Brydon, private communication

127. M. L. Jackson, L. D. Wittig and R. P. Pennington, Soil Sci. Soc. Amer. Proc. *14*, 77 (1949).

128. R. C. Mackenzie, Clay Min. Bull. *3*, 4 (1956).

129. C. B. Tanner and M. L. Jackson, Soil Sci. Soc. Amer. Proc. *12*, 60 (1947).

130. J. W. Verhoeven, A. M. Verhoeven-Schoff, A. Masson and R. Schwuzer, Helv. Chim. Acta *53*, 2503 (1974).

131. S. B. Weed and J. B. Weber, Am. Mineral. *53*, 478 (1968).

132. D. Carrol, Geol. Soc. Am. *126*, 1 (1970).

133. M. Zuker, A. G. Szabo, L. Bramall and D. T. Krajcarski, Rev. Sci. Instrum. *56*, 14 (1985).

134. M. Raupach, W. W. Emerson and P. G. Slade, J. Colloid Interface Sci. *69*, 398 (1979).

135. J. B. Weber, P. W. Perry and R. P. Upchurch, Soil Sci. Soc. Amer. Proc. *29*, 678 (1965).

136. M. F. Traynor, M. M. Mortland and T. J. Pinnavaia, Clays Clay Miner. *26*, 318 (1978).

137. D. Krenske, S. Abdo, H. van Damme, M. Cruz and J. J. Fripiat, J. Phys. Chem. *84*, 2447 (1980).

138. M. H. B. Hayes, M. E. Pick and B. A. Toms, Residue Rev. *57*, 1 (1975).

139. M. H. B. Hayes, M. E. Pick and B. A. Toms, J. Colloid Interf. Sci. *65*, 254 (1978).

140. J. H. White and A. J. Bard, J. Electroanal. Chem. *197*, 233 (1986).

141. S. B. Weed and J. B. Weber, Soil Sci. Soc. Amer. Proc. *33*, 379 (1969).

142. D. P. Rillema and D. S. Jones, J. Chem. Soc. Chem. Commun. 849 (1979).

143. J. H. Russell and S. C. Wallwork, Acta Crystallogr. Sect. B *28*, 1527 (1972).

144. O. Poizat, C. Sourisseau and Y. Mathey, J. Chem. Soc. Faraday Trans. 1 *80*, 3257 (1984).

145. R. Greene-Kelly, Trans. Faraday Soc. *51*, 412 (1955).

146. L. G. Strange, Proc. Int. Clay Conf. (Madrid) 693 (1972).

147. J. E. Derry, T. A. Hanor, Nature *221*, 464 (1969).

148. S. Abdo, P. Canesson, M. Cruz, J. J. Fripiat and H. van Damme, J. Phys. Chem. *88*, 5519 (1984).

149. B. A. G. Knight and P. J. Denny, Weed. Res. *10*, 40 (1970).

150. P. K. Ghosh and A. J. Bard, J. Phys. Chem. *88*, 5519 (1984).

151. In the presence of hectorite at pH 7, hydrogen is evolved at $[MV^{2+}] = 0$. In fact the largest yield is obtained with no methylviologen. (see reference 155) In this case the mechanism of hydrogen evolution must be different since it does not involve the reduction of MV^{2+}.

152. S. Aono, N. Kaji and I. Okura, J. Chem. Soc. Chem. Commun. 170 (1986).

153. T. F. Ho, A. R. McIntosh and J. R. Bolton, Nature *286*, 254 (1980).

154. W. E. Rudzinski and A. J. Bard, J. Electroanal. Chem. *199*, 323 (1986).

155. C. Detellier, H. D. H. Stover, G. Bazan and G. Villemure, to be published.

156. C. Sehzal, R. G. Sutherland and R. F. Verral, J. Phys. Chem. *84*, 388 (1980).

157. N. J. Turro, "Modern Molecular Photochemistry", Benjamin/Cummings Publ. Co., Menlo Park (1978).

158. G. M. Barrow, "Physical Chemistry", McGraw Hill, Inc (1979).

159. J. F. Rabek, "Experimental Methods in Photochemistry and Photophysics" Vol. 2, John Wiley and Sons, New York (1982).

160. G. G. Guilbault, "Practical Fluorescence, Theory, Methods and Techniques", Marcel Dekker, Inc New York (1973).

161. J. R Lakowicz, "Principles of Fluorescence Spectroscopy", Plenum Press, New York (1983).

162. G. Beck and J. K. Thomas, Chem. Phys. Lett. *94* 553 (1983).

163. N. J. Turro and T. Okudo, J. Phys. Chem. *86*, 159 (1982).

164. J. Wheeler and J. K. Thomas, J. Phys. Chem. *86*, 4540 (1982).

165. R. A. Shoonheydt, P. DePauw, D. Villiers and F. C. DeSchrijver, J. Phys. Chem. *88*, 5133 (1984).

166. T. Nakamura and J. K. Thomas, Langmuir *1*, 568 (1985).

167. J. K. Thomas, Chem. Rev. *80*, 283 (1980).

168. M. Shinitzky, A. C. Dianoux, G. Gilter and G. Weber, Biochem. *10*, 2106 (1971).

169. G. Weber, Ann. Rev. Biophys. Bioeng. *1*, 553 (1972).

170. E. Blatt, K. P. Ghiggino and W. H. Sawyer, J. Phys. Chem. *86*, 4461 (1982).

171. E. Keh, and B. Valeur, J. Coll. Interf. Sci. *79*, 465 (1981).

172. B. Valeur and E. Keh, J. Phys. Chem. *83*, 3307 (1979).

173. K. Chandrasekaran and J. K Thomas, J. Am. Chem. Soc. *105*, 6383 (1983).

174. W. Shi, S. Wolfgang, T. C. Strekas and H. D. Gafney, J. Phys. Chem. *89*, 974 (1985).

175. T. Kennelly, H. D. Gafney and M. Braun, J. Am. Chem. Soc. *107*, 4431 (1985).

176. F. W. J. Teale, Photochem. Photobiol. *10*, 363 (1969).

177. B. R. Lentz, B. M. Moore and D. A. Barrow, Biophys. J. *25*, 289 (1979).

178. C. R. Bock, T. J. Meyer and D. G. Whitten, J. Am. Chem. Soc. *96*, 4710 (1974).

179. N. Sutin and C. Creutz, Adv. Chem. Ser. *1*, 168 (1978).

180. R. A. Marcus and P. Siders, J. Phys. Chem. *86*, 622 (1982).

181. A. Habti, D. Keravis, P. Levitz and H. van Damme, J. Chem. Soc. Faraday Trans. 2 *80*, 67 (1984).

182. G. Villemure, C. Detellier and A. G. Szabo, J. Am. Chem. Soc. *108*, 4658 (1986).

183. R. Haque, S. Lilley and W. R. Coshow, J. Coll. Interf. Sci. *33*, 185 (1970).

184. A. S. Hoptkins, A. Ledwith and M. F. Stam, J. Chem. Soc. Chem Commun. 494 (1970).

185. D. R. Prasad and M. Z. Hoffman, J. Phys. Chem. *88*, 5660 (1984).

186. T. W. Ebbesen, L. E. Manning and K. S. Paters, J. Am. Chem. Soc. *106*, 7400 (1984).

187. J. P. Kuczynski, B. H. Milosavljevic, A. G. Lappin and J. K. Thomas, Chem. Phys. Lett. *104*, 149 (1984).

188. A. T. Poulos and C. K. Kelly, J. Chem. Soc. Faraday Trans. 1 *79*, 55 (1983).

189. M. Z. Hoffman, D. R. Prassad, G. Jones II and V. Malba, J. Am. Chem. Soc. *105*, 6360 (1983).

190. A. W-H. Mau, J. M. Overbeek, J. W. Loder and W. H. F. Sasse, J. Chem. Soc. Faraday Trans. 2 *82*, 869 (1986).

191. A. Camerman and L. H. Jensen, J. Am. Chem. Soc. *92*, 4200 (1970).

192. R. Haque, W. R. Coshow and L. F. Johnson, J. Amer. Chem. Soc. *91*, 3822 (1969).

193. A. J. Macfarlane and R. J. P. Williams, J. Chem. Soc. (A) 1517 (1969).

194. E. W. Nuffield, "X-ray Diffraction Methods", John Wiley and Sons, Inc, New York (1966).

195. B. E. Warren, "X-ray Diffraction", Addison-Wesly Publishing Company, Inc, Don Mills (1969).

196. G. Brown and G. W. Brindley, chapter 5 of "Crystal Stuctures of Clay Minerals and their X-ray Identification" Edited by G. W. Brindley and G. Brown, Mineralogical Society London (1984).

197. T. Sudo, K. Oinuna and K. Kobayashi, Acta Univ. Carol. Geol. Supp. *1*, 189 (1961).

198. R. J. Gibbs, Am. Mineral. *50*, 741 (1965).

199. R. M. Barrer and K. Brummer, Trans. Faraday Soc. *59*, 959 (1963).

200. D. M. Clementz and M. M. Mortland, Clays Clay Miner. *22*, 233 (1974).

201. M. B. McBride and M. M. Mortland, Clays Clay Miner. *10*, 357 (1975).

202. R. C. Reynolds Jr and J. Hower, Clays Clay Miner. *18*, 25 (1970).

203. G. V. Henderson and W. F. Bradley, Clays Clay Miner. *18*, 115 (1970).

204. S. Hendricks and E. Teller, J. Chem. Phys. *10*, 147 (1942).

205. D. M. C. MacEwan, Kolloid. *149*, 96 (1956).

206. D. M. C. MacEwan, Kolloid. *156*, 61 (1958).

207. R. C. Reynolds, Chapter 4 of reference 202

208. E. Slansky, Clays Clay Miner. *33*, 361 (1985).

209. C. M. Bethke and R. C. Reynolds, Clays Clay Miner. *34*, 224 (1986).

210. K. Tomita and H. Takahashi, Clays Clay Miner. *34*, 323 (1986).

211. J. H. Ahn and D. R. Peacor, Clays Clay Miner. *34*, 165 (1986).

212. A. Ruiz-Amil, A. R. Garcia and D. M. C. MacEwan, "X-ray Diffraction Curve for the Analysis of Interstratified Structures", Volturna Press Edinburgh (1967).

213. P. D. Cradwick and M. J. Wilson, Clay Miner. *13*, 53 (1978).

214. G. Lagaly, Clay Miner. *16*, 1 (1981).

215. M. B. McBride and M. M. Mortland, Clays Clay Miner. *21*, 323 (1973).

216. J. Ohnsorge and R. Holm, "Scanning Electron Microscopy An Introduction for Physicians and Biologists", Georg Thieme Publishers Stuttgart (1978).

217. C. W. Oathey, J. Appl. Phys. *53*, R1 (1982).

218. D. L. Davidson, Chemtech, *13*, 670 (1983).

219. T. F. Bates and J. J. Comer, Clays Clay Miner. *3*, 1 (1955).

220. A. Antonorsky and M. J. Sandy, Can. Mineral. *22*, 373 (1984).

221. T. A. Peters, Scanning Electron Microscopy, Part I 603 (1981).

222. B. F. Bohor and R. E. Huges, Clays Clay Miner. *19*, 49 (1971).

223. M. D. Wilson and E. D. Pittman, J. Sediment. Petrology *47*, 3 (1977).

224. R. E. Tompkins, Clays Clay Miner. *29*, 233(1981).

225. W. D. Keller, Clays Clay Miner. *30*, 150 (1982).

226. D. J. Cebula, R. K. Thomas, S. Middleton, R. H. Otterwill and J. R. White, Clays Clay Miner. *27*, 39 (1979).

227. W. D. Keller, R. C. Reynolds and A. Inoue, Clays Clay Miner. *34*, 187 (1986).

228. D. R. Peacor, V. E. Williams and G. E. Mustoe, Clays Clay Miner. *28*, 241 (1980).

229. H. Eswaran, J. Soil. Sci. *30*, 547 (1979).

230. U. Mingelgrin and F. Tsvetkov, Clays Clay Miner. *33*, 285 (1985).

231. S. Tomura, Y. Shibasaki, H. Mizuta and M. Kitamura, Clays Clay Miner. *31*, 413 (1983).

232. J. R. Glasmann, Clays Clay Miner. *30*, 253 (1982).

233. S. Diamond and J. W. Bloor, Clays Clay Miner. *18*, 309 (1970).

234. H. N. Khoury and D. D. Eberl, Clays Clay Miner. *27*, 291 (1979).

CLAIMS TO ORIGINAL RESEARCH.

1. $Ru(bpy)_3^{2+}$ photosensitized hydrogen evolution in the presence of the clay minerals montmorillonite, hectorite and nontronite.
2. $ZnTMPyP^{4+}$ photosensitized hydrogen evolution in the presence of the clay minerals montmorillonite and hectorite.
3. Effect of the presence of the iron-sulfur cluster $[n\text{-}Bu_4N]_2[Fe_4S_4(Ph)_4]$ on the $Ru(bpy)_3^{2+}$ photosensitized hydrogen evolution in the presence of montmorillonite.
4. Competitive adsorption of MV^{2+} and $Ru(bpy)_3^{2+}$ by montmorillonite.
5. Competitive adsorption of MV^{2+} and $ZnTMPyP^{4+}$ by montmorillonite.
6. Fluorescence of MV^{2+} intercalated in montmorillonite.
7. Fluorescence of MV^{2+} intercalated in hectorite.
8. Anisotropy of the fluorescence of MV^{2+} intercalated in montmorillonite and hectorite.
9. Lifetime of the fluorescence of MV^{2+} intercalated in hectorite and montmorillonite.
10. Application of X-ray diffraction to the analysis of interlayering in clay minerals showing segregation of $Ru(bpy)_3^{2+}$ and MV^{2+} by montmorillonite and hectorite.
11. Examination of isolated montmorillonite particles exchanged with MV^{2+} or $Ru(bpy)_3^{2+}$ by scanning electron microscopy.

I hereby declare that I am the sole author of this thesis. I authorize the University of Ottawa to lend this thesis to other institutions or individuals for the purpose of scholarly research.

Gilles Villemure

I further authorize the University of Ottawa to reproduce this thesis by photocopying or by other means, in total or in part, at the request of other institutions or individuals for the purpose of scholarly research.

Gilles Villemure